Insights into Unfolded Protein Response in the Heart

by

Qian Wang

A thesis submitted in partial fulfillment of the requirements for the degree of

Doctor of Philosophy

Department of Biochemistry

University of Alberta

Abstract

Cellular responses to stress are an integral part of cardiovascular physiology and pathology, and endoplasmic reticulum (ER) stress is the key component in the development and progression of various heart diseases. However, the relative contribution of ER stress pathways to muscle damage and molecular mechanisms governing muscle ER stress regulation are still unclear. The objectives of this thesis were to investigate a role and regulation of IRE1α, an ER membrane associated stress sensor, in skeletal and cardiac muscle and to determine structural and function features of catecholaminergic polymorphic ventricular tachycardia (CPVT) related Casq2 mutants and their role in heart pathology.

We identified two distinct pools of IRE1α in skeletal muscle fibers and in cardiomyocytes. One pool localized at the perinuclear ER membrane system and other at the junctional sarcoplasmic reticulum (SR). We also discovered that, at the junctional SR, calsequestrin interacts directly with the ER luminal domain of IRE1α preventing its dimerization, an initial step in activation IRE1α signaling. We generated a mouse model with cardiomyocyte specific, inducible deletion of the IRE1α gene. Heart with silenced IRE1α developed dilated cardiomyopathy and impaired cardiomyocyte Ca^{2+} transient indicating important role of IRE1α in the heart physiology and potential functional impact on muscle excitation-contraction coupling.

Mutations in the gene encoding for cardiac calsequestrin, CASQ2, cause a stress-induced arrhythmia, CPVT. We carried out functional and structural analysis of six CPVT related CASQ2 mutations (R33Q, L167H, D307H, D351G, G332R, and P329S). The six mutations are distributed in diverse locations of the calsequestrin and impact on structure and function of the protein including folding, aggregation, and impaired or reduced Ca^{2+} binding. Remarkably these mutations are manifested in a similar phenotype in humans.

Overall, in this thesis, we show that IRE1α is a new component of the junctional SR where it interacts with calsequestrin. This novel protein-protein interaction provides new insight into muscle specific regulatory mechanisms associated with IRE1α mediated UPR. We also provide the first direct evidence that IRE1α is required to maintain health of the heart. Finally, we provide the first evolutionary insights into the calsequestrin gene and showed that different Casq2 mutations may have distinct underlying molecular mechanisms leading to CPVT.

Preface

Chapter 1. The literature review on calsequestrin presented in the section 1.5 of Chapter 1 has been modified from Wang Q, Michalak M. 2020. Calsequestrin. Structure, function, and evolution. *Cell Calcium*. 90. 102242

Chapter 2 of my thesis has been published as Wang Q, Groenendyk J, Paskevicius T, Qin W, Kor KC, Liu Y, Hiess F, Knollmann, BC, Chen SRW, Tang J, Chen XZ, Agellon LB, Michalak M. Two pools of IRE1α in cardiac and skeletal muscle cells. *FASEB Journal*. 2019;33:8892-8904.

Liu Y, .Hiess F, form the laboratory of Dr. Chen S.R.W. at the University of Calgary performed cardiomyocyte isolation and confocal microscopy experiments presented in the Figure 2-4. Dr. Groenendyk J performed initial surface plasmon resonance analysis of IRE1α interacting with calsequestrin presented in the Figure 2 5F and Figure 2-6B. Qin W. from laboratories of Drs. Tang J. and Chen XZ. at the Hubei University of Technology and University of Alberta, respectively, assisted in experiments and analysis of the data presented in the Figure 2-11C (Cross-linking of IRE1-NLD in the absence and presence of Casq2). I was responsible for coordinating the work, data collection and analysis for the remaining figures. I wrote the manuscript with contributions from Groenendyk J and editing help from Dr. Agellon LB. and Dr. Michalak M.

Chapter 3. Dr. Singh J. form the laboratory of Dr. Light P. (Department of Pharmacology, University of Alberta) assisted in Ca^{2+} transient analysis presented in the Figure 3-7. Dr. Li W. assisted in the wheat germ agglutinin staining of heart tissue for the identification of T-tubule membrane and extracellular matrix detection presented in the Figure 3-6. Robinson A. assisted in animal care, breeding, handling, and isolation of cardiomyocytes and cardiofibroblasts. I was responsible for coordinating the work, data collection and analysis for the remaining Figures. I wrote the Chapter with contributions from Dr. Singh J and editing help from Dr. Michalak M.

Chapter 4 of my thesis will be published as: Wang Q, Paskevicius T, Filbert A, Qin W, Chen X, Tang J, Dacks J, Agellon LB, Michalak M. Evolutionary conservation and diversity of human calsequestrin function. *Scientific Report*. 2020. Revisions requested. Filbert A. form the laboratory of Dr. Dacks J. carried out phylogenetic analysis of the calsequestrin gene presented in the Figure 4-1, Figure 4-2, Figure 4-3, Figure 4-4, and Table 4-1. Paskevicius T. assisted in purification of cardiac calsequestrin protein used for experiments presented in the Figure 4-5, Figure 4-7, Figure

4-8**,** Figure 4-9, Figure 4-10, and Figure 4-11. Qin W. from laboratories of Drs. Tang J. and Dr. Chen XZ. at the Hubei University of Technology and University of Alberta, respectively, assisted in polymerization of cardiac muscle calsequestrin experiments presented in the Figure 4-9 and Figure 4-10. I was responsible for coordinating the work, data collection and analysis for the remaining Figures. I wrote the manuscript with contributions from Filbert A. and editing help from Dr. Dacks J., Dr. Agellon LB., and Dr. Michalak M.

Appendix. The data and analysis presented in Appendices is my original work.

Acknowledgments

The research described in this thesis would not have been possible without the assistance of numerous people and organizations.

I would like to express my special thanks and deepest gratitude to my supervisor Dr. Marek Michalak. For this great research opportunity, and most importantly, for his kind endless help, advices, supports, and inspirations.

I would like to thank current and previous members of the Michalak laboratory. Thank you for being wonderful colleagues, friends, and adventure companions.

I would like to thank my committee members, Dr. Larry Fliegel, Dr. Nicolas Touret for research guidance and collaborations over the years and thank for all the helps in thesis preparation. I thank Dr. Elaine Leslie and Dr. Lorrie Kirshenbaum for taking the time to serve on my PhD defense committee.

I am grateful to all our collaborators from laboratory of Dr. Peter Light, Dr. Wayne S.R. Chen, Dr. Joel Dacks, Dr. Björn C. Knollmann, Dr. Xing-Zhen Chen, and Dr. Luis B. Agellon. For all the incredible collaborations. I would like to thank Canada Foundation for Innovation, University Hospital Foundation, and Natural Sciences Engineering Research Council of Canada for funding supports.

Last but not least, to my dear family and friends, life is not so colorful without you all.

Table of Contents

Chapter 1: Literature review 1
1.1 Endoplasmic reticulum and sarcoplasmic reticulum in the heart 1
1.2 ER stress and Unfolded Protein Response 3
1.3 Unfolded protein response in heart disease 7
1.4 IRE1α, a multifunctional protein 7
1.4.1 IRE1α and structure of ER luminal domain 8
1.4.2 The ER/SR luminal modulators of IRE1α activity 10
1.5 Calsequestrin 12
1.5.1 Calsequestrin protein 12
1.5.2 Functions of calsequestrin 16
1.5.3 Cardiac calsequestrin and catecholaminergic polymorphic ventricular tachycardia 20
1.6 Objectives and hypothesis 25
1.7 References 26

Chapter 2: Identification of two pools of IRE1α in cardiac and skeletal muscle cells 39
2.1 Abstract 39
2.2 Introduction 39
2.3 Materials and Methods 41
2.3.1 Plasmids and site-specific mutagenesis 41
2.3.2 Adenovirus construction 41
2.3.3 Protein purification 41
2.3.4 Microscale thermophoresis 42
2.3.5 Surface plasmon resonance analysis 43
2.3.6 Immunoprecipitation 44
2.3.7 Skeletal muscle immunohistochemistry 44
2.3.8 Cardiomyocyte isolation and immunostaining 45
2.3.9 Mouse embryonic fibroblasts confocal 46
2.3.10 Subcellular fractionation 46
2.3.11 IRE1α cross-linking 47
2.3.12 Statistical analysis 48
2.4 Results 49
2.4.1 IRE1α is localized to the junctional SR and perinuclear space in skeletal muscle and cardiomyocytes 49
2.4.2 The luminal domain of IRE1α interacts with calsequestrin, an SR junctional protein 55
2.4.3 Mapping of calsequestrin binding to IRE1α 61
2.4.4 Calsequestrin prevents dimerization of IRE1α via interaction with the IRE1a luminal domain 65

2.5 Discussion 68
2.6 References 71

Chapter 3: Functional consequences of inositol-requiring enzyme -1α (IRE1α) deficiency in cardiomyocytes 77
3.1 Abstract 77
3.2 Introduction 77
3.3 Materials and Methods 79
3.3.1 Ethics statement and animals 79
3.3.2 Generation of transgenic mice 79
3.3.3 Echocardiography and electrocardiography 80
3.3.4 Trichrome staining and fibrosis analysis 80
3.3.5 Cardiomyocyte and cardiac fibroblast isolation 81
3.3.6 Calcium transient 82
3.3.7 Genomic DNA isolation and PCR 82
3.3.8 Real-time PCR 83
3.3.9 Immunostaining and confocal microscopy 84
3.3.10 Statistical analysis 84
3.4 Results 85
3.4.1 IRE1α reduction in conditional knockout mice 85
3.4.2 Cardiac-specific IRE1α deletion leads to severe dilated cardiomyopathy 89
3.4.3 IRE1α deficient hearts develop cardiac fibrosis 94
3.4.4 IRE1α deficient myocytes has reduced t-tubule and increased extracellular staining 95
3.4.5 IRE1α deletion cause dysfunction in Ca^{2+} handling 97
3.5 Discussion 99
3.6 References 101

Chapter 4: Phylogenetic and biochemical analysis of calsequestrin structure and association of its variants with cardiac disorders 107
4.1 Abstract 107
4.2 Introduction 107
4.3 Materials and Methods 109
4.3.1 Genome databases 109
4.3.2 Comparative genomics, phylogenetic and sequence alignments 109
4.3.3 Site-directed mutagenesis 110
4.3.4 Protein purification 111
4.3.5 CD Analysis 111
4.3.6 Microscale thermophoresis and thermal denaturation analyses 112
4.3.7 Native polyacrylamide gel electrophoresis 112
4.3.8 Limited proteolysis 113

4.3.9 Cross-linking 113
4.3.10 Statistical Analysis 114
4.4 Results 115
4.4.1 Emergence and specialization of calsequestrin within animals 115
4.4.2 Conservation of CPVT associated Casq2 mutants throughout animal kingdom 129
4.4.3 Ca^{2+} binding to Casq2 mutants 132
4.4.4 Conformational changes and protein folding of Casq2 mutants 135
4.4.5 Ca^{2+} dependent polymerization of Casq2 mutants 143
4.4.6 Casq2 binding to IRE1α, an ER/SR stress sensor 148
4.5 Discussion 151
4.6 References 158

Chapter 5: General conclusions 164
5.1 Reference 167

Bibliography 168

Appendix I: IRE1α and Casq2 knockout in mouse embryonic stem cells 198
Appendix II: The overexpression of Casq2 in non-muscle cells 200
Appendix III: Unfolded protein response in Casq2 deficient cardiomyocytes 203
Appendix IV: IRE1α and Calsequestrin co-localization using super-resolution imaging 204

List of Tables

Chapter 1

Table 1-1. Calsequestrin isoforms. 14

Table 1-2. Cardiac calsequestrin (CASQ2) mutations. 23

Chapter 3

Table 3-1. Echocardiography of control and IRE1α cmc KO mice after 3 weeks of tamoxifen administration. 92

Table 3-2. Electrocardigram of control and IRE1α cmc KO mice after 3 weeks of tamoxifen administration. 93

Chapter 4

Table 4-1. BLASTp (Basic Local Alignment Search Tool protein) searches of the genomes of 28 metazoan organisms by using *H. sapiens* CASQ1 (NP_001222.3) and CASQ2 (NP_001223.2) nucleoide sequences as queries. 116

Table 4-2. CD analysis of calsequestrin mutants 138

Table 4-3. Inflection temperature for Casq2 and Casq2 mutants 143

List of Figures and Illustrations

Chapter 1

Figure 1-1. Schematic view of SR and transverse tubules in cardiomyocytes. 2
Figure 1-2. The unfolded protein response (UPR) pathway. 5
Figure 1-3. Structure of IRE1α dimer. 9
Figure 1-4. The calsequestrin gene and the protein. 15
Figure 1-5. A model for calsequestrin-dependent regulation of the ryanodine receptor/Ca^{2+} channel (RyR). 19
Figure 1-6. Catecholaminergic polymorphic ventricular tachycardia related missense mutations in *CASQ2*. 22

Chapter 2

Figure 2-1. Immunolocalization of IRE1α in skeletal muscle. 50
Figure 2-2. Immunostaining of wild-type and IREα-deficient mouse embryonic fibroblasts. 51
Figure 2-3. Perinuclear ER-like membrane network in skeletal muscle. 52
Figure 2-4. IRE1α in isolated cardiomyocytes. 54
Figure 2-5. Calsequestrin (Casq1 and Casq2) binds to the ER luminal domain of IRE1α. 57
Figure 2-6. Calsquestrin binding to the IRE1α is independent of cysteine residues. 59
Figure 2-7. Calsequestrin-IRE1-NLD interaction in the presence of Ca^{2+}. 60
Figure 2-8. Ca^{2+} binding to cardiac muscle calsequestrin. 61
Figure 2-9. Mapping of cardiac muscle calsequestrin binding to IRE1α. 64
Figure 2-10. Schematic representation of the IRE1α dimerization assay. 65
Figure 2-11. Calsequestrin prevents IRE1α dimerization. 67
Figure 2-12. A schematic representation of two pools of IRE1α in muscle SR or ER. 69

Chapter 3

Figure 3-1. Generatingon of mice with IRE1α-deficient cardiomyocytes. 86
Figure 3-2. Body weight of IRE1α mice. 87
Figure 3-3. Real-time Q-PCR analysis of XBP1 mRNA splicing and abundance of mRNA encoding UPR markers. 88
Figure 3-4. Heart morphology and cardiac function of adult hearts with cardiomyocytes-specific IRE1α deletion. 91
Figure 3-5. Cardiomyocytes-specific IRE1α deletion in adult mice develops cardiac fibrosis. 94

Figure 3-6. T-tubule and extracellular matrixes in IRE1α cmc KO ventricle. 96
Figure 3-7. Ca^{2+} transient recordings in IRE1α cmc KO cardiomyocytes. 98

Chapter 4

Figure 4-1. Calsequestrin homologues in the vertebrate and invertebrate lineages. 124
Figure 4-2. Phyolgenetic tree of calsequestrin. 126
Figure 4-3. Short-branch phylogenetic tree of calsequestrin. 128
Figure 4-4. Amino acid sequence alignments and calsequestrin 3D structure. 131
Figure 4-5. Ca^{2+} binding to calsequestrin mutants. 134
Figure 4-6. CD analysis of Casq2 mutants. 137
Figure 4-7. Limited trypsin digestion of Casq2 mutants. 139
Figure 4-8. Thermal denaturation analysis of Casq2 and Casq2 mutants. 142
Figure 4-9. Ca^{2+}-dependent polymerization of Casq2 and Casq2 mutants. 145
Figure 4-10. Polymerization of Casq2 mutants. 147
Figure 4-11. Casq2 mutants binding to the ER luminal domain of IRE1α. 150
Figure 4-12. Abundance of Casq2 and Casq1 mRNA in selected tissues across species. 152
Figure 4-13. Summary of protein characteristics from disease related Casq2 mutants. 157

Chapter 5

Figure 5-1. Schematic representation of UPR component at the junctional SR. 164
Figure 5-2. Structure and functional impact of CPVT related cardiac calsequestrin mutations. 166

Appendix

Figure A-1. CRISPR/Cas9 knockout of the IREα or Casq2 gene in mouse embryonic stem cells. 198
Figure A-2. *IREα*$^{-/-}$ mouse embryonic stem cells lost RNase activity. 199
Figure A-3. IRE1α- and Casq2-deficient mouse embryonic stem cells able to differentiated into beating cardiomyocytes. 199
Figure B-1. Overexpression of Casq2 in HEK293 cell induces activation of IRE1α mediated UPR as monitored by XBP1 mRNA splicing. 200
Figure B- 2. Transient transfection to overexpress proteins can induce ER stress in HEK293 cells. 201
Figure B-3. HEK293 cell line stable expressing Casq2 has elevated IRE1α-mediated UPR activation. 202

Figure C-1. qPCR of mRNA isolated from wild-type and *Casq2*$^{-/-}$ cardiomyocytes. 203

Figure D-1. Skeletal muscle tissue immunostaining imaged with Nikon structured illumination microscopy (SIM, N-SIM S system).....204

List of Abbreviations

ASK1: apoptosis signal-regulating kinase 1
ATF6: Activating transcription factor 6
BiP: Binding-immunoglobulin protein aka GRP-78
Casq1: Skeletal muscle isoform of calsequestrin
Casq2: Cardiac muscle isoform of calsequestrin
Cav1.2: Voltage-gated L-type Ca^{2+} channel
CD: Circular dichroism
CHOP: Transcriptional factor C/EBP homologous protein
Cox2: Cyclooxygenase-2
CPVT: Catecholaminergic polymorphic ventricular tachycardia
DAPI: 4',6-diamidino-2-phenylindole
DHPR: Dihydropyridine receptor/Ca^{2+} channel
EC: Excitation-contraction coupling
ECG: Electrocardiogram
Echo: Echocardiography
EGTA: Ethylene glycol-bis (β-aminoethyl ether
Eif2α: Eukaryotic translation initiation factor 2α
ER: Endoplasmic reticulum
ERAD: ER-associated degradation
Ern1: Name of the gene encoding IRE1α
FITC: Fluorescein isothiocyanate
GADD34: Growth arrest and DNA damage-inducible 34
GRP94: Glucose-regulated protein 94
HEPES: 4-(2-hydroxyethyl)-1-piperazineethanesulfonic acid
Hsp47: Heat shock protein 47
IRE1-NLD: N-terminus domain of IRE1α
IRE1α: Serine/threonine-protein kinase/endoribonuclease; Inositol-requiring enzyme -1α
JNK: cJun-N-terminal kinase
MST: Microscale thermophoresis
NCX: Na^{+}/Ca^{2+} exchanger
Obsc: Obscurin
ORAI1: Ca^{2+} release-activated Ca^{2+} channel protein 1
PAGE: Polyacrylamide gel electrophoresis
PDI: Protein disulfide-isomerase
PDIA6: Protein disulfide isomerase A6
PERK: ER kinase dsRNA-activated protein kinase-like ER kinase
RIDD: Regulated IRE1-dependent decay
RYR1: Skeletal muscle isoform of Ca^{2+} release channel/ryanodine receptor
RYR2: Cardiac muscle isoform of Ca^{2+} release channel/ryanodine receptor
S1P: Site-1 protease
S2P: Site-2 protease
SDS: Sodium dodecyl sulfate
SERCA: Sarcoplasmic/endoplasmic reticulum Ca^{2+}-ATPase
SOCE: Store-operated Ca^{2+} entry
SR: Sarcoplasmic reticulum

STIM1: Stromal Interaction Molecule 1
TRAF2: TNFR-associated factor 2
T-tubule: Transverse tubules
UPR: Unfolded protein response
XBP1: X-box binding protein 1
XBP1s: Spliced X-box binding protein 1
αMHC: Alpha-myosin heavy chain

Chapter 1: Literature review

1.1 Endoplasmic reticulum and sarcoplasmic reticulum in the heart

The endoplasmic reticulum (ER) is a large, dynamic membrane system that orchestrates many vital roles in the cell including Ca^{2+} storage, protein synthesis, folding and post-translational modification, phospholipid and steroid synthesis, and stress responses[1-5]. The diverse functions of the ER are performed by distinct domains consisting of bilayer membranes formed tubules, sheets, and the nuclear envelope[2]. ER continuously communicates with other cellular organelles including Golgi apparatus, nucleus, and mitochondria; mediates lipid synthesis and transfer, Ca^{2+} transfer, inflammatory signaling, and transcriptional regulation[6, 7]. ER also forms close contacts with plasma membrane that are involved in Ca^{2+} signaling[8]. Therefore, ER is a multifunctional organelle that coordinates energy metabolism, stress signals sensing and integration, and cell fate decisions to name a few.

In cardiac muscle a highly specialized and unique ER called sarcoplasmic reticulum (SR), is dedicated to the regulation of Ca^{2+} homeostasis and excitation-contraction (E-C) coupling for activation of myofilament contraction[9, 10]. In muscle, the SR has two well defined structure and functional membrane networks: longitudinal SR and junctional SR (Figure 1-1)[11, 12]. The longitudinal SR consist of extended tubular membrane network around myofibrils and the mitochondria and it is enriched in Ca^{2+}- ATPase (SERCA) responsible for Ca^{2+} uptake to initiate muscle relaxation[12, 81, 82]. The junctional SR is the membrane of extended sacs from the longitudinal SR and faces the T tubule[11, 12]. The junctional SR contains calsequestrin responsible for Ca^{2+} storage and ryanodine receptor/Ca^{2+} channels (RyR) responsible for Ca^{2+} release to trigger muscle contraction[11, 13](Figure 1-1). Upon depolarization, voltage-gated L-type Ca^{2+} channels (Cav1.2), located primarily in the transverse T-tubular membrane, opens to increase local cytosolic Ca^{2+} concentration that triggers SR Ca^{2+} release from *via* RyR2, Ca^{2+} release from few RyR2 promotes Ca^{2+} release of neighboring RyR2 channels to amplify Ca^{2+} signals (Figure 1-1). This process is termed Ca^{2+} induced Ca^{2+} release. Released Ca^{2+} binds to troponin complex, activates contractile apparatus and initiate heart muscle contractions. Muscle relaxation cytosolic Ca^{2+} is taken up by SR *via* SERCA2a and removed to extracellular space via the Na^{+}/Ca^{2+} exchanger (NCX) to trigger muscle relaxation. This process is referred to cardiac E-C coupling, where

electrical excitation of the myocyte (action potential) generates a mechanical contractile response[14].

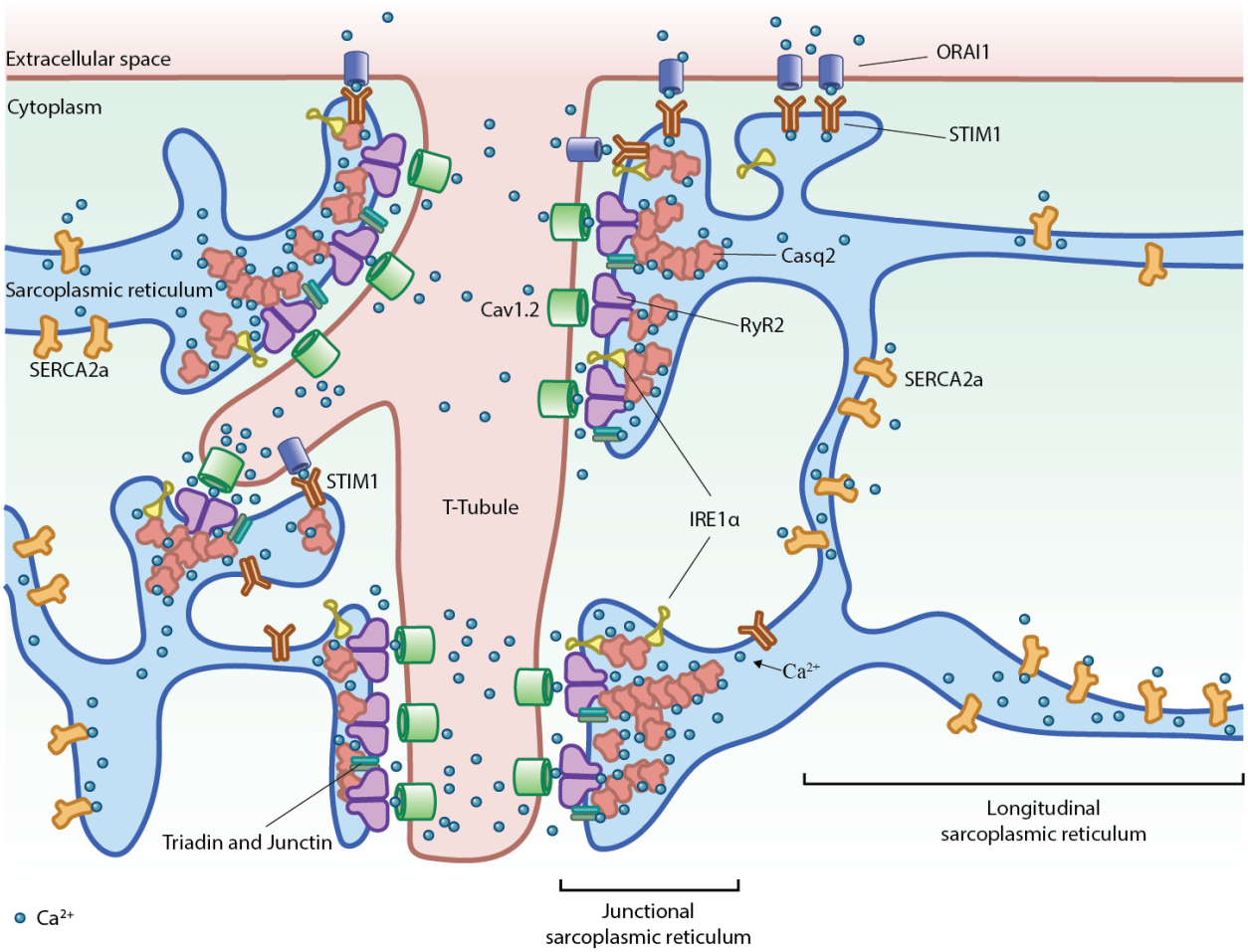

Figure 1-1. Schematic view of SR and transverse tubules in cardiomyocytes.

The longitudinal SR is occupied by high concentrations of Ca^{2+}-ATPase (SERCA). At the junctional SR, the ryanodine receptor/Ca^{2+} release channel (RyR2) faces the transverse tubules, while in the lumen of the junctional SR RyR2 interacts with calsequestrin. Two membrane-spanning junctional SR proteins, triadin and junctin, form complexes with calsequestrin and RyR2 to regulate RyR2 Ca^{2+} channel activity. In the junctional SR, calsequestrin also interacts with the UPR stress sensor IRE1α and luminal Ca^{2+} sensor STIM1. *Casq2*, cardiac calsequestrin; *Cav 1.2*, voltage-gated L-type Ca^{2+} channels; *IRE1α*, Inositol-requiring enzyme 1α; *STIM1*, stroma interaction molecule 1; *ORAI1*, Ca^{2+} release-activated Ca^{2+} channel protein 1.

Cardiomyocytes also contain functionally independent ER to carry out vital cell processes[9, 15, 16]. ER forms contiguous membrane system with SR, Golgi apparatus, and nuclear envelope[17]. Ultrastructure analysis of cardiomyocytes reveals 48% of rough ER appears in the interfibrillar and perinuclear sarcoplasm[18]. ER resident and integral membrane proteins including calreticulin, calnexin, immunoglobulin binding protein (BiP), protein disulfide-isomerase (PDI), and ribophorin II are all localized at perinuclear area, and along the I band areas whereas calsequestrin is localized at the junctional SR in the muscle cells[15, 19-22]. These ER proteins play critical roles in cardiomyocytes supporting Ca^{2+} and redox homeostasis, cardiogenesis, cardiac contractility and other functions that are essential for cardiomyocyte cell survival[23-25].

1.2 ER stress and Unfolded Protein Response

Disruption of ER homeostasis create a cellular state referred to as ER stress. Many cellular disturbances can cause ER stress including nutrient deprivation, Ca^{2+} depletion, hypoxia, metabolic disturbances, mechanical pressure, and protein aggregation. These features are often observed in ischemic, hypertrophic, and failing hearts[26-28]. Cells have developed a sophisticated surveillance system to sense and respond to ER stress with the goal of restoring ER homeostasis and ensuring cell survival. This process involves activation of complex cytoplasmic and nuclear signaling pathways collectively called unfolded protein response (UPR) (Figure 1-2). There are three ER transmembrane proteins functioning as ER stress sensors and signal transducers, including the ER kinase dsRNA-activated protein kinase-like ER kinase (PERK), activating transcription factor 6 (ATF6), and inositol-requiring enzyme 1 (IRE1). Activation of these three signaling arms of UPR trigger distinct cellular events to re-establish protein homeostasis in the ER, these include (i) translational attenuation to stop entry of new proteins to the ER, (ii) transcriptional activation of genes encoding proteins involved in protein folding (chaperones and folding enzymes) to assist protein folding and maturation, (iii) transcriptional activation of genes responsible for ER-associated degradation (ERAD) to degrade misfolded protein. However, when ER stress is prolonged and ER protein load greatly exceeds its fold capacity, continued activation of UPR will lead to (iv) apoptosis and cell death. Among the UPR signaling pathways, IRE1α is the key component that functions as master regulator in cell fate determination under ER stress[27, 28]

IRE1α, the widely expressed IRE1 paralog of the most conserved UPR signaling branch, is a type I transmembrane protein containing a serine/threonine kinase and an endoribonuclease (RNase) domain on its cytosolic face. In response to ER stress, the luminal domain of IRE1α dimerizes/oligomerizes, initiates trans-autophosphorylation of its cytosolic domain inducing a conformational change that lead to activation of IRE1α RNase activity located in the cytoplasmic domain[29, 30]. RNase activity of IRE1α catalyzes excision of 26 nucleotides within mRNA encoding the X-box binding protein 1 (XBP1). This unconventional splicing event causes frameshift allows to generate a longer, stable, and activated transcription factor known as spliced XBP1 (XBP1s)[31, 32]. XBP1s binds to a specific promoter element, known as the ER stress element and unfolded protein response element, turns on expression of genes encoding proteins that modulate protein folding, secretion, ERAD, protein translocation into the ER, and lipid synthesis[32, 33]. The RNase domain of IRE1α can cleave multiple mRNA targets with consensus sequences and secondary structure that are similar to the XBP1 mRNA, via process known as regulated IRE1-dependent decay (RIDD)[34]. Although the significance of RIDD activity is not fully understood, the function appears to play a role in adaptive response as well as inducer of apoptosis during prolonged ER stress[34-36]. In addition, IRE1α can interact and activate tumor necrosis factor (TRAF2) and apoptosis signal regulated kinase (ASK1) to initiate apoptosis[37].

Similar to IRE1α, PERK and ATF6 function as distinct ER stress sensors (Figure 1-2). They both are ER transmembrane proteins that contain an ER luminal stress sensing domain and cytoplasmic enzymatic domain. Upon ER stress, PERK phosphorylates the eukaryotic translation initiation factor 2α (eIF2α) to inhibit protein translation[38-40]. There is also a selective translation of mRNAs encoding ATF4 transcription factor that targets the UPR genes. ATF4 induces expression of CHOP/GADD153(transcriptional factor C/EBP homologous protein) and GADD34 (growth arrest and DNA damage-inducible 34), which activate ER stress-mediated apoptosis[41]. ER stress triggers relocation of ATF6 from ER to the Golgi, where its transcription factor domain cleaved by S1P and S2P proteases and released to nucleus for UPR regulation[33, 42, 43].

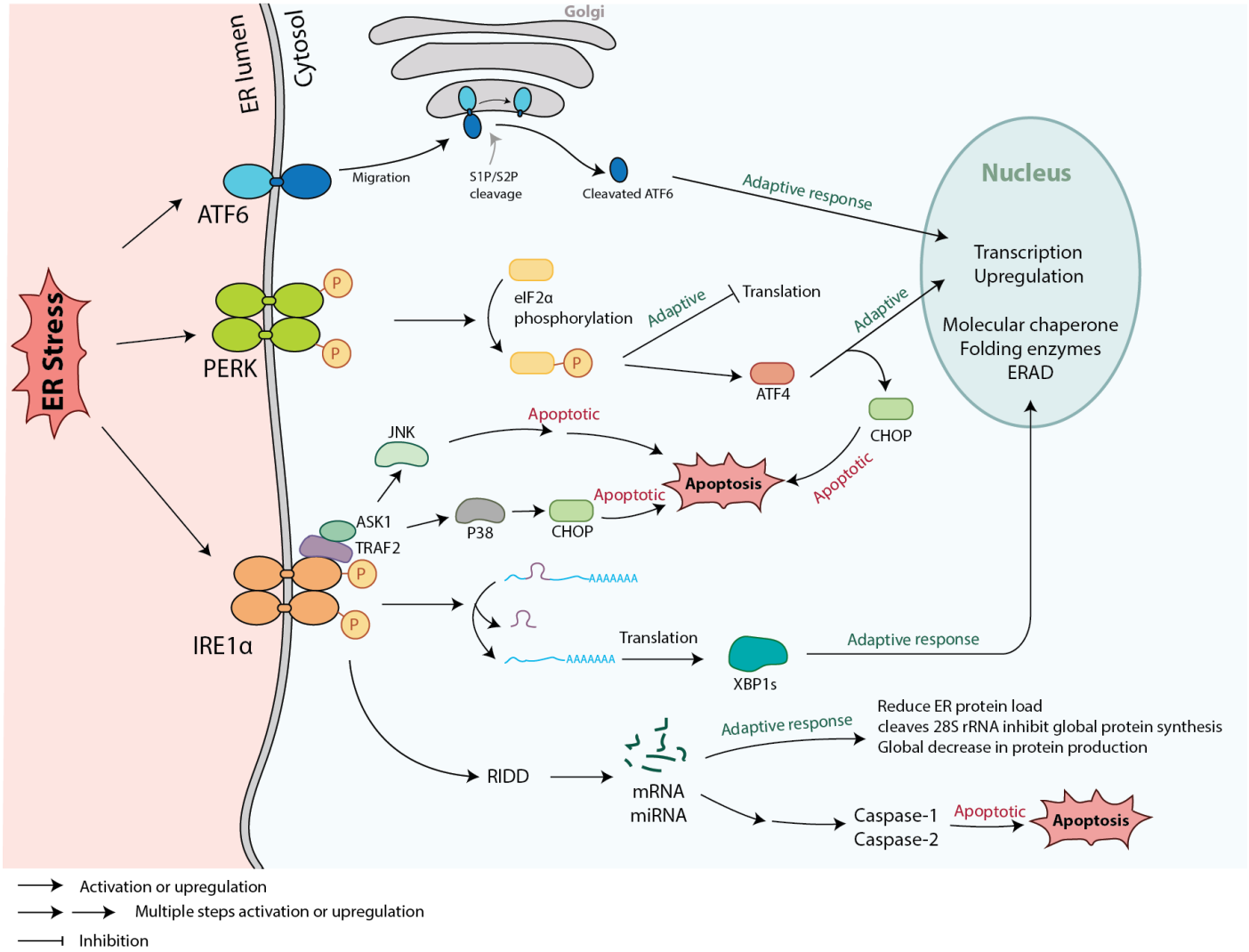

Figure 1-2. The unfolded protein response (UPR) pathway.

ER stress induces activation of three sensors located at the ER membrane: activating transcription factor 6 (ATF6), the ER kinase dsRNA-activated protein kinase-like ER kinase (PERK), and inositol-requiring 1 alpha (IRE1α). Figure adapted from [28].

ATF6: Under stressed conditions, ATF6 translocated to Golgi complex, and undergoes specific cleavage by site-1 and site-2 proteases (S1P and S2P). Cleavage of ATF6 produces a 50 kDa soluble basic leucine zipper transcription factor (cleaved ATF6), which moves to nucleus and binds to ER stress response elements (ERSE-1 and –II) or to ATF/cyclic AMP (cAMP) response element to induce transcriptional activation of ER stress response gene.

PERK: ER stress triggers dimerization and autophosphorylation of PERK, followed by targeted phosphorylation of the translation initiation factor eIF2α (eukaryotic translation initiation factor 2α), preventing initiation of translation to reduce ER protein load. But allows translation of few specific mRNAs, such as transcription factor ATF4 (activating transcription factor 4). ATF4 induction leads to expression of pro-apoptotic transcription factor CHOP (C/EBP-homologous protein).

IRE1α: IRE1α is the master regulator that is capable of cell fate determination under ER stress. Upon dimerization and autophosphorylation, IRE1α splices XBP1 mRNA (removes 26-nucleotide 3' intron) causes a frameshift allows translation of stable, and active transcriptional factor named spliced XBP1 (XBP1s). XBP1 binds to the specific promoter elements, ERSE and UPR element (UPRE), and triggers transactivation of downstream ER stress-responsive genes, including those involved in protein-folding and degradation machinery, all aimed at restoring ER homeostasis. IRE1α can also recruit TRAF2 and apoptosis signal-regulating kinase 1 (ASK1), leading to downstream activation of c-Jun NH_2-terminal kinase (JNK) and p38 MAPK. Activated JNK translocate to mitochondrial membrane, promotes activation of Bim (Bcl2-like protein 11, pro-apoptotic Bcl-2 members) and inhibition of Bcl-2 (B-cell CLL/lymphoma 2, apoptosis-suppressing oncoprotein). p38 MAPK phosphorylates and activates CHOP. CHOP induces transcriptional activation of genes that contribute to cell death.

The RNase domain of IRE1α also cleaves hundreds of ER-localized and cytosolic mRNA, ribosomal RNA, and microRNAs, a process known as regulated IRE1-dependent decay (RIDD). However, the biological significant of these targets are not fully understood. RIDD targeted RNA have been suggested to preserve ER homeostasis or induce cell death. RIDD can reduce ER protein load through mRNA degradation and global inhibition of protein synthesis by cleavage of 28S rRNA. Under chronic ER stress, IRE1α induce activation or upregulation of many pro-inflammatory and pro-apoptotic proteins. Reduces levels of select microRNAs (miRNAs), for example miRNAs that normally repress pro-apoptotic targets, results in activation of downstream caspase-1 and/or caspase-2-dependent pro-death pathways, leading to sterile inflammation and pyroptotic cell death.

1.3 Unfolded protein response in heart disease

ER stress and UPR plays an important role in cardiac health and pathology. In failing hearts, ER stress can be induced by enhanced protein synthesis, hypoxia, mechanical stress, nutrient starvation, and change in lipid metabolism. Activation of UPR has been observed in many cardiovascular diseases including myocardial infarction, oxygen starvation, ischemia/reperfusion injuries, hypertension/pressure overload, myocardium remodeling (hypertrophy and dilation), and heart failure [44-48]. However, the role of ER stress signaling in these disease conditions remains unclear.

ATF6 mediated UPR activation appear to be cardioprotective. Silencing ATF6 *via* knockdown or knockout in adult cardiomyocytes results in increased damage and decreased cardiac function upon ischemic/reperfusion injury[49]. Furthermore, transgenic mice expressing constitutively active N-terminal fragment of ATF6 in cardiomyocytes exhibit a better functional recovery from *ex vivo* ischemic/reperfusion with significantly reduced necrosis and apoptosis [49,50].

Activation of IRE1α and PERK in heart disease is cardioprotective but can also activate cell death signaling pathways and contribute to cardiomyocyte apoptosis and heart failure. PERK-deficient hearts show severe cardiomyopathy in response to pressure overload-induced heart failure, suggestive of a cardioprotective role of PERK[51]. However, inhibition of CHOP, a molecule downstream of PERK, can reduce cardiomyocyte apoptosis induced by aortic coarctation or proteasome inhibition[52, 53]. Overexpressing IRE1α in cardiomyocytes can protect the heart against pressure overload-induced heart failure[54]. XBP1 silencing leads to increased injury from ischemia/reperfusion, and overexpressing XBP1s, a spliced form of XBP1, protects hearts from ischemia/reperfusion injury[55]. On the other hand, inhibition of the apoptosis signal-regulating kinase 1 (ASK1) in IRE1α mediated apoptosis pathway reduces cardiomyocyte apoptosis after transverse aortic constriction[56].

1.4 IRE1α, a multifunctional protein

IRE1α is the most ancient ER stress sensor, conserved from yeast to mammals[57]. It is an administrator/executor of cell fate determination under ER stress conditions as discussed above. IRE1α is able to initiate adaptive responses to enhance cell survival in response to ER stress but also able to trigger apoptosis signaling to induce cell death when ER stress is not resolved. Among

the three UPR signaling branches, IRE1α is the major trigger in ER stress-induced apoptosis, whereas PERK and ATF6 are dispensable in activation of apoptosis during prolonged ER stress[36].

Recent studies have shown diverse roles of IRE1α beyond unfolded protein response. IRE1-dependent decay (RIDD) degrades RNAs, including mRNA encoding ER and cytosolic localized proteins, ribosomal RNA, and microRNAs, involved in many cellular functions such as energy metabolism, inflammation, and apoptosis[34]. Activation of RIDD can preserve ER homeostasis or induce cell death, although the mechanisms controlling the switch between cytoprotective to cytotoxic RIDD remains to be establish[34]. Sulfonation of IRE1α inhibits its signaling and activates p38/Nrf2 antioxidant responses under oxidative stress conditions[58]. Moreover, IRE1α interacts with an ER associated inositol-1,4,5-trisphosphate receptor/Ca^{2+} channels ($InsP_3R$), affects $InsP_3R$ intracellular distribution and Ca^{2+} channel activity both important for formation of functional ER-mitochondria contacts and for transport of Ca^{2+} from the ER to the mitochondria, respectively[59].

1.4.1 IRE1α and structure of ER luminal domain

In mammals, there are two homologs of IRE1, IRE1α and IRE1β. IRE1α is the more predominant isoform ubiquitously expressed. IRE1α-deficiency in mice is embryonic lethal[60]. IRE1β is restrictively expressed in the gut and IRE1β knockout mice are viable[61, 62] Both IRE1 homologs are transmembrane proteins with kinase/nuclease activities triggered by oligomerization of IRE1 in response to ER stress[61, 63].

IRE1α contains an N-terminal ER luminal domain responsible for stress sensing and C-terminal kinase and endoribonuclease domain in the cytosol involved in splicing of XBP1 mRNA and RIDD activities. A monomer of the luminal domain of IRE1α is composed of unique protein fold of a triangular shaped β-sheet clusters, which provide a dimerization interface stabilized by hydrogen bonds and hydrophobic interactions[30] (Figure 1-3). Dimerization of IRE1α luminal domain initiates auto-phosphorylation of IRE1 cytosolic domain leading to activation of IRE1 RNase activity[30, 64] Moreover, dimerization of IRE1α creates a shared central groove that resembles a major histocompatibility complex-like fold allowing for peptide binding. This suggests that IRE1α is able to interact with peptides and misfolded peptides primarily composed of basic and hydrophobic residues that mimic misfolded proteins in ER[30, 65]. Mutation of amino acid residues within the groove prevents interaction with peptides *in vitro*[65] and leads to impaired IRE1α signaling in yeast[65, 66].

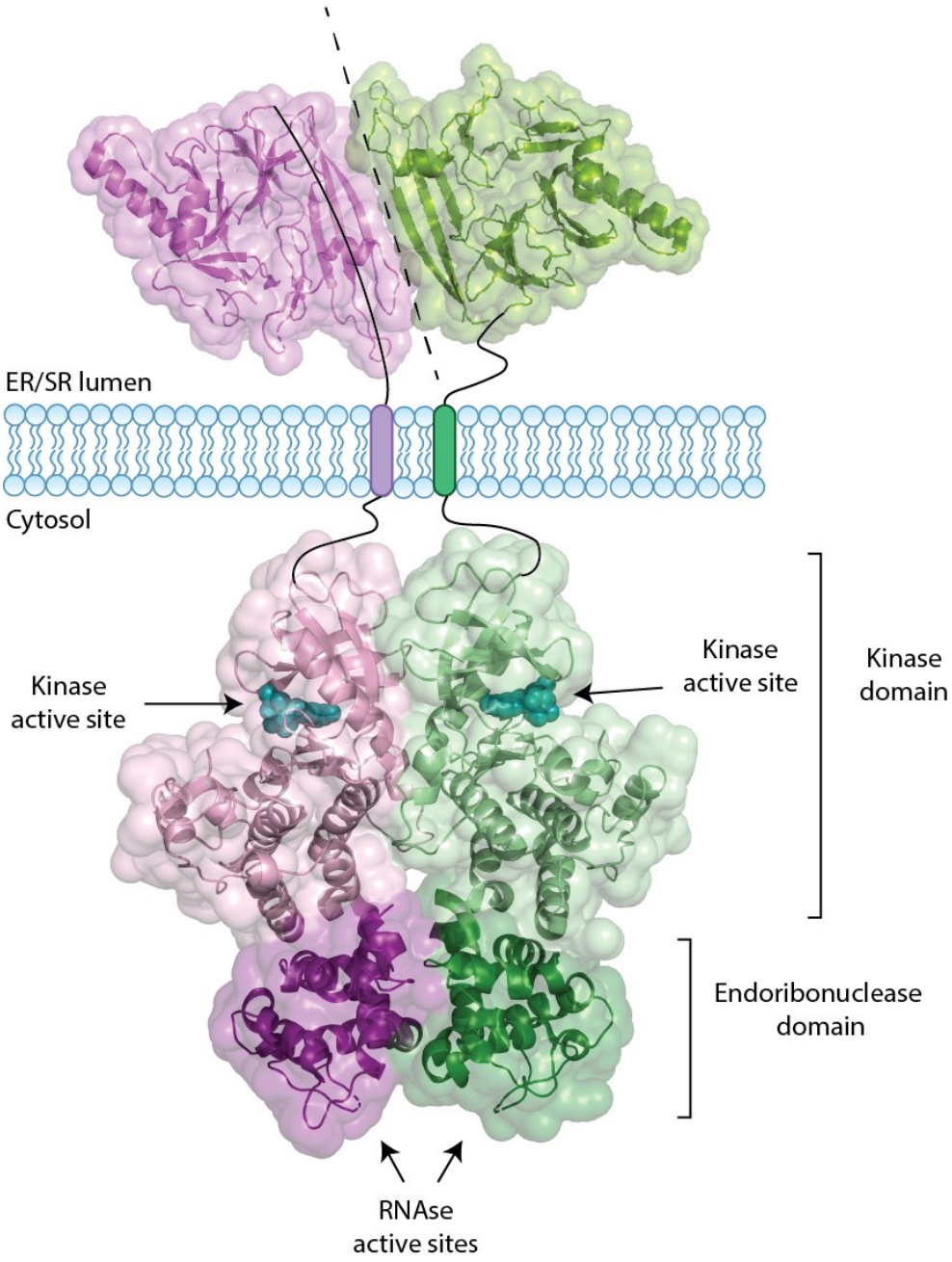

Figure 1-3. Structure of IRE1α dimer.

IRE1α is a type I transmembrane protein that consists of N-terminus domain facing ER/SR lumen, a single transmembrane domain, and cytosolic domain with kinase and endoribonuclease activity. The figure shows two monomers of IRE1α, in purple and green, with solvent accessible surfaces. The luminal domain of IRE1α (PDB: 2HZ6) forms stable dimer by hydrogen bonds and hydrophobic interactions; the dimer interface is marked by the dashed line. The cytosolic domain of IRE1α (PDB: 2RIO) contains kinase domain in light purple/green and endoribonuclease (RNase) shown in dark purple/green. The location of the kinase and RNase active site is indicated by the arrows. ADP molecules bound to the kinase active sites are shown in cyan.

1.4.2 The ER/SR luminal modulators of IRE1α activity

Several ER/SR resident proteins have been identified binding to the ER luminal domain of IRE1α and to modulate IRE1 stress sensing and ER stress response activity. These include BiP (immunoglobulin binding protein also known as GRP78), PDIA6 (protein disulfide isomerase A6), Hsp47 (heat shock protein 47), Cox2 (cyclooxygenase 2), and junctional SR protein calsequestrin.

BiP, one of the most abundant ER localized chaperones, was the first identified modulator of the IRE1α luminal domain[67, 68] BiP interacts with ER luminal domain of IRE1α and prevents its dimerization and UPR signaling. Dissociation of BiP from IRE1α triggers activation of IRE1α to mediate UPR responses[67-69]. BiP dissociation from IRE1α may be mediated by direct interaction of between BiP and misfolded proteins to sequester BiP away from IRE1α[70, 71]. BiP also binds to the luminal domain of PERK and ATF6 under resting conditions, and dissociates from PERK and ATF6 under ER stress[67, 72]. These observations indicate that BiP is a common negative regulator of UPR by binding to the luminal regions of ER stress sensors (IRE1α, PERK and ATF6) to maintain them in an inactive state.

PDIA6 is an ER luminal oxidoreductase that catalyzes protein disulfide bond formation, assists with protein folding, and maintains redox homeostasis in the ER[73]. PDIA6 interacts with ER luminal domain of IRE1α and enhances IRE1α activity upon ER stress[74]. PDIA6 effects three UPR sensors differently, silencing PDIA6 does not affect PERK pathway but suppress IRE1α activity and increases ATF6 activity in response to ER stress induced by ER Ca^{2+} store depletion[74]. Interestingly, in ischemia/reperfusion injury, ATF6 protects cardiomyocytes by inducing expression of PDIA6[75].

Hsp47 is an ER localized foldase that belongs to the family of heat shock proteins and functions as a specific carrier for different types of collagen. It assists the transport of triple-helix procollagen from ER lumen to the cis-Golgi[76, 77]. Upon ER stress, Hsp47 associates with the ER luminal domain of IRE1α, reduces binding of BiP to the IRE1α, promotes IRE1α dimerization/oligomerization and activates IRE1α-mediated UPR[78]. Importantly, Hsp47 enhances UPR upon ER stress specifically via IRE1α signaling branch. Overexpression or knockdown of Hsp47 does not alter PERK and ATF6-mediated UPR signaling[78].

Cox2, an inducible cyclooxygenase that drives inflammation, interacts with ER luminal domain of IRE1α and enhance its XBP1 splicing. Cyclosporine, a small polypeptide widely used

as an immunosuppressant in organ transplantation and treatment of autoimmune diseases, triggers activation of IRE1α through binding to Cox2, which forms complex with IRE1α[79]. Cox2-dependent activation of IRE1α is via mechanism different from that described for ER stress induced by Ca^{2+} store depletion. Cyclosporine associates to Cox2 resulting in enhanced Cox2 enzymatic activity that is required for IRE1α activation. This provide a novel mechanisms for cyclosporine-induced IRE1α signaling[79].

Calsequestrin is one of the most abundant SR proteins exclusively localized to the junctional SR in cardiac and skeletal muscle. This Ca^{2+} binding protein functions as Ca^{2+} storage and buffer to support muscle contraction. I discovered a novel interaction between ER luminal domain of IRE1α and calsequestrin[80]. Association between calsequestrin and IRE1α prevents IRE1α dimerization/oligomerization – an initiation step for its activation[80]. These findings indicate that calsequestrin is a muscle specific modulator of IRE1α (Chapter 2).

While the ER luminal domain of IRE1α is important in stress sensing, IRE1α activation is tightly controlled by interacting with number of proteins with its cytosolic domain. A comprehensive list of IRE1α cytosolic domain interacting proteins have been reviewed previously[81]. Many of these interacting proteins involved in apoptosis, supporting fine-tuning of IRE1α mediated apoptosis activation. IRE1α cytosolic domain interacting proteins can enhance or inhibit IRE1α RNase activity, or act as a scaffold and recruit other proteins to activate apoptosis signaling[81, 82]. For example, the cytosolic domain of oligomerized IRE1α binds to the adapter protein TNFR-associated factor 2 (TRAF2), triggering the activation of apoptosis signal-regulating kinase 1 (ASK1) and cJun-N-terminal kinase (JNK) pathway[83, 84] (Figure 1-2).

In conclusion, regulation of ER luminal and cytoplasmic domains of IRE1α involve a complex regulatory network. Multiple modulators may provide multiple level of regulation to fine-tuning IRE1α stress sensing. Tissue-specific regulation of IRE1α maybe mediated by distinct regulatory protein complexes. However, exact integration of these modulators with complex ER stress-sensing mechanism and/or contribution to UPR-independent IRE1α functions is yet to be determined.

1.5 Calsequestrin

Calsequestrin is the major Ca^{2+} binding protein in the SR where it serves as the main Ca^{2+} storage and buffering protein and is an important regulator of Ca^{2+} release channels in both skeletal and cardiac muscles. Calsequestrin is anchored at the junctional SR membrane through interactions with membrane proteins and undergoes reversible polymerization with increasing Ca^{2+} concentration. The protein provides high local Ca^{2+} concentration at the junctional SR and communicates changes in luminal Ca^{2+} concentration to Ca^{2+} release channels, thus it is an essential component of E-C coupling. In this section, I focus on calsequestrin structure, function, and its role in cardiac arrhythmia – catecholaminergic polymorphic ventricular tachycardia (CPVT).

1.5.1 Calsequestrin protein

Calsequestrin was first isolated from skeletal muscle by MacLennan and Wang in 1971 as the most abundant Ca^{2+} binding protein in the SR[85-88]. The protein is localized exclusively in the lumen of junctional SR, where it interacts with other junctional SR membrane proteins and forms highly abundant, polymerized branches[89-91]. Calsequestrin binds up to ~40 mol of Ca^{2+} per mol of protein with relatively low affinity[85, 86, 92-94] (Table 1-1). This allows high local Ca^{2+} storage at the junctional SR membrane to support fast Ca^{2+} release to trigger muscle contraction[85, 86]. Moreover, calsequestrin undergo reversible conformational change and polymerization upon Ca^{2+} binding (≥1mM) creating additional Ca^{2+} binding pockets for increased Ca^{2+} binding capacity[94-96]. Ca^{2+}-induced polymerization of calsequestrin plays an important role in regulation of RyR/Ca^{2+} release channel[97, 98].

There are two isoforms of calsequestrin encoded by two different genes, namely *casq1* and *casq2* (Figure 1-4)[99, 100]. In mammals, Casq1 (skeletal muscle calsequestrin) is exclusively expressed in skeletal muscle, and Casq2 (cardiac calsequestrin) is mainly expressed in the heart[101-104]. Both isoforms of calsequestrin bind to Ca^{2+} with high capacity but low affinity (Table 1-1). When the total Ca^{2+} concentration increases, Ca^{2+} binding capacity of human Casq1 and Casq2 increases non-linearly and plateaus at about 12 mM Ca^{2+} concentration[92, 93, 105, 106]. The aspartic acid rich C-tail domain of calsequestrin is the major Ca^{2+} binding site on the calsequestrin monomer, with deletion of the C-tail domain from Casq1 or Casq2 resulting in over 50% reduction in Ca^{2+} binding capacity[92, 106, 107]. In skeletal muscle, considering that calsequestrin (Casq1)

concentration in the rat extensor digitorum longus muscle at 36 ± 2 μmol per 1 fiber volume[101] and binding capacity of the protein at 40 to 80 mol Ca^{2+} per mol of protein (Table 1-1), Casq1 would store up 80% of the SR Ca^{2+}. Mammalian Casq1 and Casq2 are glycosylated, phosphorylated[105, 108-111], and ubiquitinated [112, 113]. Moreover, acetylated peptides from Casq2 were detected using anti-lysine antibodies followed by mass spectrometry[112].

Table 1-1. Calsequestrin isoforms.

	Casq1	Casq2
Gene and chromosomal location	CASQ1, chromosome 1q21 [99]	CASQ2, chromosome 1p23 [100]
Number of amino acid residues (human)	396 amino acids	399 amino acids
Molecular mass (human)	45.2 kDa	46.4 kDa
Isoelectric point (human)	4.03	4.22
Tissue expression	Fast-twitch skeletal muscle and <20% in slow-twitch skeletal muscle [101-104]	Heart and Slow-twitch skeletal muscle [101-103]
Ca^{2+} binding capacity (nmol Ca^{2+}/nmol Casq)	~80 Ca^{2+} [92], 70-80 [93], 40 [94], 43 [86], 41 [85]	~60 Ca^{2+} [92], 12-13 [114], 20 [94]
Ca^{2+} binding affinity (K_d)	1 mM [115],0.04 mM [86], 0.25 mM [116]	0.872 mM[117], 2.15 mM [118]
Polymerization state at 1 mM luminal Ca^{2+}	Mostly in a polymer form[91]	Mostly monomer and a dimer [119]
Regulation of RyR at 1 mM luminal Ca^{2+}	Inhibits RyR1, requires present of junctin alone or junctin and triadin [97, 119]; activates RyR2 [120]	Activates RyR1 and RyR2, requires triadin and/or junctin [119-121]
Post-translational modification (in mammalian)	Rabbit Casq1 is glycosylated ($GlcNAc_2Man_1$), enhance Ca^{2+}-dependent polymerization [111, 122] Rabbit Casq1 is phosphorylated to enhance Ca^{2+} binding capacity, but it does not affect RyR1 function, nor its interaction with junctin and triadin [97, 105, 108] Ubiquitinated [112]	Glycosylated ($GlcNAc_2Man_6$) and phosphorylated at C-tail domain [108-110, 122, 123] Acetylated (Lys180) [112], and ubiquitinated [113]

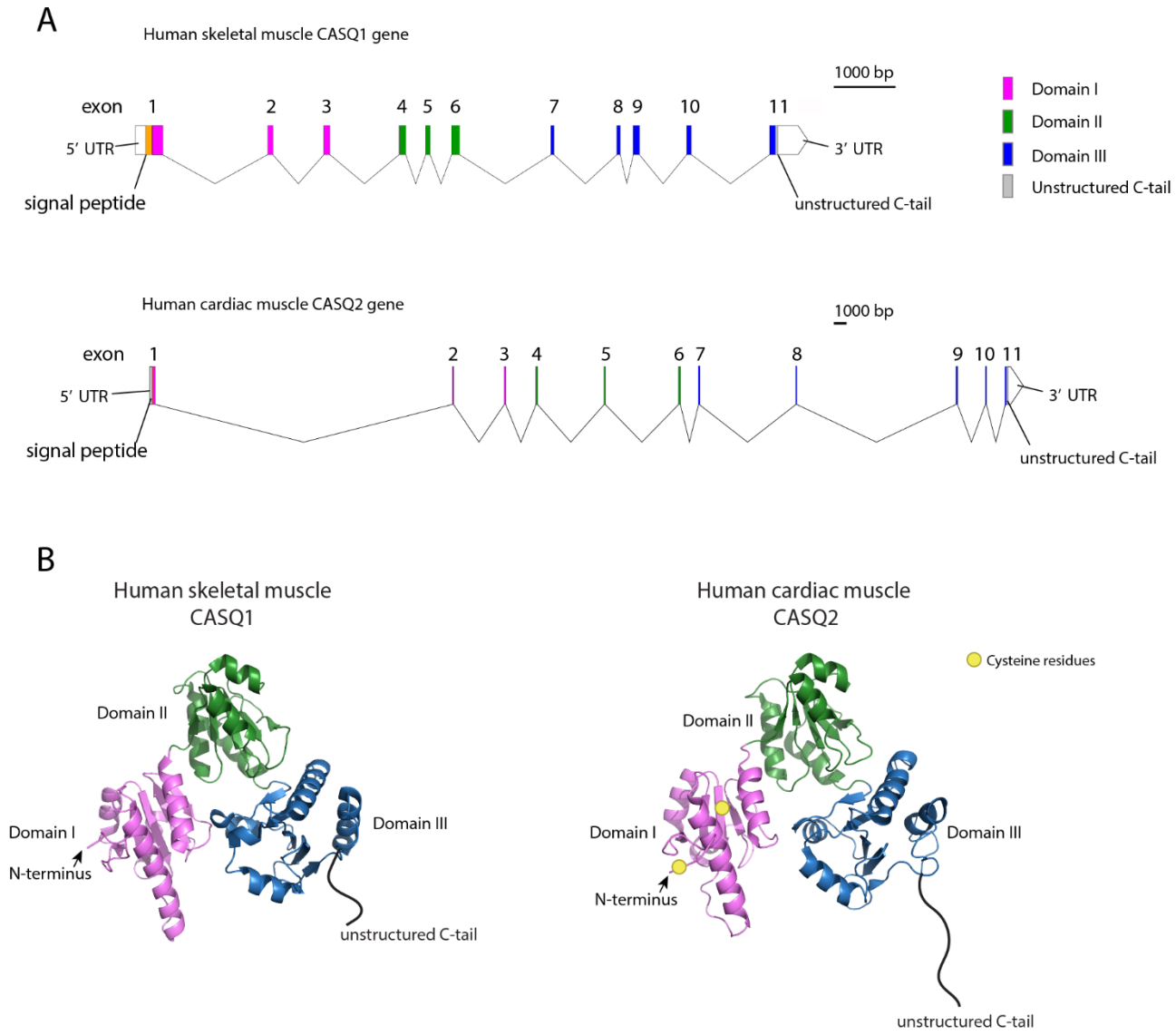

Figure 1-4. The calsequestrin gene and the protein.

A) The human skeletal muscle calsequestrin *CASQ1* gene (top, gene ID: 844), and the human cardiac calsequestrin *CASQ2* gene (bottom, gene ID: 845). The *CASQ2* gene has longer intron sequences but a similar overall genomic organization when compared to the *CASQ1* gene.

B) X-ray crystal structure of CASQ1 (left, PBD: 5CRD), and CASQ2 (right, PDB: 2VAF). Both isoforms share high primary amino acid sequence identity and structural similarity. The highly conserved cysteine residues found only in CASQ2 are indicated as yellow dots. *UTR*, untranslated region; *bp*, base pair.

1.5.2 Functions of calsequestrin

1.5.2.1 Ca^{2+} storage and buffering in the junctional SR

The major function of calsequestrin is Ca^{2+} storage and buffering at junctional SR (Table 1-1 and Figure 1-1)[86, 88]. In working muscle, about 75% of the releasable Ca^{2+} inside the SR is bound to calsequestrin[124]. In skeletal muscle fiber, deletion of Casq1 causes a 20-50 % reduction in total releasable SR Ca^{2+} induced by caffeine[125-127]. SR Ca^{2+} content increases with increased abundance of Casq1 in skinned skeletal fiber[101], and overexpression of Casq1 in myotubule results in increased releasable SR Ca^{2+} [128]. Casq2-deficient cardiomyocytes have decreased SR Ca^{2+} content[129, 130], all supporting Ca^{2+} storage function of calsequestrin.

Free Ca^{2+} concentration in the lumen of the SR does not change significantly during sustained contraction, but it varies in calsequestrin-deficient fibers[124, 131], indicating that calsequestrin plays a role as Ca^{2+} buffer in the SR. In the resting muscle, there is a comparable level of free SR Ca^{2+} concentration in wild-type and Casq1-deficient fibers indicating that calsequestrin does not modulate free Ca^{2+} concentration at the junctional SR. However, with increased frequency of stimulation and induced contractions, the free SR Ca^{2+} concentration in wild-type cells does not change significantly, whereas Casq1-deficient fibers show rapid depletion of free SR Ca^{2+} concentration and highly reduced buffering power[124, 131], supporting Ca^{2+} buffering function of calsequestrin

1.5.2.2 Calsequestrin and regulation of the SR ryanodine receptor/Ca^{2+} channel (RyR)

The roles of Casq1 and Casq2 in modulation of RyR Ca^{2+} channel activity have been extensively studied *in vitro* using single channel reconstitution approaches either using isolated SR vesicles that contain native RyR or with purified RyR protein incorporated into the lipid bilayer[132]. In skeletal muscle, Casq1 inhibits RyR1 at ≤ 1 mM [Ca^{2+}] (Figure 1-5)[97, 98, 133-135], but it dissociates from RyR1 at high Ca^{2+} concentration (≥ 5 mM)[97, 134, 136]. Removing Casq1 from the RyR1 complex containing junctin, triadin, leads to increased probability and duration of the opening of RyR1 channel[97, 134]. Re-addition of Casq1 back to native RyR1 leads to reduced channel opening duration[97, 134] supporting a notion, that Casq1 inhibits RyR1 channel activity.

Junctin plays an important role in Casq1-dependent regulation of RyR1. Casq1 does not have any effect on RyR1 incorporated into lipid bilayer in the absence of junctin[106, 133, 134]. The C-tail

Ca^{2+} binding domain of Casq1 involved in protein polymerization, and interactions with triadin and junctin, is necessary for Casq1-dependent effects on RyR1 activity[106]. Clearly, interplay between Ca^{2+}, junctin, triadin, RyR1, and Casq1 is essential for Casq1-dependent modulation of RyR1 channel activity, and consequently skeletal muscle E-C coupling.

Casq2 activates RyR2 at ≥ 250 μM Ca^{2+} concentration, and has an inhibitory effect on the channel at low Ca^{2+} concentration (≤20μM) (Figure 1-5)[132, 135, 137, 138]. The channel activity of the native RyR2 isolated from SR vesicles is enhanced by increasing Ca^{2+} concentration[139, 140]. Removing Casq2 from native RyR2 by a high Ca^{2+} concentration reduces the open probability of the RyR2, and it becomes insensitive to increasing Ca^{2+} concentration. Importantly, this is reversed by addition of Casq2[132, 135, 137, 138]. Re-association of triadin and junctin to purified RyR2 in the lipid bilayer enhances RyR2 open channel probability, but addition of Casq2 restores RyR2 sensitivity to SR luminal Ca^{2+}. In conclusion, several *in vitro* single channel reconstitution studies provided strong support for a regulatory role of calsequestrin on RyR, and this regulation requires calsequestrin interacting with junctional SR proteins such as triadin and junctin.

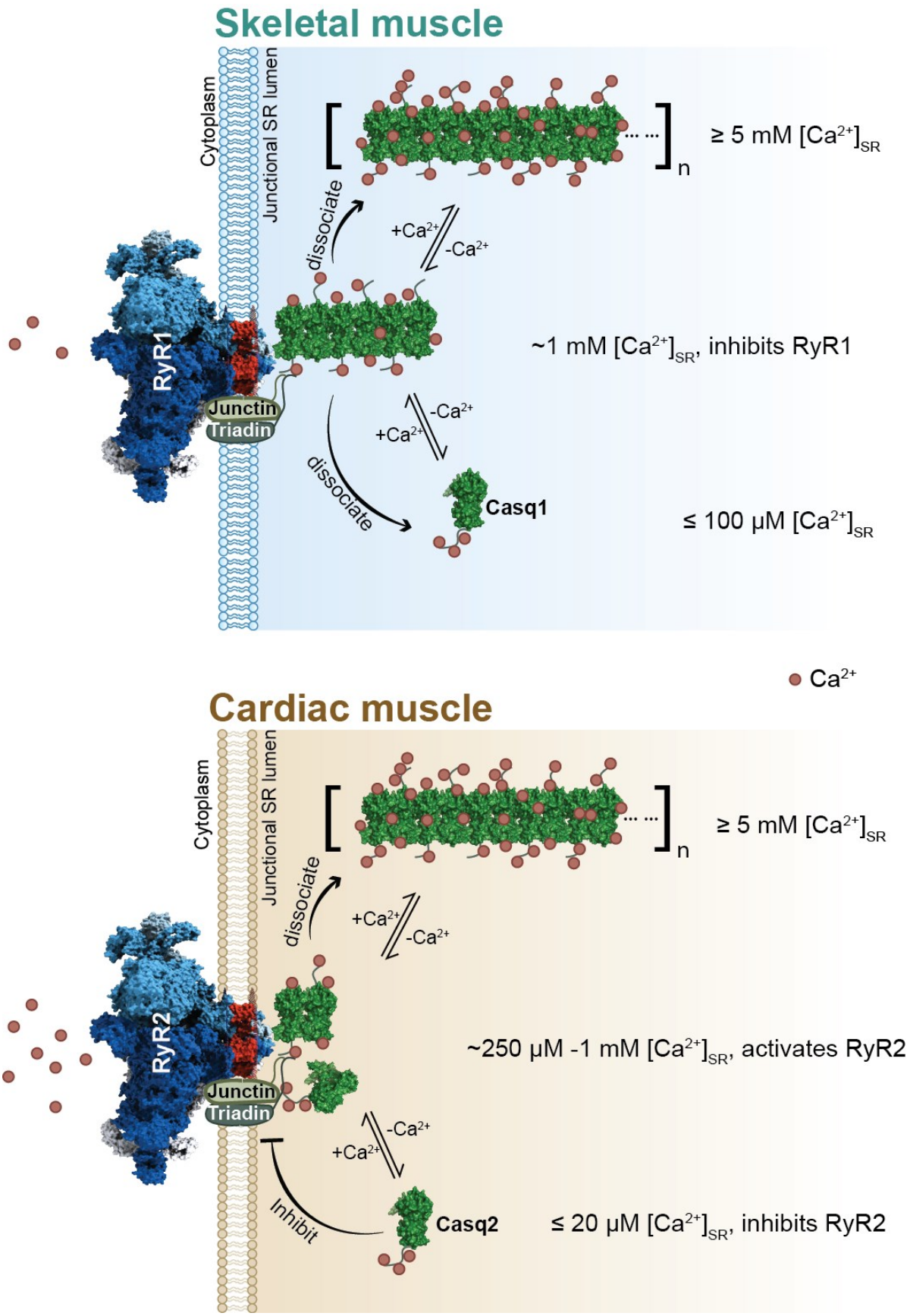
Skeletal muscle
Cytoplasm
Junctional SR lumen
≥ 5 mM [Ca2+]SR
dissociate
+Ca2+
-Ca2+
RyR1
~1 mM [Ca2+]SR, inhibits RyR1
Junctin
Triadin
-Ca2+
+Ca2+
dissociate
Casq1
≤ 100 μM [Ca2+]SR
Ca2+
Cardiac muscle
Cytoplasm
Junctional SR lumen
≥ 5 mM [Ca2+]SR
dissociate
+Ca2+
-Ca2+
RyR2
~250 μM -1 mM [Ca2+]SR, activates RyR2
Junctin
Triadin
-Ca2+
+Ca2+
Inhibit
Casq2
≤ 20 μM [Ca2+]SR, inhibits RyR2

Figure 1-5. A model for calsequestrin-dependent regulation of the ryanodine receptor/Ca^{2+} channel (RyR).

At the junctional SR, calsequestrin interacts with RyR, triadin, and junctin in a Ca^{2+} dependent manner. Changes in Ca^{2+} concentration induce a conformational change in calsequestrin. In skeletal muscle, Casq1 inhibits RyR1 at $\leq$ 1 mM Ca^{2+} concentration and dissociates from RyR1/junctin/triadin complex at $[Ca^{2+}] \geq$ 5mM or $\leq$ 100 μM. In cardiomyocytes, Casq2 activates RyR2 at $\geq$ 250 μM Ca^{2+} concentration and inhibits the RyR Ca^{2+} channel at low Ca^{2+} concentration $\leq$ 20 μM. Calsequestrin dissociates from the RyR2/junctin/triadin complex at a high Ca^{2+} concentration due to a Ca^{2+} dependent conformational change. SR, sarcoplasmic reticulum; RyR, ryanodine receptor/Ca^{2+} channel.

1.5.2.3 Calsequestrin and store-operated Ca^{2+} entry

In response to Ca^{2+} depletion, the ER luminal Ca^{2+} sensor, STIM1, dimerizes and interacts with the plasma membrane Ca^{2+} channel (ORAI1) to trigger Ca^{2+} entry from the extracellular space via so called store-operated Ca^{2+} entry (SOCE)[141, 142]. SOCE is a major Ca^{2+} entry pathway in non-muscle cells in response to depletion of Ca^{2+} in the ER and is used to maintain ER Ca^{2+} homeostasis[141, 143]. SOCE is also involved in refilling the SR Ca^{2+} store, and plays a role during skeletal muscle and heart development[120, 144].

In skeletal muscle, Casq1 has been proposed to inhibit SOCE[128]. STIM1 is co-localized with calsequestrin and RyR1 at the junctional SR/T-tubule interface[145]. During exercise, the ORAI1 Ca^{2+} channel in the T-tubule makes contacts with STIM1 at the junctional SR (Figure 1-1)[145]. Overexpression of Casq1 in C_2C_{12} myotubes inhibits SOCE under the conditions of thapsigargin-dependent Ca^{2+} depletion of the ER Ca^{2+} store[128]. Knockdown of Casq1 (>80%) with shRNA, in mouse *flexor digitorum brevis* muscle, results in reduced abundance of STIM1 and ORAI1 and enhanced SOCE following depletion of SR Ca^{2+} [146]. Furthermore, SOCE current is activated more rapidly during repetitive depolarization in skeletal myotubes from calsequestrin (Casq1 and Casq2) null mice when compared to wild-type muscle[147]. Casq1 effects on SOCE are intriguing, but it is not clear whether the protein exerts its effects on SOCE via direct interaction with STIM1, or indirectly by affecting junctional SR Ca^{2+} homeostasis and/or regulation of RyR1/Ca^{2+} channel.

1.5.3 Cardiac calsequestrin and catecholaminergic polymorphic ventricular tachycardia

Mutations in *casq2* are linked to catecholaminergic polymorphic ventricular tachycardia (CPVT) (Table 1-2, Figure 1-6)[148-150]. Arrhythmia patients have been reported as homozygous carriers of frameshift or splicing Casq2 mutations causing very early premature stop codons (62delA, 532+1 G>A, and G112+5X), which results in nonfunctional Casq2. Patients have structurally normal hearts, but display a severe form of CPVT in the early stage of life (6-7 years old)[118, 151]. This indicates that the absence of functional Casq2 in humans is not lethal, and may have no effect on cardiac development, but affected individuals develop life threating arrhythmia conditions as early as in childhood.

CPVT is an inherited arrhythmia characterized by polymorphic ventricular tachycardia induced by stress[148, 152-154]. Mutations in *casq2* account for about 3-5% of all CPVT[148, 155]. There are 17 Casq2 mutations identified to date associated with CPVT in humans (Table 1-2). Five

homozygous mutation are autosomal recessive, six heterozygous mutations appear to be autosomal dominant mutations, three are compound heterozygous mutations, two single nucleotide polymorphisms, and one heterozygous mutation found from whole-exon-sequencing are predicted to be pathogenic and may be a candidate for autosomal dominant inheritance mutations (Table 1-2).

Casq2 mutations show different defects on protein structure, Ca^{2+} binding, polymerization, and RyR2 regulation *in vitro* (Table 1-2)[114, 117, 118, 121, 156, 157], yet mutations knock-in mice all lead to stress-induced arrhythmia[130, 158, 159]. Different Casq2 mutations may have distinct underlying molecular mechanisms leading to CPVT, however, one unifying feature of Casq2 mutants associated with CPVT is dysfunction in the protein's Ca^{2+}-depend polymerization/depolymerization that affects filament formation.

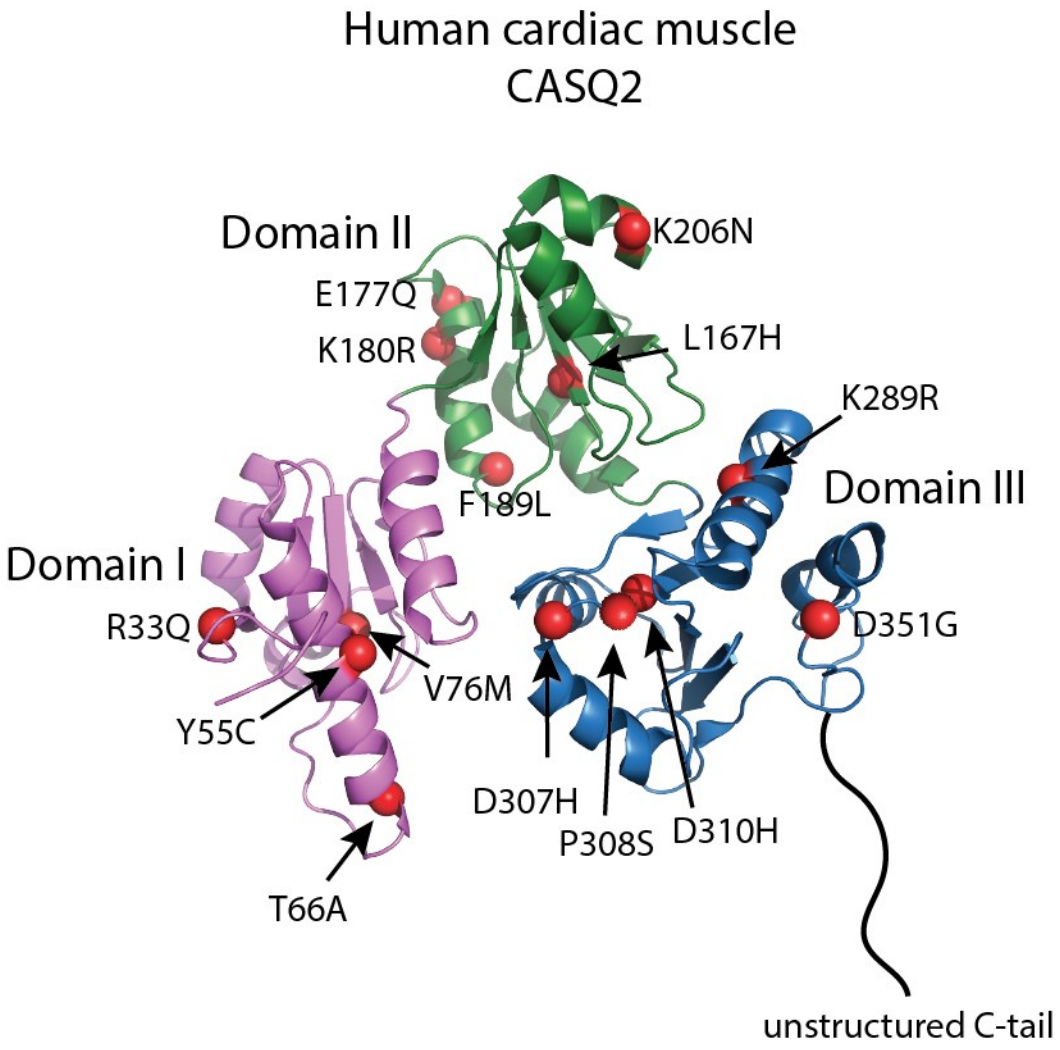

Figure 1-6. Catecholaminergic polymorphic ventricular tachycardia related missense mutations in *CASQ2*.

X-ray crystal structure adapted from PDB: 2VAF for human CASQ2. Mutated residues are labeled as red dots.

Table 1-2. Cardiac calsequestrin (CASQ2) mutations.

Mutation type	Mutation	Phenotype	Notes	Knock-in mouse model
Missense	D307H	CPVT	- Homozygous carrier with symptoms, heterozygous carrier shows no symptoms[160]	- Unaffected cardiac architecture, and normal ventricle function, but display catecholamine induced ventricular arrhythmia. Stable expression and targeting to junctional SR[113, 159] - Increased RyR2 leakiness when challenged with catecholamines[159] - No significant change in total SR Ca^{2+} content[130], [159]. - 95% reduction in protein abundance[130]
Missense	R33Q	Arrhythmia, non-sustained VT during exercise	- Homozygous carrier [161]	- Bidirectional VT on exposure to environmental stress in absence of pharmacological challenge[158] - Reduced SR Ca^{2+} capacity, dilated junctional SR but normal total SR volume [158] - Reduced abundance of Casq2-R33Q protein [158]
Non-sense	R33X	CPVT	Heterozygous carrier, autosomal dominant [151] Arginine changed to a stop codon at position 33	
Incorrect Splicing	532+1G>A	Severe CPVT	Patient is homozygous carrier, heterozygous siblings show no symptom[151].	- Caused be a premature stop codon Null mice features: - structural normal heart with stress-inducible arrhythmia[129, 130] - Unaffected SR Ca^{2+} content but increased SR volume[129]. Yet another research group reported >50% reduction in SR Ca^{2+} content [130] - Spontaneous SR Ca^{2+} releases and SR Ca^{2+} leak through RyR2 upon stress [129]
Deletion	62delA	Severe CPVT	Patient is homozygous carrier, heterozygous siblings show no symptom[151].	
Deletion	G112 +5X	Severe CPVT, Stress-induced VT and cardiac arrest [118]	- Homozygous mutation - Does not bind Ca^{2+}[118]	
Missense	L167H	Severe CPVT [118]	- Compound heterozygous with G11^{2+}5X [118]	Not available

Missense	K180R	Severe CPVT	- Heterozygous dominant inheritance [162]	- Structural normal heart but stress inducible VT
Missense	Y55C	CPVT	- Compound heterozygous[163]	Not available
Missense	P308L	CPVT		
Missense	F189L	CPVT [164] Sudden death during struggle [165]	- Heterozygous carrier[164-166]	Not available
Missense	E177Q	- Sudden unexplained death victims	-Heterozygous mutation, not characterized[167]	Not available
Missense	K206N	Cardiac arrest	- Heterozygous carrier [168]	Not available
SNP*	T66A	CPVT sudden unexplained death victims	- Unknown clinical significance - Finnish families[169] & Asian population[167]	Not available
SNP*	V76M			
Missense	K289R, P308S, D310H	In chickens, sudden death	- Unknown clinical significance in human[170]	Not available
Missense	D351G	Two male infants with SIDS (sudden infant death syndrome)	-Heterozygous variants determined from whole-exome analysis, likely pathologic[166, 171]	Not available
Missense	S173I	CPVT-like and Sudden unexplained death	-Heterozygous carrier -Unknown pathogenicity[96]	Not available

* SNP: Single nucleotide polymorphisms

1.6 Objectives and hypothesis

Objectives

i) Examine the role and regulation of IRE1α in skeletal and cardiac muscle.

ii) Investigate how mutations in Casq2 lead to stress-induced arrhythmia CPVT. Determine structural and functional features of the CPVT related Casq2 mutants and their role in heart pathology.

Hypothesis:

i) ER stress sensor IRE1α plays an important role in the physiology and pathophysiology of the heart, and IRE1α mediated signaling may be regulated via protein-protein interaction(s) in skeletal and cardiac muscle.

ii) CPVT related Casq2 mutations may affect structure and function of the protein and this impacts SR Ca^{2+} store and control of Ca^{2+} in excitation-contraction coupling.

1.7 References

1. Wang M, Kaufman RJ. Protein misfolding in the endoplasmic reticulum as a conduit to human disease. *Nature*. 2016;529:326-335
2. Schwarz DS, Blower MD. The endoplasmic reticulum: structure, function and response to cellular signaling. *Cellular and Molecular Life Sciences*. 2016;73:79-94
3. Schröder M. Endoplasmic reticulum stress responses. *Cellular and Molecular Life Sciences*. 2008;65:862-894
4. Lam AK, Galione A. The endoplasmic reticulum and junctional membrane communication during calcium signaling. *Biochimica et Biophysica Acta (BBA) - Biomembranes*. 2013;1833:2542-2559
5. Schröder M, Kaufman RJ. The mammalian unfolded protein response. *Annual Review of Biochemistry*. 2005;74:739-789
6. Lombardi AA, Elrod JW. Mediating ER-mitochondrial cross-talk. *Science*. 2017;358:591-592
7. Phillips MJ, Voeltz GK. Structure and function of ER membrane contact sites with other organelles. *Nature Reviews Molecular Cell Biology*. 2016;17:69-82
8. Saheki Y, De Camilli P. Endoplasmic reticulum–plasma membrane contact sites. *Annual Review of Biochemistry*. 2017;86:659-684
9. Michalak M, Opas M. Endoplasmic and sarcoplasmic reticulum in the heart. *Trends in Cell Biology*. 2009;19:253-259
10. Sorrentino V. Sarcoplasmic reticulum: structural determinants and protein dynamics. *International Journal of Biochemistry & Cell Biology*. 2011;43:1075-1078
11. Wray S, Burdyga T. Sarcoplasmic reticulum function in smooth muscle. *Physiological Reviews*. 2010;90:113-178
12. Bers DM. Cardiac sarcoplasmic reticulum calcium leak: basis and roles in cardiac dysfunction. *Annual Review of Physiology*. 2014;76:107-127
13. Pinali C, Bennett H, Davenport JB, Trafford Andrew W, Kitmitto A. Three-dimensional reconstruction of cardiac sarcoplasmic reticulum reveals a continuous network linking transverse-tubules. *Circulation Research*. 2013;113:1219-1230
14. Bers DM. Cardiac excitation–contraction coupling. *Nature*. 2002;415:198-205
15. Allen BG, Katz S. Calreticulin and calsequestrin are differentially distributed in canine heart. *Journal of Molecular and Cellular Cardiology*. 2000;32:2379-2384
16. Lee D, Michalak M. Membrane associated Ca^{2+} buffers in the heart. *BMB Reports*. 2010;43:151-157
17. Doroudgar S, Glembotski CC. New concepts of endoplasmic reticulum function in the heart: programmed to conserve. *Journal of Molecular and Cellular Cardiology*. 2013;55:85-91

18. Slade AM, Severs NJ. Rough endoplasmic reticulum in the adult mammalian cardiac muscle cell. *Journal of Submicroscopic Cytology and Pathology*. 1985;17:531-536

19. Koyabu S, Imanaka-Yoshida K, Ioshii SO, Nakano T, Yoshida T. Switching of the dominant calcium sequestering protein during skeletal muscle differentiation. *Cell Motility and the Cytoskeleton*. 1994;29:259-270

20. Kaisto T, Metsikkö K. Distribution of the endoplasmic reticulum and its relationship with the sarcoplasmic reticulum in skeletal myofibers. *Experimental Cell Research*. 2003;289:47-57

21. Kaakinen M, Papponen H, Metsikkö K. Microdomains of endoplasmic reticulum within the sarcoplasmic reticulum of skeletal myofibers. *Experimental Cell Research*. 2008;314:237-245

22. Volpe P, Villa A, Podini P, Martini A, Nori A, Panzeri MC, Meldolesi J. The endoplasmic reticulum-sarcoplasmic reticulum connection: distribution of endoplasmic reticulum markers in the sarcoplasmic reticulum of skeletal muscle fibers. *Proceedings of the National Academy of Sciences of the United States of America*. 1992;89:6142-6146

23. Mesaeli N, Nakamura K, Zvaritch E, Dickie P, Dziak E, Krause KH, Opas M, MacLennan DH, Michalak M. Calreticulin is essential for cardiac development. *Journal of Cell Biology*. 1999;144:857-868

24. Xiong B, Jha V, Min J-K, Cho J. Protein disulfide isomerase in cardiovascular disease. *Experimental & Molecular Medicine*. 2020;52:390-399

25. Wang X, Bi X, Zhang G, Deng Y, Luo X, Xu L, Scherer PE, Ferdous A, Fu G, Gillette TG, Lee AS, Jiang X, Wang ZV. Glucose-regulated protein 78 is essential for cardiac myocyte survival. *Cell Death and Differentiation*. 2018;25:2181-2194

26. Walter P, Ron D. The unfolded protein response: From stress pathway to homeostatic regulation. *Science*. 2011;334:1081-1086

27. Groenendyk J, Sreenivasaiah PK, Kim DH, Agellon LB, Michalak M. Biology of endoplasmic reticulum stress in the heart. *Circulation Research*. 2010;107:1185-1197

28. Groenendyk J, Agellon LB, Michalak M. Coping with endoplasmic reticulum stress in the cardiovascular system. *Annual Review of Physiology*. 2013;75:49-67

29. Liu CY, Schroder M, Kaufman RJ. Ligand-independent dimerization activates the stress response kinases IRE1 and PERK in the lumen of the endoplasmic reticulum. *Journal of Biological Chemistry*. 2000;275:24881-24885

30. Zhou J, Liu CY, Back SH, Clark RL, Peisach D, Xu Z, Kaufman RJ. The crystal structure of human IRE1 luminal domain reveals a conserved dimerization interface required for activation of the unfolded protein response. *Proceedings of the National Academy of Sciences of the United States of America*. 2006;103:14343-14348

31. Calfon M, Zeng H, Urano F, Till JH, Hubbard SR, Harding HP, Clark SG, Ron D. IRE1 couples endoplasmic reticulum load to secretory capacity by processing the XBP-1 mRNA. *Nature*. 2002;415:92-96

32. Yoshida H, Matsui T, Yamamoto A, Okada T, Mori K. XBP1 mRNA is induced by ATF6 and spliced by IRE1 in response to ER stress to produce a highly active transcription factor. *Cell*. 2001;107:881-891

33. Yamamoto K, Yoshida H, Kokame K, Kaufman RJ, Mori K. Differential contributions of ATF6 and XBP1 to the activation of endoplasmic reticulum stress-responsive cis-acting elements ERSE, UPRE and ERSE-II. *Journal of Biochemistry*. 2004;136:343-350

34. Maurel M, Chevet E, Tavernier J, Gerlo S. Getting RIDD of RNA: IRE1 in cell fate regulation. *Trends in Biochemical Sciences*. 2014;39:245-254

35. Lerner AG, Upton J-P, Praveen PVK, Ghosh R, Nakagawa Y, Igbaria A, Shen S, Nguyen V, Backes BJ, Heiman M, Heintz N, Greengard P, Hui S, Tang Q, Trusina A, Oakes SA, Papa FR. IRE1α Induces Thioredoxin-Interacting Protein to Activate the NLRP3 Inflammasome and Promote Programmed Cell Death under Irremediable ER Stress. *Cell Metabolism*. 2012;16:250-264

36. Upton J-P, Wang L, Han D, Wang ES, Huskey NE, Lim L, Truitt M, McManus MT, Ruggero D, Goga A, Papa FR, Oakes SA. IRE1α cleaves select microRNAs during ER stress to derepress translation of proapoptotic Caspase-2. *Science* 2012;338:818-822

37. Sano R, Reed JC. ER stress-induced cell death mechanisms. *Biochimica et Biophysica Acta (BBA) - Molecular Cell Research*. 2013;1833:3460-3470

38. Harding HP, Zhang Y, Ron D. Protein translation and folding are coupled by an endoplasmic-reticulum-resident kinase. *Nature*. 1999;397:271-274

39. Shi Y, Vattem KM, Sood R, An J, Liang J, Stramm L, Wek RC. Identification and characterization of pancreatic eukaryotic initiation factor 2 α-subunit kinase, PEK, involved in translational control. *Molecular and Cellular Biology*. 1998;18:7499-7509

40. Bravo R, Parra V, Gatica D, Rodriguez AE, Torrealba N, Paredes F, Wang ZV, Zorzano A, Hill JA, Jaimovich E, Quest AFG, Lavandero S. Endoplasmic reticulum and the unfolded protein response: dynamics and metabolic integration. *International Review of Cell and Molecular Biology*. 2013;301:215-290

41. Oyadomari S, Mori M. Roles of CHOP/GADD153 in endoplasmic reticulum stress. *Cell Death & Differentiation*. 2004;11:381-389

42. Kokame K, Kato H, Miyata T. Identification of ERSE-II, a new cis-acting element responsible for the ATF6-dependent mammalian unfolded protein response. *Journal of Biological Chemistry*. 2001;276:9199-9205

43. Yoshida H, Haze K, Yanagi H, Yura T, Mori K. Identification of the cis-acting endoplasmic reticulum stress response element responsible for transcriptional induction of mammalian glucose-regulated proteins. Involvement of basic leucine zipper transcription factors. *Journal of Biological Chemistry*. 1998;273:33741-33749

44. Okada K, Minamino T, Tsukamoto Y, Liao Y, Tsukamoto O, Takashima S, Hirata A, Fujita M, Nagamachi Y, Nakatani T, Yutani C, Ozawa K, Ogawa S, Tomoike H, Hori M, Kitakaze M. Prolonged endoplasmic reticulum stress in hypertrophic and failing heart after aortic constriction: possible contribution of endoplasmic reticulum stress to cardiac myocyte apoptosis. *Circulation*. 2004;110:705-712

45. Gao G, Xie A, Zhang J, Herman AM, Jeong EM, Gu L, Liu M, Yang KC, Kamp TJ, Dudley SC. Unfolded protein response regulates cardiac sodium current in systolic human heart failure. *Circulation: Arrhythmia and Electrophysiology*. 2013;6:1018-1024

46. Szegezdi E, Duffy A, O'Mahoney ME, Logue SE, Mylotte LA, O'Brien T, Samali A. ER stress contributes to ischemia-induced cardiomyocyte apoptosis. *Biochemical and Biophysical Research Communications*. 2006;349:1406-1411

47. Thuerauf Donna J, Marcinko M, Gude N, Rubio M, Sussman Mark A, Glembotski Christopher C. Activation of the unfolded protein response in infarcted mouse heart and hypoxic cultured cardiac myocytes. *Circulation Research*. 2006;99:275-282

48. Sawada T, Minamino T, Fu HY, Asai M, Okuda K, Isomura T, Yamazaki S, Asano Y, Okada K, Tsukamoto O, Sanada S, Asanuma H, Asakura M, Takashima S, Kitakaze M, Komuro I. X-box binding protein 1 regulates brain natriuretic peptide through a novel AP1/CRE-like element in cardiomyocytes. *Journal of Molecular and Cellular Cardiology*. 2010;48:1280-1289

49. Jin J-K, Blackwood EA, Azizi K, Thuerauf DJ, Fahem AG, Hofmann C, Kaufman RJ, Doroudgar S, Glembotski CC. ATF6 decreases myocardial ischemia/reperfusion damage and links er stress and oxidative stress signaling pathways in the heart. *Circulation Research*. 2017;120:862-875

50. Martindale Joshua J, Fernandez R, Thuerauf D, Whittaker R, Gude N, Sussman Mark A, Glembotski Christopher C. Endoplasmic reticulum stress gene induction and protection from ischemia/reperfusion injury in the hearts of transgenic mice with a tamoxifen-regulated form of ATF6. *Circulation Research*. 2006;98:1186-1193

51. Liu X, Kwak D, Lu Z, Xu X, Fassett J, Wang H, Wei Y, Cavener DR, Hu X, Hall J, Bache RJ, Chen Y. Endoplasmic reticulum stress sensor protein kinase R-like endoplasmic reticulum kinase (PERK) protects against pressure overload-induced heart failure and lung remodeling. *Hypertension (Dallas, Tex. : 1979)*. 2014;64:738-744

52. Guan HS, Shangguan HJ, Shang Z, Yang L, Meng XM, Qiao SB. Endoplasmic reticulum stress caused by left ventricular hypertrophy in rats: effects of telmisartan. *American Journal of the Medical Sciences*. 2011;342:318-323

53. Fu HY, Minamino T, Tsukamoto O, Sawada T, Asai M, Kato H, Asano Y, Fujita M, Takashima S, Hori M, Kitakaze M. Overexpression of endoplasmic reticulum-resident chaperone attenuates cardiomyocyte death induced by proteasome inhibition. *Cardiovascular Research*. 2008;79:600-610

54. Steiger D, Yokota T, Li J, Ren S, Minamisawa S, Wang Y. The serine/threonine-protein kinase/endoribonuclease IRE1α protects the heart against pressure overload-induced heart failure. *The Journal of Biological Chemistry*. 2018;293:9652-9661

55. Wang ZV, Deng Y, Gao N, Pedrozo Z, Li DL, Morales CR, Criollo A, Luo X, Tan W, Jiang N, Lehrman MA, Rothermel BA, Lee A-H, Lavandero S, Mammen PPA, Ferdous A, Gillette TG, Scherer PE, Hill JA. Spliced X-box binding protein 1 couples the unfolded protein response to hexosamine biosynthetic pathway. *Cell*. 2014;156:1179-1192

56. Yamaguchi O, Higuchi Y, Hirotani S, Kashiwase K, Nakayama H, Hikoso S, Takeda T, Watanabe T, Asahi M, Taniike M, Matsumura Y, Tsujimoto I, Hongo K, Kusakari Y,

Kurihara S, Nishida K, Ichijo H, Hori M, Otsu K. Targeted deletion of apoptosis signal-regulating kinase 1 attenuates left ventricular remodeling. *Proceedings of the National Academy of Sciences of the United States of America*. 2003;100:15883-15888

57. Hollien J. Evolution of the unfolded protein response. *Biochimica et Biophysica Acta (BBA) - Molecular Cell Research*. 2013;1833:2458-2463

58. Hourihan JM, Moronetti Mazzeo LE, Fernández-Cárdenas LP, Blackwell TK. Cysteine sulfenylation directs IRE-1 to activate the SKN-1/Nrf2 antioxidant response. *Molecular Cell*. 2016;63:553-566

59. Carreras-Sureda A, Jaña F, Urra H, Durand S, Mortenson DE, Sagredo A, Bustos G, Hazari Y, Ramos-Fernández E, Sassano ML, Pihán P, van Vliet AR, González-Quiroz M, Torres AK, Tapia-Rojas C, Kerkhofs M, Vicente R, Kaufman RJ, Inestrosa NC, Gonzalez-Billault C, Wiseman RL, Agostinis P, Bultynck G, Court FA, Kroemer G, Cárdenas JC, Hetz C. Non-canonical function of IRE1α determines mitochondria-associated endoplasmic reticulum composition to control calcium transfer and bioenergetics. *Nature Cell Biology*. 2019;21:755-767

60. Iwawaki T, Akai R, Yamanaka S, Kohno K. Function of IRE1 alpha in the placenta is essential for placental development and embryonic viability. *Proceedings of the National Academy of Sciences*. 2009;106:16657

61. Tirasophon W, Lee K, Callaghan B, Welihinda A, Kaufman RJ. The endoribonuclease activity of mammalian IRE1 autoregulates its mRNA and is required for the unfolded protein response. *Genes & Development*. 2000;14:2725-2736

62. Tsuru A, Fujimoto N, Takahashi S, Saito M, Nakamura D, Iwano M, Iwawaki T, Kadokura H, Ron D, Kohno K. Negative feedback by IRE1β optimizes mucin production in goblet cells. *Proceedings of the National Academy of Sciences of the United States of America*. 2013;110:2864-2869

63. Imagawa Y, Hosoda A, Sasaka S-i, Tsuru A, Kohno K. RNase domains determine the functional difference between IRE1α and IRE1β. *FEBS Letters*. 2008;582:656-660

64. Li H, Korennykh AV, Behrman SL, Walter P. Mammalian endoplasmic reticulum stress sensor IRE1 signals by dynamic clustering. *Proceedings of the National Academy of Sciences of the United States of America*. 2010;107:16113-16118

65. Gardner BM, Walter P. Unfolded proteins are Ire1-activating ligands that directly induce the unfolded protein response. *Science* 2011;333:1891-1894

66. Credle JJ, Finer-Moore JS, Papa FR, Stroud RM, Walter P. On the mechanism of sensing unfolded protein in the endoplasmic reticulum. *Proceedings of the National Academy of Sciences of the United States of America*. 2005;102:18773-18784

67. Bertolotti A, Zhang Y, Hendershot LM, Harding HP, Ron D. Dynamic interaction of BiP and ER stress transducers in the unfolded-protein response. *Nature Cell Biology*. 2000;2:326-332

68. Okamura K, Kimata Y, Higashio H, Tsuru A, Kohno K. Dissociation of Kar2p/BiP from an ER sensory molecule, Ire1p, triggers the unfolded protein response in yeast. *Biochemical and Biophysical Research Communications*. 2000;279:445-450

69. Kimata Y, Oikawa D, Shimizu Y, Ishiwata-Kimata Y, Kohno K. A role for BiP as an adjustor for the endoplasmic reticulum stress-sensing protein Ire1. *Journal of Cell Biology*. 2004;167:445-456

70. Kopp MC, Nowak PR, Larburu N, Adams CJ, Ali MM. In vitro FRET analysis of IRE1 and BiP association and dissociation upon endoplasmic reticulum stress. *eLife*. 2018;7:e30257

71. Adams CJ, Kopp MC, Larburu N, Nowak PR, Ali MMU. Structure and molecular mechanism of ER stress signaling by the unfolded protein response signal activator IRE1. *Frontiers in Molecular Biosciences*. 2019;6

72. Shen J, Chen X, Hendershot L, Prywes R. ER stress regulation of ATF6 localization by dissociation of BiP/GRP78 binding and unmasking of Golgi localization signals. *Developmental Cell*. 2002;3:99-111

73. Ali Khan H, Mutus B. Protein disulfide isomerase a multifunctional protein with multiple physiological roles. *Frontiers in Chemistry*. 2014;2

74. Groenendyk J, Peng Z, Dudek E, Fan X, Mizianty MJ, Dufey E, Urra H, Sepulveda D, Rojas-Rivera D, Lim Y, Kim DH, Baretta K, Srikanth S, Gwack Y, Ahnn J, Kaufman RJ, Lee SK, Hetz C, Kurgan L, Michalak M. Interplay between the oxidoreductase PDIA6 and microRNA-322 controls the response to disrupted endoplasmic reticulum calcium homeostasis. *Science Signaling*. 2014;7:ra54

75. Vekich JA, Belmont PJ, Thuerauf DJ, Glembotski CC. Protein disulfide isomerase-associated 6 is an ATF6-inducible ER stress response protein that protects cardiac myocytes from ischemia/reperfusion-mediated cell death. *Journal of Molecular and Cellular Cardiology*. 2012;53:259-267

76. Nagata K. Hsp47: a collagen-specific molecular chaperone. *Trends in Biochemical Sciences*. 1996;21:22-26

77. Nagata K, Hosokawa N. Regulation and function of collagen-specific molecular chaperone, HSP47. *Cell Structure and Function*. 1996;21:425-430

78. Sepulveda D, Rojas-Rivera D, Rodríguez DA, Groenendyk J, Köhler A, Lebeaupin C, Ito S, Urra H, Carreras-Sureda A, Hazari Y, Vasseur-Cognet M, Ali MMU, Chevet E, Campos G, Godoy P, Vaisar T, Bailly-Maitre B, Nagata K, Michalak M, Sierralta J, Hetz C. Interactome screening identifies the ER luminal chaperone Hsp47 as a regulator of the unfolded protein response transducer IRE1α. *Molecular Cell*. 2018;69:238-252.e237

79. Groenendyk J, Paskevicius T, Urra H, Viricel C, Wang K, Barakat K, Hetz C, Kurgan L, Agellon LB, Michalak M. Cyclosporine A binding to COX-2 reveals a novel signaling pathway that activates IRE1α unfolded protein response sensor. *Scientific Reports*. 2018;8:16678

80. Wang Q, Groenendyk J, Paskevicius T, Qin W, Kor KC, Liu Y, Hiess F, Knollmann BC, Chen SRW, Tang J, Chen XZ, Agellon LB, Michalak M. Two pools of IRE1α in cardiac and skeletal muscle cells. *FEBS Journal*. 2019;33:8892-8904

81. Chen Y, Brandizzi F. IRE1: ER stress sensor and cell fate executor. *Trends in Cell Biology*. 2013;23:547-555

82. Hetz C, Glimcher LH. Fine-tuning of the unfolded protein response: Assembling the IRE1alpha interactome. *Molecular Cell*. 2009;35:551-561

83. Urano F, Wang X, Bertolotti A, Zhang Y, Chung P, Harding HP, Ron D. Coupling of stress in the ER to activation of JNK protein kinases by transmembrane protein kinase IRE1. *Science*. 2000;287:664-666

84. Nishitoh H, Matsuzawa A, Tobiume K, Saegusa K, Takeda K, Inoue K, Hori S, Kakizuka A, Ichijo H. ASK1 is essential for endoplasmic reticulum stress-induced neuronal cell death triggered by expanded polyglutamine repeats. *Genes & Development*. 2002;16:1345-1355

85. Ikemoto N, Bhatnagar GM, Nagy B, Gergely J. Interaction of divalent cations with the 55,000-dalton protein component of the sarcoplasmic reticulum. Studies of fluorescence and circular dichroism. *Journal of Biological Chemistry*. 1972;247:7835-7837

86. MacLennan DH, Wong PT. Isolation of a calcium-sequestering protein from sarcoplasmic reticulum. *Proceedings of the National Academy of Sciences of the United States of America*. 1971;68:1231-1235

87. Meissner G, Conner GE, Fleischer S. Isolation of sarcoplasmic reticulum by zonal centrifugation and purification of Ca^{2+}-pump and Ca^{2+}-binding proteins. *Biochimica et Biophysica Acta (BBA) - Biomembranes*. 1973;298:246-269

88. Ikemoto N, Nagy B, Bhatnagar GM, Gergely J. Studies on a metal-binding protein of the sarcoplasmic reticulum. *Journal of Biological Chemistry*. 1974;249:2357-2365

89. Franzini-Armstrong C. STUDIES OF THE TRIAD : I. Structure of the junction in frog twitch fibers. *Journal of Cell Biology*. 1970;47:488-499

90. Franzini-Armstrong C, Kenney LJ, Varriano-Marston E. The structure of calsequestrin in triads of vertebrate skeletal muscle: a deep-etch study. *Journal of Cell Biology*. 1987;105:49-56

91. Perni S, Close M, Franzini-Armstrong C. Novel details of calsequestrin gel conformation in situ. *Journal of Biological Chemistry*. 2013;288:31358-31362

92. Park H, Park IY, Kim E, Youn B, Fields K, Dunker AK, Kang C. Comparing skeletal and cardiac calsequestrin structures and their calcium binding: a proposed mechanism for coupled calcium binding and protein polymerization. *Journal of Biological Chemistry*. 2004;279:18026-18033

93. Sanchez EJ, Lewis KM, Danna BR, Kang C. High-capacity Ca^{2+} binding of human skeletal calsequestrin. *Journal of Biological Chemistry*. 2012;287:11592-11601

94. Park H, Wu S, Dunker AK, Kang C. Polymerization of calsequestrin. Implications for Ca^{2+} regulation. *Journal of Biological Chemistry*. 2003;278:16176-16182

95. Wang S, Trumble WR, Liao H, Wesson CR, Dunker AK, Kang C. Crystal structure of calsequestrin from rabbit skeletal muscle sarcoplasmic reticulum. *Nature Structural Biology*. 1998;5:476-483

96. Titus EW, Deiter FH, Shi C, Wojciak J, Scheinman M, Jura N, Deo RC. The structure of a calsequestrin filament reveals mechanisms of familial arrhythmia. *bioRxiv*. 2019:672303

97. Beard NA, Casarotto MG, Wei L, Varsanyi M, Laver DR, Dulhunty AF. Regulation of ryanodine receptors by calsequestrin: effect of high luminal Ca^{2+} and phosphorylation. *Biophysical Journal*. 2005;88:3444-3454

98. Wei L, Varsányi M, Dulhunty AF, Beard NA. The conformation of calsequestrin determines its ability to regulate skeletal ryanodine receptors. *Biophysical Journal*. 2006;91:1288-1301

99. Fliegel L, Newton E, Burns K, Michalak M. Molecular cloning of cDNA encoding a 55-kDa multifunctional thyroid hormone binding protein of skeletal muscle sarcoplasmic reticulum. *Journal of Biological Chemistry*. 1990;265:15496-15502

100. Scott BT, Simmerman HK, Collins JH, Nadal-Ginard B, Jones LR. Complete amino acid sequence of canine cardiac calsequestrin deduced by cDNA cloning. *Journal of Biological Chemistry*. 1988;263:8958-8964

101. Murphy RM, Larkins NT, Mollica JP, Beard NA, Lamb GD. Calsequestrin content and SERCA determine normal and maximal Ca^{2+} storage levels in sarcoplasmic reticulum of fast- and slow-twitch fibres of rat. *The Journal of Physiology*. 2009;587:443-460

102. Sacchetto R, Volpe P, Damiani E, Margreth A. Postnatal development of rabbit fast-twitch skeletal muscle: accumulation, isoform transition and fibre distribution of calsequestrin. *Journal of Muscle Research and Cell Motility*. 1993;14:646-653

103. Biral D, Volpe P, Damiani E, Margreth A. Coexistence of two calsequestrin isoforms in rabbit slow-twitch skeletal muscle fibers. *FEBS Letters*. 1992;299:175-178

104. Damiani E, Volpe P, Margreth A. Coexpression of two isoforms of calsequestrin in rabbit slow-twitch muscle. *Journal of Muscle Research and Cell Motility*. 1990;11:522-530

105. Beard NA, Wei L, Cheung SN, Kimura T, Varsanyi M, Dulhunty AF. Phosphorylation of skeletal muscle calsequestrin enhances its Ca^{2+} binding capacity and promotes its association with junctin. *Cell Calcium*. 2008;44:363-373

106. Beard NA, Dulhunty AF. C-terminal residues of skeletal muscle calsequestrin are essential for calcium binding and for skeletal ryanodine receptor inhibition. *Skelet Muscle*. 2015;5:6

107. Royer L, Ríos E. Deconstructing calsequestrin. Complex buffering in the calcium store of skeletal muscle. *The Journal of Physiology*. 2009;587:3101-3111

108. Cala SE, Jones LR. Phosphorylation of cardiac and skeletal muscle calsequestrin isoforms by casein kinase II. Demonstration of a cluster of unique rapidly phosphorylated sites in cardiac calsequestrin. *Journal of Biological Chemistry*. 1991;266:391-398

109. Kiarash A, Kelly CE, Phinney BS, Valdivia HH, Abrams J, Cala SE. Defective glycosylation of calsequestrin in heart failure. *Cardiovascular Research*. 2004;63:264-272

110. Sanchez EJ, Munske GR, Criswell A, Milting H, Dunker AK, Kang C. Phosphorylation of human calsequestrin: implications for calcium regulation. *Molecular and Cellular Biochemistry*. 2011;353:195

111. Sanchez EJ, Lewis KM, Munske GR, Nissen MS, Kang C. Glycosylation of skeletal calsequestrin: implications for its function. *Journal of Biological Chemistry*. 2012;287:3042-3050

112. Ryder DJ, Judge SM, Beharry AW, Farnsworth CL, Silva JC, Judge AR. Identification of the acetylation and ubiquitin-modified proteome during the progression of skeletal muscle atrophy. *PLOS One*. 2015;10:e0136247

113. Kalyanasundaram A, Bal NC, Franzini-Armstrong C, Knollmann BC, Periasamy M. The calsequestrin mutation CASQ2D307H does not affect protein stability and targeting to the junctional sarcoplasmic reticulum but compromises its dynamic regulation of calcium buffering. *Journal of Biological Chemistry*. 2010;285:3076-3083

114. Kim E, Youn B, Kemper L, Campbell C, Milting H, Varsanyi M, Kang C. Characterization of human cardiac calsequestrin and its deleterious mutants. *Journal of Molecular Biology*. 2007;373:1047-1057

115. Slupsky JR, Ohnishi M, Carpenter MR, Reithmeier RA. Characterization of cardiac calsequestrin. *Biochemistry*. 1987;26:6539-6544

116. Aaron BM, Oikawa K, Reithmeier RA, Sykes BD. Characterization of skeletal muscle calsequestrin by 1H NMR spectroscopy. *Journal of Biological Chemistry*. 1984;259:11876-11881

117. Wang Q, Paskevicius T, Filbert A, Qin W, Chen X, Tang J, Dacks J, Agellon L, Michalak M. Evolutionary conservation and diversity of human calsequestrin function. *Scientific Report*. 2020; Revisions requested

118. di Barletta MR, Viatchenko-Karpinski S, Nori A, Memmi M, Terentyev D, Turcato F, Valle G, Rizzi N, Napolitano C, Gyorke S, Volpe P, Priori SG. Clinical phenotype and functional characterization of CASQ2 mutations associated with catecholaminergic polymorphic ventricular tachycardia. *Circulation*. 2006;114:1012-1019

119. Wei L, Hanna AD, Beard NA, Dulhunty AF. Unique isoform-specific properties of calsequestrin in the heart and skeletal muscle. *Cell Calcium*. 2009;45:474-484

120. Rosenberg P, Katz D, Bryson V. SOCE and STIM1 signaling in the heart: Timing and location matter. *Cell Calcium*. 2019;77:20-28

121. Qin J, Valle G, Nani A, Nori A, Rizzi N, Priori SG, Volpe P, Fill M. Luminal Ca^{2+} regulation of single cardiac ryanodine receptors: insights provided by calsequestrin and its mutants. *The Journal of General Physiology*. 2008;131:325-334

122. Lewis KM, Munske GR, Byrd SS, Kang J, Cho H, Ríos E, Kang C. Characterization of post-translational modifications to calsequestrins of cardiac and skeletal muscle. *International journal of molecular sciences*. 2016;17:1539

123. Jacob S, Sleiman NH, Kern S, Jones LR, Sala-Mercado JA, McFarland TP, Sabbah HH, Cala SE. Altered calsequestrin glycan processing is common to diverse models of canine heart failure. *Molecular and Cellular Biochemistry*. 2013;377:11-21

124. Manno C, Sztretye M, Figueroa L, Allen PD, Rios E. Dynamic measurement of the calcium buffering properties of the sarcoplasmic reticulum in mouse skeletal muscle. *The Journal of Physiology*. 2013;591:423-442

125. Dainese M, Quarta M, Lyfenko AD, Paolini C, Canato M, Reggiani C, Dirksen RT, Protasi F. Anesthetic- and heat-induced sudden death in calsequestrin-1-knockout mice. *The FASEB Journal*. 2009;23:1710-1720

126. Paolini C, Quarta M, Nori A, Boncompagni S, Canato M, Volpe P, Allen PD, Reggiani C, Protasi F. Reorganized stores and impaired calcium handling in skeletal muscle of mice lacking calsequestrin-1. *The Journal of Physiology*. 2007;583:767-784

127. Royer L, Sztretye M, Manno C, Pouvreau S, Zhou J, Knollmann BC, Protasi F, Allen PD, Ríos E. Paradoxical buffering of calcium by calsequestrin demonstrated for the calcium store of skeletal muscle. *The Journal of General Physiology*. 2010;136:325-338

128. Shin DW, Pan Z, Kim EK, Lee JM, Bhat MB, Parness J, Kim DH, Ma J. A retrograde signal from calsequestrin for the regulation of store-operated Ca^{2+} entry in skeletal muscle. *Journal of Biological Chemistry*. 2003;278:3286-3292

129. Knollmann BC, Chopra N, Hlaing T, Akin B, Yang T, Ettensohn K, Knollmann BE, Horton KD, Weissman NJ, Holinstat I, Zhang W, Roden DM, Jones LR, Franzini-Armstrong C, Pfeifer K. Casq2 deletion causes sarcoplasmic reticulum volume increase, premature Ca^{2+} release, and catecholaminergic polymorphic ventricular tachycardia. *Journal of Clinical Investigation*. 2006;116:2510-2520

130. Song L, Alcalai R, Arad M, Wolf CM, Toka O, Conner DA, Berul CI, Eldar M, Seidman CE, Seidman JG. Calsequestrin 2 (CASQ2) mutations increase expression of calreticulin and ryanodine receptors, causing catecholaminergic polymorphic ventricular tachycardia. *Journal of Clinical Investigation*. 2007;117:1814-1823

131. Canato M, Scorzeto M, Giacomello M, Protasi F, Reggiani C, Stienen GJM. Massive alterations of sarcoplasmic reticulum free calcium in skeletal muscle fibers lacking calsequestrin revealed by a genetically encoded probe. *Proceedings of the National Academy of Sciences of the United States of America*. 2010;107:22326-22331

132. Lai FA, Erickson HP, Rousseau E, Liu QY, Meissner G. Purification and reconstitution of the calcium release channel from skeletal muscle. *Nature*. 1988;331:315-319

133. Wei L, Gallant EM, Dulhunty AF, Beard NA. Junctin and triadin each activate skeletal ryanodine receptors but junctin alone mediates functional interactions with calsequestrin. *International Journal of Biochemistry & Cell Biology*. 2009;41:2214-2224

134. Beard NA, Sakowska MM, Dulhunty AF, Laver DR. Calsequestrin is an inhibitor of skeletal muscle ryanodine receptor calcium release channels. *Biophysical Journal*. 2002;82:310-320

135. Terentyev D, Viatchenko-Karpinski S, Vedamoorthyrao S, Oduru S, Gyorke I, Williams SC, Gyorke S. Protein protein interactions between triadin and calsequestrin are involved in modulation of sarcoplasmic reticulum calcium release in cardiac myocytes. *The Journal of Physiology*. 2007;583:71-80

136. Zhang L, Kelley J, Schmeisser G, Kobayashi YM, Jones LR. Complex formation between junctin, triadin, calsequestrin, and the ryanodine receptor. Proteins of the cardiac junctional sarcoplasmic reticulum membrane. *Journal of Biological Chemistry*. 1997;272:23389-23397

137. Qin J, Valle G, Nani A, Chen H, Ramos-Franco J, Nori A, Volpe P, Fill M. Ryanodine receptor luminal Ca^{2+} regulation: swapping calsequestrin and channel isoforms. *Biophysical Journal*. 2009;97:1961-1970

138. Gyorke I, Hester N, Jones LR, Gyorke S. The role of calsequestrin, triadin, and junctin in conferring cardiac ryanodine receptor responsiveness to luminal calcium. *Biophysical Journal*. 2004;86:2121-2128

139. Gyorke I, Gyorke S. Regulation of the cardiac ryanodine receptor channel by luminal Ca^{2+} involves luminal Ca^{2+} sensing sites. *Biophysical Journal*. 1998;75:2801-2810

140. Lukyanenko V, Gyorke I, Gyorke S. Regulation of calcium release by calcium inside the sarcoplasmic reticulum in ventricular myocytes. *Pflügers Archiv: European journal of physiology*. 1996;432:1047-1054

141. Prakriya M, Lewis RS. Store-operated calcium channels. *Physiological Reviews*. 2015;95:1383-1436

142. Lewis RS. The molecular choreography of a store-operated calcium channel. *Nature*. 2007;446:284-287

143. Parekh AB, James W. Putney J. Store-operated calcium channels. *Physiological Reviews*. 2005;85:757-810

144. Michelucci A, García-Castañeda M, Boncompagni S, Dirksen RT. Role of STIM1/ORAI1-mediated store-operated Ca^{2+} entry in skeletal muscle physiology and disease. *Cell Calcium*. 2018;76:101-115

145. Boncompagni S, Michelucci A, Pietrangelo L, Dirksen RT, Protasi F. Exercise-dependent formation of new junctions that promote STIM1-Orai1 assembly in skeletal muscle. *Scientific Reports* 2017;7:14286

146. Zhao X, Min CK, Ko J-K, Parness J, Kim DH, Weisleder N, Ma J. Increased store-operated Ca^{2+} entry in skeletal muscle with reduced calsequestrin-1 expression. *Biophysical Journal*. 2010;99:1556-1564

147. Yarotskyy V, Protasi F, Dirksen RT. Accelerated activation of SOCE current in myotubes from two mouse models of anesthetic- and heat-induced sudden death. *PLOS One*. 2013;8:e77633-e77633

148. Faggioni M, Knollmann BC. Calsequestrin 2 and arrhythmias. *American Journal of Physiology: Heart and Circulatory Physiology*. 2012;302:H1250-1260

149. Gyorke S, Stevens SC, Terentyev D. Cardiac calsequestrin: quest inside the SR. *The Journal of Physiology*. 2009;587:3091-3094

150. Faggioni M, Kryshtal DO, Knollmann BC. Calsequestrin mutations and catecholaminergic polymorphic ventricular tachycardia. *Pediatric Cardiology*. 2012;33:959-967

151. Postma AV, Denjoy I, Hoorntje TM, Lupoglazoff JM, Da Costa A, Sebillon P, Mannens MM, Wilde AA, Guicheney P. Absence of calsequestrin 2 causes severe forms of catecholaminergic polymorphic ventricular tachycardia. *Circulation Research*. 2002;91:e21-26

152. Venetucci LA, Eisner DA. Calsequestrin mutations and sudden death: a case of too little sarcoplasmic reticulum calcium buffering? *Circulation Research*. 2008;103:223-225

153. Knollmann BC. New roles of calsequestrin and triadin in cardiac muscle. *The Journal of Physiology*. 2009;587:3081-3087

154. Baltogiannis GG, Lysitsas DN, di Giovanni G, Ciconte G, Sieira J, Conte G, Kolettis TM, Chierchia GB, de Asmundis C, Brugada P. CPVT: arrhythmogenesis, therapeutic management, and future perspectives. A brief review of the literature. *Frontiers in Cardiovascular Medicine*. 2019;6:92

155. Ackerman MJ, Priori SG, Willems S, Berul C, Brugada R, Calkins H, Camm AJ, Ellinor PT, Gollob M, Hamilton R, Hershberger RE, Judge DP, Le Marec H, McKenna WJ, Schulze-Bahr E, Semsarian C, Towbin JA, Watkins H, Wilde A, Wolpert C, Zipes DP. HRS/EHRA expert consensus statement on the state of genetic testing for the channelopathies and cardiomyopathies this document was developed as a partnership between the Heart Rhythm Society (HRS) and the European Heart Rhythm Association (EHRA). *Heart Rhythm*. 2011;8:1308-1339

156. Terentyev D, Kubalova Z, Valle G, Nori A, Vedamoorthyrao S, Terentyeva R, Viatchenko-Karpinski S, Bers DM, Williams SC, Volpe P, Gyorke S. Modulation of SR Ca release by luminal Ca and calsequestrin in cardiac myocytes: effects of CASQ2 mutations linked to sudden cardiac death. *Biophysical Journal*. 2008;95:2037-2048

157. Valle G, Galla D, Nori A, Priori SG, Gyorke S, de Filippis V, Volpe P. Catecholaminergic polymorphic ventricular tachycardia-related mutations R33Q and L167H alter calcium sensitivity of human cardiac calsequestrin. *Biochemical Journal*. 2008;413:291-303

158. Rizzi N, Liu N, Napolitano C, Nori A, Turcato F, Colombi B, Bicciato S, Arcelli D, Spedito A, Scelsi M, Villani L, Esposito G, Boncompagni S, Protasi F, Volpe P, Priori SG. Unexpected structural and functional consequences of the R33Q homozygous mutation in cardiac calsequestrin: a complex arrhythmogenic cascade in a knock in mouse model. *Circulation Research*. 2008;103:298-306

159. Dirksen WP, Lacombe VA, Chi M, Kalyanasundaram A, Viatchenko-Karpinski S, Terentyev D, Zhou Z, Vedamoorthyrao S, Li N, Chiamvimonvat N, Carnes CA, Franzini-Armstrong C, Gyorke S, Periasamy M. A mutation in calsequestrin, CASQ2D307H, impairs sarcoplasmic reticulum Ca^{2+} handling and causes complex ventricular arrhythmias in mice. *Cardiovascular Research*. 2007;75:69-78

160. Lahat H, Pras E, Olender T, Avidan N, Ben-Asher E, Man O, Levy-Nissenbaum E, Khoury A, Lorber A, Goldman B, Lancet D, Eldar M. A missense mutation in a highly conserved region of CASQ2 is associated with autosomal recessive catecholamine-induced polymorphic ventricular tachycardia in Bedouin families from Israel. *American Journal of Human Genetics*. 2001;69:1378-1384

161. Terentyev D, Nori A, Santoro M, Viatchenko-Karpinski S, Kubalova Z, Gyorke I, Terentyeva R, Vedamoorthyrao S, Blom NA, Valle G, Napolitano C, Williams SC, Volpe P, Priori SG, Gyorke S. Abnormal interactions of calsequestrin with the ryanodine receptor calcium release channel complex linked to exercise-induced sudden cardiac death. *Circulation Research*. 2006;98:1151-1158

162. Gray B, Bagnall RD, Lam L, Ingles J, Turner C, Haan E, Davis A, Yang PC, Clancy CE, Sy RW, Semsarian C. A novel heterozygous mutation in cardiac calsequestrin causes autosomal dominant catecholaminergic polymorphic ventricular tachycardia. *Heart Rhythm*. 2016;13:1652-1660

163. de la Fuente S, Van Langen IM, Postma AV, Bikker H, Meijer A. A case of catecholaminergic polymorphic ventricular tachycardia caused by two calsequestrin 2 mutations. *Pacing and Clinical Electrophysiology*. 2008;31:916-919

164. Liu QQ, Oberti C, Zhang XQ, Ke T, Zhang T, Scheinman M, Hu DY, Wang QK. [A Novel mutation of F189L in CASQ2 in families with catecholaminergic polymorphic ventricular tachycardia]. *Zhonghua Yi Xue Yi Chuan Xue Za Zhi*. 2008;25:334-337

165. Rajagopalan A, Pollanen MS. Sudden death during struggle in the setting of heterozygosity for a mutation in calsequesterin 2. *Forensic Science, Medicine and Pathology*. 2016;12:86-89

166. Landstrom AP, Dailey-Schwartz AL, Rosenfeld JA, Yang Y, McLean MJ, Miyake CY, Valdes SO, Fan Y, Allen HD, Penny DJ, Kim JJ. Interpreting incidentally identified variants in genes associated with catecholaminergic polymorphic ventricular tachycardia in a large cohort of clinical whole-exome genetic test referrals. *Circulation: Arrhythmia and Electrophysiology*. 2017;10

167. Wong CH, Koo SH, She GQ, Chui P, Lee EJ. Genetic variability of RyR2 and CASQ2 genes in an Asian population. *Forensic Science International*. 2009;192:53-55

168. Kirchhefer U, Wehrmeister D, Postma AV, Pohlentz G, Mormann M, Kucerova D, Muller FU, Schmitz W, Schulze-Bahr E, Wilde AA, Neumann J. The human CASQ2 mutation K206N is associated with hyperglycosylation and altered cellular calcium handling. *Journal of Molecular and Cellular Cardiology*. 2010;49:95-105

169. Laitinen PJ, Swan H, Kontula K. Molecular genetics of exercise-induced polymorphic ventricular tachycardia: identification of three novel cardiac ryanodine receptor mutations and two common calsequestrin 2 amino-acid polymorphisms. *European Journal of Human Genetics*. 2003;11:888-891

170. Basaki M, Asasi K, Tabandeh MR, Aminlari M. Polymorphism identification and cardiac gene expression analysis of the calsequestrin 2 gene in broiler chickens with sudden death syndrome. *British Poultry Science*. 2016;57:151-160

171. Neubauer J, Lecca MR, Russo G, Bartsch C, Medeiros-Domingo A, Berger W, Haas C. Post-mortem whole-exome analysis in a large sudden infant death syndrome cohort with a focus on cardiovascular and metabolic genetic diseases. *European Journal of Human Genetics*. 2017;25:404-409

Chapter 2: Identification of two pools of IRE1α in cardiac and skeletal muscle cells

2.1 Abstract

The endoplasmic reticulum (ER) plays a central role in cellular stress responses via mobilization of ER stress coping responses, such as the unfolded protein response. The inositol-requiring enzyme 1α (IRE1α) is an ER stress sensor and component of the unfolded protein response. Muscle cells also have a well-developed and highly subspecialized membrane network of smooth ER, called SR - surrounding myofibrils and specialized for Ca^{2+} storage, release, and uptake - to control muscle E-C coupling. Here we describe two distinct pools of IRE1α in cardiac and skeletal muscle cells, one localized at the perinuclear ER and the other at the junctional SR. We discovered that, at the junctional SR, calsequestrin binds to IRE1α inhibiting its dimerization. This novel interaction of IRE1α with calsequestrin, one of the highly abundant Ca^{2+} handling proteins at the junctional SR, provides new insights into the regulation of stress coping responses in muscle cells.

2.2 Introduction

Stress responses are central to cellular physiology and pathology and failure to adapt to stress leads to cell death. To mitigate cellular stress and re-establish homeostasis cells must activate stress coping response mechanisms[1-3]. In cells, including muscle cells, the ER plays a central role in cellular stress responses via mobilization of one of the stress coping responses, such as the UPR. The UPR involves three unique ER transmembrane signaling proteins: the inositol-requiring 1 (IRE1), ER kinase dsRNA-activated protein kinase-like ER kinase (PERK), and activating transcription factor 6 (ATF6)[1, 4, 5]. Activation of ER stress-induced UPR signaling pathways result in translational attenuation, transcriptional activation of genes encoding proteins involved in protein folding, and transcriptional activation of genes for components of the ERAD pathway[1, 4, 5]. Under optimal conditions IRE1, PERK and ATF6 are maintained in an inactive state by binding to BiP, an ER chaperone. Upon stress, BiP dissociates from these proteins resulting in activation of UPR signaling pathways[1, 5]. IRE1α is the most evolutionary conserved ER stress sensor and component of the UPR[6]. The protein has endoribonuclease activity that splices the mRNA encoding the transcription factor XBP1 to produce the stable form of the transcription factor that induces the expression of genes involved in many aspects of the protein secretory pathway, including protein folding, ERAD, and protein quality control [7].

In muscle cells, the ER is responsible for cellular housekeeping functions, among which are the synthesis, folding, posttranslational modification, and transport of proteins; the synthesis of lipids and steroids; the assembly and trafficking of membranes; stress signaling, and signaling to the nucleus, cytoplasm, mitochondria, and plasma membrane[8-10]. Muscle cells also have a well-developed and highly specialized membrane network of smooth ER, called SR, surrounding myofibrils[11, 12]. The SR is specialized for Ca^{2+} storage, release and uptake, to control muscle E-C coupling[13]. The SR luminal Ca^{2+} binding proteins, calsequestrin, histidine-rich Ca^{2+}-binding protein, junctate, and sarcalumenin, are responsible for Ca^{2+} storage, while ryanodine receptor/Ca^{2+} release channel (RyR) is responsible for Ca^{2+} release to trigger muscle contraction. Sarcoplasmic/endoplasmic reticulum Ca^{2+} ATPase (SERCA) pumps Ca^{2+} back to the lumen of the SR, driving muscle relaxation. Additionally, the SR forms two distinct regions in the muscle: the longitudinal SR which is enriched with the SERCA pump, and the junctional SR where the RyR and calsequestrin are localized[14, 15]. Calsequestrin is involved in binding and storing Ca^{2+} and it comprises approximately 27% by mass of all junctional SR proteins[16]. Two isoforms of calsequestrin exist and are encoded by two different genes: cardiac muscle calsequestrin (Casq2) and skeletal muscle calsequestrin (Casq1)[17, 18]. The crystal structures of cardiac and skeletal muscle calsequestrin indicates that the proteins contain three thioredoxin-like domains reminiscent of ER luminal oxidoreductases[19].

Disruption of ER functions triggers ER stress and activation of IRE1α[1, 20]. In skeletal muscle, the IRE1α is activated during exercise[20], starvation[21], and a high fat diet[22]. Activation of IRE1α and other branches of the UPR pathway have been implicated in many cardiovascular diseases including hypoxia, ischemia/reperfusion, hypertrophy, pressure overload, and drug-induced insults[1, 23]. Previous studies have shown that inhibition of IRE1α signaling protects the heart from cardiac fibrosis[24] and atherosclerosis[25]. How IRE1α signaling is regulated in the muscle by the SR luminal environment is not known. Understanding the molecular organization of IRE1α and events controlling its activation in skeletal and cardiac muscle is necessary to assess the connection between muscle stress coping response and cellular pathophysiology[1]. In this study we report that there are two pools of IRE1α in cardiac and skeletal muscle cells, one localized to perinuclear ER, and the other at the junctional SR, a site of Ca^{2+} release for myofilament activation. We also discovered that calsequestrin binds to the ER luminal domain of IRE1α and prevents its dimerization, and this may serve to squelch the activation of IRE1α at the junctional SR.

2.3 Materials and Methods

2.3.1 Plasmids and site-specific mutagenesis

The mammalian expression vector encoding human IRE1-NLD (luminal domain of IRE1α) cDNA in pED plasmid was generous gift from Dr. Randall Kaufman[26]. The triple cysteine mutant of the IRE1-NLD, (C109,148,332A) was described previously[27]. The cDNA encoding full-length or truncated (Δ350-390 and Δ316-390) canine cardiac muscle calsequestrin (Casq2) lacking the signal sequence was cloned into pET22b vector to generate pET-Casq2 or pET-Casq2 (Δ350-390 and Δ316-390) for bacterial expression of the protein. The following expression vectors were used in this study: pcDNA3.1 expression vector containing cDNA encoding full-length Casq2, C-terminus truncation of Casq2 (Δ350-390), and C-terminus plus partial thioredoxin domain III truncation of Casq2 (Δ316-390) for mammalian cell transfection[28].

2.3.2 Adenovirus construction

Mammalian expression vector containing cDNA encoding red fluorescence protein (RFP) fused to full length mouse IRE1α was generated using ER-RFP (generous gift from Dr. Erik Snapp) and pcDNA3.1(+) mouse full length IRE1α plasmid (generous gift from Dr. Ko Miyoshi). EcoRI and NotI restriction enzyme sites were introduced by PCR. cDNA of full-length mouse IRE1α with the signal sequence omitted was cloned into ER-RFP expression vector with the C1-GFP backbone at the C-terminus of RFP. Short and flexible linker sequences, encoding the amino acid sequence GGSGEFGGSG, were added between the RFP and IRE1α coding sequences. cDNA of RFP-IRE1α was cloned and packed into adenovirus by Vector Biolabs, USA.

2.3.3 Protein purification

The ER luminal domain of IRE1α (IRE1-NLD) and IRE1-NLD cysteine triple mutant (C109,148,332A) were expressed in COS-1 cells and purified by Ni-NTA agarose chromatography[26, 27]. COS-1 cells were transfected with a vector containing cDNA encoding IRE1-NLD or IRE1-NLD cysteine mutant using turboFect transfection reagent (ThermoFisher, R0531), harvested, and lysed in a buffer containing 25 mM Tris-Cl, pH 8.0, 150 mM NaCl, and 1% NP-40. Cell lysates were centrifuged at 16,000 xg for 30 min at 4^{o}C, and supernatant was processed for protein purification. Ni-NTA-agarose affinity chromatography was performed by following the manufacture's protocol (QIAGEN Cat #30230) under native conditions in a binding

buffer containing 50 mM NaH_2PO_4, 500 mM NaCl, and 10 mM imidazole, pH 8.0[27]. The IRE1-NLD or IRE1-NLD cysteine triple mutant proteins were eluted with 250 mM imidazole[27].

Native cardiac muscle calsequestrin (Casq2) and skeletal muscle calsequestrin (Casq1) proteins were purified from pig hearts and rabbit skeletal muscle, respectively[29, 30]. In brief, 200-250 g of muscle was homogenized in a buffer containing 0.1 M KH_2PO_4, pH 7.1, 1 mM EDTA, and 2.66 M ammonium sulfate (65% saturation) followed by ammonium sulfate (85% saturation) precipitation, DEAE chromatography with a column buffer containing 50 mM NaCl, 0.1 M KH_2PO4, 1 mM EDTA, pH7.1. The protein was eluted at 300 to 400 mM NaCl. Eluted fractions containing calsequestrin were pooled and subjected to phenyl Sepharose CL-4B chromatography with a column buffer containing 50 mM NaCl, 0.1 M KH_2PO4, 1 mM EDTA, pH7.1[29, 30]. Calsequestrin containing fractions were eluted from phenyl Sepharose CL-4B with a buffer containing 10 mM $CaCl_2$[29, 30]. Fractions containing calsequestrin were pooled and stored at -80ºC in a buffer containing 50 mM HEPES, pH 7.4, 150 mM KCl, 500 µM $CaCl_2$, and 250 µM EGTA. All procedures were carried out at 4ºC, and all buffers contained a cocktail of protease inhibitors[31]. Full-length recombinant Casq2, and truncated Casq2 were expressed in *E. coli* BL21 (DE3) cells (Invitrogen) and purified with Ni-NTA affinity column chromatography following the manufacture's protocol (QIAGEN Cat #30230).

2.3.4 Microscale thermophoresis

Microscale thermophoresis analyses were carried out using a Monolith NT.115 instrument (Nano Temper Technologies, Germany) or Monolith NT.LabelFree instrument (Nano Temper Technologies, Germany). Proteins were labeled using the Monolith NT Protein Labeling Kit RED-NHS (Nano Temper Technologies, cat# MO-C030) following manufacture's protocol. All experiments were carried out at room temperature in standard capillaries (Nano Temper Technologies, cat# MO-K022, for fluorescence labeled IRE1-NLD or IRE1-NLD cysteine triple mutant) or in hydrophobic capillaries (Nano Temper Technologies, cat# MO-K025, for fluorescence labeled calsequestrin) with 20% LED power (fluorescence lamp intensity) and 40% microscale thermophoresis power (IR-laser intensity). The assay buffer contained 50 mM HEPES, pH 7.4, 150 mM KCl, 500 µM $CaCl_2$, 250 µM EGTA, 0.05% Tween-20, and 2.5% glycerol. $CaCl_2$ and EGTA concentrations were adjusted to obtain the desired free Ca^{2+} concentration: 80 µM (350 µM $CaCl_2$ and 850 µM EGTA), 125 µM (175 µM $CaCl_2$ and 50 µM EGTA), 1000 µM (1100 µM

$CaCl_2$ and 100 µM EGTA). Free Ca^{2+} concentration was calculated using the Ca-EGTA Calculator TS v1.3 web tool[32].

Ca^{2+} binding to full-length Casq2 or Casq2 truncated were carried out using Monolith NT.LabelFree instrument in standard capillaries (Nano Temper Technologies, cat# MO-Z022) with 20% LED power and 40% microscale thermophoresis power. The proteins were incubated for 10 min in a buffer containing 50 mM HEPES, pH 7.4, 150 mM KCl, 0.1% pluronic F-127, and 50 µM EGTA. An increasing concentration of $CaCl_2$ (0.01-20 mM, in 50 mM HEPES, pH 7.4, 150 mM KCl) was used. All microscale thermophoresis data were analyzed by Monolith Affinity Analysis v2.2.6 software.

2.3.5 Surface plasmon resonance analysis

Surface plasmon resonance (SPR) was performed to monitor the interaction between IRE1-NLD and calsequestrin (BIACore, GE Life Sciences). The CM5 chip was activated using a 1:1 dilution of 1-ethyl-3-(3-dimethylaminopropyl) carbodiimide:N-hydroxysuccinimide (EDC:NHS) as previously described[27]. Purified IRE1-NLD protein was diluted in 10 mM sodium acetate, pH 5, injected over the activated CM5 chip, and captured at a flow rate of 5 µl/min to a total of ~2000 Response Units (RU). Uncoupled amine reactive sites on the CMD surface were then blocked by an injection of 1 M ethanolamine, pH 9.0. An uncoupled reference lane was generated to subtract background binding. The running buffer was composed of 10 mM HEPES, pH 7.2, 150 mM KCl, 1 mM EDTA, and 0.005% surfactant P20. Purified IRE1-NLD triple cysteine mutant protein[27] was coupled to a CM5 chip to a total of ~1500 RU followed by addition of increasing concentration of calsequestrin (10000 nM - 39 nM). For each measurement, the signal was corrected against the control surface response to eliminate any refractive index changes due to buffer change. The data was collected at 25°C at a flow rate of 30 µl/min to minimize mass transfer effects. Kinetic analysis was performed using the BiaEvaluation software (GE Life Sciences) with a 1:1 Langmuir binding model. Association and dissociation rates and affinity (K_d) were calculated for each experiment and averaged. The binding response signal in RUs was continuously recorded and presented graphically as a function of time. All experiments and analysis were conducted on a BIACore T200 instrument (GE Life Sciences).

2.3.6 Immunoprecipitation

COS-1 cells were co-transfected with pED-IRE1-NLD-6His expression vector and pcDNA3.1 expression vector containing cDNA encoding full-length Casq2 or truncated Casq2 using TurboFect transfection reagent (ThermoFisher, R0531). At 48 hours after transfection, cells were washed and harvested into 600 µl of the lysis buffer containing 50 mM HEPES, pH7.4, 200 mM NaCl, 2% CHAPS, and a mixture of protease inhibitors. The lysate was incubated on ice for 30 min and centrifuged at 13,000 xg for 15 min at 4°C. Two µl of antibodies [control immunoglobulin G, or mouse anti-6xHis (ThermoFisher,MA1-21315), or rabbit anti-calsequestrin (Abcam ab3516)] were added to supernatant and mixture was incubated overnight at 4°C with rotation. A 10% slurry of protein A/G Sepharose CL-4B beads (100 µl) was added, and mixture were incubated for an additional 4 hours with rotation at 4°C. Beads were pelleted and washed three times with a buffer containing 50 mM HEPES, pH 7.4, 200 mM NaCl, 1% CHAPS; and then once with a buffer containing 50 mM HEPES, pH 7.4, 200 mM NaCl. Pellets were re-suspended in 30 µl of SDS-PAGE sample buffer and loaded on an SDS-PAGE followed by immunoblot analysis with mouse anti-6xHis or rabbit anti-calsequestrin antibodies, and then with goat anti-mouse (Millipore, AP200P) or mouse anti-rabbit light chain specific horseradish peroxidase-conjugated polyclonal antibodies.

2.3.7 Skeletal muscle immunohistochemistry

For histological analysis, paraffin sections of rabbit hind leg muscle were prepared and processed by the Alberta Diabetes Institute HistoCore Facility at the University of Alberta. Heat-induced epitope retrieval was used to break potential protein cross-linking during fixation. Tissue sections were heated in 10 mM sodium citrate, pH 6.0, at 90-95ºC for 20 min. Sections were permeabilized with 0.1% Triton X-100 in phosphate-buffered saline (PBS) for 5 min at room temperature, then blocked with a solution containing 5% bovine serum albumin (BSA) and 2% normal goat serum in PBS. Sections were incubated with primary antibodies (diluted in blocking buffer) for 18 hours, washed with PBS, and incubated with Alexa Fluor 488 conjugated goat anti-rabbit IgG (ThermoFisher A11034, 1:200), or Alexa Fluor 546 conjugated goat anti-mouse IgG antibodies (ThermoFisher A11003, 1:200). Sections were washed with PBS and mounted with Prolong Diamond Antifade Mountant (Thermo Fisher Scientific, P36961), and visualized using a Leica TCS SP5 confocal microscope with Leica inverted DMI 6000 B microscope base. Images

were acquired with oil immersion objectives 40X/numerical aperture (NA) 1.25 or 100X/numerical aperture (NA) 1.44 at 22.5°C. For Alexa Fluor 488 visualization (detects rabbit anti-RyR, anti-IRE1α, and anti-obscurin antibodies), the argon laser was used with excitation at 488 nm and emission peak at 525 nm. For Alexa Fluor 546 (detects mouse anti-RyR, anti-α-actinin, and anti-Casq1 antibodies), the HeNe laser was used with excitation at 543 nm and emission peak at 573 nm. The following primary antibodies were used: rabbit anti-ryanodine receptor antibodies[33] at 1:500 dilution, mouse anti-ryanodine receptor 1 antibodies[34] at 1:200 dilution, rabbit anti-IRE1α antibodies (Abcam, ab37073) at 1:200 dilution, rabbit anti-obscurin antibodies (Abcam, ab121652) at 1:2500, mouse anti-α-actinin antibodies (Sigma, A7811) at 1:800 dilution, mouse anti-Casq1 VIIID1-2C monoclonal antibodies at 1:40 dilution[35] (generous gift from K.P. Campbell). Skeletal muscle sections were also stained with DAPI (ThermoFisher 62248) and FITC (Fluorescein isothiocyanate) conjugated Concanavalin A (1:50). Images were acquired with Leica Application Suite Advanced Fluorescence (Leica LAS-AF) microscopy software, exported as Leica Image File format (LIF) and processed using ImageJ software (https://imagej.net/Fiji/Downloads) with 8 bit image type.

Overlap of IRE1α with calsequestrin or ryanodine receptor signals was analyzed using ImageJ software (https://imagej.net/Fiji/Downloads). A straight line was drawn along the triad (junctional SR + T-tubule) at the longitudinal axis of muscle fiber and identified as a region of interest (ROI). The fluorescence signal intensity of each channel (green for Alexa Fluor 488, red for Alexa Fluor 546) for each immunostained section was calculated using corresponding ROI and the values were plotted along the X axis (distance in μm) to identify regions of overlap.

2.3.8 Cardiomyocyte isolation and immunostaining

Ventricular myocytes from GFP-RyR2 knock-in mice[36] were isolated using retrograde aortic perfusion as described previously[37]. Freshly isolated cells were collected by centrifugation; reintroduced with Ca^{2+} (0.5 mM); re-suspended in minimum essential medium (MEM) (Invitrogen) supplemented with 0.2% fetal bovine serum, insulin (1 μg/ml), transferrin (0.55 μg/ml), selenium (0.5 ng/ml), penicillin (100 U/ml), streptomycin (100 μg/ml), 2 mM glutamine, 4 mM $NaHCO_3$, 10 mM HEPES, pH 7.4, and 10 μM blebbistatin; plated on glass coverslips pre-coated with laminin (50 μg/ml); and cultured in 5% CO_2 at 37°C in 6-well dishes. After 4-6 hours, unattached myocytes were gently removed by PBS wash, and fresh culture media was added to

the wells. The IRE1α encoding adenovirus was added to the culture media at a MOI 1000. Culture media was changed every day. After 5 days in culture, the coverslips were gently washed with PBS and mounted on an inverted Nikon A1R scanning confocal microscope system equipped with a Nikon 60X/numerical aperture (NA) 1.2 Plan-Apochromat water immersion objective and selective excitation and emission filters. Excitation light was provided by argon (488 nm; Coherent Sapphire) and yellow diode (561 nm; Coherent Sapphire) lasers to detect GFP ($Excitation_{Max}$ 488 nm/$Emission_{Max}$ 510 nm) and IRE1α abundance ($Excitation_{Max}$ 581 nm/$Emission_{Max}$ 644 nm) in cardiomyocytes. Basic image processing and spectral fluorescence un-mixing for co-detection and analysis of GFP and IRE1α fluorescence signals were performed using the NIS Elements AR 4.13 software (Nikon).

2.3.9 Mouse embryonic fibroblasts confocal

Ern1$^{-/-}$ mouse embryonic fibroblasts (IRE1α-deficient cells) and wild-type mouse embryonic fibroblasts (both a generous gift from Dr. Randal Kaufman) were fixed with 3.7% paraformaldehyde (Electron Microscopy Sciences 15710) and 0.1% Glutaraldehyde for 12 min at 37ºC. Cells were permeabilized with 0.05% Saponin diluted in PBS, washed with PBS, blocked with 5% goat normal serum in PBS with 0.05% saponin for 1 hour, followed by incubation with anti-IRE1α antibodies (Abcam, ab37073) at 1:200 dilution and Alexa Fluor 488 conjugated goat anti-rabbit IgG (ThermoFisher A11034, 1:200). Slides were mounted with Prolong Diamond Antifade Mountant (Thermo Fisher Scientific, P36961), and visualized with a Leica TCS SP5 confocal microscope.

2.3.10 Subcellular fractionation

SR membrane fractions were isolated from rabbit skeletal muscle as previously described[38]. In brief, the hind leg muscle was collected from New Zealand white rabbits (1-3 kg weight), the muscle was homogenized in buffer containing 250 ml of 300 mM sucrose, 5 mM imidazole-HCl, pH 7.4. The homogenate was centrifuged at 7,700 xg for 10 min at 4°C. The supernatant was saved, and the pellets were re-homogenized with the same buffer. The supernatants from both homogenates were combined and centrifuged. The microsomal pellet (containing longitudinal and terminal cisternae of SR vesicles) was obtained by centrifugation of the low speed supernatant for 90 min at 110,000 xg, at 4°C. The microsomal pellet was re-suspended in homogenization buffer and layered onto a sucrose gradient consisting of 45% (weight/weight) sucrose (1.6 M), 38%

sucrose (1.3 M), 32% sucrose (1.1 M), and 27% sucrose (0.8 M) in 5 mM imidazole-HCl, pH 7.4. The gradient was centrifuged overnight at 70,000 xg for 90 min, at 4°C. The membrane fractions at the interfaces between the gradients were collected and diluted with 5 mM imidazole-HCl, pH 7.4, followed with centrifugation at 125,000 xg for 2 hours, at 4°C. The pellets were re-suspended in homogenization buffer and stored at -80°C until use.

Two hundred µl of each fraction obtained from the sucrose gradient was further fractionated with the OptiPrep system (Sigma-Aldrich), an iodixanol-based density gradient for subcellular organelle separation and isolation. OptiPrep (60% iodoxanol in water) were diluted to 25%, 22%, 19%, 16%, 10%, 7%, and 5% (% iodoxanol) in a homogenization buffer containing 10 mM HEPES, pH 7.4, 250 mM sucrose, 1 mM EDTA, and 1 mM EGTA. The OptiPrep gradient was centrifuged at 184,501 xg in a SW55 Ti swinging bucket rotor for 6 hours. Twelve fractions (300 µl per fraction) were collected from the top of gradient followed by incubation overnight at -20°C. 1.2 ml of 90% acetone was used to precipitate proteins. Precipitated proteins were centrifuged at 16,100 xg for 10 min at 4°C. The pellets were washed with 200 µl of 100% ethanol and re-centrifuged at 16,100 xg for 10 min at 4°C. The final pellets were dissolved in 100 µl of SDS-PAGE sample buffer containing 40 mM Tris, pH 6.8, 1% SDS, 5% glycerol, 0.0003% Bromophenol blue, 50 mM DTT followed by SDS-PAGE and immunoblot analyses.

2.3.11 IRE1α cross-linking

The homobifunctional protein cross linker disuccinimidyl suberate (DSS) (Thermo Scientific Pierce, cat#:21555) was dissolved in DMSO at a final concentration of 10 mM. His-IRE1-NLD was diluted to a final concentration of 3.6 µM in a reaction buffer containing 50 mM HEPES, pH 7.4, 150 mM NaCl, 250 µM EGTA, 500 µM $CaCl_2$, 0.05% Tween-20, 5% Glycerol. Casq2 was added to a final concentration of 18 µM (1 to 5 molar ratio, IRE1-NLD to Casq2). Mixtures were incubated with 20-fold molar excess of DSS for 1 hour at 22.5°C. The reaction was then quenched for 15 min with 100 mM Tris pH 7.4 followed by SDS-PAGE (12% acrylamide). Proteins were transferred to nitrocellulose membrane follow by immunoblotting with mouse anti-6xHis antibodies (ThermoFisher, MA1-21315).

2.3.12 Statistical analysis

Statistical analysis was performed using GraphPad Prism version 7.0. The Student's t-test was used to compare the mean of two independent groups, and one-way Anova was used to compare the mean of three or more independent groups, with a *p*-value determined to be significant if less than 0.05.

2.4 Results

2.4.1 IRE1α is localized to the junctional SR and perinuclear space in skeletal muscle and cardiomyocytes

We examined the intracellular distribution of IRE1α, an ER stress coping response sensor and signaling molecule[1, 20-22], to address its molecular organization and regulation in muscle cells. Anti-RyR1 and anti-Casq1 (skeletal muscle calsequestrin isoform) antibodies were used as markers of the junctional SR membrane[39], and anti-obscurin antibodies, a sarcomeric protein localized to the M-line[40], as a marker for the region occupied by the longitudinal SR. As expected, RyR1 and calsequestrin were co-localized to the junctional SR (Figure 2-1A)[41] but not to the longitudinal SR stained with anti-obscurin antibodies (Figure 2-1C). Next, we used anti-IRE1α antibodies (Figure 2-2) to localize IRE1α in muscle cells. Surprisingly, we discovered IRE1α positive staining in the junctional SR that overlapped with anti-calsequestrin staining (Figure 2-1B). This was in addition to the anticipated IRE1α positive staining in the nuclear envelope and the perinuclear region containing ER membrane network (Figure 2-1D), a cellular region lacking any detectable staining for both calsequestrin and RyR1 (Figure 2-1D). Perinuclear region ER was identified using FITC conjugated Concanavalin A staining, a lectin binds specifically to high mannose N-glycans[42] (Figure 2-3).

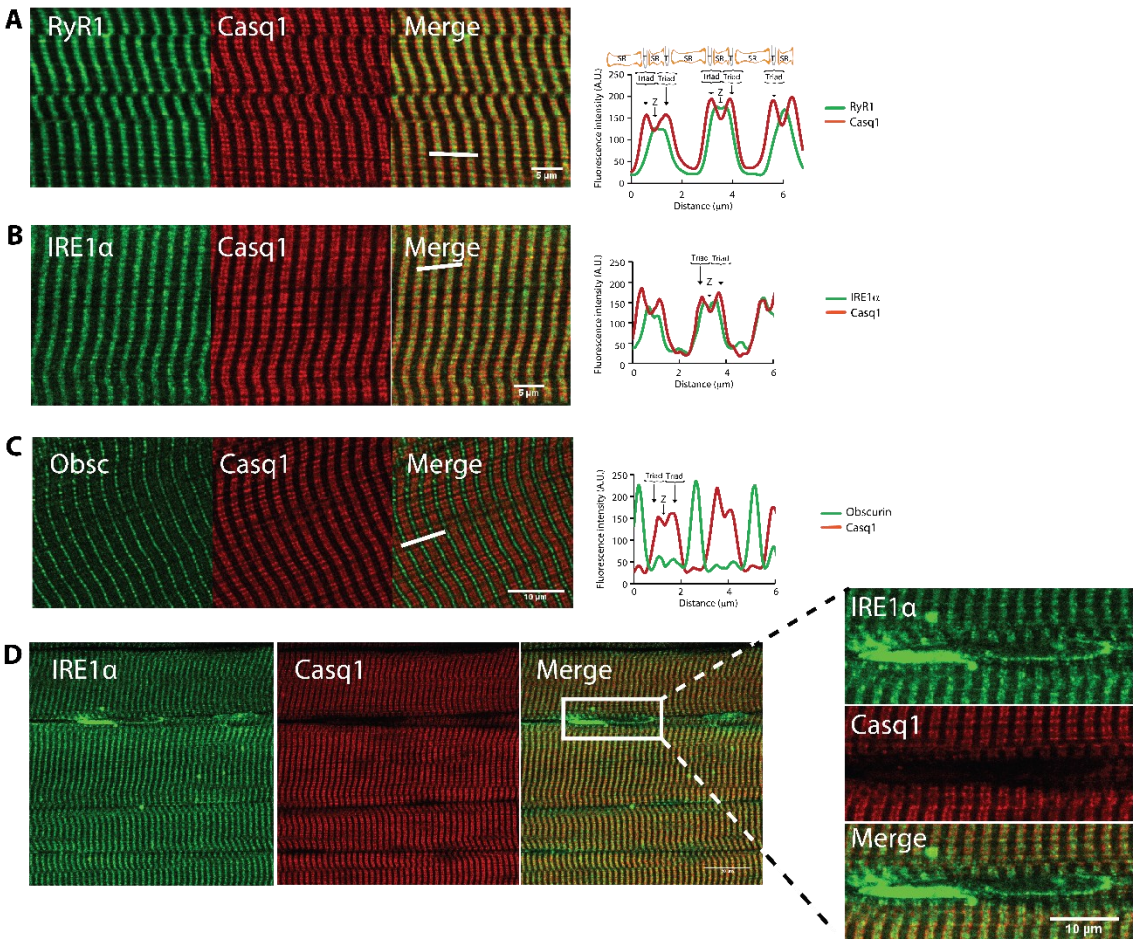

Figure 2-1. Immunolocalization of IRE1α in skeletal muscle.

A) Immunostaining longitudinal sections of skeletal muscle with antibodies against RyR1 or Casq1. Right panel, graphic representation of overlap between RyR1 and Casq1. The white bars indicate the scanned area represented in the graphs. Location of the triad (T) (junctional SR + T-tubule membrane) and the Z line are indicated in the graphs.

B) Immunostaining of skeletal muscle sections with anti-obscurin antibodies (Obsc) indicating the location of the M-band or with anti-calsequestrin antibodies (Casq1). The white bars indicate the scanned area represented in the graphs.

C) Immunostaining of skeletal muscle with antibodies against IRE1α or Casq1. Right panel, graphic representation of overlap between IRE1α and Casq1. The white bars indicate the scanned area represented in the graphs.

D) Immunostaining of IRE1α and Casq1 in the perinuclear region of skeletal muscle. Right panel shows a large magnification of the perinuclear space section indicated by the rectangle.

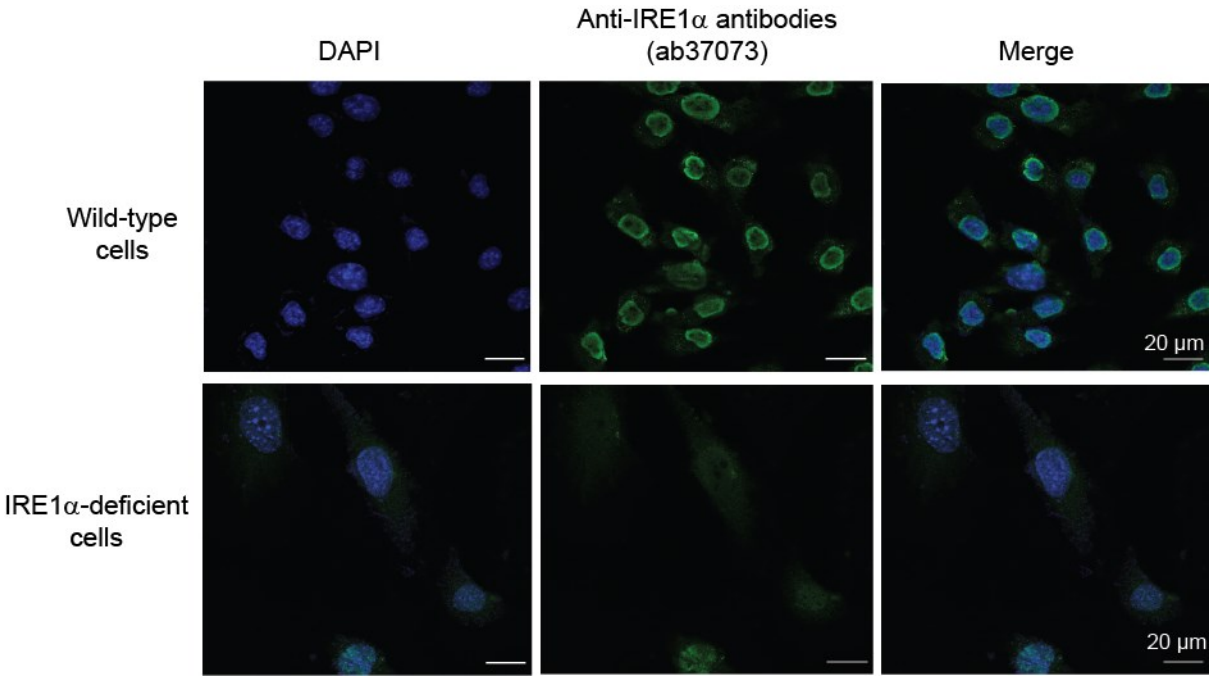

Figure 2-2. Immunostaining of wild-type and IREα-deficient mouse embryonic fibroblasts.

To determine the specificity of anti-IRE1α antibodies, wild-type and *Ern1*$^{-/-}$ mouse embryonic fibroblasts (IRE1α-deficient cells) were probed with anti-IRE1α antibodies (Abcam, ab37073) and visualized using a Leica TCS SP5 confocal microscope. IREα-deficient cells show minimum to no signal when stained with anti-IRE1α antibodies compare with wild-type confirming the specificity of anti-IRE1α antibodies to recognize IRE1α.

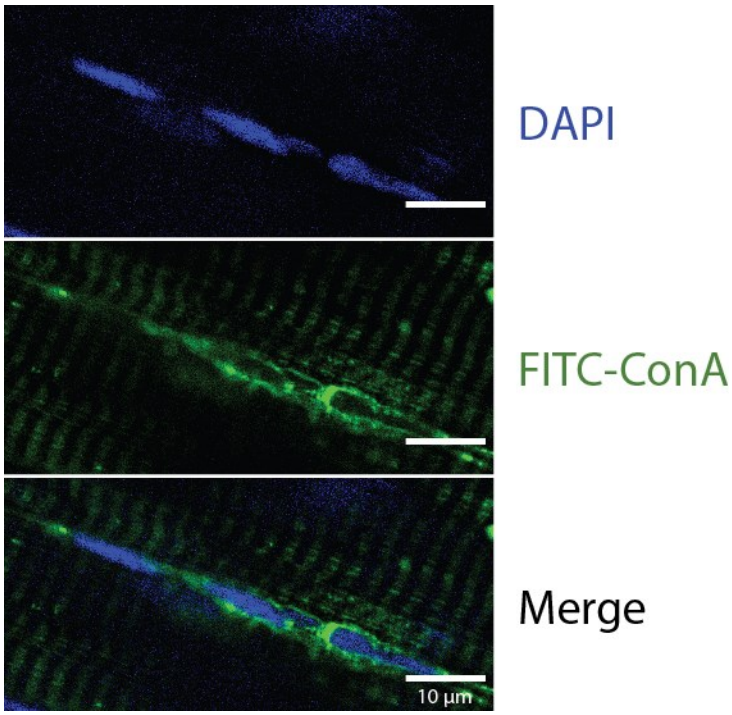

Figure 2-3. Perinuclear ER-like membrane network in skeletal muscle.

Longitudinal sections of skeletal muscle were stained with fluorescein isothiocyanate (FITC) conjugated Concanavalin A (FITC-ConA) and 4',6-diamidino-2-phenylindole (DAPI).

Next, we examined IRE1α localization in isolated cardiomyocytes that express green fluorescent protein (GFP) tagged-RyR2[36]. Similar to the skeletal muscle (Figure 2-1), IRE1α co-localized with RyR2 in the cardiac junctional SR (Figure 2-4) and was detected in the nuclear envelope and perinuclear ER membrane region, which did not show any detectable RyR2 signal (Figure 2-4). Thus, we concluded that both skeletal and cardiac muscle cells contained two pools of IRE1α, one localized at the perinuclear region and the other at the junctional SR containing calsequestrin and RyR1 (or RyR2).

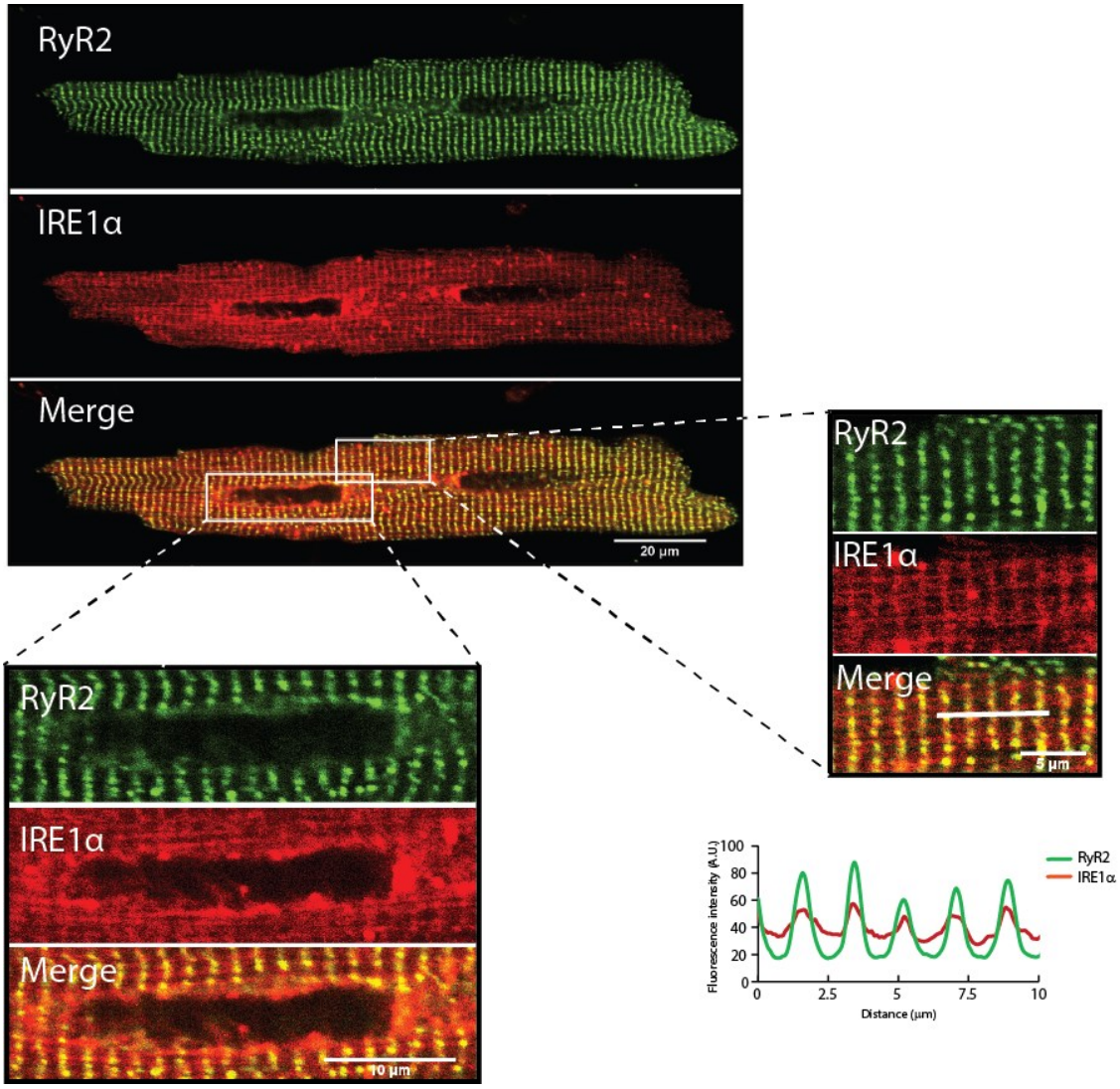

Figure 2-4. IRE1α in isolated cardiomyocytes.

Isolated rat cardiomyocytes from green fluorescence protein tagged ryanodine receptor (RyR2) knock-in transgenic mice[36] were transduced with adenovirus packed with the red fluorescent protein tagged IRE1α (IRE1α). Large magnification of the sarcomere and perinuclear areas are shown as indicated by the boxes. Graphic representation of overlap between RyR2 and IRE1α is shown. The white bars indicate the scanned area represented in the graphs.

2.4.2 The luminal domain of IRE1α interacts with calsequestrin, an SR junctional protein

Previously, the ER resident oxidoreductase PDIA6 was identified as an IRE1α binding protein that modulates IRE1α activity[27 43]. Calsequestrin contains three thioredoxin domains[19] typical for ER resident oxidoreductases[44]. Therefore, we asked whether in muscle cells calsequestrin can also form complexes with IRE1α at the junctional SR. To evaluate this, tissue purified skeletal (Casq1) and cardiac (Casq2) muscle calsequestrin and recombinant His-tagged cardiac muscle calsequestrin Casq2 (Figure 2-5A) were tested for direct binding to the ER luminal domain of IRE1α (IRE1-NLD). Using microscale thermophoresis, we discovered that native skeletal muscle Casq1 bound to IRE1-NLD with a K_d of 698 nM (Figure 2-5B). Both native Casq2 and recombinant His-tagged cardiac muscle calsequestrin (Casq2) also bound to IRE1-NLD with a K_d of 2 μM (Figure 2-5C,D). Calreticulin was used as a negative control and showed no binding to IRE1-NLD (Figure 2-5E).

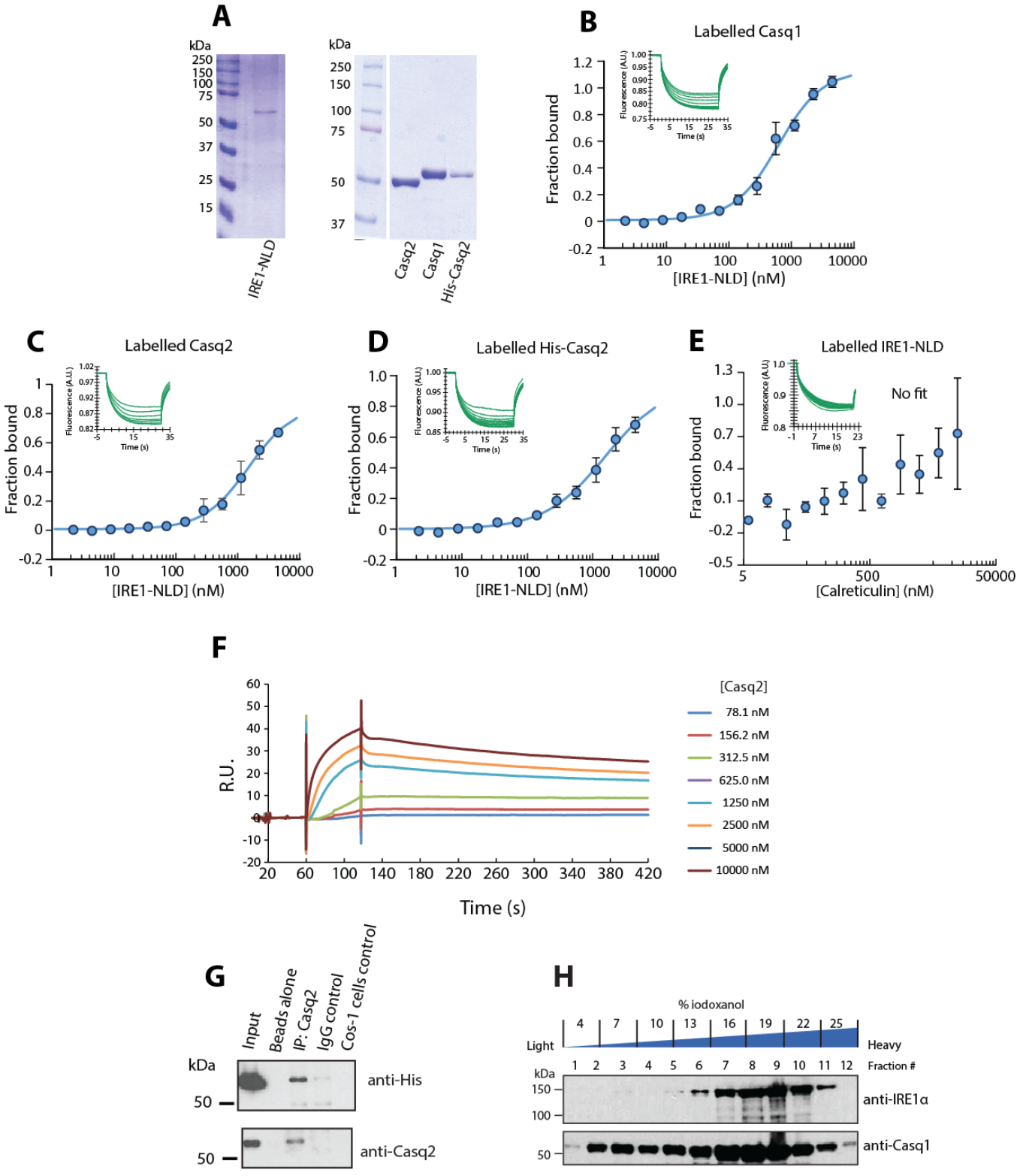
A
kDa
250
150
100
75
50
37
25
15
IRE1-NLD
kDa
250
150
100
75
50
37
Casq2
Casq1
His-Casq2
B
Labelled Casq1
Fraction bound
[IRE1-NLD] (nM)
C
Labelled Casq2
Fraction bound
[IRE1-NLD] (nM)
D
Labelled His-Casq2
Fraction bound
[IRE1-NLD] (nM)
E
Labelled IRE1-NLD
No fit
Fraction bound
[Calreticulin] (nM)
F
R.U.
Time (s)
[Casq2]
78.1 nM
156.2 nM
312.5 nM
625.0 nM
1250 nM
2500 nM
5000 nM
10000 nM
G
Input
Beads alone
IP: Casq2
IgG control
Cos-1 cells control
kDa
50
anti-His
50
anti-Casq2
H
% iodoxanol
4
7
10
13
16
19
22
25
Light
Heavy
1 2 3 4 5 6 7 8 9 10 11 12
Fraction #
kDa
150
100
anti-IRE1α
50
anti-Casq1

Figure 2-5. Calsequestrin (Casq1 and Casq2) binds to the ER luminal domain of IRE1α.

A) SDS-PAGE analysis of proteins used for microscale thermophoresis.

B) Casq1 protein was covalently labeled with a red fluorescent tag and incubated with increasing amounts of the purified IRE1-NLD protein followed by microscale thermophoresis. Each data point is the mean of 3 independent microscale thermophoresis measurements.

C) Fluorescently labeled native Casq2 protein was incubated with increasing amounts of purified IRE1-NLD protein followed by microscale thermophoresis. Each data point is the mean of 3 independent microscale thermophoresis measurements; error bars represent the standard error mean.

D) Recombinant Casq2 protein was covalently labeled with a red fluorescent tag and incubated with increasing amounts of purified IRE1-NLD protein followed by microscale thermophoresis. Each data point is the mean of 6 independent microscale thermophoresis measurements. Normalized microscale thermophoresis time traces are shown in graphs B–D.

E) Calreticulin does not bind to IRE1α luminal domain. Luminal domain of IRE1α (IRE1-NLD) was covalently labeled with a red fluorescent tag and incubated with increasing amounts of purified calreticulin followed by microscale thermophoresis. Normalized microscale thermophoresis time traces are shown above. Each data point is the average of three independent microscale thermophoresis measurements.

F) IRE1-NLD was immobilized on a CM5 chip followed by flow of increasing concentrations of Casq2 as indicated in the figure and analyzed by SPR.

G) His-tagged ER luminal domain of IRE1α (IRE1-NLD) and Casq2 were expressed in COS-1 cells followed by immunoprecipitation with anti-His antibodies or IgG control. Immunoblot analysis was carried out with anti-His or anti-Casq2 antibodies. Immunoprecipitation experiments were performed in triplicate with representative blot shown.

H) Iodixanol-based density gradient (OptiPrep) gradient fractionation of heavy SR vesicles (junctional SR) followed by immunoblot analysis with anti-IRE1α and anti-calsequestrin (Casq1). A.U., arbitrary units; R.U., relative units.

We used surface plasmon resonance (SPR) and immunoprecipitation techniques to further examine Casq2-IRE1α interactions (Figure 2-5F, G). SPR analysis revealed that cardiac muscle calsequestrin interacted with the luminal domain of IRE1α in a concentration-dependent manner (Figure 2-5F). Next, His-tagged IRE1-NLD and Casq2 were expressed in COS-1 cells followed by immunoprecipitation with anti-Casq2 antibodies (Figure 2-5G). Full-length Casq2 co-immunoprecipitated with His-tagged IRE1-NLD (Figure 2-5G). Finally, Opti-Prep gradient fractionation of heavy SR vesicles (enriched in junctional SR) showed that calsequestrin and IRE1α were enriched in the fractions containing heavy SR vesicles representing the junctional SR (Figure 2-5H, fractions #6-11). These findings demonstrated that IRE1α co-localized with Casq1 and Casq2 at the junctional SR and that calsequestrin formed complexes with the ER luminal domain of IRE1α.

There are three cysteine residues in IRE1-NLD (i.e., Cys^{109}, Cys^{148}, and Cys^{332})[45] that are essential for binding of the oxidoreductase PDIA6 to IRE1α [27]. Since calsequestrin contains three thioredoxin domains[19], typical for ER resident oxidoreductases [44], we asked whether the cysteine residues in IRE1α were involved in the binding of calsequestrin. Mutation of three cysteines in the ER luminal domain of IRE1α did not have any effect on calsequestrin binding to IRE1-NLD as measured by microscale thermophoresis (Figure 2-6A) nor by BIACore (Figure 2-6B) techniques, indicating that calsequestrin binding to the IRE1α luminal domain did not involve cysteine residues.

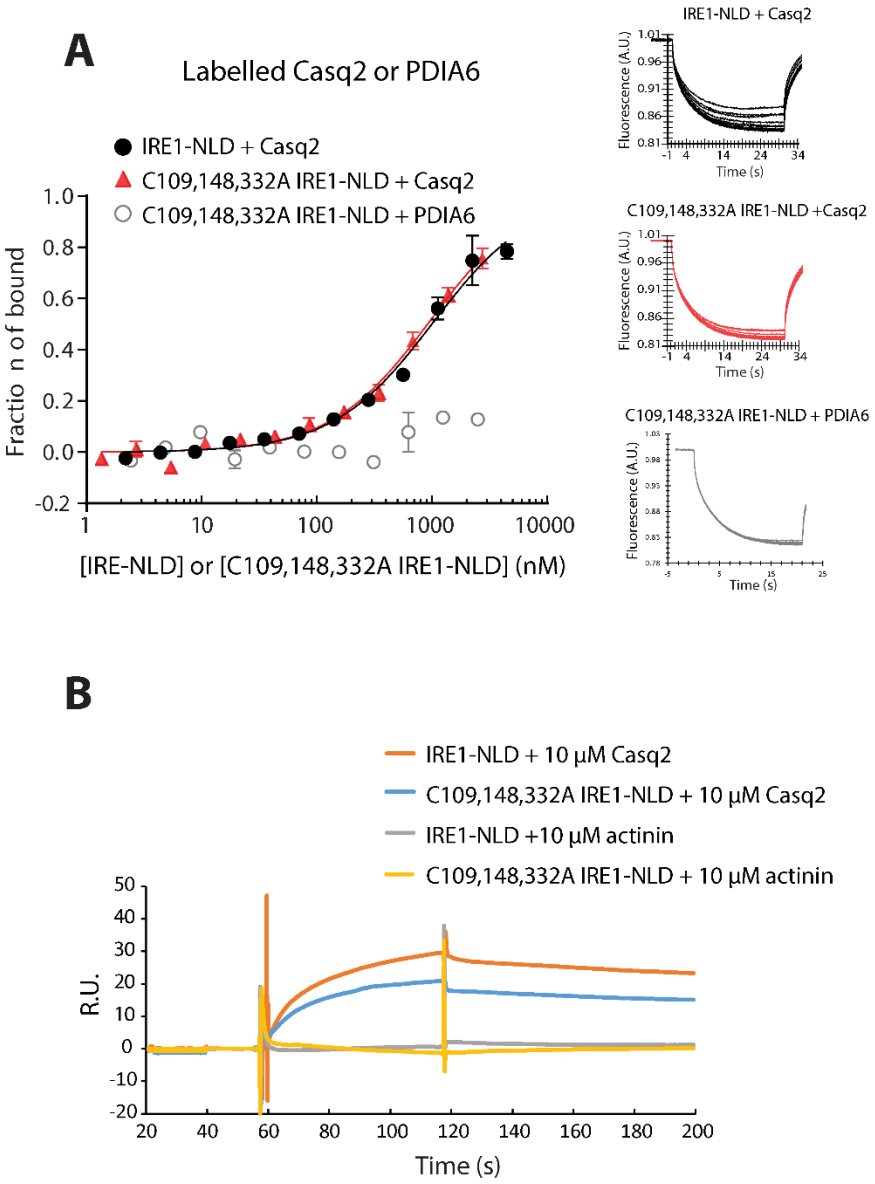

Figure 2-6. Calsquestrin binding to the IRE1α is independent of cysteine residues.

A) cardiac muscle calsequestrin (Casq2) protein was covalently labeled with a red fluorescent tag and incubated with increasing amounts of N-terminus luminal domain of IRE1α (IRE1-NLD) or IRE1-NLD triple cysteine mutant (C109, 148, 332A IRE1-NLD) protein followed by microscale thermophoresis. Covalently labeled PDIA6 binding to the IRE1-NLD triple cysteine mutant was used as a control[27]. Normalized microscale thermophoresis time traces are shown to the right of the graph. Each data point is the mean of 3 independent microscale thermophoresis measurements.

B) Casq2 was injected over immobilized IRE1-NLD or immobilized C109, 148, 332A IRE1-NLD. α-Actinin was used as a negative control.

Finally, we asked whether binding of calsequestrin to the IRE1α luminal domain was sensitive to changes in Ca^{2+} concentration. Microscale thermophoresis analysis indicated that complex formation between native Casq2 or recombinant Casq2 and the luminal domain of IRE1α was independent of Ca^{2+} at concentrations ranging from 80 to 1000 µM (Figure 2-7).

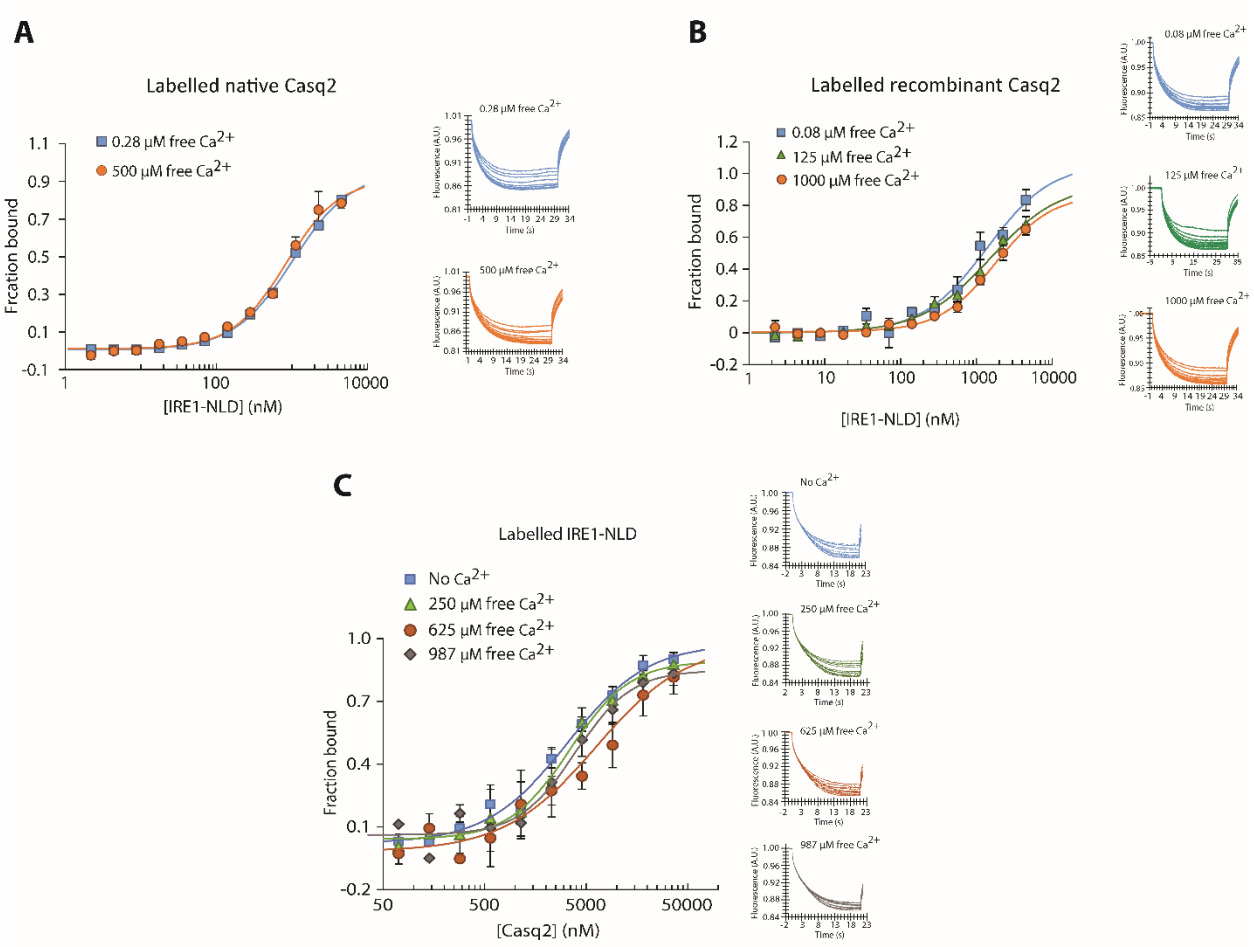

Figure 2-7. Calsequestrin-IRE1-NLD interaction in the presence of Ca^{2+}.

A) Native cardiac muscle calsequestrin (Casq2) protein was covalently labeled with a red fluorescent tag and incubated in the presence of different Ca^{2+} concentrations as indicated in the Figure followed by microscale thermophoresis analysis.

B) Labeled recombinant cardiac muscle calsequestrin protein was incubated with increasing Ca^{2+} concentrations as indicated in the Figure followed by microscale thermophoresis.

C) Fluorescent labeled N-terminus luminal domain of IRE1α (IRE1-NLD) protein was incubated with native cardiac Casq2 and increasing Ca^{2+} concentrations as indicated in the Figure followed by microscale thermophoresis. Normalized time traces are shown in the graph. Normalized microscale thermophoresis time traces are shown to the right of the graphs. Each data point is the average of three independent microscale thermophoresis measurements.

2.4.3 Mapping of calsequestrin binding to IRE1α

Structurally, in addition to the three thioredoxin domains, Casq2 contains an acidic C-terminal domain[19], a site of high capacity Ca^{2+} binding[46, 47]. To map the region of Casq2 protein involved in binding to IRE1α, we expressed in *E. coli* and purified two Casq2 truncated proteins (Figure 2-8A) then analyzed their ability to bind Ca^{2+} and the ER luminal domain of IRE1α. As expected, full-length calsequestrin bound Ca^{2+} with a K_d value of 1 mM (Figure 2-8B). The Casq2 Δ350-390 protein, missing the 41 C-terminal acidic amino acid residues (Figure 2-8C), exhibited Ca^{2+} binding with a K_d value similar to that seen for a full-length protein (Figure 2-8B). In contrast, Casq2 Δ316-390 protein, containing only 11 acid amino acid residues of the third thioredoxin domain, showed no measurable Ca^{2+} binding (Figure 2-8D).

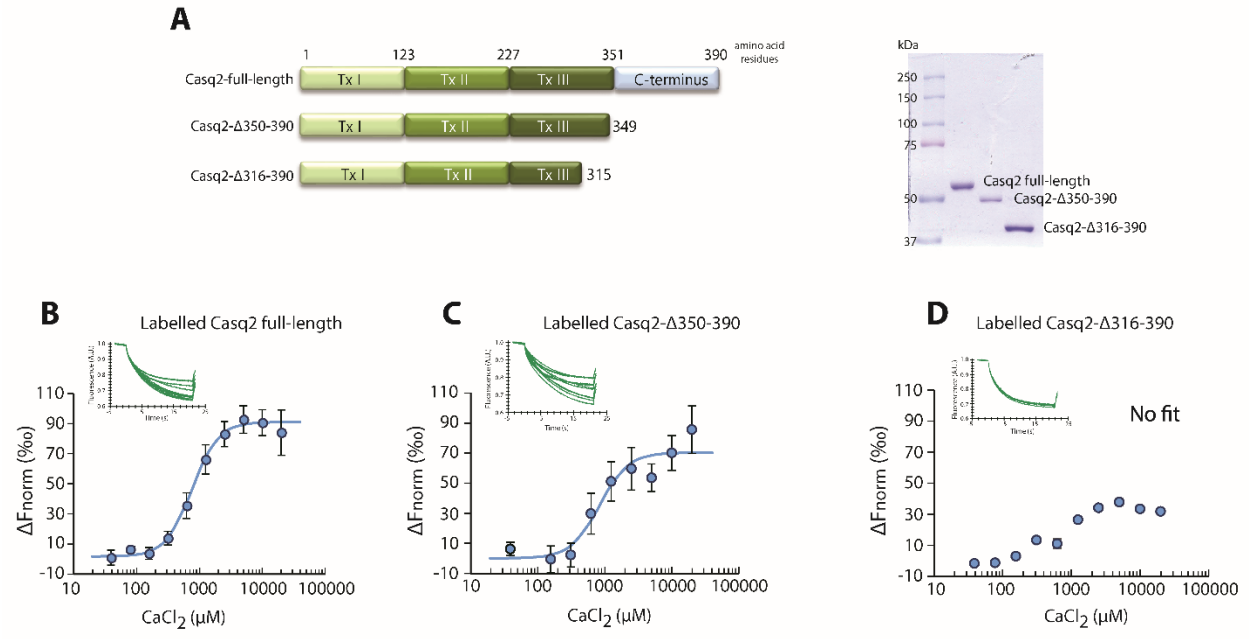

Figure 2-8. Ca^{2+} binding to cardiac muscle calsequestrin.

A) Schematic representation of truncated calsequestrin protein used for label free microscale thermophoresis analysis shown in panels B, C and D. The C-terminus truncations of cardiac muscle calsequestrin with deleted residues 350 to 390 (Casq2 Δ350-390) or residues 316 to 390 (Casq2 Δ316-390). Right panel: Coomassie blue stained SDS-PAGE of purified full-length and truncated recombinant cardiac muscle calsequestrin used for microscale thermophoresis analysis.

B, C, D) Recombinant cardiac muscle calsequestrin (B), residues 350 to 390 truncated calsequestrin (Casq2 Δ350-390) (C) or residues 316 to 390 truncated protein (Casq2 Δ316-390) (D) were incubated with increasing concentration of Ca^{2+}. Each data point is the average of three to six independent microscale thermophoresis measurements.

We used microscale thermophoresis analysis to test whether truncated cardiac muscle calsequestrin could bind to the ER luminal domain of IRE1α. Calsequestrin truncated at the C-terminal acidic region (Casq2-Δ350-390) bound to the IRE1-NLD (Figure 2-9A). Deletion of an additional 34 amino acid residues (Casq2-Δ316-390) resulted in loss of binding to IRE1-NLD (Figure 2-9B). This was supported by co-immunoprecipitation experiments showing that both full-length cardiac muscle calsequestrin and Casq2-Δ350-390 expressed in COS-1 cells were efficiently pulled-down with His-IRE1-NLD (Figure 2-9C) whereas Casq2-Δ316-390 was not (Figure 2-9C). Thus, we concluded that the last 34 amino acid residues in the third thioredoxin domain of calsequestrin that forms two short α-helices and two short β-strands of calsequestrin (Figure 2-9D) were important for binding of Casq2 to the ER luminal domain of IRE1α.

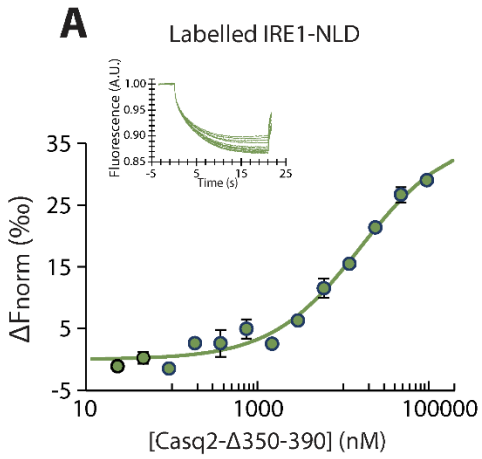
A
Labelled IRE1-NLD
Fluorescence (A.U.)
Time (s)
ΔFnorm (‰)
[Casq2-Δ350-390] (nM)

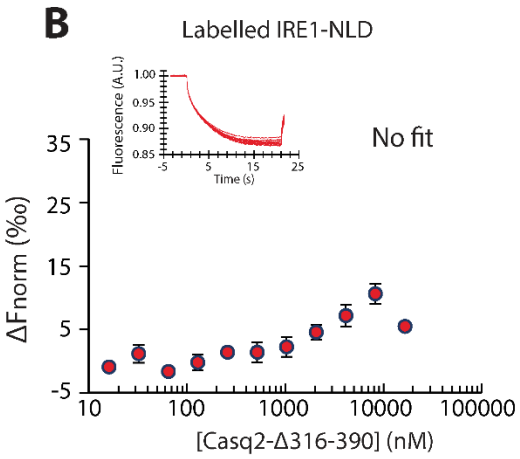
B
Labelled IRE1-NLD
No fit
Fluorescence (A.U.)
Time (s)
ΔFnorm (‰)
[Casq2-Δ316-390] (nM)

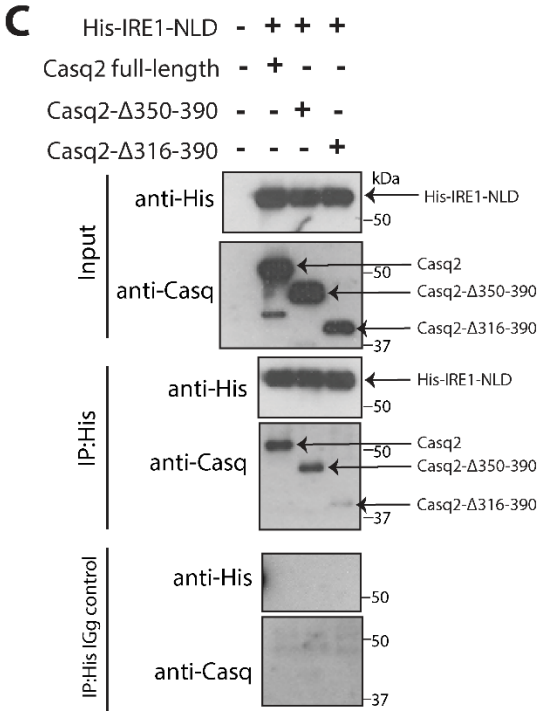
C
His-IRE1-NLD
Casq2 full-length
Casq2-Δ350-390
Casq2-Δ316-390
kDa
anti-His
anti-Casq
Input
IP:His
IP:His IGg control
His-IRE1-NLD
Casq2
Casq2-Δ350-390
Casq2-Δ316-390

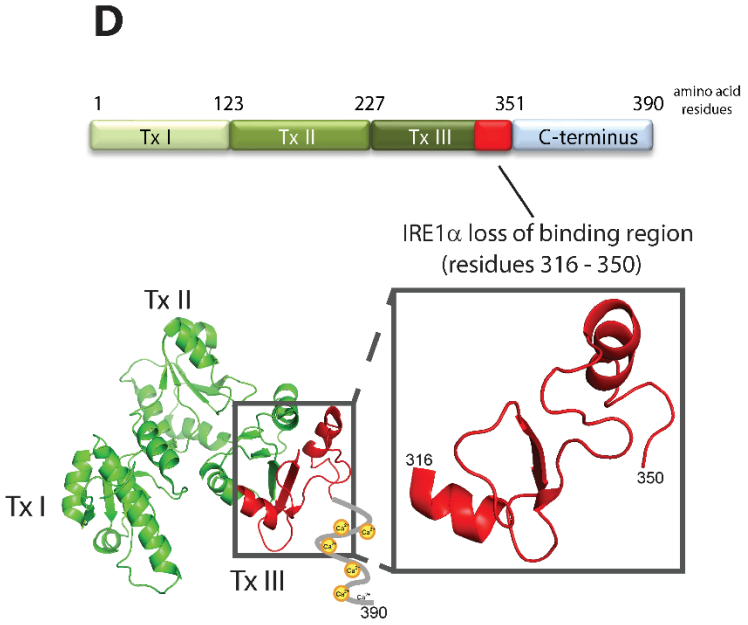
D
Tx I
Tx II
Tx III
C-terminus
amino acid residues
IRE1α loss of binding region
(residues 316 - 350)
316
350
390

Figure 2-9. Mapping of cardiac muscle calsequestrin binding to IRE1α.

A) Labeled N-terminus domain of IRE1α (IRE1-NLD) was incubated with increasing concentrations of truncated cardiac muscle calsequestrin (Casq2Δ350–390) followed by microscale thermophoresis analysis. Normalized time traces are shown on the top of the graph.

B) Recombinant IRE1-NLD protein was covalently labeled with a red fluorescent tag and incubated with increasing amounts of residues 316–390–truncated Casq2 (Casq2 Δ316–390) followed by microscale thermophoresis analysis. Normalized time traces are shown on the top of the graph.

C) His-tagged ER IRE1-NLD (His-IRE1-NLD) and full-length or truncated (Casq2Δ350–390 or Casq2Δ316–390) Casq2 were expressed in COS-1 cells followed by immunoprecipitation with anti-His antibodies or IgG control. Immunoblot analysis was carried out with anti-His or anti-Casq2 antibodies. Immunoprecipitation experiments were performed in triplicate with a representative blot shown. The location of full-length, Δ316–390 and Δ350–390 calsequestrin is indicated by the arrows. A.U., arbitrary units; ΔFnorm, normalized fluorescence unit, 1000 × [Fnorm(bound) – Fnorm(unbound)]; R.U., relative units.

D) A model of the third thioredoxin-like domain in cardiac muscle calsequestrin binding to the ER luminal domain of IRE1α binding. Schematic representation of the cardiac muscle calsequestrin with red labeled 316-350 region of the Δ316-390 protein. Tx, thioredoxin domains. PDB ID: 2VAF.

2.4.4 Calsequestrin prevents dimerization of IRE1α via interaction with the IRE1a luminal domain

The dimerization and oligomerization of the IRE1α luminal domain brings the cytosolic domains of IRE1α into close proximity[48-50]. The process reconstitutes IRE1α endoribonuclease activity, which is a key step in the activation of the IRE1α branch of the UPR pathway[48-50]. Based on our findings, we hypothesized that the binding of calsequestrin to IRE1α interferes with IRE1α dimerization. To test this hypothesis, we developed an IRE1α dimerization assay using microscale thermophoresis (Figure 2-10) and carried out an IRE1α dimerization/cross-linking assay. In the absence of calsequestrin, IRE1-NLD underwent dimerization with increasing concentrations of IRE1-NLD (Figure 2-11A, B, green traces). Strikingly, in the presence of either native (Figure 2-11A) or recombinant (Figure 2-11B) cardiac muscle calsequestrin, the dimerization of IRE1α cytosolic domains was not detected. To further understand how calsequestrin prevented the oligomerization of the luminal domain of IRE1α, we carried out the dimerization/cross-linking analysis of IRE1α in the absence or presence of calsequestrin. Upon addition of cross-linker, there was a substantial decrease in IRE1α monomers and the corresponding appearance IRE1α dimers and tetramers (Figure 2-11C). In agreement with the microscale thermophoresis analysis, there was a large proportion of IRE1α protein remaining in monomeric form in the presence of Casq2, consistent with the reduced formation of IRE1α multimers (Figure 2-11C). Taken together, these findings demonstrate that the binding of calsequestrin to the luminal domain of IRE1α impeded oligomerization of IRE1α.

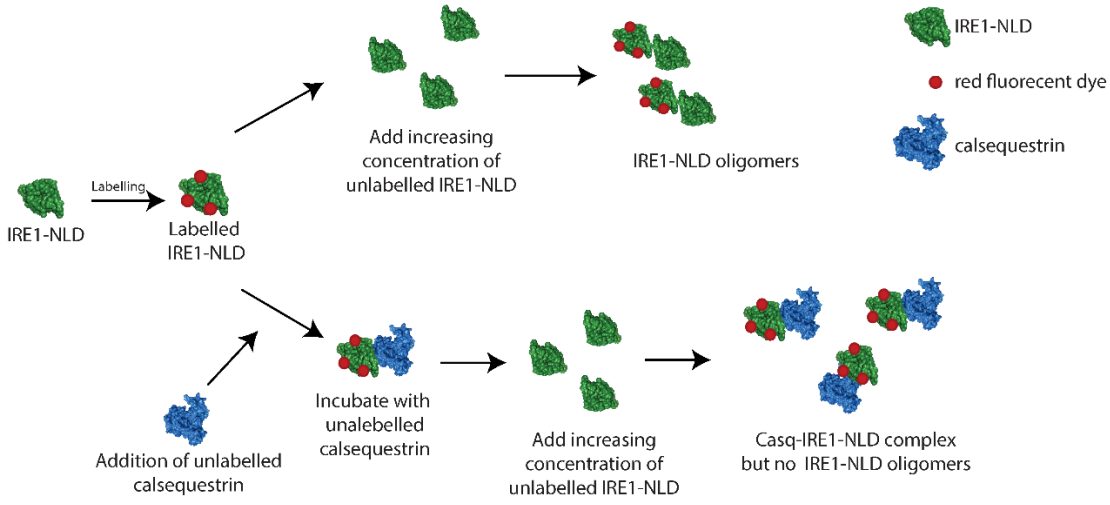

Figure 2-10. Schematic representation of the IRE1α dimerization assay.

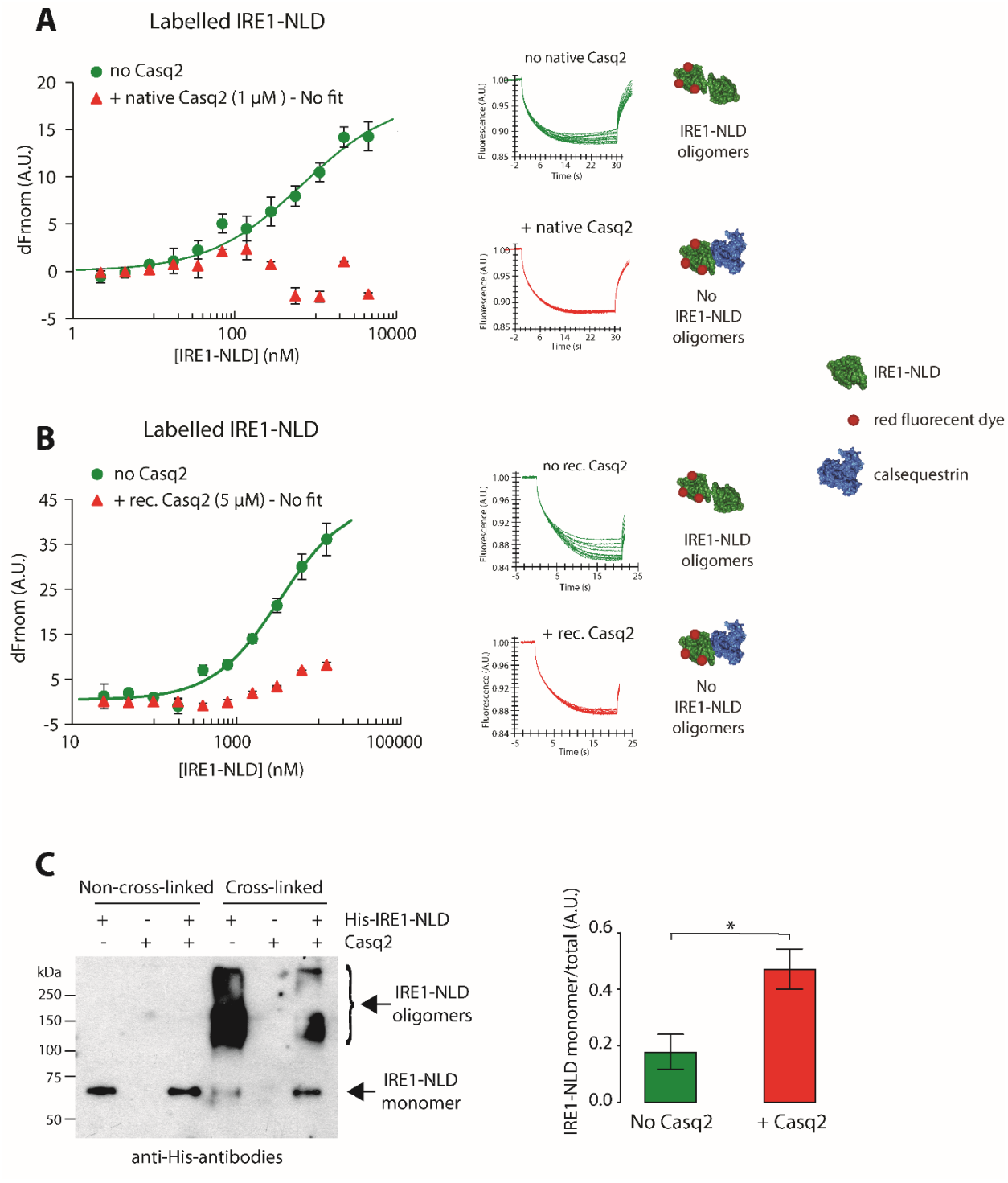
A
Labelled IRE1-NLD
no Casq2
+ native Casq2 (1 µM) - No fit
dFrnom (A.U.)
[IRE1-NLD] (nM)
no native Casq2
Fluorescence (A.U.)
Time (s)
IRE1-NLD oligomers
+ native Casq2
No IRE1-NLD oligomers
IRE1-NLD
red fluorecent dye
calsequestrin
B
Labelled IRE1-NLD
no Casq2
+ rec. Casq2 (5 µM) - No fit
dFrnom (A.U.)
[IRE1-NLD] (nM)
no rec. Casq2
Fluorescence (A.U.)
Time (s)
IRE1-NLD oligomers
+ rec. Casq2
No IRE1-NLD oligomers
C
Non-cross-linked
Cross-linked
His-IRE1-NLD
Casq2
kDa
250
150
100
75
50
IRE1-NLD oligomers
IRE1-NLD monomer
anti-His-antibodies
IRE1-NLD monomer/total (A.U.)
No Casq2
+ Casq2
*

Figure 2-11. Calsequestrin prevents IRE1α dimerization.

A) Fluorescent-labeled IRE1-NLD was incubated with increasing concentrations of unlabeled IRE1-NLD in the absence (no Casq2) or presence (+ Casq2) of native Casq2 followed by microscale thermophoresis analysis. Normalized microscale thermophoresis time traces are shown to the right of the graph. Each data point is the mean of 3 independent microscale thermophoresis measurements.

B) Recombinant IRE1-NLD protein was covalently labeled with a red fluorescent tag and incubated with increasing concentration of unlabeled IRE1-NLD in the absence (no recombinant Casq2) or presence (+ recombinant Casq2) of recombinant Casq2 followed by microscale thermophoresis. Normalized time traces are shown to the right of the graph. Each data point is the mean of 3 independent microscale thermophoresis measurements.

C) Cross-linking of IRE1-NLD in the absence and presence of Casq2 was carried out as described in Materials and Methods. The abundance of IRE1-NLD monomer relative to the total IRE1-NLD is shown in the graph; n = 3. *p = 0.0307.

2.5 Discussion

In eukaryotic cells, including muscle cells, the ER is responsible for many basic cellular processes such as stress responses, protein synthesis and folding, synthesis of lipids and sterols, storage and release of intracellular Ca^{2+}, and signaling to the nucleus, mitochondria, and plasma membrane[1, 9, 51]. In cardiomyocytes and skeletal muscle cells, many of the ER housekeeping functions are the responsibility of the perinuclear rough/smooth ER[52]. The ER of muscle is further structurally and functionally subspecialized into longitudinal and junctional SR, instrumental in the regulation of E-C coupling to facilitate muscle mechanical functions[53, 54], but less involved with respect to cellular processes traditionally associated with the ER[52]. In this study, we discovered that there are two pools of IRE1α, one in the perinuclear area corresponding to the ER-like network of intracellular membrane and the second one at the junctional SR. This specialized region of the SR membrane network (Figure 2-12) is enriched in RyR/Ca^{2+} release channel and Ca^{2+} binding and buffering protein calsequestrin, and the site of Ca^{2+} release for myofilament activation[13-15]. Importantly, we discovered that at the junctional SR the luminal domain of IRE1α interacts with calsequestrin preventing IRE1α oligomerization. The binding of IRE1α to calsequestrin at the junctional SR may represent a unique strategy for squelching IRE1α signaling under physiological conditions when junctional SR experiences repeated fluctuations of SR Ca^{2+} concentration. This strategy might serve to insulate IRE1α signaling and function in SR, leaving IRE1α in the perinuclear ER to remain responsive to cellular stress and to activate UPR independent of the constant fluctuations in Ca^{2+} concentration that occur in the SR.

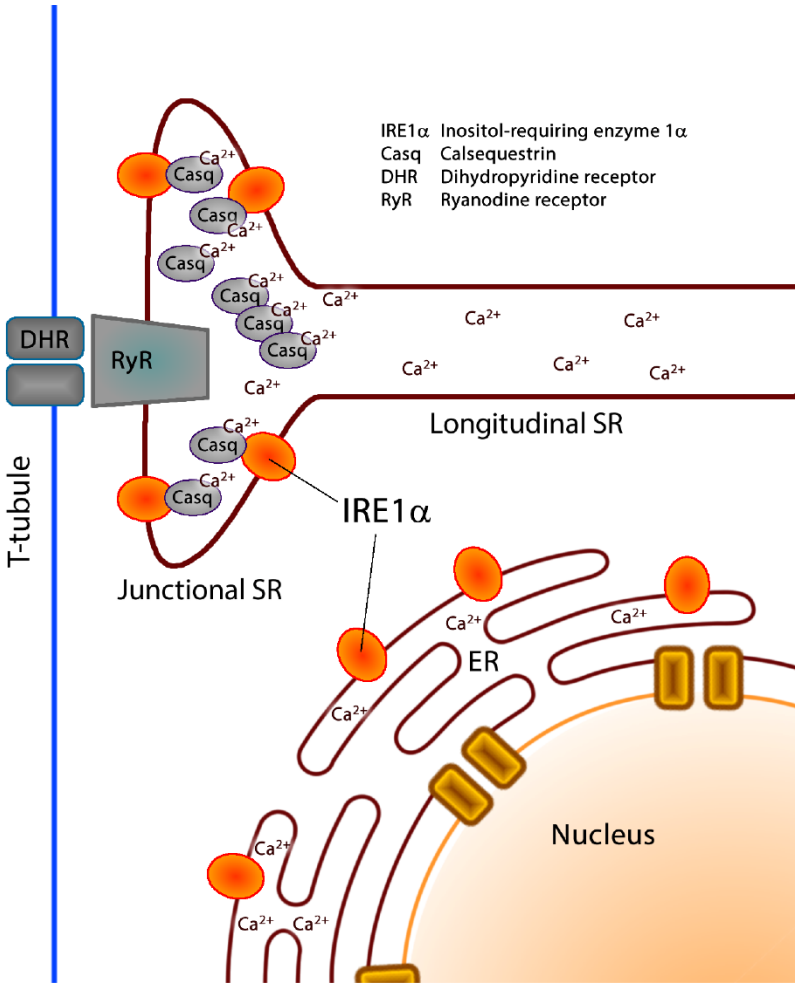

Figure 2-12. A schematic representation of two pools of IRE1α in muscle SR or ER.

In muscle ER, the membrane network is organized into a perinuclear ER and a highly specialized smooth ER called SR[52]. IRE1α is found in the perinuclear area corresponding to the ER-like network of intracellular membrane and at the junctional SR that is enriched in the RyR and Ca^{2+} release channel and Ca^{2+} binding protein calsequestrin and is the site of Ca^{2+} release for myofilament activation.

Several proteins have been identified as components of junctional SR to support Ca^{2+} release to trigger muscle contraction, e.g., RyR/Ca^{2+} release channel, and the Ca^{2+} storage proteins calsequestrin, junctin, triadin, junctate, junctophilins and mitsugumin 56[14]. Calsequestrin interacts with RyR, triadin, and junctin in the junctional SR, and regulates RyR activity[18, 55-60]. Binding of calsequestrin to STIM1 has also been observed in non-muscle cells with forced overexpression of calsequestrin, and this interaction suppresses store-operated Ca^{2+} entry[61]. Calsequestrin binding to triadin, junctin, and STIM1 involves the C-terminal acidic high capacity Ca^{2+} binding domain of the protein. This site is independent from binding of calsequestrin to IRE1α since the deletion of

the calsequestrin C-terminal high capacity Ca^{2+} binding domain (Δ350-390) had no effect on the interaction between the truncated calsequestrin and IRE1α luminal domain.

It is apparent that IRE1α signaling involves interaction with different proteins (including phosphatases, kinases, apoptosis-related proteins and the cytoskeleton) that modulate its activity through binding to its cytoplasmic domain[1, 62, 63]. It is well documented that in non-excitable cells BiP binds IRE1α directly inhibiting its activity under non-stress conditions, and dissociates from IRE1α to trigger its activity when ER stress is induced[49, 64-66]. However, deletion of the BiP binding domain of IRE1α does not cause constitutive IRE1α kinase activity[67, 68], indicating there is additional complexity in BiP-dependent regulation of IRE1α. PDIA6, an oxidoreductase and ER luminal resident protein, has also been identified as an IRE1α binding partner[27, 43] and modulator of IRE1α activity[27], and more recently, Hsp47[69] and COX-2[70] were identified as a regulator of IRE1α. Here we show that calsequestrin is a novel IRE1α interaction partner that constitute the complex regulatory network controlled by IRE1α, one that is specialized at the junctional SR in the muscle.

2.6 References

1. Groenendyk J, Agellon LB, Michalak M. Coping with endoplasmic reticulum stress in the cardiovascular system. *Annual Review of Physiology*. 2013;75:49-67
2. Cao SS, Kaufman RJ. Endoplasmic reticulum stress and oxidative stress in cell fate decision and human disease. *Antioxidants & Redox Signaling*. 2014;21:396-413
3. Dicks N, Gutierrez K, Michalak M, Bordignon V, Agellon LB. Endoplasmic reticulum stress, genome damage, and cancer. *Frontiers in Oncology*. 2015;5:11
4. Wang M, Kaufman RJ. Protein misfolding in the endoplasmic reticulum as a conduit to human disease. *Nature*. 2016;529:326-335
5. Hetz C, Papa FR. The Unfolded Protein Response and Cell Fate Control. *Molecular Cell*. 2018;69:169-181
6. Hollien J. Evolution of the unfolded protein response. *Biochimica et Biophysica Acta (BBA) - Molecular Cell Research*. 2013;1833:2458-2463
7. Acosta-Alvear D, Zhou Y, Blais A, Tsikitis M, Lents NH, Arias C, Lennon CJ, Kluger Y, Dynlacht BD. XBP1 controls diverse cell type- and condition-specific transcriptional regulatory networks. *Molecular Cell*. 2007;27:53-66
8. Schwarz DS, Blower MD. The endoplasmic reticulum: structure, function and response to cellular signaling. *Cellular and Molecular Life Sciences*. 2016;73:79-94
9. Krebs J, Agellon LB, Michalak M. Ca^{2+} homeostasis and endoplasmic reticulum (ER) stress: An integrated view of calcium signaling. *Biochemical and Biophysical Research Communications*. 2015;460:114-121
10. Braakman I, Hebert DN. Protein folding in the endoplasmic reticulum. *Cold Spring Harbor Perspectives in Biology*. 2013;5:a013201
11. Rossi AE, Dirksen RT. Sarcoplasmic reticulum: the dynamic calcium governor of muscle. *Muscle & Nerve*. 2006;33:715-731
12. Reddish FN, Miller CL, Gorkhali R, Yang JJ. Calcium Dynamics Mediated by the Endoplasmic/Sarcoplasmic Reticulum and Related Diseases. *International Journal of Molecular Sciences*. 2017;18
13. Eisner DA, Caldwell JL, Kistamas K, Trafford AW. Calcium and Excitation-Contraction Coupling in the Heart. *Circulation Research*. 2017;121:181-195
14. Barone V, Randazzo D, Del Re V, Sorrentino V, Rossi D. Organization of junctional sarcoplasmic reticulum proteins in skeletal muscle fibers. *Journal of Muscle Research and Cell Motility*. 2015;36:501-515
15. Chopra N, Knollmann BC. Triadin regulates cardiac muscle couplon structure and microdomain Ca^{2+} signalling: a path towards ventricular arrhythmias. *Cardiovascular Research*. 2013;98:187-191
16. Costello B, Chadwick C, Saito A, Chu A, Maurer A, Fleischer S. Characterization of the junctional face membrane from terminal cisternae of sarcoplasmic reticulum. *Journal of Cell Biology*. 1986;103:741-753

17. Gyorke S, Stevens SC, Terentyev D. Cardiac calsequestrin: quest inside the SR. *The Journal of Physiology*. 2009;587:3091-3094

18. Knollmann BC. New roles of calsequestrin and triadin in cardiac muscle. *The Journal of Physiology*. 2009;587:3081-3087

19. Wang S, Trumble WR, Liao H, Wesson CR, Dunker AK, Kang CH. Crystal structure of calsequestrin from rabbit skeletal muscle sarcoplasmic reticulum. *Nature Structural Biology*. 1998;5:476-483

20. Wu J, Ruas JL, Estall JL, Rasbach KA, Choi JH, Ye L, Bostrom P, Tyra HM, Crawford RW, Campbell KP, Rutkowski DT, Kaufman RJ, Spiegelman BM. The unfolded protein response mediates adaptation to exercise in skeletal muscle through a PGC-1alpha/ATF6alpha complex. *Cell Metabolism*. 2011;13:160-169

21. Paul PK, Bhatnagar S, Mishra V, Srivastava S, Darnay BG, Choi Y, Kumar A. The E3 ubiquitin ligase TRAF6 intercedes in starvation-induced skeletal muscle atrophy through multiple mechanisms. *Molecular and Cellular Biology*. 2012;32:1248-1259

22. Pierre N, Deldicque L, Barbe C, Naslain D, Cani PD, Francaux M. Toll-like receptor 4 knockout mice are protected against endoplasmic reticulum stress induced by a high-fat diet. *PLOS One*. 2013;8:e65061

23. Marambio P, Toro B, Sanhueza C, Troncoso R, Parra V, Verdejo H, Garcia L, Quiroga C, Munafo D, Diaz-Elizondo J, Bravo R, Gonzalez MJ, Diaz-Araya G, Pedrozo Z, Chiong M, Colombo MI, Lavandero S. Glucose deprivation causes oxidative stress and stimulates aggresome formation and autophagy in cultured cardiac myocytes. *Biochimica et Biophysica Acta (BBA) - Biomembranes*. 2010;1802:509-518

24. Groenendyk J, Lee D, Jung J, Dyck JR, Lopaschuk GD, Agellon LB, Michalak M. Inhibition of the Unfolded Protein Response Mechanism Prevents Cardiac Fibrosis. *PLOS One*. 2016;11:e0159682

25. Tufanli O, Telkoparan Akillilar P, Acosta-Alvear D, Kocaturk B, Onat UI, Hamid SM, Cimen I, Walter P, Weber C, Erbay E. Targeting IRE1 with small molecules counteracts progression of atherosclerosis. *Proceedings of the National Academy of Sciences of the United States of America*. 2017;114:E1395-E1404

26. Liu CY, Wong HN, Schauerte JA, Kaufman RJ. The protein kinase/endoribonuclease IRE1alpha that signals the unfolded protein response has a luminal N-terminal ligand-independent dimerization domain. *Journal of Biological Chemistry*. 2002;277:18346-18356

27. Groenendyk J, Peng Z, Dudek E, Fan X, Mizianty MJ, Dufey E, Urra H, Sepulveda D, Rojas-Rivera D, Lim Y, Kim DH, Baretta K, Srikanth S, Gwack Y, Ahnn J, Kaufman RJ, Lee SK, Hetz C, Kurgan L, Michalak M. Interplay between the oxidoreductase PDIA6 and microRNA-322 controls the response to disrupted endoplasmic reticulum calcium homeostasis. *Science Signaling*. 2014;7:ra54

28. Gatti G, Trifari S, Mesaeli N, Parker JM, Michalak M, Meldolesi J. Head-to-tail oligomerization of calsequestrin: a novel mechanism for heterogeneous distribution of endoplasmic reticulum luminal proteins. *Journal of Cell Biology*. 2001;154:525-534

29. MacLennan DH, Wong PT. Isolation of a calcium-sequestering protein from sarcoplasmic reticulum. *Proceedings of the National Academy of Sciences of the United States of America*. 1971;68:1231-1235

30. Cala SE, Jones LR. Rapid purification of calsequestrin from cardiac and skeletal muscle sarcoplasmic reticulum vesicles by Ca^{2+}-dependent elution from phenyl-sepharose. *Journal of Biological Chemistry*. 1983;258:11932-11936

31. Milner RE, Baksh S, Shemanko C, Carpenter MR, Smillie L, Vance JE, Opas M, Michalak M. Calreticulin, and not calsequestrin, is the major calcium binding protein of smooth muscle sarcoplasmic reticulum and liver endoplasmic reticulum. *Journal of Biological Chemistry*. 1991;266:7155-7165

32. Schoenmakers TJ, Visser GJ, Flik G, Theuvenet AP. CHELATOR: an improved method for computing metal ion concentrations in physiological solutions. *Biotechniques*. 1992;12:870-874, 876-879

33. McPherson PS, Kim YK, Valdivia H, Knudson CM, Takekura H, Franzini-Armstrong C, Coronado R, Campbell KP. The brain ryanodine receptor: a caffeine-sensitive calcium release channel. *Neuron*. 1991;7:17-25

34. Campbell KP, Knudson CM, Imagawa T, Leung AT, Sutko JL, Kahl SD, Raab CR, Madson L. Identification and characterization of the high affinity [3H]ryanodine receptor of the junctional sarcoplasmic reticulum Ca^{2+} release channel. *Journal of Biological Chemistry*. 1987;262:6460-6463

35. Knudson CM, Chaudhari N, Sharp AH, Powell JA, Beam KG, Campbell KP. Specific absence of the alpha 1 subunit of the dihydropyridine receptor in mice with muscular dysgenesis. *Journal of Biological Chemistry*. 1989;264:1345-1348

36. Hiess F, Vallmitjana A, Wang R, Cheng H, ter Keurs HE, Chen J, Hove-Madsen L, Benitez R, Chen SR. Distribution and Function of Cardiac Ryanodine Receptor Clusters in Live Ventricular Myocytes. *Journal of Biological Chemistry*. 2015;290:20477-20487

37. Hunt DJ, Jones PP, Wang R, Chen W, Bolstad J, Chen K, Shimoni Y, Chen SR. K201 (JTV519) suppresses spontaneous Ca^{2+} release and [3H]ryanodine binding to RyR2 irrespective of FKBP12.6 association. *Biophysical Journal*. 2007;404:431-438

38. Saito A, Seiler S, Chu A, Fleischer S. Preparation and morphology of sarcoplasmic reticulum terminal cisternae from rabbit skeletal muscle. *Journal of Cell Biology*. 1984;99:875-885

39. Lanner JT, Georgiou DK, Joshi AD, Hamilton SL. Ryanodine receptors: structure, expression, molecular details, and function in calcium release. *Cold Spring Harbor Perspectives in Biology*. 2010;2:a003996

40. Young P, Ehler E, Gautel M. Obscurin, a giant sarcomeric Rho guanine nucleotide exchange factor protein involved in sarcomere assembly. *Journal of Cell Biology*. 2001;154:123-136

41. Jorgensen AO, Shen AC, Campbell KP. Ultrastructural localization of calsequestrin in adult rat atrial and ventricular muscle cells. *Journal of Cell Biology*. 1985;101:257

42. Mega T, Oku H, Hase S. Characterization of carbohydrate-binding specificity of concanavalin A by competitive binding of pyridylamino sugar chains. *Journal of Biochemistry*. 1992;111:396-400

43. Eletto D, Eletto D, Dersh D, Gidalevitz T, Argon Y. Protein disulfide isomerase A6 controls the decay of IRE1alpha signaling via disulfide-dependent association. *Molecular Cell*. 2014;53:562-576

44. Kozlov G, Maattanen P, Thomas DY, Gehring K. A structural overview of the PDI family of proteins. *FEBS Journal*. 2010;277:3924-3936

45. Liu CY, Xu Z, Kaufman RJ. Structure and intermolecular interactions of the luminal dimerization domain of human IRE1alpha. *Journal of Biological Chemistry*. 2003;278:17680-17687

46. Park H, Park IY, Kim E, Youn B, Fields K, Dunker AK, Kang C. Comparing skeletal and cardiac calsequestrin structures and their calcium binding: a proposed mechanism for coupled calcium binding and protein polymerization. *Journal of Biological Chemistry*. 2004;279:18026-18033

47. Beard NA, Dulhunty AF. C-terminal residues of skeletal muscle calsequestrin are essential for calcium binding and for skeletal ryanodine receptor inhibition. *Skelet Muscle*. 2015;5:6

48. Zhou J, Liu CY, Back SH, Clark RL, Peisach D, Xu Z, Kaufman RJ. The crystal structure of human IRE1 luminal domain reveals a conserved dimerization interface required for activation of the unfolded protein response. *Proceedings of the National Academy of Sciences of the United States of America*. 2006;103:14343-14348

49. Liu CY, Schroder M, Kaufman RJ. Ligand-independent dimerization activates the stress response kinases IRE1 and PERK in the lumen of the endoplasmic reticulum. *Journal of Biological Chemistry*. 2000;275:24881-24885

50. Li H, Korennykh AV, Behrman SL, Walter P. Mammalian endoplasmic reticulum stress sensor IRE1 signals by dynamic clustering. *Proceedings of the National Academy of Sciences of the United States of America*. 2010;107:16113-16118

51. Baumann O, Walz B. Endoplasmic reticulum of animal cells and its organization into structural and functional domains. *International Review of Cytology*. 2001;205:149-214

52. Michalak M, Opas M. Endoplasmic and sarcoplasmic reticulum in the heart. *Trends in Cell Biology*. 2009;19:253-259

53. Wray S, Burdyga T. Sarcoplasmic reticulum function in smooth muscle. *Physiological Reviews*. 2010;90:113-178

54. Bers DM. Cardiac sarcoplasmic reticulum calcium leak: basis and roles in cardiac dysfunction. *Annual Review of Physiology*. 2014;76:107-127

55. Beard NA, Wei L, Dulhunty AF. Ca^{2+} signaling in striated muscle: the elusive roles of triadin, junctin, and calsequestrin. *European Biophysics Journal*. 2009;39:27-36

56. Lee JM, Rho SH, Shin DW, Cho C, Park WJ, Eom SH, Ma J, Kim DH. Negatively charged amino acids within the intraluminal loop of ryanodine receptor are involved in the interaction with triadin. *Journal of Biological Chemistry*. 2004;279:6994-7000

57. Kobayashi YM, Alseikhan BA, Jones LR. Localization and characterization of the calsequestrin-binding domain of triadin 1. Evidence for a charged beta-strand in mediating the protein-protein interaction. *Journal of Biological Chemistry*. 2000;275:17639-17646

58. Gyorke I, Hester N, Jones LR, Gyorke S. The role of calsequestrin, triadin, and junctin in conferring cardiac ryanodine receptor responsiveness to luminal calcium. *Biophysical Journal*. 2004;86:2121-2128

59. Zhang L, Kelley J, Schmeisser G, Kobayashi YM, Jones LR. Complex formation between junctin, triadin, calsequestrin, and the ryanodine receptor. Proteins of the cardiac junctional sarcoplasmic reticulum membrane. *Journal of Biological Chemistry*. 1997;272:23389-23397

60. Gaburjakova M, Bal NC, Gaburjakova J, Periasamy M. Functional interaction between calsequestrin and ryanodine receptor in the heart. *Cellular and Molecular Life Sciences*. 2013;70:2935-2945

61. Wang L, Zhang L, Li S, Zheng Y, Yan X, Chen M, Wang H, Putney JW, Luo D. Retrograde regulation of STIM1-Orai1 interaction and store-operated Ca^{2+} entry by calsequestrin. *Scientific Reports*. 2015;5:11349-11349

62. Kraskiewicz H, FitzGerald U. InterfERing with endoplasmic reticulum stress. *Trends in Pharmacological Sciences*. 2012;33:53-63

63. Hetz C. The unfolded protein response: controlling cell fate decisions under ER stress and beyond. *Nature Reviews Molecular Cell Biology*. 2012;13:89-102

64. Bertolotti A, Zhang Y, Hendershot LM, Harding HP, Ron D. Dynamic interaction of BiP and ER stress transducers in the unfolded-protein response. *Nature Cell Biology*. 2000;2:326-332

65. Oikawa D, Kimata Y, Kohno K, Iwawaki T. Activation of mammalian IRE1alpha upon ER stress depends on dissociation of BiP rather than on direct interaction with unfolded proteins. *Experimental Cell Research* 2009;315:2496-2504

66. Ma K, Vattem KM, Wek RC. Dimerization and release of molecular chaperone inhibition facilitate activation of eukaryotic initiation factor-2 kinase in response to endoplasmic reticulum stress. *Journal of Biological Chemistry*. 2002;277:18728-18735

67. Oikawa D, Kimata Y, Kohno K. Self-association and BiP dissociation are not sufficient for activation of the ER stress sensor Ire1. *Journal of Cell Science*. 2007;120:1681-1688

68. Kimata Y, Oikawa D, Shimizu Y, Ishiwata-Kimata Y, Kohno K. A role for BiP as an adjustor for the endoplasmic reticulum stress-sensing protein Ire1. *Journal of Cell Biology*. 2004;167:445-456

69. Sepulveda D, Rojas-Rivera D, Rodríguez DA, Groenendyk J, Köhler A, Lebeaupin C, Ito S, Urra H, Carreras-Sureda A, Hazari Y, Vasseur-Cognet M, Ali MMU, Chevet E, Campos G, Godoy P, Vaisar T, Bailly-Maitre B, Nagata K, Michalak M, Sierralta J, Hetz C. Interactome screening identifies the ER luminal chaperone Hsp47 as a regulator of the unfolded protein response transducer IRE1α. *Molecular Cell*. 2018;69:238-252.e237

70. Groenendyk J, Paskevicius T, Urra H, Viricel C, Wang K, Barakat K, Hetz C, Kurgan L, Agellon LB, Michalak M. Cyclosporine A binding to COX-2 reveals a novel signaling

pathway that activates IRE1α unfolded protein response sensor. *Scientific Reports*. 2018;8:16678

Chapter 3: Functional consequences of inositol-requiring enzyme -1α (IRE1α) deficiency in cardiomyocytes

3.1 Abstract

The endoplasmic reticulum (ER) stress and activation of unfolded protein response (UPR) is involved in the development and progression of various heart disease, such as cardiac hypertrophy, ischemic heart disease, and heart failure. The serine/threonine protein kinase/endoribonuclease IRE1α is a key component of UPR that can induce both adaptive UPR and apoptotic signaling pathways to determine cell fate. However, the specific role of IRE1α in the heart is unknown. In this study, we aimed to characterize the specific contribution of IRE1α in cardiac physiology and pathogenesis. We generated a mouse model with cardiomyocyte specific, inducible silencing of the IRE1α gene. We discovered that silencing the IRE1α gene in adult heart results in dilated cardiomyopathy with severely impaired cardiac function. Moreover, IRE1α-deficient cardiomyocytes show impaired Ca^{2+} transient, suggesting IRE1α deficiency in the heart leads to dysfunction in Ca^{2+} handling by cardiomyocytes.

3.2 Introduction

The ER is a specialized organelle composed of a single bilayer that forms the nuclear envelope, dynamic branched tubules, and a network of sheets[1]. It governs lipid and steroid synthesis, carbohydrate metabolism, Ca^{2+} storage, synthesis, folding and processing of over one third of all cellular proteins[2]. Disruptions to ER homeostasis, including oxidative stress, protein aggregation, Ca^{2+} flux, or accumulation of misfolded protein can cause ER stress and activate a highly conserved adaptive response namely UPR[2]. There are three major ER stress sensors and signaling transducers in UPR including ATF6, PERK, and IRE1α. Activation of these sensors leads to protein translational attenuation, transcriptional activation of chaperones and folding enzyme genes, and activation protein degradation pathway to reduce accumulation of misfolded protein and restore ER homeostasis[2, 3].

ER stress is an integral part of heart physiology and pathology. ER stress signaling is activated in response to many types of myocardial assaults, including ischemia, ischemia/reperfusion injuries, hypoxia, and mechanical overload[4-9]. However, the role of ER stress signaling in these disease conditions remains unclear. Different ER stress pathways appear to have specific roles in the heart. ATF6 activation can protect myocardium from ischemia/reperfusion

injury via inducing cytoprotective ER stress proteins: BiP, GRP94 (glucose-regulated protein 94), and oxidative stress response genes[10, 11]. PERK deficient heart shows more severe cardiomyopathy in response to pressure overload-induced heart failure, suggests PERK singling pathway is cardioprotective[12]. Overexpressing IRE1α in cardiomyocytes can protect the heart against pressure overload-induced heart failure[13]. Transcription factor XBP1, downstream of IRE1α activation, can protect heart from hypoxia during myocardium infarction by increasing BiP expression[14]. Inhibition of XBP1 in cultured cardiomyocytes significantly increases cardiac myocyte apoptosis and cell death in response to hypoxia/reoxygenation stress[14]. Moreover, XBP1 silencing led to increased injury from ischemia/reperfusion, and overexpressing spliced active form of XBP1 (XBP1s) can protect hearts from ischemia/reperfusion injury with nearly 50% reduction in infarct sizes[15]. XBP1s deficient heart shows exacerbated heart failure progression under pressure overload (a common pathological condition in hypertensive patients), indicating XBP1 is part of adaptive response to protect heart in response to pressure overload[16].

ER stress can also activate cell death signaling pathways and contributes to myocyte apoptosis and heart failure[17-21]. The apoptosis signal-regulating kinase 1 (ASK1) in IRE1α pathway-mediated ER stress is essential for ER stress-induced apoptosis[22], deletion of the ASK1 gene in mice is cardioprotective with reduced cardiomyocyte apoptosis after transverse aortic constriction[20]. Moreover, IRE1α-XBP1 signaling mediates expression of key proatherogenic cytokines and chemokines that could drive the atherosclerotic process under metabolic stress. Inhibition of IRE1α-driven XBP1 splicing with small molecules alleviates atherosclerosis in apolipoprotein E-deficient mice (atherogenesis disease model)[23], [24, 25]. In a heart failure mice model with severe cardiac fibrosis, inhibiting IRE1α activity able prevents cardiac fibrosis[26]. These findings suggest that activation of IRE1α arm of UPR could contribute to disease progression. PERK mediated ER stress can also contribute to cardiomyocyte apoptosis. Inhibiting CHOP, downstream of PERK, can reduce cardiomyocyte apoptosis induced by aortic coarctation or proteasome inhibition[21, 27]. In heart failure mice model induced by transverse aortic constriction, CHOP-deficient mice do not develop as severe cardiac hypertrophy, fibrosis, and cardiac dysfunction as wild-type mice indicating that CHOP contributes to development of cardiac hypertrophy and failure induced by pressure overload[28]. Similarly, preventing eIF2α phosphorylation in PERK signaling pathway, can counteract disease progression in atrial fibrillation[29] and improve cardiac pathology caused by parasitic infection[30]. These emerging

evidences show that ER stress contributes to both adaptive response and pathological remodeling of the heart. However, understanding a contribution of IRE1α to the heart physiology and pathology remains to be further established.

In this study, we investigated the direct impact of IRE1α deficiency in cardiomyocytes using animal model with cardiomyocyte-specific, tamoxifen-inducible deletion of the IRE1α gene. In the absence of any external stress, silencing of IRE1α in cardiomyocytes of the adult hearts lead to severe dilation, systolic dysfunction, and cardiac fibrosis. Importantly, IRE1α-deficient cardiomyocytes show prolonged Ca^{2+} release response followed by oscillating and elevated cytosolic Ca^{2+} after stimulation, as well as increased premature spontaneous Ca^{2+} release events. This indicates that IRE1α plays a role in cardiomyocyte E-C coupling, and that IRE1α deficiency induced dilated cardiomyopathy is likely due to alternations in cardiomyocytes Ca^{2+} handling.

3.3 Materials and Methods

3.3.1 Ethics statement and animals

All animal experiments were carried out according to the University of Alberta Animal Policy and Welfare Committee and the Canadian Council on Animal Care Guidelines. The approval for use of animals in research was granted by the Animal Care and Use Committee for Health Science, a University of Alberta ethics review committee. The protocol was approved by the Committee (AUP297).

3.3.2 Generation of transgenic mice

Heart-specific, inducible IRE1α deletion mice were generated using CRE/LoxP system. IRE1α flox/flox mice generously provided by Dr. Kenji Kohno[31] from Department of Stem cell Biology, Kyoto University, Japan. Homozygous carrier for the loxP flank IRE1α exon 21 and 22 with mixed (C57BL/6 x 129/SvJae) background. IRE1α flox/flox mice were cross-bred with αMHC (myosin heavy chain)-Cre mice (C57BL/6) single time to generate double transgenic mice (designated IRE1α cmc KO) which carried transgenes containing both MerCreMer driven by αMHC promoters and loxP-IRE1α-loxP. To induce deletion of the IRE1α exon 21 and 22, we delivered tamoxifen as food mixture[32] (Figure 3-1). Wild-type and floxed single-transgenic (IRE1α flox/flox) mice treated with tamoxifen or double-transgenic IRE1α cmc KO mice treated with

standard chow (normal food) were used as controls. Both male and female mice age 12-14 weeks were included in the study.

3.3.3 Echocardiography and electrocardiography

Mice were anesthetized with 1.0% to 1.5% isoflurane with 1 to 1.5 l/min 100% oxygen, and *in vivo* cardiac function was assessed by transthoracic echocardiography using a Vevo 3100 high-resolution imaging system equipped with a 30-MHz transducer (model RMV-707B, VisualSonics, Toronto, Ontario, Canada). The following measurements were obtained during both systole and diastole: inter-ventricular septal thickness (IVS), left ventricular posterior wall thickness (LVPW), left ventricular internal diameter (LVID), heart rate, ejection fraction (EF). Measurements were averaged from 3 to 6 cardiac cycles according to the American Society of Echocardiography. Percent ejection fraction (%EF) was calculated as follows: 100 * [(end-diastolic volume - end-systolic volume)/end-diastolic volume)]. The Tei index (a measure of myocardial performance) was calculated as the ratio of time intervals (a-b/b), derived by pulsed Doppler echocardiography, where *a* is the time between the end and the start of transmitral flow, and *b* is the LV ejection time.

For electrocardiography (ECG), mice were anesthetized with 1.0% to 1.5% isoflurane with 1 to 1.5 l/min 100% oxygen, depilatory cream applied to chest area. Animals were placed in dorsal recumbency and limbs gently taped down. ECGs were measured using surface electrode clips, and readings were recorded using Power Lab (ADInstruments). Microneedles attached to electrodes were inserted just under the skin. By convention, lead I has the positive electrode on the left arm, and lead II, the negative electrode on the right arm, and lead III on the left leg serves as a reference (ground). Record for1-3min using LabChart (version: 7.3, ADInstruments)

3.3.4 Trichrome staining and fibrosis analysis

Cardiac tissue was fixed in 10% formalin in phosphate buffered saline (137 mM NaCl, 2.7 mM KCl, 10 mM Na_2HPO_4, 1.8 mM KH_2PO_4, pH 7.2). Fixed tissues were embedded into paraffin, sectioned by 5 μm, mounted on to glass slide, and stained with Masson's Trichrome for collagen in the Alberta Diabetes Institute HistoCore Facility at the University of Alberta. In brief, sectioned hearts were placed in filtered Bouin's solution (1% saturated picric acid, 9% formaldehyde, and 5% acetic acid) at 60^{o}C for 30 minutes and let sit for another 30 minutes at room temperature. After washing the slide with water, the slide was stained with filtered trichrome for 20 minutes

and placed in 0.5% acetic water for 2 minutes. Slides were imaged using Zeiss COLIBRI fluorescence Microscope with 20x objective, 20-40 images were captured for each slice in random views. Total of 3 control heart (single transgenic floxed IRE1α mice fed tamoxifen for 3 weeks) and 3 IRE1α cmc KO mice fed tamoxifen for 3 weeks.

Semiautomated image analysis of fibrotic areas were carried by Fiji ImageJ (version 1.52n, https://imagej.net/Fiji/Downloads) as described previously[33]. In brief, images were converted to RBG stacked providing grayscale pictures for the red, green, and blue channels separately. For the grayscale image corresponding to the green channels, the threshold was adjusted to detect collagen stained area (blue), and the detected regions were measured using measure tool.

3.3.5 Cardiomyocyte and cardiac fibroblast isolation

Adult mice fibroblasts were isolated from hearts of 6-8 weeks old C57BL/6J background male mice. The heart were perfused using a Langendorff-Free method[34]. In brief, immediately after cervical dislocation and opening the chest cavity, the descending aorta was cut, and 7 mL of EDTA buffer (130 mM NaCl, 5 mM KCl, 0.5 mM NaH_2PO4, 10 mM HEPES, pH 7.8, 10 mM Glucose, 10 mM 2,3-butanedione monoxime, 10 mM Taurine, 5 mM EDTA) was injected immediately into the apex of the right ventricle. Then the ascending aorta was clamped using surgical hemostats, and the heart was transferred to fresh EDTA buffer. To digest the heart, the following buffers were injected sequentially to the apex of the left ventricle at 2 ml/mins: 10 mL EDTA buffer, 3 mL perfusion buffer (130 mM NaCl, 5 mM KCl, 0.5 mM NaH_2PO4, 10 mM HEPES, pH 7.8, 10 mM Glucose, 10 mM BDM, 10 mM Taurine, 1 mM MaCl2), and 50 ml collagenase buffer (0.5 mg/ml collagenase 2 (Sigma-Aldrich C6885); 0.1 mg/ml collagenase 4 (Sigma-Aldrich C5138); Protease type XIV, 0.05 mg/ml (Sigma-Aldrich P5147); dissolved in perfusion buffer. The right and left ventricle from digested hearts were then separated and gently pulled into about 1 mm pieces using forceps. Cells were dissociated with gentle trituration, and enzyme activity was stop by addition of 5 ml/heart stop buffer contains 5% FBS in perfusion buffer. Cell suspension was passed through a 100 µm cell strainer and centrifuged at 40 xg for 3 mins and pellets enriched in cardiomyocyte were collected. Supernatant containing cardiac fibroblasts was collected and centrifuged again at 400 xg for 5 mins, and pellet was washed in DMEM (Gibco, 11995) with 10% FBS. The cell suspension was centrifuged again at 400 xg for 5

mins then the pellet was re-suspended in 10% FBS DMEM, 10 U/mL penicillin, and 100 µg/ml streptomycin and plated onto 10 cm culture dish (Corning, 430167).

3.3.6 Calcium transient

Cardiac ventricular myocytes were incubated with 1 µM Fluo-4 acetoxymethylester for 20 min at room temperature and re-suspended in dye-free perfusion buffer with incubation at 37 °C for 20 min to allow complete de-esterification of AM esters. The Ca^{2+} imaging was performed using an Olympus IX83 inverted microscope and myocytes were perfused with Ca^{2+} imaging solution (in: 140 mM NaCl, 5 mM KCl, 10 mM HEPES, pH 7.4, 1.4 mM $MgSO_4$. 7 mM H_2O, 2 mM $CaCl_2$, 5 mM Glucose) with multi-channel superfusion system. The fluorescence of Ca^{2+} transient was emitted after excitation at 480 nm and 5 % intensity (X-cite 120 LED Boost Excelitas light source) for 10 ms and Ca^{2+} transients were measured at 20 Hz using 30X objective and Andor iXon Ultra 897camera. Electric field stimulation of myocytes was performed using Warner instruments SIU-102 stimulator with platinum electrodes. The region of interest (ROI) enclosing rod-shaped myocyte was selected and the cells were paced at 1 Hz using GRASS SD9 pulse generator for 60 seconds followed by 0.05 Hz for 2 min. The Ca^{2+} sparks and average fluorescence intensity of paced Ca^{2+} events evoked at 0.05 Hz were then analyzed. The time of peak and end of each event was analyzed using LabChart and Clampfit software (Molecular Devices, CA, USA) and 75% of time to reach baseline from peak was calculated. Statistical analyses were performed with unpaired Student's t-test using Graphpad prism 5.0 software.

3.3.7 Genomic DNA isolation and PCR

Genomic DNA was isolated from cardiomyocytes and mouse tails using Qiagen DNeasy Blood & Tissue kits (Qiagen, 69504). Taq polymerase (FroggaBio, FBTAQM) was used for polymerase chain reaction (PCR) with thermocycling conditions as follows:

Initial denaturation – 94ºC for 5 minutes

40 cycles of 94ºC for 30 seconds

58ºC for 30 seconds

72 C for 90 seconds

Final extension – 72ºC for 10 minutes

PCR primers used for genotyping of the IRE1α exon 20-21 deletion:

Forward primer (5’ to 3’) AGCCAGTACACTGGTCATGCTA

Reverse primer (5’ to 3’) ACCCCAAGACTAGCCCTTACA

αMHC-MerCreMer primer:

Forward primer (5’ to 3’): GCCAGCTAAACATGCTTCATC

Reverse primer (5’ to 3’): ATTGCCCCTGTTTCACTATCC

3.3.8 Real-time PCR

Total RNA was isolated from cardiomyocytes or cardiac fibroblasts using Qiagen RNeasy mini kit (Qiagen, 74104) according to the manufacturer’s instructions. A Rotor-Gene RG-3000 (Corbett Research) and iQ SYBR Green Supermix (Bio-Rad) were used for real-time PCR experiments. Five hundred ng RNA was used for reverse transcription by using iScript cDNA synthesis kit (Bio-Rad, 1708891), 20 ng cDNA was mixed with iQ SYBR Green Supermix (Bio-Rad, 170-8882) for real-time PCR reaction. The final quantitation of the amount of target (Ct value) in a real-time PCR reaction was converted to the amount of transcript and normalized by glyceraldehyde 3-phosphate dehydrogenase (GAPDH). PCR primers used in this study is listed as follow:

ERN1 (IRE1α) exon 21-22: forward (5’ to 3’) CGAGCCATGAGAAACAAGAAAC
reverse (5’ to 3’) GGAAGCGGGAAGTGAAGTAG

Spliced XBP1 (XBP1s): forward (5’ to 3’) GAGTCCGCAGCAGGTG
reverse (5’ to 3’) GTGTCAGAGTCCATGGGA

BiP: forward (5’ to 3’) AAG CTC AAA GAG CGC ATT GAC ACC
reverse (5’ to 3’) AGT CTT CAA TGT CCG CAT CCT GGT

Calreticulin: forward (5’ to 3’) AAG ACT GGG ATG AAC GAG CCA AGA
reverse (5’ to 3’) AAT TTG ACG TGG TTT CCA CTC GCC

CHOP: forward (5’ to 3’) TCACACGCACATCCCAAA
reverse (5’ to 3’) CCTAGTTCTTCCTTGCTCTTC

ATF4: forward (5’ to 3’) TCG ATG CTC TGT TTC GAA TG
reverse (5’ to 3’) AGA ATG TAA AGG GGG CAA CC

ATF6: forward (5’ to 3’) CCA ATA GCC AAC AGA AAG CCC GCA
reverse (5’ to 3’) TGG TTT CTG TGT ACT GGA CAG CCA

GAPDH: forward (5’ to 3’) TTC ACC ACC ATG GAG AAG GC
reverse (5’ to 3’) GGC ATG GAC TGT GGT CAT GA

3.3.9 Immunostaining and confocal microscopy

Paraffin embedded sections of mice hearts were prepared and processed at the Alberta Diabetes Institute HistoCore Facility at the University of Alberta. Sections were baked at 60°C for 45 min to 1 hour to help tissue better stick to the glass slide. Then de-paraffined and rehydrated with 2x5 min 100% Xylene, 2x5 min 100% ethanol, 2x5 min 70% ethanol, and finally washed with tap water for 2x5 min. Heat-induced epitope retrieval was used to break potential protein cross-linking during fixation. Tissue sections were heated in 10 mM sodium citrate, pH 6.0, at 90-95°C for 2x5 minutes. Sections were incubated with fluorescein isothiocyanate (FITC) conjugated wheat germ agglutinin (FITC-WGA, GeneTex GTX01502) at 100 µg/ml and 4',6-Diamidino-2-Phenylindole, Dihydrochloride (DAPI, ThermoFisher Scientific 62248) at 3 µM final concentration both diluted in phosphate buffered saline (137 mM NaCl, 2.7 mM KCl, 10 mM Na_2HPO_4, 1.8 mM KH_2PO_4, pH 7.2) for 30 minutes at room temperature in the dark. Sections were washed with PBS 2x5 minutes and mounted with Prolong Diamond Antifade Mountant (Thermo Fisher Scientific, P36961).

Slides were visualized using a Leica TCS SP5 confocal microscope with Leica inverted DMI 6000 B microscope base. Images were acquired with oil immersion objectives 40X/numerical aperture (NA) 1.25 or 100X/numerical aperture (NA) 1.44 at 22.5°C. For FITC-WGA visualization, the argon laser was used with excitation at 488 nm and emission peak at 525 nm. Images were acquired with Leica Application Suite Advanced Fluorescence (Leica LAS-AF) microscopy software, exported as Leica Image File format (LIF) and processed using ImageJ software (https://imagej.net/Fiji/Downloads) with 8 bit image type.

3.3.10 Statistical analysis

Statistical analysis was performed using GraphPad Prism version 7.0. The Student's t-test was used to compare the mean of two independent groups, and one-way Anova was used to compare the mean of three or more independent groups, with a *p*-value determined to be significant if less than 0.05.

3.4 Results

3.4.1 IRE1α reduction in conditional knockout mice

To elucidate IRE1α function in adult heart, we generated a transgenic mouse model with inducible and cardiac-specific IRE1α knockout using a Cre-loxP-mediated gene switch strategy (Figure 3-1A). Flox-IRE1α mice were cross-bred with αMHC-Cre mice containing a cardiac-specific MerCreMer transgene where the Cre recombinase gene was under the control of the cardiomyocytes specific alpha-myosin heavy chain (αMHC) promoter. The Cre-dependent deletion of exons 20-21 from the floxed IRE1α allele was induced by administration of tamoxifen as described previously[32]. Tamoxifen binds to MerCreMer transgene product to promote nuclear translocation of the Cre recombinase in cardiomyocytes resulting in deletion of exons 20-21 from the IRE1α gene. We have previously shown that administration of tamoxifen alone does not have adverse effects, including no side effects on cardiac function, and optimal induction was achieved at 3 weeks post-tamoxifen feeding[32]. Deletion of the floxed IRE1α allele was seen only in heart tissue of transgenic mice carrying both MerCreMer and Flox-IRE1α (refer as cardiomyocyte specific IRE1α knockout, IRE1α cmc KO) (Figure 3-1B). Tamoxifen feeding for 3 weeks resulted in over 75% reduction in IRE1α mRNA as quantified by real-time PCR of mRNA isolated from cardiomyocytes (Figure 3-1D).

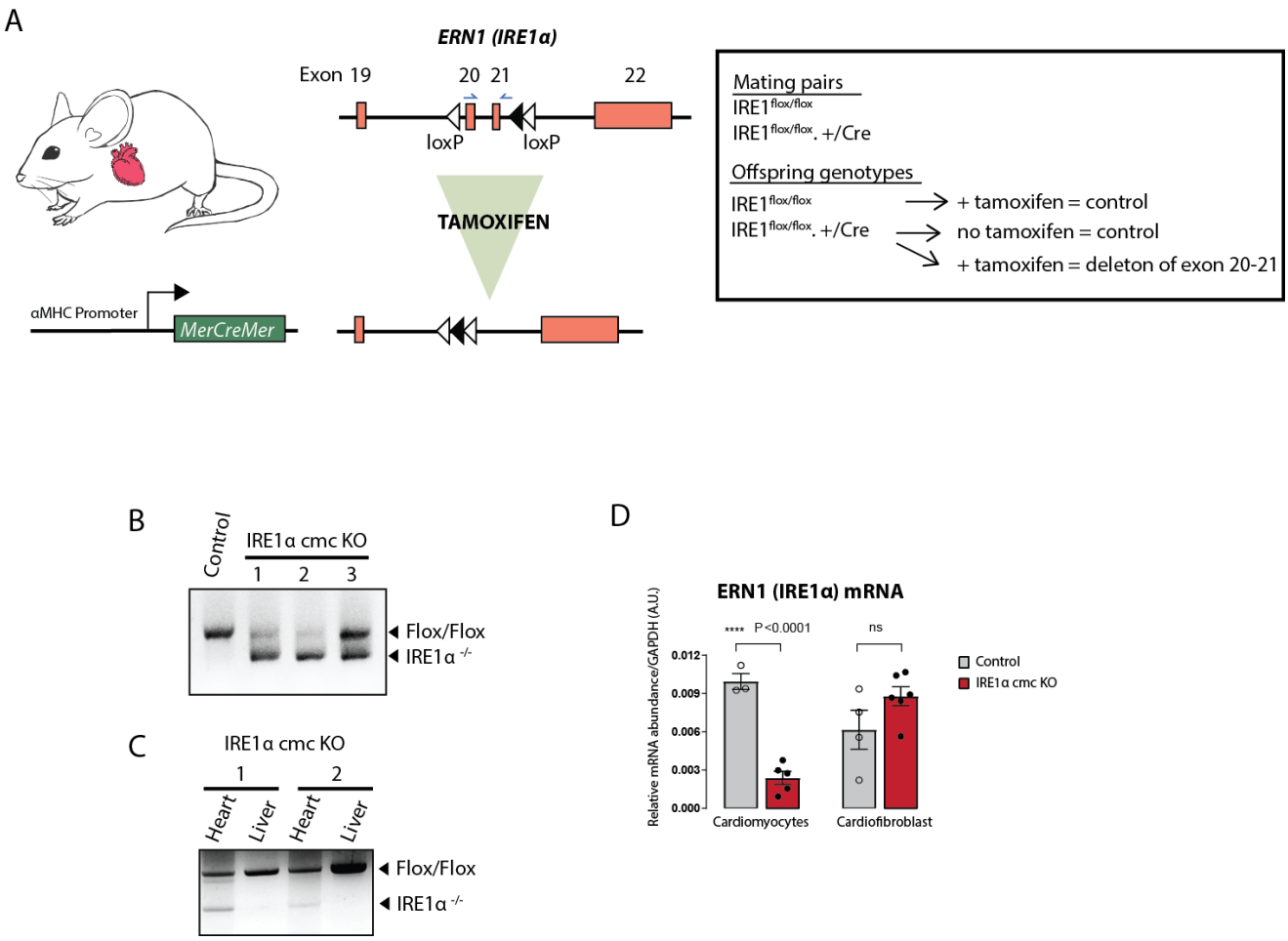

Figure 3-1. Generatingon of mice with IRE1α-deficient cardiomyocytes.

A) A schematic diagram of strategy used for generation of cardiomyocytes specific silencing of the IRE1α gene. IRE1α$^{flox/flox}$ mice with loxP site flanking exon 20 and 21 were generated generously provided by Dr. Kenji Kohno[31]. Closed and open arrowheads indicate flippase recombinase target (FRT) and loxP elements, respectively, IRE1α flox/flox mice were cross-bred with the αMHC (myosin heavy chain)-Cre mice (C57BL/6) to generate transgenic mice (designated IRE1α cmc KO) with transgene encoding MerCreMer driven by the αMHC promoters and the loxP-IRE1α-loxP. To induce deletion exon 20 and exon 21 of the IRE1α gene mice were fed tamoxifen mixed in their food as described previously[32]. IRE1α$^{flox/flox}$ without Cre + tamoxifen was used as a control and it is referred to as IRE1α$^{flox/flox}$.

B) PCR analysis of genomic DNA isolated from control mice (IRE1α flox/flox fed tamoxifen) and IRE1α cmc KO mice after 3 weeks tamoxifen feeding.

C) PCR analysis of genomic DNA isolated from heart or liver of IRE1α cmc KO mice.

D) Real-time PCR analysis of IRE1α mRNA in control mice (IRE1α flox/flox fed tamoxifen) and IRE1α cmc KO mice after fed tamoxifen for 3 weeks. DNA primer were designed to target exon 20 and exon 21 as shown in A). NS, not significant. Unpaired two tail student t-test was used for statistical analysis.

There were no differences in body weight (Figure 3-2), survival rate, and behavior between tamoxifen induced transgenic mice and control mice over 3 weeks of tamoxifen feeding (IRE1α$^{flox/flox}$ no Cre). Cardiomyocyte specific deletion of IRE1α did not cause transient activation of UPR as ATF6 and PERK and their downstream effectors (transcription factors CHOP and ATF4, chaperone calreticulin and BiP) showed no significant changes in the abundance of their mRNA in IRE1α-deficient cardiomyocytes as compared to IRE1α$^{flox/flox}$ control (Figure 3-3).

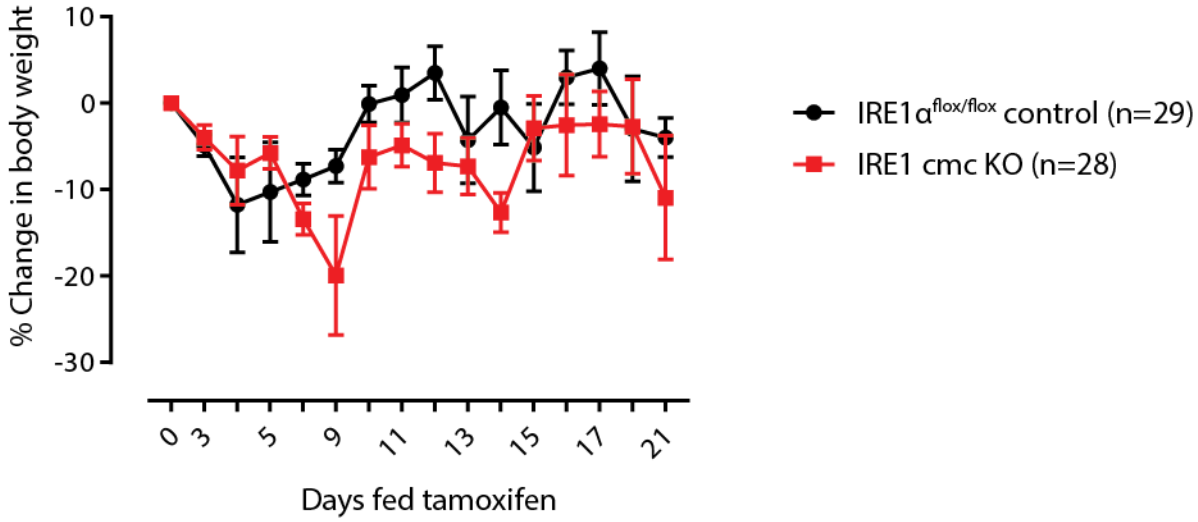

Figure 3-2. Body weight of IRE1α mice.

IRE1α cmc KO mice showed no significant changes in the body weight over 3 weeks of tamoxifen feeding as compared to control animal (IRE1α$^{flox/flox}$ without Cre). The percentage of change in body weight $= \frac{\text{body weight at day(x)tamoxifen} - \text{body weight at day(0)}}{\text{body weight at day(0)}} \times 100\%$. Unpaired two tail student t-test was used for statistical analysis. Data shown are mean ± standard error.

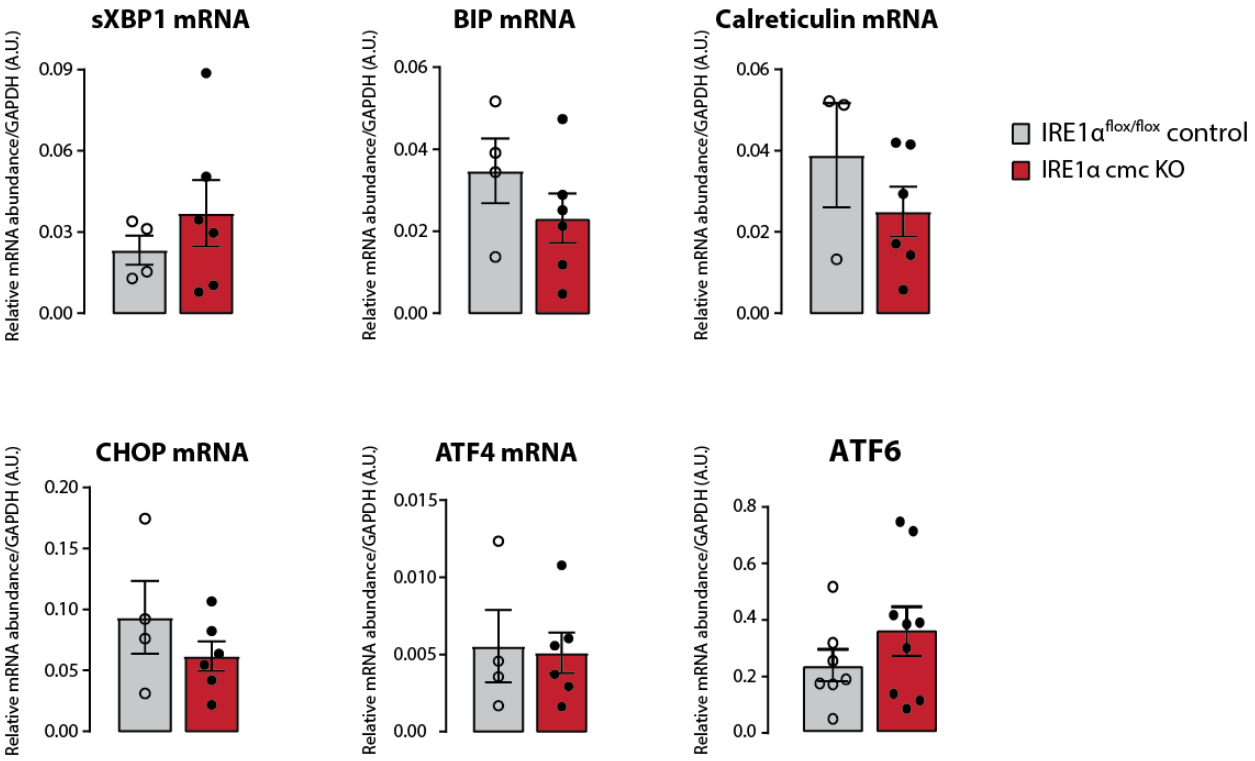

Figure 3-3. Real-time Q-PCR analysis of XBP1 mRNA splicing and abundance of mRNA encoding UPR markers.

RNA was extracted from isolated cardiomyocytes of control IRE1α$^{flox/flox}$ without Cre and IRE1α cmc KO hearts fed tamoxifen for 3 weeks. Unpaired two tail student t-test was used for statistical analysis - no significant differences were found for any of the analyzed targets. Unpaired two tail student t-test was used for statistical analysis. Data shown are mean ± standard error.

3.4.2 Cardiac-specific IRE1α deletion leads to severe dilated cardiomyopathy

Echocardiography and four-lead electrocardiogram (ECG) were used to assess heart function of the IRE1α cmc KO animals. In these experiments, tamoxifen fed and normal food (chow) fed IRE1α$^{flox/flox}$ control mice showed similar parameters and, therefore, the data presented together as pooled parameters. M-mode non-invasive transthoracic echocardiography analysis of tamoxifen-induced cardiomyocyte IRE1α knockout (IRE1α cmc KO) hearts shows severe left ventricle dilation and impaired systolic function (Figure 3-4B,C). The systolic function of the left ventricle, represented by ejection fraction (%EF), was significantly reduced after 3 weeks of tamoxifen administration (Figure 3-4C). Moreover, IRE1α cmc KO hearts displayed a significant increase in the left ventricle inner diameter (LVID), decreased left ventricle posterior wall thickness (LVPW), and increased left ventricle end-systolic volume all indicating cardiac dilation. Left ventricle diastolic function was assessed by left ventricle inflow doppler imaging (Table 3-1). Control (IRE1α$^{flox/flox}$ + tamoxifen) mice did not show any abnormal heart morphology (Figure 3-4A). Interestingly, IRE1α cmc KO hearts showed a very small to absent A wave, indicating a highly restricted pattern of transmitral flow velocity. Pulmonary pulse wave velocity (the velocity of pressure waves traveling through the arterial system) was also reduced in IRE1α cmc KO hearts likely due to weak systolic function of the left ventricle (Table 3-1). In summary, IRE1α deficiency in cardiomyocytes results in rapid development of dilated cardiomyopathy and heart failure.

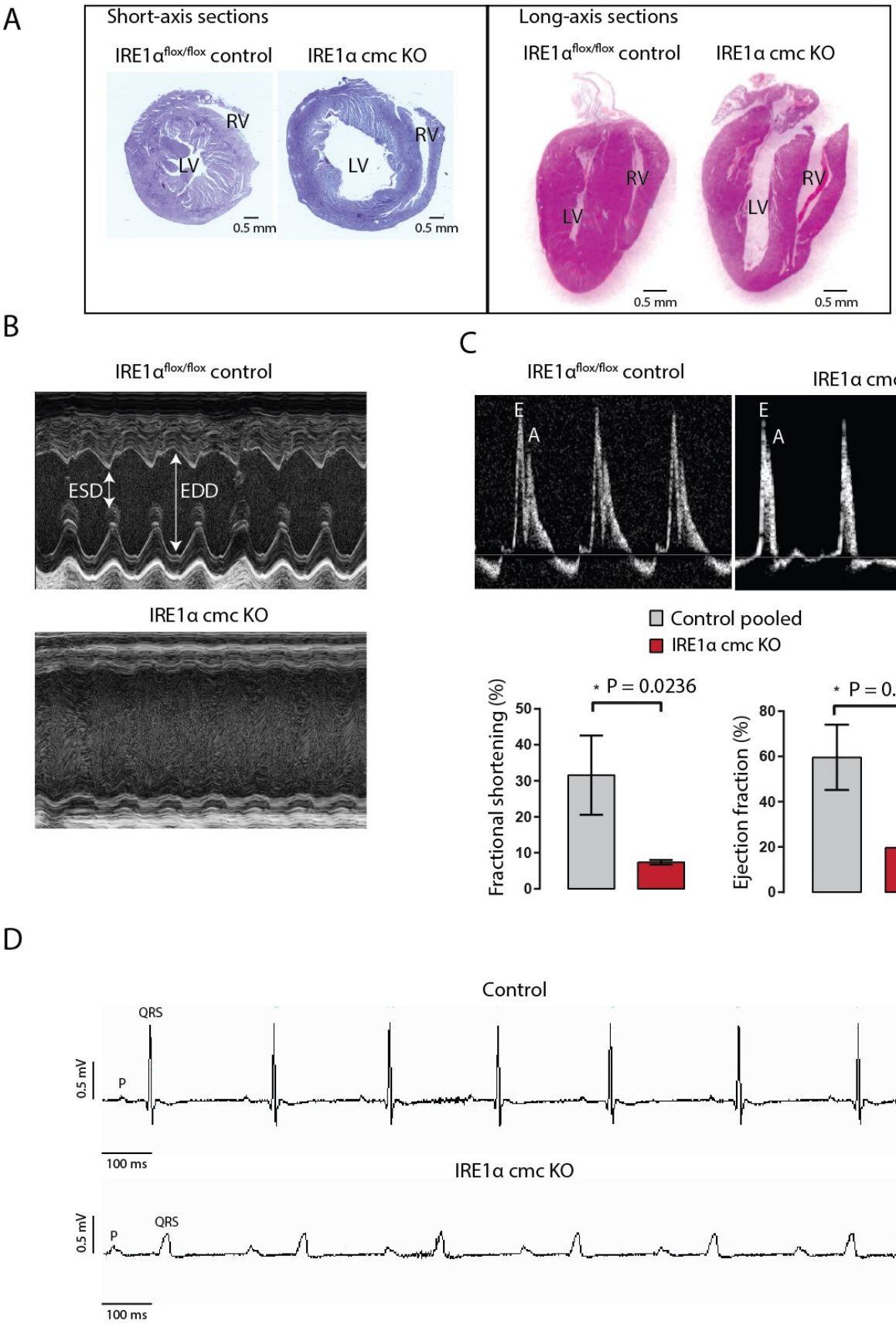
A
Short-axis sections
IRE1α flox/flox control
IRE1α cmc KO
RV
LV
0.5 mm
Long-axis sections
B
C
ESD
EDD
E
A
Control pooled
* P = 0.0236
* P = 0.0129
Fractional shortening (%)
Ejection fraction (%)
D
Control
QRS
P
0.5 mV
100 ms

Figure 3-4. Heart morphology and cardiac function of adult hearts with cardiomyocytes-specific IRE1α deletion.

A) Hematoxylin and eosin staining of hearts (longitudinal cross-section) of control (IRE1α$^{flox/flox}$ without Cre) and IRE1α cmc KO mice fed tamoxifen for 3 weeks. LV: left ventricle, RV: Right ventricle.

B) Representative M-mode echocardiography images of control (IRE1α$^{flox/flox}$ without Cre) and IRE1α cmc KO fed tamoxifen for 3 weeks. ESD, end systolic diameter; EDD, end diastolic diameter.

C) Representative images of transmitral flow velocity pattern in the pulmonary venous flow from echocardiography of control (IRE1α$^{flox/flox}$ without Cre) and IRE1α cmc KO hearts fed tamoxifen for 3 weeks. E, E-wave indicating early ventricular filling; A: A-wave indicating late filling caused by atrial contraction. Percentage of fractional shortening and percentage of ejection fraction measured from echocardiography were plotted below with mean ± standard error (n = 2 for control pooled from IRE1α$^{flox/flox}$ + tamoxifen mice and IRE1α$^{flox/flox}$ with Cre + chow mice, and n = 4 for IRE1α cmc KO). Unpaired two tail student t-test was used for statistical analysis. Data shown are mean ± standard error.

D) Representative electrocardiography recording images of hearts from control (n=5) and IRE1α cmc KO (n=4) fed tamoxifen for 3 weeks.

Table 3-1. Echocardiography of control and IRE1α cmc KO mice after 3 weeks of tamoxifen administration.

	unit	Control (n=2)	IRE1α (n=4)	significance
Body weight	g	23.48 ± 0.58	21.22 ± 1.13	ns
Heat rate	bpm	368.63 ± 91.37	454.14 ± 23.28	ns
LV dimensions and functions				
IVSd	mm	0.65 ± 0.01	0.60 ± 0.05	ns
IVSs	mm	0.93 ± 0.01	0.66 ± 0.05	*
LVIDd	mm	4.08 ± 0.23	4.94 ± 0.25	ns
LVIDs	mm	2.81 ± 0.61	4.58 ± 0.26	*
LVPWd	mm	0.72 ± 0.01	0.63 ± 0.04	ns
LVPWs	mm	1.05 ± 0.08	0.70 ± 0.03	**
Vol.;d	µl	72.34 ± 9.63	119.13 ± 14.79	ns
Vol.;s	µl	30.62 ± 14.33	96.47 ± 14.00	*
Stroke Vol.	µl	41.73 ± 4.69	22.66 ± 1.49	**
% EF		58.29 ± 16.03	16.33 ± 1.47	*
%FS		31.57 ± 11.00	7.35 ± 0.66	*
Cardiac Output	(ml/min)	16.06 ± 5.79	10.23 ± 0.49	ns
LV mass	g	78.90 ± 8.80	98.68 ± 14.70	ns
Mitral inflow				
E velocity	mm/sec	540.5 ± 91.2	506.1 ± 54.8	ns
A velocity	mm/sec	349.7 ± 77.7	189.1 ± 58.4	ns
Mitral E/A ratio	mitral	1.56 ± 0.08	4.49 ± 2.2	ns
Tei index		0.90 ± 0.03	1.43 ± 0.16	ns
Pulmonary				
Pulse wave velocity	mm/s	674.5 ± 45.5	432.75 ± 59.05	*

LV = left ventricle
IVSd = intraventricular septum wall thickness (diastolic)
IVSs = intraventricular septum wall thickness (systolic)
LVIDd = left ventricle inner diameter (diastolic)
LVIDs = left ventricle inner diameter (systolic)
LVPWd = left ventricle posterior wall thickness (diastolic)
LVPWs = left ventricle posterior wall thickness (systolic)
Vol:d = LV end-diastolic volume
Vol:s = LV end-systolic volume
%EF= percentage of ejection fraction
%FS = LV fractional shortening = $\frac{LV\ end\ diastolic\ dimension - LV\ end\ systolic\ dimention}{LV\ end\ diastolic\ dimension} \times 100\%$
LV mass = left ventricular mass
LV diastolic function assess by mitral inflow doppler tracing, E velocity: measured from E wave, early left ventricle filling waves. A velocity: measured from A wave, late atrial contraction wave.
Mitral E/A ratio: ratio of E wave to A-wave velocity
Tei index, an index of myocardial performance in systolic and diastolic function
Statistical significance: *$p < 0.05$ and **$p < 0.01$, ns: not significant. Analyzed by unpaired student t-test, two tail. Data presented are mean ± standard error.

Next, we carry out electrocardiogram to detect potential conduction delays and arrhythmias associated with dilated cardiomyopathy in IRE1α cmc KO mice. The P wave amplitude as a proportion of the QRS amplitude was increased in the IRE1α cmc KO hearts indicative of an enlarged cardiac chambers (Figure 3-4D). The QRS amplitude was also significantly reduced in IRE1α cmc KO hearts (Figure 3-4D, Table 3-2). Taken together, the ECG analysis further supported our conclusions that IRE1α deficiency in cardiomyocytes in adult heart leads to dilated cardiomyopathy with left ventricle enlargement and severe impairment of systolic function.

Table 3-2. Electrocardigram of control and IRE1α cmc KO mice after 3 weeks of tamoxifen administration.

	unit	Control (n=5)	IRE1α cmc KO (n=4)	significance
Body weight	g	22.9 ± 1.533	20.9 ± 1.451	ns
Heart rate	bpm	442.2 ±43.6	465.9 ± 31.444	ns
RR interval	s	0.1414 ± 0.015	0.1308 ± 0.010	ns
PR interval	s	0.038 ± 0.002	0.03675 ± 0.004	ns
P duration	s	0.018 ± 0.003	0.01275 ± 0.001	ns
QRS interval	s	0.0102 ± 0.001	0.01125 ± 0.002	ns
QT interval	s	0.0176 ± 0.0002	0.0225 ± 0.006	ns
QTc	s	0.047 ± 0.003	0.0635 ± 0.019	ns
JT interval	s	0.0058 ± 0.001	0.011 ± 0.005	ns
Tpeak Tend interval	s	0.0038 ± 0.001	0.00825 ± 0.004	ns
P Amplitude	mV	0.1054 ± 0.012	0.1058 ± 0.013	ns
Q Amplitude	mV	-0.1404 ± 0.054	-0.02 ± 0.021	ns
R Amplitude	mV	1.476 ± 0.195	0.4925 ± 0.032	**
S Amplitude	mV	-0.2634 ± 0.163	-0.1943 ± 0.108	ns
ST Height	mV	0.0526 ± 0.028	-0.1033 ± 0.066	*
T Amplitude	mV	0.1086 ± 0.098	-0.02475 ± 0.114	ns

Statistical significance: *$p < 0.05$ and **$p < 0.01$, ns: not significant. Analyzed by unpaired student t-test, two tail. Data presented are mean ± standard error.

3.4.3 IRE1α deficient hearts develop cardiac fibrosis

Fibrosis remodeling is associated with non-ischemic dilated myopathy[35, 36]. Inhibiting IRE1α endonuclease activity prevents cardiac fibrosis with improved prognosis[26]. Surprisingly, IRE1α cmc KO hearts developed fibrosis. Trichrome staining of the myocardium and quantitative analysis of the fibrotic areas shows increased deposition of collagen in the IRE1α cmc KO hearts (Figure 3-5) indicating that cardiomyocyte specific deletion of IRE1α lead to development of cardiac fibrosis.

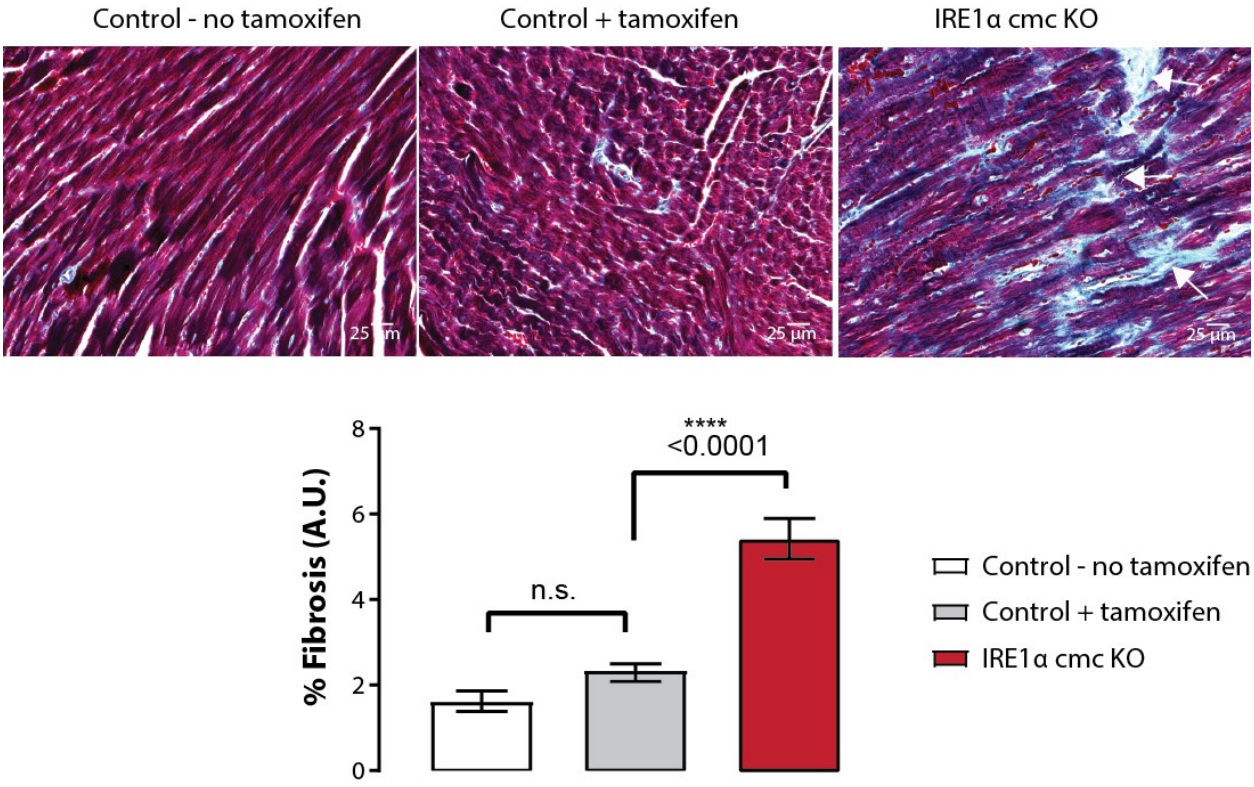

Figure 3-5. Cardiomyocytes-specific IRE1α deletion in adult mice develops cardiac fibrosis.

Gomori's trichrome staining for collage depositions of control ($IRE1\alpha^{flox/flox}$ without Cre) and IRE1α cmc KO myocardium. IRE1α cmc KO mice without tamoxifen induction control ($IRE1\alpha^{flox/flox}$ + Cre, fed with chow food) were also included. The arrows indicate the location of the blue staining for collage. Quantitative analysis of the percentage of areas with collagen deposition in all three groups were measured and analyzed by imageJ. Unpaired two tail student t-test was used for statistical analysis. ****: $p < 0.0001$. n.s. not significant. Data shown are mean ± standard error.

3.4.4 IRE1α deficient myocytes has reduced t-tubule and increased extracellular staining

Cardiomyocytes from failing hearts have reduced number or even absence of T-tubules[37, 38]. To determine if T-tubule remodeling was associated with cardiomyocyte specific IRE1α deletion-induced dilated myopathy, we use FITC conjugated wheat germ agglutinin (WGA) to stain sarcolemma and T-tubule within myocardium. WGA is a lectin that selectively binds to N-acetylglucosamine-oligomers and sialic acid residues on glycoproteins[39], including dystrophin-associated glycoprotein complex localized at T-tubule[40] and collagen in extracellular matrix[41], and been used to label cell boundary and T-tubules of the cardiomyocytes[42-44]. Fluorescence probe conjugated WGA has been previously used as a tool for detecting T-tubule remodeling and measuring cardiomyocyte sizes within myocardium[40, 45, 46].

Confocal imaging of heart from IRE1α cmc KO mice showed significant reduction in the T-tubule fractional area (7.9 ± 0.4%, mean ± standard error), quantified by FITC-WGA staining area versus longitudinal cross-section area of a single cardiomyocyte (14.6 ± 0.5 %)(Figure 3-6). Moreover, cardiomyocyte specific IRE1α deletion causes enlarged cardiomyocytes size. The mean cardiomyocytes cross-section area in IRE1α$^{flox/flox}$ control heart was 648.6 ± 22.5 μm^2 (longitudinal) and 243.6 ± 9.3 μm^2 (short axis) compare to a significantly increased cardiomyocyte size in IRE1α cmc KO hearts - 833.9 ± 32.6 μm^2 (longitudinal) and 291.6 ± 7.5 μm^2 (short axis), $p < 0.0001$, 220 for control group and 280 cells IRE1α cmc KO hearts, and $n = 3$ for both groups (Figure 3-6).

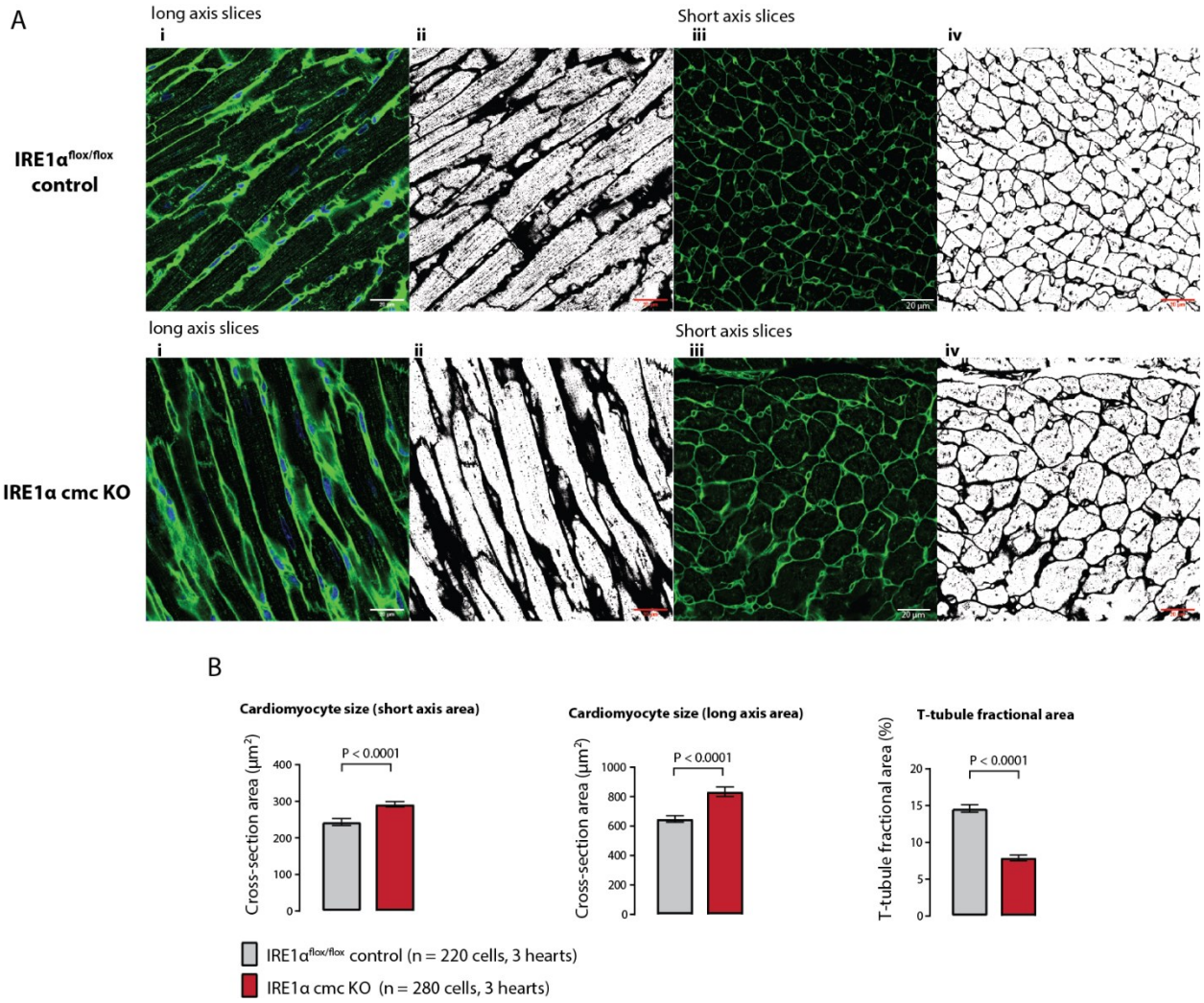

Figure 3-6. T-tubule and extracellular matrixes in IRE1α cmc KO ventricle.

FITC conjugated wheat germ agglutinin staining (green) of heart sections from control (IRE1α$^{flox/flox}$) and IRE1α cmc KO hearts fed tamoxifen for 3 weeks. Representative images in the longitudinal-axis plane (i) and short-axis cross-section (iii). DAPI nucleus co-staining shown in blue. The binary images with manual adjusted threshold show stained area in black and non-stained area in white were produced for better visualization and analysis (ii and iv). Confocal images were taken from random regions of ventricle sections. Images were analyzed using Fiji ImageJ.

3.4.5 IRE1α deletion cause dysfunction in Ca^{2+} handling

To determine whether IRE1α deletion in cardiomyocytes alters Ca^{2+} handling, we measured intracellular Ca^{2+} concentration ($[Ca^{2+}]_i$) in the isolated, field-stimulated ventricular cardiomyocytes loaded with the fluorescent, cell permeable, Ca^{2+} indicator fluo-4/AM. Global Ca^{2+} transient from IRE1α deficient cardiomyocytes shows frequently small transient rises in diastolic Ca^{2+} and after contractions following each paced beat (Figure 3-7A). These spontaneous premature Ca^{2+} release events occurred in a statistically significant higher frequency in IRE1α deficient cardiomyocytes (0.92 ± 0.13 versus 0.33 ± 0.10 spontaneous Ca^{2+} release events per 20 seconds) than cells isolated from control hearts. This alternation in Ca^{2+} transient is typical in store-overload-induced Ca^{2+} release, where SR Ca^{2+} overload leads to spontaneous Ca^{2+} release through RyR2 and triggers arrhythmias[47].

Moreover, IRE1α deficient cardiomyocytes shows significantly prolonged response in recovering cytosolic Ca^{2+} back to baseline (the pre-stimulation baseline value of the recorded signal), and random occurrence of a sustained, low amplitude phase of Ca^{2+} release after peak (Figure 3-7B). Similar to diastolic SR Ca^{2+} leaks caused by RyR2 mutations or Casq2 deletion[48-50]. Interestingly, our preliminary result shows partial inhibition of RyR2 channels via ryanodine able to abolish Ca^{2+} oscillation in the isolated IRE1α cmc KO cardiomyocytes and recovery of transient duration comparable to control myocytes. This indicates that spontaneous Ca^{2+} releases seen in IRE1α cmc KO cardiomyocytes may be caused by enhanced RyR2 activity.

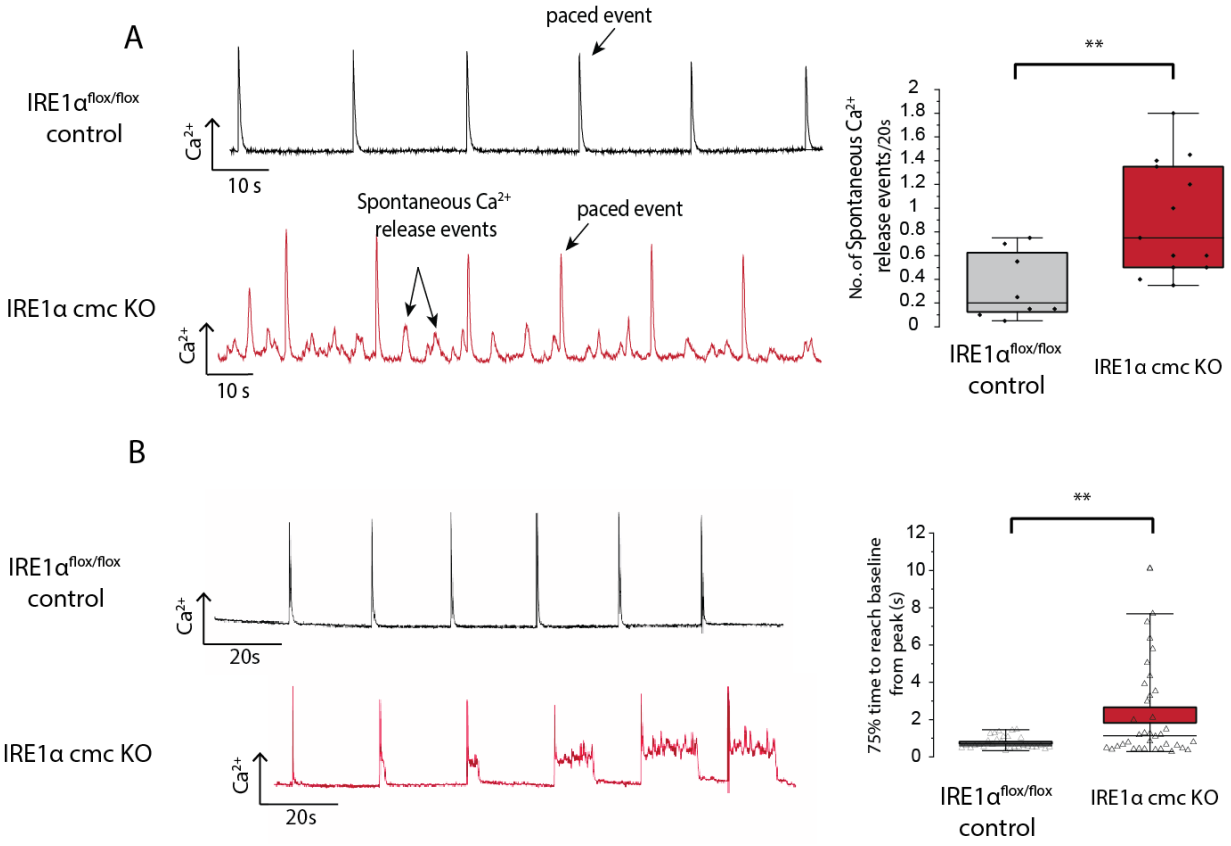

Figure 3-7. Ca^{2+} transient recordings in IRE1α cmc KO cardiomyocytes.

A) Representative Ca^{2+} transient recording showing spontaneous Ca^{2+} release events at rest (without electrical stimuli) in cardiomyocytes isolated from IRE1α cmc KO hearts (left). Quantification of spontaneous Ca^{2+} release events per 20s of recording (right). IRE1α deficient cardiomyocytes shows increased unsynchronized spontaneous Ca^{2+} release events. n=8 and 13 for control and IRE1α cmc KO cardiomyocytes recordings respectively from three hearts each group. **, $p < 0.01$.

B) Representative Ca^{2+}transient recordings for cardiomyocytes isolated from control ($IRE1\alpha^{flox/flox}$) and IRE1α cmc KO hearts fed tamoxifen for 3 weeks (left). Ca^{2+} transients were recorded from fluo 4/AM loaded, field-stimulated myocytes at 0.05 Hz. Cardiomyocytes isolated from IRE1α cmc KO hearts showed prolonged $[Ca^{2+}]_i$ transient and Ca^{2+} oscillations. n=30 cells from three $IRE1\alpha^{flox/flox}$ control heart and n=36 cells from three IRE1α cmc KO hearts. **, $p < 0.01$. 75% of time (transient duration) to reach baseline from the transient peak: the plateau duration measured at 75% below the peak level (right)

3.5 Discussion

Although work presented in Chapter 3 is still part of an ongoing and active research project a few exciting conclusions can be drown from currently available data. We demonstrated here that IRE1α plays an important role in maintaining cardiac health and function. IRE1α silencing in adult heart results in a severe dilated cardiomyopathy with impaired systolic function (Figure 3-4 and Table 3-1). The hearts develop cardiac fibrosis, have reduced T-tubules, and enlarged cardiomyocytes (Figure 3-5 and Figure 3-6). Most importantly and surprisingly, IRE1α-deficient cardiomyocytes showed impaired Ca^{2+} handling, with a prolonged Ca^{2+} release response and increased spontaneous Ca^{2+} release events (Figure 3-7).

IRE1α mediated UPR is essential for development and cell survival[31, 51, 52]. Whole body knockout of the IRE1α gene in mice results in embryonic lethality at 12.5 days of gestation due to placental malformation[31]. Whole-body knockout of the XBP1 gene, a well characterized adaptive response part of IRE1α pathway, in mice results in embryonic lethality at E12.5-14.5 due to impaired hepatocyte development[53]. In adult hearts, XBP1 deficiency leads to different phenotype when compared to the IRE1α gene knockout[16, 54]. Silencing XBP1 adult cardiomyocytes do not alter cardiac size and function, but exacerbated cardiac hypertrophy after isoproterenol infusion compare with wild-type mice[54]. XBP1 knockout in adult hearts have preserved cardiac function at young age (≤ 3 month) but shows progressive loss of cardiac contractility leading to mortality during aging, and exacerbation of heart failure progression under pressure overload[16]. This unique phenotype of XBP1-deficient adult hearts indicates that functions of IRE1α other than splicing of XBP1 mRNA, contribute to the phenotype of IRE1α-deficient hearts we generated in this study. Moreover, when compared to other UPR branches, whole body knockout of the ATF6 gene or cardiomyocyte specific knockout of the PERK gene in adult mice hearts exhibit normal cardiac structure and contractile properties under non-stressed conditions[11, 12]. These animals, however, show increased cell damage and decreased cardiac function under stress conditions and ischemic/reperfusion damage[11, 12]. These findings indicate that adaptive UPR responses are cardioprotective under stressed condition, however, at rest, cardiac structure and function is not affected in the absence of UPR components, ATF6, PERK, and XBP1. Taken together, the severe cardiac remodeling and impaired cardiac systolic function seen by us in IRE1α gene knockout hearts under non-stressed conditions are unexpected, and we propose that a novel and unique function of IRE1α may be responsible for its effects on cardiac physiology.

Cardiomyocyte specific IRE1α knockout causes Ca^{2+} handling dysfunction during stimulated contraction (Figure 3-7). There is limited information on the link between UPR and arrhythmia [55]. In human induced pluripotent stem cell-derived cardiomyocytes, activation of UPR induced by tunicamycin results in downregulation of multiple cardiac ion channels, including Nav1.5, Kv4.3, KvLQT1, and Cav1.2, leads to altered action potential morphology (prolonged duration and decreased upstroke velocity)[56]. To our knowledge, the functional association between IRE1α and electrophysiology of the heart have not been investigated We have previously shown that in cardiomyocytes, IRE1α is localized to both perinuclear ER and the junctional SR (Chapter 2). IRE1α as a junctional SR component colocalized with RyR2/Ca^{2+} release channel and interacts with Ca^{2+} storage/buffering protein calsequestrin, both RyR2 and calsequestrin play important roles in the control of muscle EC-coupling. Can IRE1α interact with RyR2 and control RyR2 Ca^{2+} release properties? Recent study have shown that IRE1α interacts directly with inositol 1,4,5-trisphosphate ($InsP_3R1$) and controls $InsP_3R1$ cellular distribution and enhance Ca^{2+} channel activity[57]. The $InsP_3Rs$ and RyRs are transmembrane proteins with similar functional characteristics, similar protein structures and membrane arrangement[58-61]. Similar to $InsP_3Rs$, IRE1α may be able to interact with RyR2 and affect its Ca^{2+} release properties. To support this hypothesis, our preliminary result indicates that normal Ca^{2+} transient can be restored in IRE1α -deficient cardiomyocytes with administration of ryanodine.

ER stress have been implicated in many cardiovascular diseases[2, 3]. Adaptive UPR have shown be cardioprotective, but irremediable ER stress can push the UPR toward proinflammatory and proapoptotic signaling. IRE1α as master regulator that is capable of cell fate determination have shown both cardioprotective and ability to contribute to disease progression. For example, overexpressing IRE1α in cardiomyocytes can protect heart against pressure overload-induced heart failure[13], on other hand, inhibiting IRE1α can protect heart from cardiac fibrosis[26] and atherosclerosis[25]. A better understanding of the underlying physiological role of IRE1α in the heart can help us develop therapeutic strategies aimed at mitigating ER stress in heart diseases. Here, we show that IRE1α is essential for cardiac health and function, IRE1α deficient adult heart exhibit severe dilation and reduced cardiac function under non stressed condition, and this may be due to dysfunctions in cardiomyocytes Ca^{2+} handling. However, the underlying mechanism is yet to be uncovered.

3.6 References

1. Westrate LM, Lee JE, Prinz WA, Voeltz GK. Form follows function: the importance of endoplasmic reticulum shape. *Annual Review of Biochemistry*. 2015;84:791-811
2. Groenendyk J, Agellon LB, Michalak M. Coping with endoplasmic reticulum stress in the cardiovascular system. *Annual Review of Physiology*. 2013;75:49-67
3. Groenendyk J, Sreenivasaiah PK, Kim DH, Agellon LB, Michalak M. Biology of endoplasmic reticulum stress in the heart. *Circulation Research*. 2010;107:1185-1197
4. Doroudgar S, Thuerauf DJ, Marcinko MC, Belmont PJ, Glembotski CC. Ischemia activates the ATF6 branch of the endoplasmic reticulum stress response. *Journal of Biological Chemistry*. 2009;284:29735-29745
5. Okada K, Minamino T, Tsukamoto Y, Liao Y, Tsukamoto O, Takashima S, Hirata A, Fujita M, Nagamachi Y, Nakatani T, Yutani C, Ozawa K, Ogawa S, Tomoike H, Hori M, Kitakaze M. Prolonged endoplasmic reticulum stress in hypertrophic and failing heart after aortic constriction: possible contribution of endoplasmic reticulum stress to cardiac myocyte apoptosis. *Circulation*. 2004;110:705-712
6. Li SY, Gilbert SA, Li Q, Ren J. Aldehyde dehydrogenase-2 (ALDH2) ameliorates chronic alcohol ingestion-induced myocardial insulin resistance and endoplasmic reticulum stress. *Journal of Molecular and Cellular Cardiology*. 2009;47:247-255
7. Severino A, Campioni M, Straino S, Salloum FN, Schmidt N, Herbrand U, Frede S, Toietta G, Di Rocco G, Bussani R, Silvestri F, Piro M, Liuzzo G, Biasucci LM, Mellone P, Feroce F, Capogrossi M, Baldi F, Fandrey J, Ehrmann M, Crea F, Abbate A, Baldi A. Identification of Protein Disulfide Isomerase as a Cardiomyocyte Survival Factor in Ischemic Cardiomyopathy. *Journal of the American College of Cardiology*. 2007;50:1029-1037
8. Myoishi M, Hao H, Minamino T, Watanabe K, Nishihira K, Hatakeyama K, Asada Y, Okada K, Ishibashi-Ueda H, Gabbiani G, Bochaton-Piallat ML, Mochizuki N, Kitakaze M. Increased endoplasmic reticulum stress in atherosclerotic plaques associated with acute coronary syndrome. *Circulation*. 2007;116:1226-1233
9. Jia LX, Zhang WM, Zhang HJ, Li TT, Wang YL, Qin YW, Gu H, Du J. Mechanical stretch-induced endoplasmic reticulum stress, apoptosis and inflammation contribute to thoracic aortic aneurysm and dissection. *Journal of Pathology*. 2015;236:373-383
10. Martindale Joshua J, Fernandez R, Thuerauf D, Whittaker R, Gude N, Sussman Mark A, Glembotski Christopher C. Endoplasmic reticulum stress gene induction and protection from ischemia/reperfusion injury in the hearts of transgenic mice with a tamoxifen-regulated form of ATF6. *Circulation Research*. 2006;98:1186-1193
11. Jin J-K, Blackwood EA, Azizi K, Thuerauf DJ, Fahem AG, Hofmann C, Kaufman RJ, Doroudgar S, Glembotski CC. ATF6 decreases myocardial ischemia/reperfusion damage and links er stress and oxidative stress signaling pathways in the heart. *Circulation Research*. 2017;120:862-875
12. Liu X, Kwak D, Lu Z, Xu X, Fassett J, Wang H, Wei Y, Cavener DR, Hu X, Hall J, Bache RJ, Chen Y. Endoplasmic reticulum stress sensor protein kinase R-like endoplasmic

reticulum kinase (PERK) protects against pressure overload-induced heart failure and lung remodeling. *Hypertension (Dallas, Tex. : 1979)*. 2014;64:738-744

13. Steiger D, Yokota T, Li J, Ren S, Minamisawa S, Wang Y. The serine/threonine-protein kinase/endoribonuclease IRE1α protects the heart against pressure overload-induced heart failure. *The Journal of Biological Chemistry*. 2018;293:9652-9661

14. Thuerauf Donna J, Marcinko M, Gude N, Rubio M, Sussman Mark A, Glembotski Christopher C. Activation of the unfolded protein response in infarcted mouse heart and hypoxic cultured cardiac myocytes. *Circulation Research*. 2006;99:275-282

15. Wang ZV, Deng Y, Gao N, Pedrozo Z, Li DL, Morales CR, Criollo A, Luo X, Tan W, Jiang N, Lehrman MA, Rothermel BA, Lee A-H, Lavandero S, Mammen PPA, Ferdous A, Gillette TG, Scherer PE, Hill JA. Spliced X-box binding protein 1 couples the unfolded protein response to hexosamine biosynthetic pathway. *Cell*. 2014;156:1179-1192

16. Wang X, Deng Y, Zhang G, Li C, Ding G, May Herman I, Tran Diem H, Luo X, Jiang D-S, Li Dan L, Wei X, Xu L, Ferdous A, Gillette Thomas G, Scherer Philipp E, Jiang X, Wang Zhao V. Spliced x-box binding protein 1 stimulates adaptive growth through activation of mTOR. *Circulation*. 2019;140:566-579

17. Sano R, Reed JC. ER stress-induced cell death mechanisms. *Biochimica et Biophysica Acta (BBA) - Molecular Cell Research*. 2013;1833:3460-3470

18. Wang S, Binder P, Fang Q, Wang Z, Xiao W, Liu W, Wang X. Endoplasmic reticulum stress in the heart: insights into mechanisms and drug targets. *British Journal of Pharmacology*. 2018;175:1293-1304

19. Terai K, Hiramoto Y, Masaki M, Sugiyama S, Kuroda T, Hori M, Kawase I, Hirota H. AMP-activated protein kinase protects cardiomyocytes against hypoxic injury through attenuation of endoplasmic reticulum stress. *Molecular and Cellular Biology*. 2005;25:9554-9575

20. Yamaguchi O, Higuchi Y, Hirotani S, Kashiwase K, Nakayama H, Hikoso S, Takeda T, Watanabe T, Asahi M, Taniike M, Matsumura Y, Tsujimoto I, Hongo K, Kusakari Y, Kurihara S, Nishida K, Ichijo H, Hori M, Otsu K. Targeted deletion of apoptosis signal-regulating kinase 1 attenuates left ventricular remodeling. *Proceedings of the National Academy of Sciences of the United States of America*. 2003;100:15883-15888

21. Fu HY, Minamino T, Tsukamoto O, Sawada T, Asai M, Kato H, Asano Y, Fujita M, Takashima S, Hori M, Kitakaze M. Overexpression of endoplasmic reticulum-resident chaperone attenuates cardiomyocyte death induced by proteasome inhibition. *Cardiovascular Research*. 2008;79:600-610

22. Nishitoh H, Matsuzawa A, Tobiume K, Saegusa K, Takeda K, Inoue K, Hori S, Kakizuka A, Ichijo H. ASK1 is essential for endoplasmic reticulum stress-induced neuronal cell death triggered by expanded polyglutamine repeats. *Genes & Development*. 2002;16:1345-1355

23. Pendse AA, Arbones-Mainar JM, Johnson LA, Altenburg MK, Maeda N. Apolipoprotein E knock-out and knock-in mice: atherosclerosis, metabolic syndrome, and beyond. *Journal of Lipid Research*. 2009;50 Suppl:S178-S182

24. Erbay E, Babaev VR, Mayers JR, Makowski L, Charles KN, Snitow ME, Fazio S, Wiest MM, Watkins SM, Linton MF, Hotamisligil GS. Reducing endoplasmic reticulum stress through a macrophage lipid chaperone alleviates atherosclerosis. *Nature Medicine*. 2009;15:1383-1391

25. Tufanli O, Telkoparan Akillilar P, Acosta-Alvear D, Kocaturk B, Onat UI, Hamid SM, Cimen I, Walter P, Weber C, Erbay E. Targeting IRE1 with small molecules counteracts progression of atherosclerosis. *Proceedings of the National Academy of Sciences of the United States of America*. 2017;114:E1395-E1404

26. Groenendyk J, Lee D, Jung J, Dyck JR, Lopaschuk GD, Agellon LB, Michalak M. Inhibition of the Unfolded Protein Response Mechanism Prevents Cardiac Fibrosis. *PLOS One*. 2016;11:e0159682

27. Guan HS, Shangguan HJ, Shang Z, Yang L, Meng XM, Qiao SB. Endoplasmic reticulum stress caused by left ventricular hypertrophy in rats: effects of telmisartan. *American Journal of the Medical Sciences*. 2011;342:318-323

28. Fu Hai Y, Okada K-i, Liao Y, Tsukamoto O, Isomura T, Asai M, Sawada T, Okuda K, Asano Y, Sanada S, Asanuma H, Asakura M, Takashima S, Komuro I, Kitakaze M, Minamino T. Ablation of C/EBP homologous protein attenuates endoplasmic reticulum–mediated apoptosis and cardiac dysfunction induced by pressure overload. *Circulation*. 2010;122:361-369

29. Wiersma M, Meijering RAM, Qi X-Y, Zhang D, Liu T, Hoogstra-Berends F, Sibon OCM, Henning RH, Nattel S, Brundel BJJM. Endoplasmic reticulum stress is associated with autophagy and cardiomyocyte remodeling in experimental and human atrial fibrillation. *Journal of the American Heart Association*. 2017;6:e006458

30. Ayyappan JP, Lizardo K, Wang S, Yurkow E, Nagajyothi JF. Inhibition of ER stress by 2-aminopurine treatment modulates cardiomyopathy in a murine chronic chagas disease model. *Biomolecules & Therapeutics (Seoul)*. 2019;27:386-394

31. Iwawaki T, Akai R, Yamanaka S, Kohno K. Function of IRE1 alpha in the placenta is essential for placental development and embryonic viability. *Proceedings of the National Academy of Sciences*. 2009;106:16657

32. Lee D, Oka T, Hunter B, Robinson A, Papp S, Nakamura K, Srisakuldee W, Nickel BE, Light PE, Dyck JRB, Lopaschuk GD, Kardami E, Opas M, Michalak M. Calreticulin induces dilated cardiomyopathy. *PloS one*. 2013;8:e56387-e56387

33. Schipke J, Brandenberger C, Rajces A, Manninger M, Alogna A, Post H, Mühlfeld C. Assessment of cardiac fibrosis: a morphometric method comparison for collagen quantification. *Journal of Applied Physiology*. 2017;122:1019-1030

34. Ackers-Johnson M, Li PY, Holmes AP, O'Brien SM, Pavlovic D, Foo RS. A simplified, langendorff-free method for concomitant isolation of viable cardiac myocytes and nonmyocytes from the adult mouse heart. *Circulation Research*. 2016;119:909-920

35. Cojan-Minzat BO, Zlibut A, Agoston-Coldea L. Non-ischemic dilated cardiomyopathy and cardiac fibrosis. *Heart Failure Reviews*. 2020

36. Liu T, Song D, Dong J, Zhu P, Liu J, Liu W, Ma X, Zhao L, Ling S. Current understanding of the pathophysiology of myocardial fibrosis and its quantitative assessment in heart failure. *Frontiers in Physiology*. 2017;8

37. Kaprielian RR, Stevenson S, Rothery SM, Cullen MJ, Severs NJ. Distinct patterns of dystrophin organization in myocyte sarcolemma and transverse tubules of normal and diseased human myocardium. *Circulation*. 2000;101:2586-2594

38. Crossman DJ, Young AA, Ruygrok PN, Nason GP, Baddelely D, Soeller C, Cannell MB. T-tubule disease: Relationship between t-tubule organization and regional contractile performance in human dilated cardiomyopathy. *Journal of Molecular and Cellular Cardiology*. 2015;84:170-178

39. Bhavanandan VP, Katlic AW. The interaction of wheat germ agglutinin with sialoglycoproteins. The role of sialic acid. *Journal of Biological Chemistry*. 1979;254:4000-4008

40. Campbell KP, Kahl SD. Association of dystrophin and an integral membrane glycoprotein. *Nature*. 1989;338:259-262

41. Pandya K, Kim H-S, Smithies O. Fibrosis, not cell size, delineates β-myosin heavy chain reexpression during cardiac hypertrophy and normal aging in vivo. *Proceedings of the National Academy of Sciences of the United States of America*. 2006;103:16864-16869

42. Balijepalli RC, Lokuta AJ, Maertz NA, Buck JM, Haworth RA, Valdivia HH, Kamp TJ. Depletion of T-tubules and specific subcellular changes in sarcolemmal proteins in tachycardia-induced heart failure. *Cardiovascular Research*. 2003;59:67-77

43. Emde B, Heinen A, Gödecke A, Bottermann K. Wheat germ agglutinin staining as a suitable method for detection and quantification of fibrosis in cardiac tissue after myocardial infarction. *European Journal of Histochemistry*. 2014;58:2448-2448

44. Richards MA, Clarke JD, Saravanan P, Voigt N, Dobrev D, Eisner DA, Trafford AW, Dibb KM. Transverse tubules are a common feature in large mammalian atrial myocytes including human. *American Journal of Physiology. Heart and Circulatory Physiology*. 2011;301:H1996-H2005

45. Bensley JG, De Matteo R, Harding R, Black MJ. Three-dimensional direct measurement of cardiomyocyte volume, nuclearity, and ploidy in thick histological sections. *Scientific Reports*. 2016;6:23756

46. Crossman DJ, Shen X, Jüllig M, Munro M, Hou Y, Middleditch M, Shrestha D, Li A, Lal S, dos Remedios CG, Baddeley D, Ruygrok PN, Soeller C. Increased collagen within the transverse tubules in human heart failure. *Cardiovascular Research*. 2017;113:879-891

47. Priori SG, Chen SRW. Inherited dysfunction of sarcoplasmic reticulum Ca^{2+} handling and arrhythmogenesis. *Circulation Research*. 2011;108:871-883

48. Acimovic I, Refaat MM, Moreau A, Salykin A, Reiken S, Sleiman Y, Souidi M, Přibyl J, Kajava AV, Richard S, Lu JT, Chevalier P, Skládal P, Dvořak P, Rotrekl V, Marks AR, Scheinman MM, Lacampagne A, Meli AC. Post-translational modifications and diastolic calcium leak associated to the novel RYR2-D3638A mutation lead to cpvt in patient-specific hipsc-derived cardiomyocytes. *Journal of Clinical Medicine*. 2018;7:423

49. Knollmann BC, Chopra N, Hlaing T, Akin B, Yang T, Ettensohn K, Knollmann BE, Horton KD, Weissman NJ, Holinstat I, Zhang W, Roden DM, Jones LR, Franzini-Armstrong C, Pfeifer K. Casq2 deletion causes sarcoplasmic reticulum volume increase, premature Ca^{2+} release, and catecholaminergic polymorphic ventricular tachycardia. *Journal of Clinical Investigation*. 2006;116:2510-2520

50. Iyer V, Hajjar Roger J, Armoundas Antonis A. Mechanisms of abnormal calcium homeostasis in mutations responsible for catecholaminergic polymorphic ventricular tachycardia. *Circulation Research*. 2007;100:e22-e31

51. Mishiba K-I, Iwata Y, Mochizuki T, Matsumura A, Nishioka N, Hirata R, Koizumi N. Unfolded protein-independent IRE1 activation contributes to multifaceted developmental processes in Arabidopsis. *Life Science Alliance*. 2019;2:e201900459

52. Chen Y, Brandizzi F. IRE1: ER stress sensor and cell fate executor. *Trends in Cell Biology*. 2013;23:547-555

53. Reimold AM, Etkin A, Clauss I, Perkins A, Friend DS, Zhang J, Horton HF, Scott A, Orkin SH, Byrne MC, Grusby MJ, Glimcher LH. An essential role in liver development for transcription factor XBP-1. *Genes & Development* 2000;14:152-157

54. Duan Q, Ni L, Wang P, Chen C, Yang L, Ma B, Gong W, Cai Z, Zou M-H, Wang DW. Deregulation of XBP1 expression contributes to myocardial vascular endothelial growth factor-A expression and angiogenesis during cardiac hypertrophy invivo. *Aging cell*. 2016;15:625-633

55. Liu M, Dudley SC, Jr. The role of the unfolded protein response in arrhythmias. *Channels (Austin, Tex.)*. 2018;12:335-345

56. Liu M, Shi G, Zhou A, Rupert CE, Coulombe KLK, Dudley SC, Jr. Activation of the unfolded protein response downregulates cardiac ion channels in human induced pluripotent stem cell-derived cardiomyocytes. *Journal of Molecular and Cellular Cardiology*. 2018;117:62-71

57. Carreras-Sureda A, Jaña F, Urra H, Durand S, Mortenson DE, Sagredo A, Bustos G, Hazari Y, Ramos-Fernández E, Sassano ML, Pihán P, van Vliet AR, González-Quiroz M, Torres AK, Tapia-Rojas C, Kerkhofs M, Vicente R, Kaufman RJ, Inestrosa NC, Gonzalez-Billault C, Wiseman RL, Agostinis P, Bultynck G, Court FA, Kroemer G, Cárdenas JC, Hetz C. Non-canonical function of IRE1α determines mitochondria-associated endoplasmic reticulum composition to control calcium transfer and bioenergetics. *Nature Cell Biology*. 2019;21:755-767

58. Fan G, Baker ML, Wang Z, Baker MR, Sinyagovskiy PA, Chiu W, Ludtke SJ, Serysheva, II. Gating machinery of InsP3R channels revealed by electron cryomicroscopy. *Nature*. 2015;527:336-341

59. Peng W, Shen H, Wu J, Guo W, Pan X, Wang R, Chen SR, Yan N. Structural basis for the gating mechanism of the type 2 ryanodine receptor RyR2. *Science*. 2016;354

60. Seo M-D, Enomoto M, Ishiyama N, Stathopulos PB, Ikura M. Structural insights into endoplasmic reticulum stored calcium regulation by inositol 1,4,5-trisphosphate and ryanodine receptors. *Biochimica et Biophysica Acta (BBA) - Molecular Cell Research*. 2015;1853:1980-1991

61. Mackrill JJ. Ryanodine receptor calcium release channels: an evolutionary perspective. *Advancesin Experimental Medicine and Biology*. 2012;740:159-182

Chapter 4: Phylogenetic and biochemical analysis of calsequestrin structure and association of its variants with cardiac disorders

4.1 Abstract

Calsequestrin is among the most abundant proteins in muscle SR and displays a high capacity but a low affinity for Ca^{2+} binding. In mammals, calsequestrin is encoded by two genes, *CASQ1* and *CASQ2*, which are expressed almost exclusively in skeletal and cardiac muscles, respectively. Phylogenetic analysis indicates that calsequestrin is an ancient gene in metazoans, and that the duplication of the ancestral calsequestrin gene took place after the emergence of the lancelet. Cardiac muscle calsequestrin (CASQ2) gene variants associated with catecholaminergic polymorphic ventricular tachycardia (CPVT) in humans are positively correlated with a high degree of evolutionary conservation across all calsequestrin homologues. We investigated the impact of CPVT associated mutations on protein structure and function and carried out biochemical and biophysical analysis of CPVT causing mutations including R33Q, L167H, D307H, newly discovery recessive dominant CPVT associated mutant K180R, and heterozygous variants recently discovered from whole exome sequencing (D351G, G332R, P329S). The mutations are distributed in diverse locations of the calsequestrin protein and impart functional diversity but remarkably manifest in a similar phenotype in humans.

4.2 Introduction

The SR is a high specialized membrane network that supports mechanical muscle functions requiring large fluxes of Ca^{2+}. Consequently, the SR controls E-C coupling[1-3] without compromising Ca^{2+} requiring cellular processes that are normally associated with the ER[4]. There are two well defined structural and functional regions of the SR in cardiac muscle: the longitudinal SR that runs parallel to the myofibrils and the junctional SR that forms multiple membrane contacts with T-tubule membrane contact sites[5-7]. The junctional SR is the primary site of Ca^{2+} release via the RyR/Ca^{2+} channel which triggers muscle contraction. The SR luminal Ca^{2+} binding protein calsequestrin is a high capacity, low affinity Ca^{2+} binding protein that forms oligomeric structures that regulate RyR activity *via* interactions with RyR, triadin and junctin[1, 8-14]. There are two isoforms of calsequestrin, which are encoded by two different genes: cardiac calsequestrin (*Casq2*) and skeletal muscle calsequestrin (*Casq1*)[14, 15]. The crystal structure of calsequestrin indicates that

the protein contains three thioredoxin-like domains reminiscent of ER luminal oxidoreductases[16, 17].

CPVT is an inherited disease characterized by ventricular arrhythmias leading to sudden death[18, 19]. CPVT results from defects in intracellular Ca^{2+} handling by cardiomyocytes. Two major variants have been associated with the CPVT disorder. The autosomal dominant form is associated with mutations in the RyR2 gene and accounts for ~50% cases, while a recessive form with mutations in the cardiac isoform of calsequestrin (CASQ2) accounts for 2-5 % cases. Other mutations also found in the *CALM1* (encodes calmodulin1) and *TRDN* (encodes triadin) gene account for <2% of CPVT cases[20-24]. Thirteen mutations in the CASQ2 gene have been identified in CPVT patients, in sudden death syndrome[25, 26], and three of them are non-synonymous polymorphisms (cSNP)[24, 27]. Several biochemical and cell biological studies of R33Q, L167H, and D307H calsequestrin mutants indicate that these mutations lead to impaired Ca^{2+} storage and Ca^{2+} release from the SR[22, 24-37]. Recently new calsequestrin mutations have been identified including K180R, D351G, G332R, and P329S[27, 36, 38-43].

In this study, we examined the evolutionary constraints of the CPVT related calsequestrin mutations, and included *Casq1*, *Casq2* and pre-duplicate calsequestrin in the phylogenetic analysis. We showed that calsequestrin is an ancient protein in the metazoan, and that the duplication of the calsequestrin gene took place after the divergence of the lancelet but before divergence of Chondrichthyes. We noted that calsequestrin mutations, associated with CPVT, positively correlated with an increase in the degree of evolutionary conservation of the mutated sites. Furthermore, we carried out biochemical and biophysical analysis of seven CPVT related mutants (R33Q, L167H, D307H, K180R), and whole exome sequencing variants (D351G, G332R, P329S), with a major emphasis on the mutation's impact on the structure and function of the calsequestrin protein. The mutations are distributed in diverse locations of the calsequestrin protein but remarkably manifest in a similar phenotype in humans[28, 30, 44-46].

.

4.3 Materials and Methods

4.3.1 Genome databases

The genomes used in the comparative genomics and phylogenetics analyses are publicly available and include the following from NCBI: *Homo sapiens, Canis lupus familiaris, Bos taurus, Oryctolagus cuniculus, Sus scrofa, Rattus norvegicus, Mus musculus, Xenopus tropicalis, Gallus gallus, Taeniopygia guttata, Crocodylus porosus, Latimeria chalumnae, Danio rerio, Callorhinchus milii, Leucoraja erinacea, Branchiostoma floridae, Ciona intestinalis, Helobdella robusta, Drosophila melanogaster, Apis mellifera, Manduca sexta, Daphnia pulex, Parhyale hawaiensis, Parasteatoda tepidariorum, Caenorhabditis elegans, Nematostella vectensis, Mnemiopsis leidyi, Trichoplax adhaerans, Amphimedon queenslandica, Monosiga brevicollis, Salpingoeca rosetta, Capsaspora owczarzaki.* Ensembl: *Helobdella robusta.* Skatebase.org: *Leucoraja erinacea.* hymenopteragenome.org: *Apis mellifera.* wfleabase.org: *Daphnia pulex*

4.3.2 Comparative genomics, phylogenetic and sequence alignments

Using *H. sapiens CASQ1* and *CASQ2* sequences as queries, BLASTp (Basic Local Alignment Search Tool protein) searches were performed on the genomes of 28 metazoan organisms (Table 4-1). Reciprocal BLAST was performed to verify the homology of significant hits obtained via forward BLAST. Predictions regarding the homology of a sequence were based on both the E-value and identity score. Hits that displayed the lowest E-value and greatest identity score in both the forward and reciprocal BLAST were predicted as being homologous. In cases of multiple homologous hits, the hit with the greatest identity score was predicted as being potentially orthologous. When no significant hits could be obtained using a BLASTp search, tBLASTn was used to search inside of the genome scaffolds. Additionally, HMMer was also used to search for sequences without significant BLASTp hits. Any potential HMMer hits were then verified using reciprocal BLAST.

For phylogenetic analyses, we used both RAxML consensus trees using 100 bootstraps and MrBayes Bayesian analysis trees with 10 million iterations achieving an average standard deviation of splits frequencies value of less than 0.01. Default parameters on CIPRES for RAxML-HPC v0.8 and MrBayes v3.2.6 on XSEDE were used with the following change for the RAxML trees: an LG4X protein matrix was used with the PROTGAMMA protein substitution model. The clades generated by the RAxML consensus trees were considered significant with node values of

at least 50. MrBayes tree clades were considered significant with node probability values of at least 0.8. RAxML consensus trees were generated using Consensus v3.695, while the graphical representation of the phylogenetic results was generated using Figtree v1.3.1. The calsequestrin sequences found using comparative genomics were aligned using MUSCLE v3.8.31 and visualized using MESQUITE v3.2.

4.3.3 Site-directed mutagenesis

A pET22b *E. coli* expression vector containing full-length recombinant canine *casq2* cDNA with a C-terminus 6xHis tag were used as template to obtain Casq2 mutants. Platinum pfx DNA polymerase (Invitrogen, 11708) was used for site-directed mutagenesis PCR with primers as follow with mutated residues shown in red:

R33Q: Forward primer (5' to 3') - GATGGCAAAGACCAGGTGGTCAGTCTCACTG
Reverse primer (5' to 3') -CAGTGAGACTGACCACCTGGTCTTTGCCATC

L167H : Forward primer (5' to 3') - GAGGACCAGATCAAACACATTGGCTTTTTCAAG
Reverse primer (5' to 3') -CTTGAAAAAGCCAATGTGTTTGATCTGGTCCTC

K180R : forward primer (5' to 3') - GTCAGAGTATTATAGGGCTTTTGAGGAGGC
Reverse primer (5' to 3') -GCCTCCTCAAAAGCCCTATAATACTCTGAC

D307H: Forward primer (5' to 3') - GCATCGTGTGGATTCACCCGGATGACTTTC
Reverse primer (5' to 3') -GAAAGTCATCCGGGTGAATCCACACGATGC

P329S : Forward primer (5' to 3') - TTGACCTATTCAAGTCACAGATCGGGGTGGT
Reverse primer (5' to 3') -ACCACCCCGATCTGTGACTTGAATAGGTCAA

G332R : Forward primer (5' to 3') - TCAAGCCACAGATCCGTGTGGTGAATGTGAC
Reverse primer (5' to 3') -GTCACATTCACCACACGGATCTGTGGCTTGA

D351G: Forward primer (5' to 3') - TTCCTGATGATGATGGCCTGCCCACAGCTGA
Reverse primer (5' to 3') -TCAGCTGTGGGCAGGCCATCATCATCAGGAA

Methylated non-mutated template plasmids were digested with DpnI, and the correct mutations were confirmed by DNA Sanger sequencing. Seven CPVT-related Casq2 mutants (R33Q, L167H, K180R, D307H, P329S, G332R, D351G) were generated.

4.3.4 Protein purification

cDNA encoding wild-type canine cardiac *casq2* and *casq2* mutants was cloned into pET22b expression vector. Proteins were expressed in *E. coli* BL21(DE3) and purified. Cells were grown in lysogeny broth (LB) medium until the A_{600} reaches 0.6 at 37ºC, then induced with addition of 1 mM IPTG at 37ºC for 3 hrs. Cells were crashed by pressure homogenizer into a buffer containing 50 mM Tris-HCl, pH 8.0, 300 mM NaCl, and 10% glycerol, then purified by using a HisTrap HP purification column (GE lifesciences, 17524701) and AKTA pure chromatography system (GE lifesciences 29018224). Purification was performed using binding buffer containing 50 mM Tris-HCl, pH 8.0, 300 mM NaCl, and protein eluted with a buffer containing 50 mM Tris-HCl, pH 8.0, 300 mM NaCl, and 250 mM imidazole. The 6xHis tagged ER luminal domain of IRE1α (IRE1-NLD) was expressed in COS-1 cells and purified by Ni-NTA agarose chromatography[47].

4.3.5 CD Analysis

CD spectra were recorded on a Jasco model J-810 spectropolarimeter. Far UV CD spectra were collected with 4.82 μM protein in buffer containing 10 mM NaH_2PO_4, pH 7.4, and 5 mM KCl, as NaCl interferes with CD analysis. CD scans were recorded using a quartz cell with a path length of 1 mm, response time of 2 s, scan speed of 10 nm/min, and band width of 1.0 nm. Ca^{2+}-induced changes in CD spectra were monitored in the presence of 1 mM of EGTA and 6 mM of $CaCl_2$. CD spectra analysis was carried out at 24ºC. The final spectra were an average of 5 measurements, after baseline subtraction. Analysis of the spectra was performed using K2D3[48]. The following calculations were performed for analysis:

Mean residue ellipticity was calculated with formula:

$$[\theta] = \theta_{obs} \times \frac{MRW}{(10 \times l \times c)}$$

Where [θ] with unit of Deg cm^2dmol^{-1}, θ_{obs} is the observed ellipticity in degrees, l is the optical path-length in cm, c is the protein concentration in g/ml, MRW is the mean residue molecular mass calculated with formula:

$$MRW = \frac{M}{(N-1)}$$

where M is a molecular mass of polypeptide chain in Da, and N is the number of amino acids in the chain.

4.3.6 Microscale thermophoresis and thermal denaturation analyses

Labelled microscale thermophoresis - Microscale thermophoresis analyses were carried out using a Monolith NT.115 instrument (Nano Temper Technologies, Germany) or Monolith NT.LabelFree instrument (Nano Temper Technologies, Germany). The ER-luminal domain of IRE1α (IRE1-NLD) was labelled using the Monolith NT Protein Labeling Kit RED-NHS (Nano Temper Technologies, cat# MO-C030) following the manufacture's protocol. All experiments were carried out at room temperature in standard capillaries with 20% LED power (fluorescence lamp intensity) and 40% MST power (IR-laser intensity). The assay buffer contained 50 mM HEPES, pH 7.4, 150 mM KCl, 500 μM $CaCl_2$, 250 μM EGTA, 0.05% Tween-20, and 2.5% glycerol. $CaCl_2$ and EGTA concentrations were adjusted to obtain the desired free Ca^{2+} concentration: no Ca^{2+} (500 μM EGTA, 500 μM $CaCl_2$), 5 mM (500 μM EGTA, 5.5 mM $CaCl_2$). Free Ca^{2+} concentration was calculated using the Ca^{2+}-EGTA Calculator TS v1.3 web tool[49].

Label-free microscale thermophoresis - Ca^{2+} binding to wild-type Casq2 or Casq2 mutants were carried out using a Monolith NT.LabelFree instrument in standard capillaries with 20% LED power and 60% Microscale thermophoresis power. The proteins were incubated for 10 min in a buffer containing 50 mM HEPES, pH 7.4, 150 mM KCl, 0.1% pluronic F-127, and 50 μM EGTA. An increasing concentration of $CaCl_2$ (0.01-20 mM, in 50 mM HEPES, pH 7.4, 150 mM KCl) was used. All Microscale thermophoresis data was analyzed by Monolith Affinity Analysis v2.2.6 software.

Tycho NT.6 - thermal denaturation analysis of wild-type Casq2 or Casq2 mutants was carried out using Tycho NT.6. This label-free system is based on measurement of a protein's intrinsic tryptophan fluorescence and records a protein's unfolding profile in real-time as temperature is increased from 35 to 95ºC. Ten μl of 0.25 mg/ml protein was used in buffer containing 50 mM HEPES, pH 7.4, 150 mM KCl, 500 μM $CaCl_2$, 250 μM EGTA, 0.05% Tween-20, and 2.5% glycerol.

4.3.7 Native polyacrylamide gel electrophoresis

To determining the oligomerization state of Casq2 or Casq2 mutants in the presence of different free Ca^{2+} concentrations, a discontinuous Tris-glycine polyacrylamide gel system consisting of a 5% stacking gel and a 10% separation gel was used under non-denaturing conditions. Proteins were diluted 3x with non-denaturing loading dye (240 mM Tris-HCl, pH 6.8,

30% glycerol, and 0.03% bromophenol blue). Proteins were separated in a Mini-PROTEAN electrophoresis chamber (BioRad) in a running buffer containing 25 mM Tris, pH 8.8, and 192 mM glycine, at 100 V, for 2 hr at 4ºC. The proteins were stained with Stains-all solution[50], Coomassie-blue, or transferred to nitrocellulose membrane for immunoblotting analysis.

4.3.8 Limited proteolysis

Cardiac calsequestrin (Casq2) and mutant proteins were subjected to proteolysis in a buffer containing 50 mM HEPES, pH 7.4, 150 mM KCl, 500 μM $CaCl_2$, 250 μM EGTA, 0.05% Tween-20, and 2.5% glycerol. $CaCl_2$ and EGTA concentrations were adjusted to the desired free Ca^{2+} concentration: no Ca^{2+} (250 μM EGTA, 250 μM $CaCl_2$), 5 mM (250 μM EGTA, 5.25 mM $CaCl_2$). Free Ca^{2+} concentration was calculated using the Ca-EGTA Calculator TS v1.3 web tool [49]. Proteins (150 μg of protein in 200 μl) were incubated in a reaction buffer with the desired free Ca^{2+} concentration for 20 min at 25ºC before addition of trypsin at the trypsin/protein ration of 1:50 (w/w), and samples were taken for SDS-PAGE analysis at 1, 2, 5, 10, 20, 30, 60, and 120 min. The samples were mixed with 4x SDS-PAGE sample buffer (Bio-Rad) containing serine protease inhibitor phenylmethylsufonyl fluoride (PMSF) and boiled at 100°C for 2 min before SDS-PAGE. All experiments were repeated 3 times with protein from 2 separate purifications. The gels were stained with Coomassie Blue R-250 (Bio-Rad).

4.3.9 Cross-linking

The homobiofunctional protein cross linker disuccinimidyl suberate (DSS) (Thermo Scientific Pierce, cat#:21555) was dissolved in DMSO at a final concentration of 10 mM[47]. Wild-type Casq2 or Casq2 mutant proteins were diluted to a final concentration of 10 μM in a reaction buffer containing 50 mM HEPES, pH 7.4, 150 mM NaCl, 250 μM EGTA, 500 μM $CaCl_2$, and 0.05% Tween-20. Proteins were incubated with 20-fold molar excess of DSS for 1 hr at 22.5°C. The reaction was then quenched for 15 min with 100 mM Tris pH 7.4 followed by SDS-PAGE (10% acrylamide). Proteins were transferred to nitrocellulose membrane follow by immunoblotting with mouse anti-6xHis antibodies (ThermoFisher, MA1-21315) or anti-calsequestrin antibodies (Abcam, 3516).

4.3.10 Statistical Analysis

Statistical analysis was performed using GraphPad Prism version 7.0. The Student's t-test was used to compare the mean of two independent groups, and one-way Anova was used to compare the mean of three or more independent groups, with a *p*-value determined to be significant if less than 0.05.

4.4 Results

4.4.1 Emergence and specialization of calsequestrin within animals

Phylogenetic analysis of the two calsequestrin genes (*casq1* and *casq2*) was carried out with the aim of clarifying the distribution and conservation of each paralogue across animals. This allows us to deduce the timing of the gene duplication event and relate this information to calsequestrin mutants responsible for CPVT. Homology searching was undertaken in 23 metazoan genomes and three outgroup lineages to identify calsequestrin homologues. We identified unambiguous calsequestrin homologues in most of the vertebrate and invertebrate lineages (Table 4-1). Furthermore, we revealed that *Ciona intestinalis*, *B. floridae,* and all taxa within the invertebrates possess a single calsequestrin gene, including taxa as deeply branched as Trichoplax and Nematostella (Figure 4-1). We did not identify a calsequestrin homologue in the sponge Amphimedon likely due to a database error or loss of calsequestrin in this lineage. Although the relative branching order of the basal lineages within animals is still disputed, with Nematostella or sponges as the deepest branch, calsequestrin is clearly an ancient protein within the metazoan (Figure 4-2 and Figure 4-3).

Table 4-1. BLASTp (Basic Local Alignment Search Tool protein) searches of the genomes of 28 metazoan organisms by using *H. sapiens* CASQ1 (NP_001222.3) and CASQ2 (NP_001223.2) nucleoide sequences as queries.

Subject database	**Forward BLAST hit name**	**Forward BLAST hit accession numbers**	**Forward BLAST e-values**	**Reverse BLAST hit names in** [Homo sapiens]	**Reverse BLAST hit accession numbers**	**Reverse BLAST e-values**	**Notes**
Forward query name: Homo sapiens CASQ1							
Rattus norvegicus	calsequestrin-1 precursor [Rattus norvegicus]	NP_001153066.1	0	calsequestrin-1 precursor	NP_001222.3	0	CASQ1
Gallus gallus	calsequestrin-2 precursor [Gallus gallus]	NP_989857.1	0	calsequestrin-2 precursor	NP_001223.2	0	Reverse BLAST has identity score of 81 and 91% query cover for CASQ2
Gallus gallus	calsequestrin-2 precursor [Gallus gallus]	NP_989857.1	0	calsequestrin-1 precursor	NP_001222.3	0	Reverse BLAST has identity score of 71 and 88% query cover for CASQ2
Gallus gallus	calsequestrin [Gallus gallus]	AAA48674.1	0	calsequestrin-2 precursor	NP_001223.2	0	Reverse BLAST has identity score of 83 and 91% query cover for CASQ2
Gallus gallus	calsequestrin [Gallus gallus]	AAA48674.1	0	calsequestrin-1 precursor	NP_001222.3	0	Reverse BLAST has identity score of 71 and 91% query cover for CASQ2
Xenopus tropicalis	hypothetical protein XENTR_v10002392mg [Xenopus tropicalis]	OCA27346.1	0	calsequestrin-1 precursor	NP_001222.3	0	CASQ1
Xenopus tropicalis	calsequestrin-2 precursor [Xenopus tropicalis]	NP_989136.1	8E-177	calsequestrin-2 precursor	NP_001223.2	5E-179	CASQ2
Xenopus tropicalis	calsequestrin-1 precursor	NP_988894.1	8E-162	calsequestrin-1 precursor	NP_001222.3	5E-163	CASQ1

	[Xenopus tropicalis]						
Latimeria chalumnae	PREDICTED: calsequestrin-1 [Latimeria chalumnae]	XP_006001917.1	0	calsequestrin-1 precursor	NP_001222.3	0	CASQ1
Latimeria chalumnae	PREDICTED: calsequestrin-2 [Latimeria chalumnae]	XP_006001992.1	0	calsequestrin-2 precursor	NP_001223.2	0	CASQ2
Danio rerio	calsequestrin-2 precursor [Danio rerio]	NP_001002682.1	4E-180	calsequestrin-2 precursor	NP_001223.2	0	CASQ2
Danio rerio	calsequestrin-1 precursor [Danio rerio]	NP_001070192.1	2E-174	unnamed protein product	BAC86117.1	0	CASQ1
Danio rerio	calsequestrin-1 precursor [Danio rerio]	NP_001070192.1	2E-174	calsequestrin-1 precursor	NP_001222.3	3E-172	CASQ1
Callorhinchus milii	PREDICTED: calsequestrin-2-like [Callorhinchus milii]	XP_007889783.1	2E-180	calsequestrin-2 precursor	NP_001223.2	0	Only one forward BLAST hit in NCBI - uncertain whether it is CASQ1 or CASQ2
Callorhinchus milii	PREDICTED: calsequestrin-2-like [Callorhinchus milii]	XP_007889783.1	2E-180	calsequestrin-1 precursor	NP_001222.3	0	tBLASTn did not yield any additional forward BLAST hits
Leucoraja erinacea	gnl|SkateBase|LS-transcriptB2-ctg62807	ctg62807	6E-160	calsequestrin-2 precursor	NP_001223.2	0	No hits in NCBI, used tBLASTn on skatebase.org
Petromyzon marinus							No hits identified in NCBI
Branchiostoma floridae	hypothetical protein BRAFLDRAFT_122314 [Branchiostoma floridae]	XP_002604497.1	7E-45	Chain A, Ca^{2+} Complex Of Human Skeletal Calsequestrin	3UOM_A	8E-57	Related to CASQ
Branchiostoma floridae	hypothetical protein BRAFLDRAFT	XP_002604497.1	7E-45	calsequestrin-1 precursor	NP_001222.3	1E-56	

	_122314 [Branchiostoma floridae]						
Ciona intestinalis	PREDICTED: calsequestrin-2 [Ciona intestinalis]	XP_002130664.1	3E-122	Chain A, Human Skeletal Calsequestrin, D210g Mutant	5CRE_A	5E-121	CASQ but uncertain whether it is CASQ1 or CASQ2
Ciona intestinalis	PREDICTED: calsequestrin-2 [Ciona intestinalis]	XP_002130664.1	3E-122	calsequestrin-1 precursor	NP_001222.3	7E-121	
Helobdella robusta							No hits identified in NCBI nor Ensembl
Drosophila melanogaster							No hits identified in NCBI
Caenorhabditis elegans	Calsequestrin [Caenorhabditis elegans]	NP_510438.1	2.00E-53	Chain A, Human Skeletal Calsequestrin, D210g Mutant	5CRE_A	3.00E-51	CASQ present
Caenorhabditis elegans	Calsequestrin [Caenorhabditis elegans]	NP_510438.1	2.00E-53	calsequestrin-1 precursor	NP_001222.3	5.00E-51	
Nematostella vectensis	predicted protein [Nematostella vectensis]	XP_001623501.1	9.00E-55	Chain A, Human Skeletal Calsequestrin, M53t Mutant High-calcium Complex	5CRH_A	9.00E-54	
Mnemiopsis leidyi							No hits identified in NCBI
Trichoplax adhaerens	hypothetical protein TRIADDRAFT_56011 [Trichoplax adhaerens]	XP_002111704.1	6.00E-48	calsequestrin-2 precursor	NP_001223.2	2.00E-50	
Amphimedon queenslandica							No hits identified in NCBI
Monosiga brevicollis							Only 1 hit with e-value of 2.2

Salpingoeca rosetta	hypothetical protein PTSG_02152 [Salpingoeca rosetta]	XP_004996635.1	5.00E-09	protein disulfide-isomerase precursor	NP_000909.2	3.00E-86	Not CASQ
Capsaspora owczarzaki							Not hits identified in NCBI
Oryctolagus cuniculus	calsequestrin-1 precursor [Oryctolagus cuniculus]	NP_001075737.1	0.00E+00	calsequestrin-1 precursor	NP_001222.3	0.00E+00	CASQ1
Mus musculus	calsequestrin-1 precursor [Mus musculus]	NP_033943.2	0.00E+00	calsequestrin-1 precursor	NP_001222.3	0.00E+00	CASQ1
Apis mellifera		XM_001121993.4	6.52E-05				No hits identified in NCBI
Manduca sexta							No hits identified in NCBI
Canis lupus familiaris	calsequestrin-1 [Canis lupus familiaris]	XP_850097.1	0	calsequestrin-1 precursor	NP_001222.3	0	CASQ1
Sus scrofa	calsequestrin-1 precursor [Sus scrofa]	NP_001230198.1	0	calsequestrin-1 precursor	NP_001222.3	0	CASQ1
Bos taurus	calsequestrin-1 precursor [Bos taurus]	NP_001071345.1	0	calsequestrin-1 precursor	NP_001222.3	0	CASQ1
Crocodylus porosus	PREDICTED: calsequestrin-2 [Crocodylus porosus]	XP_019404288.1	0	calsequestrin-2 precursor	NP_001223.2	0	CASQ2?
Taeniopygia guttata	PREDICTED: calsequestrin-2 [Taeniopygia guttata]	XP_002188512.1	0	calsequestrin-2 precursor	NP_001223.2	0	CASQ2?
Parasteatoda tepidariorum	calsequestrin-2-like [Parasteatoda tepidariorum]	XP_021000344.1	4.00E-21	unnamed protein product	BAG58422.1	2.00E-23	Appears to be related to CASQ; similar to calsequestrin-2 precursor
Parasteatoda	calsequestrin-2-like	XP_021000344.1	4.00E-21	calsequestrin-2 precursor	NP_001223.2	4.00E-22	Appears to be related to CASQ

tepidariorum	[Parasteatoda tepidariorum]						
Daphnia pulex							No significant hits in NCBI
Parhyale hawaiensis							No significant hits identified in NCBI
Forward query name: Homo sapiens CASQ2							
Rattus norvegicus	calsequestrin-2 precursor [Rattus norvegicus]	NP_058827.3	0	calsequestrin-2 precursor	NP_001223.2	0	CASQ2
Rattus norvegicus	calsequestrin-1 precursor [Rattus norvegicus]	NP_001153066.1	0	calsequestrin-1 precursor	NP_001222.3	0	CASQ1
Gallus gallus	calsequestrin-2 precursor [Gallus gallus]	NP_989857.1	0	calsequestrin-2 precursor	NP_001223.2	0	CASQ2
Xenopus tropicalis	calsequestrin-2 precursor [Xenopus tropicalis]	NP_989136.1	0	calsequestrin-2 precursor	NP_001223.2	5E-179	CASQ2
Latimeria chalumnae	PREDICTED: calsequestrin-2 [Latimeria chalumnae]	XP_006001992.1	0	calsequestrin-2 precursor	NP_001223.2	0	CASQ2
Danio rerio	calsequestrin-2 precursor [Danio rerio]	NP_001002682.1	0	calsequestrin-2 precursor	NP_001223.2	0	CASQ2
Callorhinchus milii	PREDICTED: calsequestrin-2-like [Callorhinchus milii]	XP_007889783.1	0	calsequestrin-2 precursor	NP_001223.2	0	CASQ2
Callorhinchus milii	PREDICTED: calsequestrin-2-like [Callorhinchus milii]	XP_007889783.1	0	calsequestrin-1 precursor	NP_001222.3	0	CASQ1
Leucoraja erinacea	gnl|SkateBase|LS-transcriptB2-ctg62807	ctg62807	3E-177	calsequestrin-2 precursor	NP_001223.2	0	Possibly CASQ2
Petromyzon marinus		JL3244	0.000001	protein disulfide-isomerase A4 precursor	NP_004902.1	0	Only 1 hit with tBLASTn in NCBI with e-value of 7.6

Branchiostoma floridae	hypothetical protein BRAFLDRAFT_122314 [Branchiostoma floridae]	XP_002604497.1	2E-38	Chain A, Ca^{2+} Complex Of Human Skeletal Calsequestrin	3UOM_A	8E-57	CASQ; not obvious representing which paralog
Branchiostoma floridae	hypothetical protein BRAFLDRAFT_122314 [Branchiostoma floridae]	XP_002604497.1	2E-38	calsequestrin-1 precursor	NP_001222.3	1E-56	
Ciona intestinalis	PREDICTED: calsequestrin-2 [Ciona intestinalis]	XP_002130664.1	3E-131	Chain A, Human Skeletal Calsequestrin, D210g Mutant	5CRE_A	5E-121	CASQ not obvious representing which paralog
Helobdella robusta							No hits in NCBI or JGI
Drosophila melanogaster							No hits on NCBI also no significant hits identified in flybase.org
Caenorhabditis elegans	Calsequestrin [Caenorhabditis elegans]	NP_510438.1	4.00E-49	Chain A, Human Skeletal Calsequestrin, D210g Mutant	5CRE_A	3.00E-51	CASQ; not obvious representing which paralog
Nematostella vectensis	predicted protein [Nematostella vectensis]	XP_001623501.1	2.00E-52	Chain A, Human Skeletal Calsequestrin, M53t Mutant	5CRH_A	9.00E-54	CASQ; not obvious hit representing paralog
Mnemiopsis leidyi							No hits identified in NCBI; best tBLASTn hit e-value of 2e-04
Trichoplax adhaerens	hypothetical protein TRIADDRAFT_56011 [Trichoplax adhaerens]	XP_002111704.1	7.00E-53	calsequestrin-2 precursor	NP_001223.2	2.00E-50	CASQ; not obvious representing which paralog
Amphimedon queenslandica							Only 1 hit with e-value of 0.49
Monosiga brevicollis							Best hit has e-value of 0.027

Salpingoeca rosetta							Best hit has e-value of 0.027
Capsaspora owczarzaki							No hits in NCBI or ensembl
Oryctolagus cuniculus	calsequestrin-2 precursor [Oryctolagus cuniculus]	NP_001095161.1	0.00E+00	calsequestrin-2 precursor	NP_001223.2	0.00E+00	CASQ2
Mus musculus	calsequestrin-2 precursor [Mus musculus]	NP_033944.2	0.00E+00	calsequestrin-2 precursor	NP_001223.2	0.00E+00	CASQ2
Apis mellifera		XM_001121993.4	4.00E-01	Homo sapiens thioredoxin-related transmembrane protein 3,	BC107422.1	9.00E-50	No hits identified in NCBI
Manduca sexta							No hits identified in NCBI
Canis lupus familiaris	calsequestrin-2 precursor [Canis lupus familiaris]	NP_001300745.1	0	calsequestrin-2 precursor	NP_001223.2	0	CASQ2
Sus scrofa	LOW QUALITY PROTEIN: calsequestrin-2 [Sus scrofa]	XP_020945654.1	0	calsequestrin-2 precursor	NP_001223.2	0	CASQ2
Bos taurus	calsequestrin-2 [Bos taurus]	NP_001030451.1	0	calsequestrin-2 precursor	NP_001223.2	0	CASQ2
Crocodylus porosus	PREDICTED: calsequestrin-2 [Crocodylus porosus]	XP_019404288.1	0	calsequestrin-2 precursor	NP_001223.2	0	CASQ2
Taeniopygia guttata	PREDICTED: calsequestrin-2 [Taeniopygia guttata]	XP_002188512.1	0	calsequestrin-2 precursor	NP_001223.2	0	CASQ2
Parasteatoda tepidariorum	calsequestrin-2-like [Parasteatoda tepidariorum]	XP_021000344.1	3.00E-23	unnamed protein product	BAG58422.1	2.00E-23	Appears to be related to CASQ. similar to calsequestrin-2 precursor
Parasteatoda tepidariorum	calsequestrin-2-like [Parasteatoda tepidariorum]	XP_021000344.1	3.00E-23	calsequestrin-2 precursor	NP_001223.2	4.00E-22	Appears to be related to CASQ

Daphnia pulex	hypothetical protein DAPPUDRAFT_305526 [Daphnia pulex]	EFX88084.1	1.1				E-value not significant
Parhyale hawaiensis							No significant hits identified in NCBI,

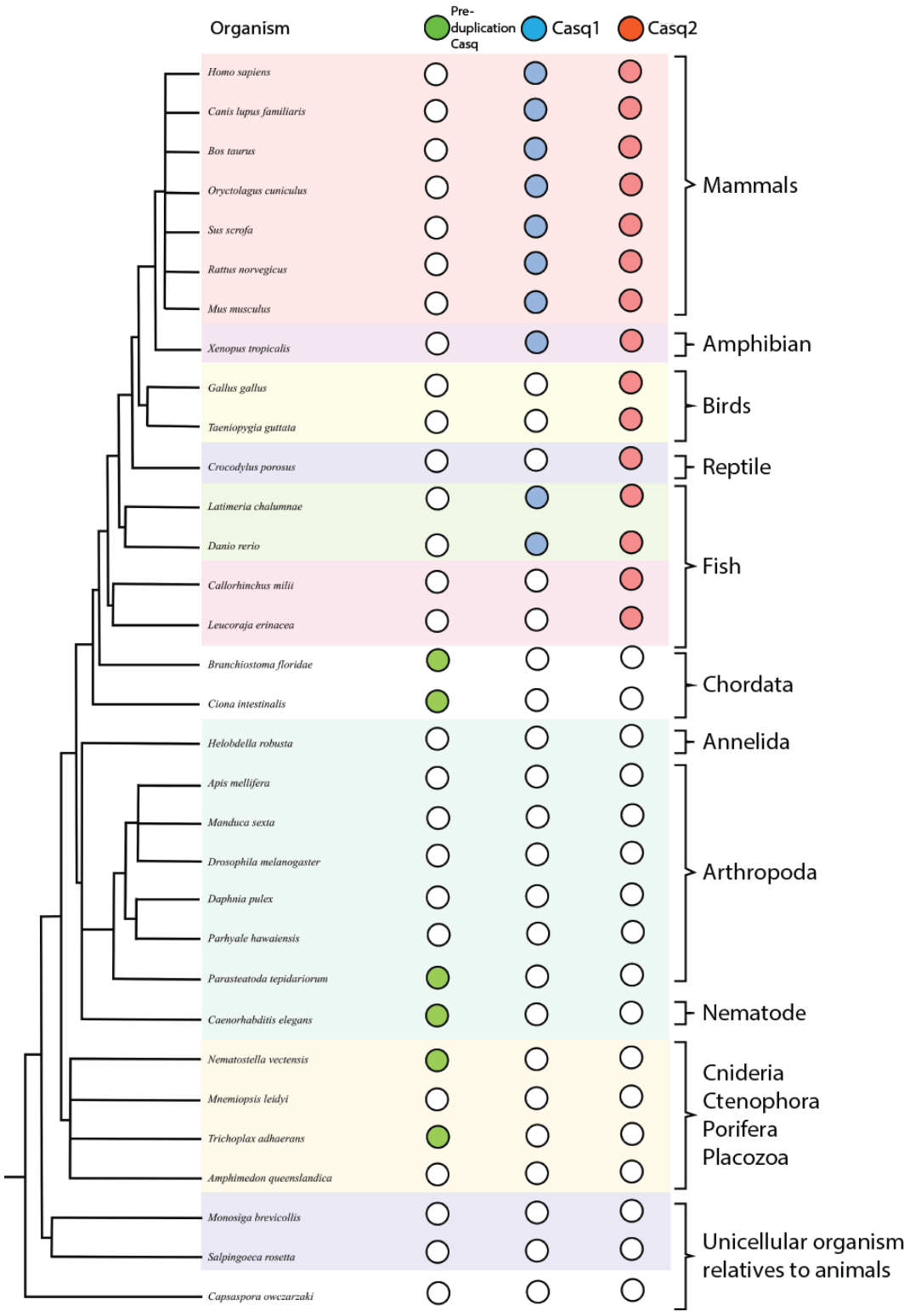

Figure 4-1. Calsequestrin homologues in the vertebrate and invertebrate lineages.

Empty circles indicate the gene is absent. Green circles indicate the presence of pre-duplication Casq, blue circles the presence of *casq1*, and red circles the presence of *casq2*.

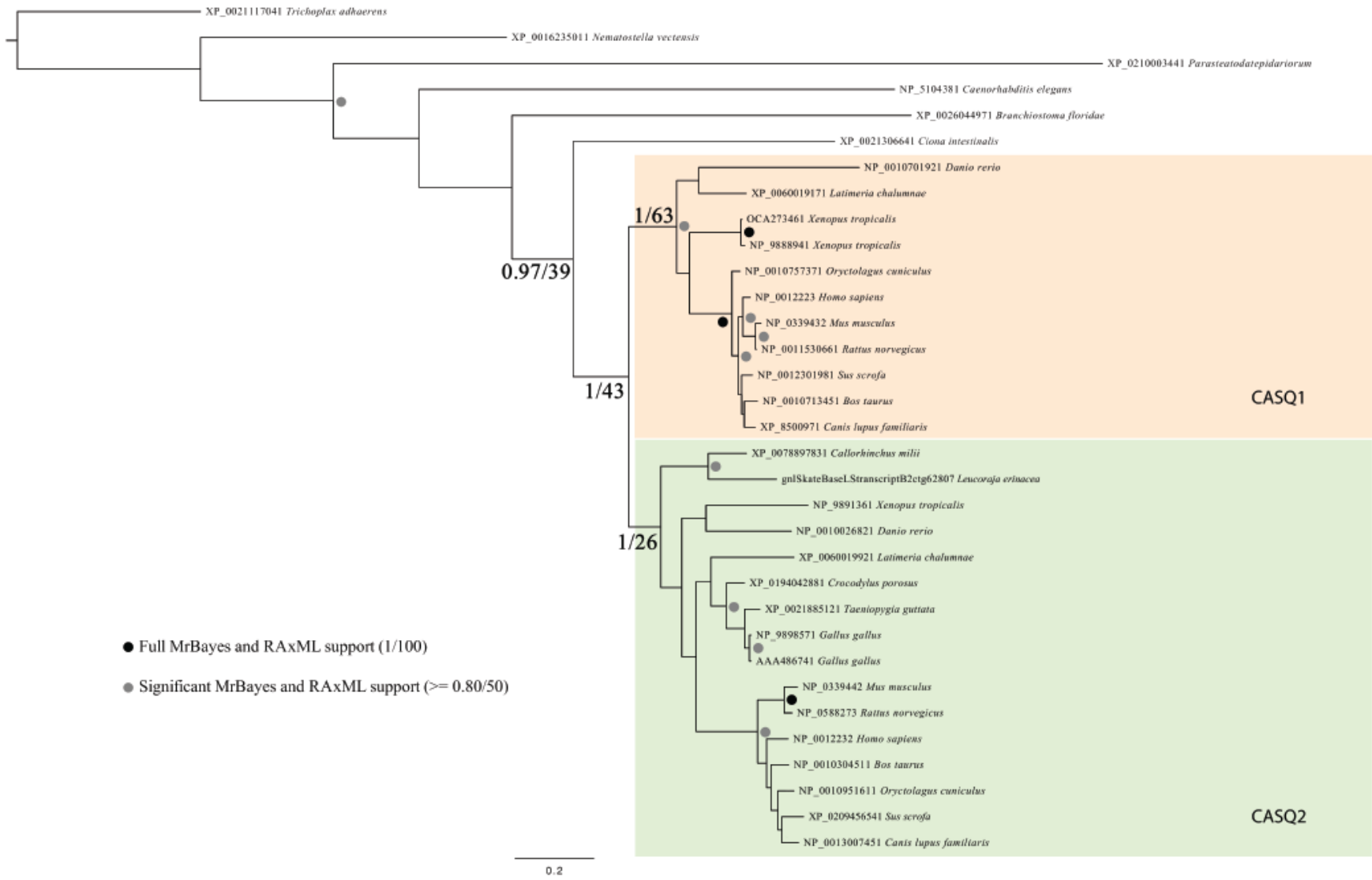
XP_0021117041 Trichoplax adhaerens
XP_0016235011 Nematostella vectensis
XP_0210003441 Parasteatodatepidariorum
NP_5104381 Caenorhabditis elegans
XP_0026044971 Branchiostoma floridae
XP_0021306641 Ciona intestinalis
NP_0010701921 Danio rerio
XP_0060019171 Latimeria chalumnae
OCA273461 Xenopus tropicalis
NP_9888941 Xenopus tropicalis
NP_0010757371 Oryctolagus cuniculus
NP_0012223 Homo sapiens
NP_0339432 Mus musculus
NP_0011530661 Rattus norvegicus
NP_0012301981 Sus scrofa
NP_0010713451 Bos taurus
XP_8500971 Canis lupus familiaris
CASQ1
XP_0078897831 Callorhinchus milii
gnlSkateBaseLStranscriptB2ctg62807 Leucoraja erinacea
NP_9891361 Xenopus tropicalis
NP_0010026821 Danio rerio
XP_0060019921 Latimeria chalumnae
XP_0194042881 Crocodylus porosus
XP_0021885121 Taeniopygia guttata
NP_9898571 Gallus gallus
AAA486741 Gallus gallus
NP_0339442 Mus musculus
NP_0588273 Rattus norvegicus
NP_0012232 Homo sapiens
NP_0010304511 Bos taurus
NP_0010951611 Oryctolagus cuniculus
XP_0209456541 Sus scrofa
NP_0013007451 Canis lupus familiaris
CASQ2
1/63
0.97/39
1/43
1/26
● Full MrBayes and RAxML support (1/100)
● Significant MrBayes and RAxML support (>= 0.80/50)
0.2

Figure 4-2. Phyolgenetic tree of calsequestrin.

A phylogenetic tree was generated by combining MrBayes and RAxML consensus data with *Branchiasotma floridae* as an outgroup. The *Danio rerio* casq1 sequence was removed from the dataset used to generate the tree due to long branch attraction causing poor RAxML consensus bootstrap values in previous iterations. The presence of *casq1* and *casq2* is highlighted by different background colors.

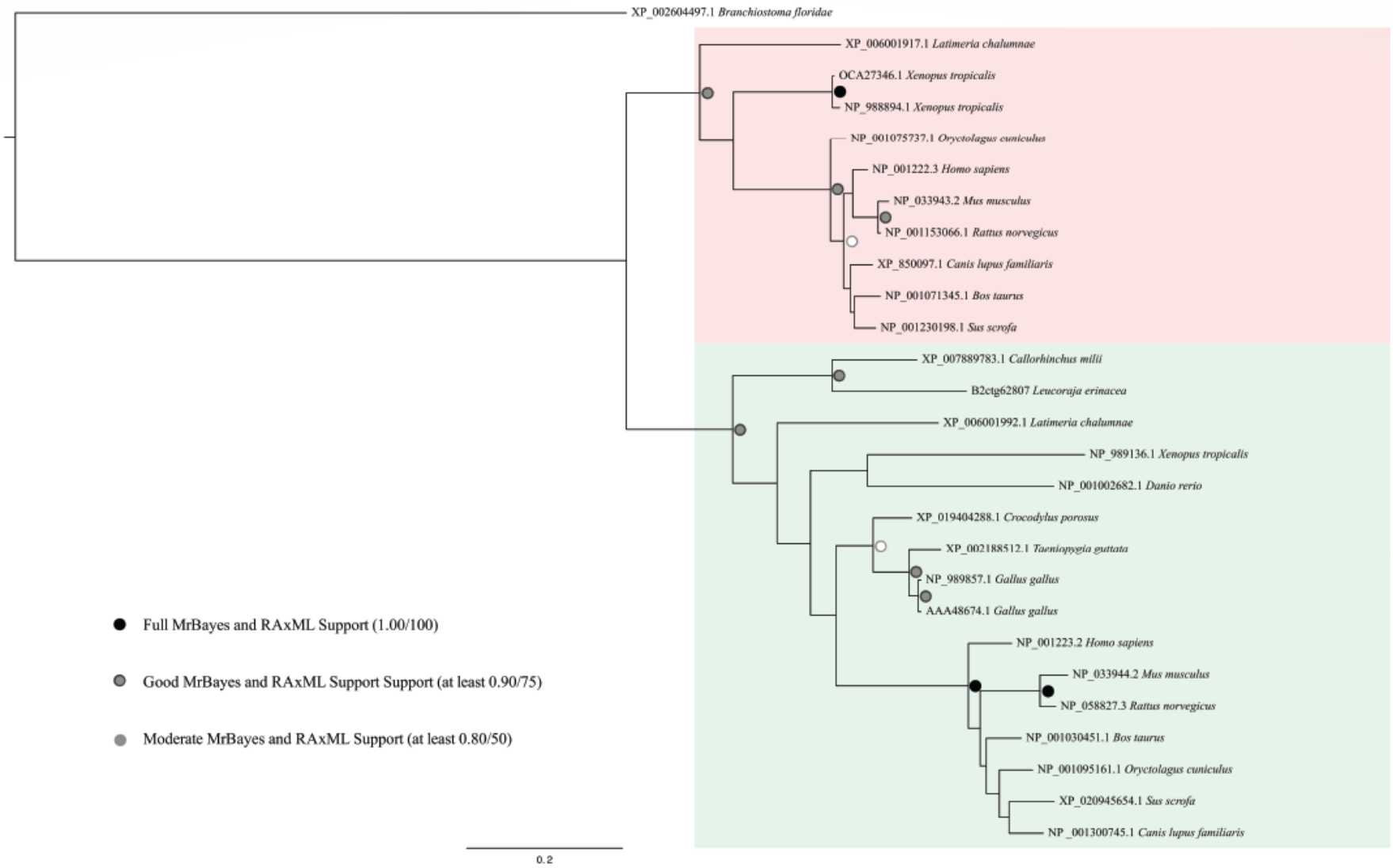
XP_002604497.1 Branchiostoma floridae
XP_006001917.1 Latimeria chalumnae
OCA27346.1 Xenopus tropicalis
NP_988894.1 Xenopus tropicalis
NP_001075737.1 Oryctolagus cuniculus
NP_001222.3 Homo sapiens
NP_033943.2 Mus musculus
NP_001153066.1 Rattus norvegicus
XP_850097.1 Canis lupus familiaris
NP_001071345.1 Bos taurus
NP_001230198.1 Sus scrofa
XP_007889783.1 Callorhinchus milii
B2ctg62807 Leucoraja erinacea
XP_006001992.1 Latimeria chalumnae
NP_989136.1 Xenopus tropicalis
NP_001002682.1 Danio rerio
XP_019404288.1 Crocodylus porosus
XP_002188512.1 Taeniopygia guttata
NP_989857.1 Gallus gallus
AAA48674.1 Gallus gallus
NP_001223.2 Homo sapiens
NP_033944.2 Mus musculus
NP_058827.3 Rattus norvegicus
NP_001030451.1 Bos taurus
NP_001095161.1 Oryctolagus cuniculus
XP_020945654.1 Sus scrofa
NP_001300745.1 Canis lupus familiaris
Full MrBayes and RAxML Support (1.00/100)
Good MrBayes and RAxML Support Support (at least 0.90/75)
Moderate MrBayes and RAxML Support (at least 0.80/50)
0.2

Figure 4-3. Short-branch phylogenetic tree of calsequestrin.

A phylogenetic tree was generated by combining MrBayes and RAxML consensus data as described in Figure 4-2. The presence of *casq1* and *casq2* is highlighted by different background colors.

Each of these lineages, as well the invertebrates and hemichordates, possess only a single calsequestrin gene, leaving the timing of when *casq1* vs c*asq2* arose as an outstanding question. Preliminary phylogeny provided moderate support for the non-vertebrate sequences emerging basal to clades of the *casq1* and *casq2*, thus being pre-duplicated versions (Figure 4-2 and Figure 4-3). Further analysis focused on vertebrate gene sequences and using the lancelet sequences as an outgroup (Figure 4-1). The analysis robustly showed that the calsequestrin gene duplication giving rise to *casq1* and *casq2* occurred after the divergence of the lancelet lineage but before the divergence of the Chondrichthyes. We were unable to identify any calsequestrin genomic DNA sequences in the insect lineage. This likely represents a bona fide loss in this line given the positive identification of a homologue in the spider *Parasteatoda tepidariorum*.

The Chondrichthyes and Avian taxa lost *casq1* independently. We identified *casq1* paralogues in the Chondrichthyes despite robustly classifying *casq2* being present and the duplication having taken place prior to this point (Figure 4-1). The same was observed for the avian taxa sampled, suggesting that *casq1* was lost independently in these three lineages. In mammalian muscles the two calsequestrin isoforms exhibit tissue specific expression[51-53]. Casq2 is expressed in cardiac and slow-twitch skeletal muscle, whereas Casq1 is expressed in adult fast-twitched muscle[51-53]. Cartilaginous fish as well as avian animals have both fast-twitch and slow-twitch skeletal muscles even though they appear to lack *casq1*.

4.4.2 Conservation of CPVT associated Casq2 mutants throughout animal kingdom

Having the evolutionary distribution of *casq1* and *casq2* allowed us to contextualize calsequestrin mutations in the human *CASQ2*, which have been associated with CPVT (Figure 4-4)[24, 54, 55]. We selected the following seven Casq2 mutants for further analyses: R33Q, L167H, D307H, K180R, P329S, G332R, and D351G (Figure 4-4). Many mutations are scattered across the three thioredoxin-like domains of Casq2 (Figure 4-4), but remarkably they all lead to a similar clinical outcome[24, 54]. L167, and D351 are conserved in Casq1 and Casq2 paralogues found in vertebrates, but are variable in the pre-duplicated non-bilaterian (Figure 4-4). In contrast, positions R33, K180, D307, P329 and G332 are fully conserved across all calsequestrin homologues including pre-duplication Casq (Figure 4-4).

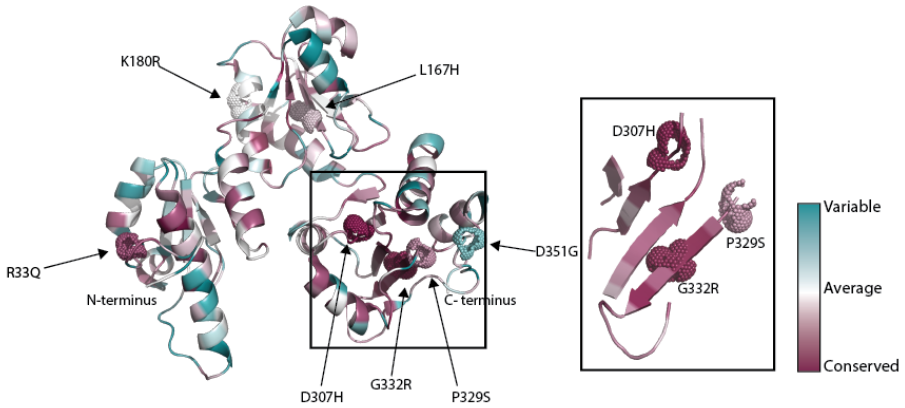
K180R
L167H
R33Q
N-terminus
C- terminus
D351G
D307H
G332R
P329S
D307H
P329S
G332R
Variable
Average
Conserved

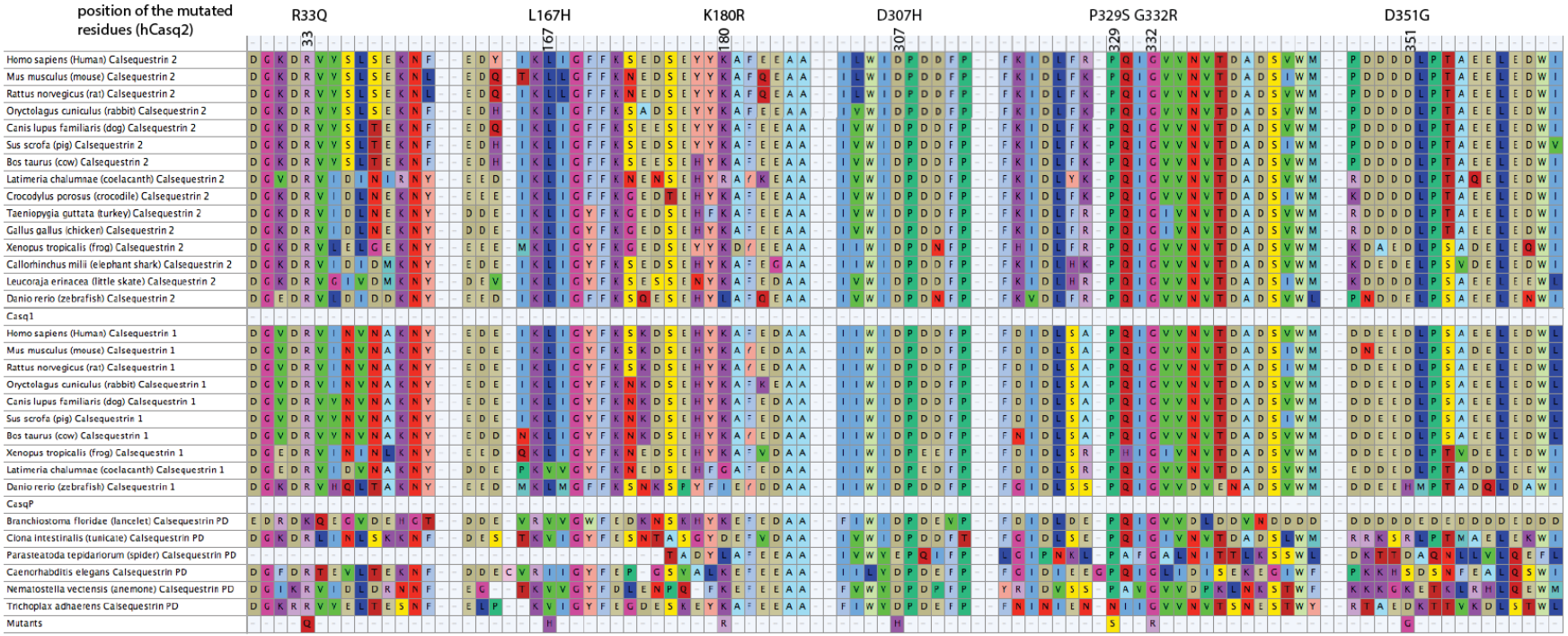
position of the mutated residues (hCasq2)
R33Q
L167H
K180R
D307H
P329S G332R
D351G
Homo sapiens (Human) Calsequestrin 2
Mus musculus (mouse) Calsequestrin 2
Rattus norvegicus (rat) Calsequestrin 2
Oryctolagus cuniculus (rabbit) Calsequestrin 2
Canis lupus familiaris (dog) Calsequestrin 2
Sus scrofa (pig) Calsequestrin 2
Bos taurus (cow) Calsequestrin 2
Latimeria chalumnae (coelacanth) Calsequestrin 2
Crocodylus porosus (crocodile) Calsequestrin 2
Taeniopygia guttata (turkey) Calsequestrin 2
Gallus gallus (chicken) Calsequestrin 2
Xenopus tropicalis (frog) Calsequestrin 2
Callorhinchus milii (elephant shark) Calsequestrin 2
Leucoraja erinacea (little skate) Calsequestrin 2
Danio rerio (zebrafish) Calsequestrin 2
Casq1
Homo sapiens (Human) Calsequestrin 1
Mus musculus (mouse) Calsequestrin 1
Rattus norvegicus (rat) Calsequestrin 1
Oryctolagus cuniculus (rabbit) Calsequestrin 1
Canis lupus familiaris (dog) Calsequestrin 1
Sus scrofa (pig) Calsequestrin 1
Bos taurus (cow) Calsequestrin 1
Xenopus tropicalis (frog) Calsequestrin 1
Latimeria chalumnae (coelacanth) Calsequestrin 1
Danio rerio (zebrafish) Calsequestrin 1
CasqP
Branchiostoma floridae (lancelet) Calsequestrin PD
Ciona intestinalis (tunicate) Calsequestrin PD
Parasteatoda tepidariorum (spider) Calsequestrin PD
Caenorhabditis elegans Calsequestrin PD
Nematostella vectensis (anemone) Calsequestrin PD
Trichoplax adhaerens Calsequestrin PD
Mutants

Figure 4-4. Amino acid sequence alignments and calsequestrin 3D structure.

The 3D structure of the cardiac isoform of calsequestrin (Casq2) is shown (2VAF). The location of R33Q, L167H, K180R, D307H, P329S, G332R, and D351G Casq2 mutants are depicted in the structure. A scale of variable to conserved residues is indicated in the Figure. Mutants are shown as dot sphere. The highly conserved 4 beta-strands from the third thioredoxin-like fold is enlarged in the box and shown separately. The table shows the alignment of calsequestrin amino acid sequences. The degree of conservation of Casq2 sequences is color-coded using ConSurf [56]. Multiple sequence alignments were input from the Casq1, Casq2, and Casqp alignment. Different colors represent similar/identical amino acid residues. The location of mutated residues is indicated in the Table. hCASQ2, human Casq2.

4.4.3 Ca^{2+} binding to Casq2 mutants

Next, we carried out biochemical and biophysical analysis of the Casq2 mutants to gain insight into the contribution of these mutations to the development of CPVT. First, we used microscale thermophoresis (MST) to investigate Ca^{2+} binding to Casq2 mutants. Mutation of Casq2 residues R33Q, L167H, K180R and D351G had no significant effect on Ca^{2+} binding to calsequestrin (Figure 4-5A-D) with K_d values ranging from 0.872 ± 0.283 mM for wild-type to 1.052 ± 0.154 mM for the D351G mutant (Figure 4-5H). However, P329S and G332R mutants exhibited altered Ca^{2+} binding affinities (Figure 4-5E,F). In agreement with previous observations[17], the D307H Casq2 mutant showed no measurable Ca^{2+} binding (Figure 4-5G). Of the seven mutants associated with CPVT examined, only three exhibited altered Ca^{2+} binding properties.

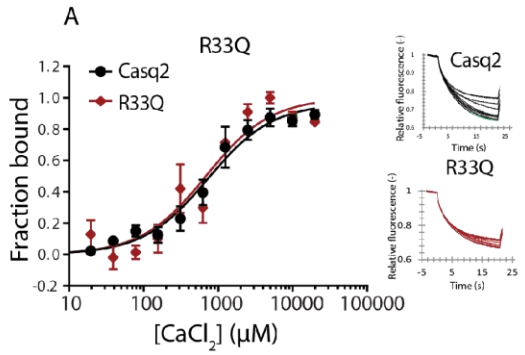

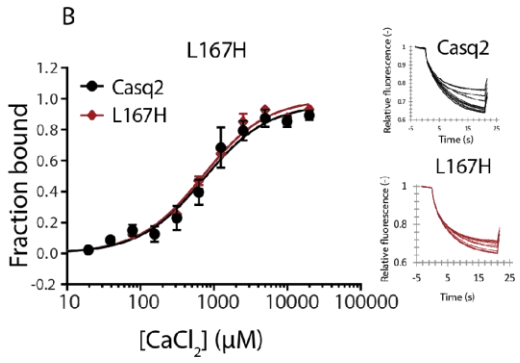

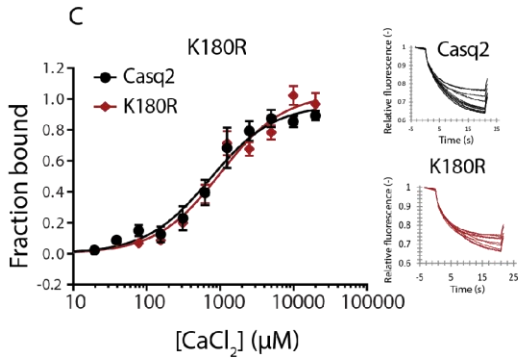

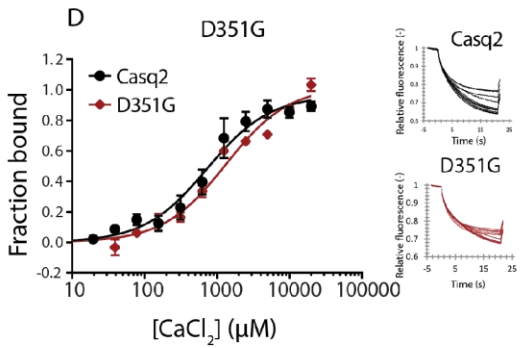

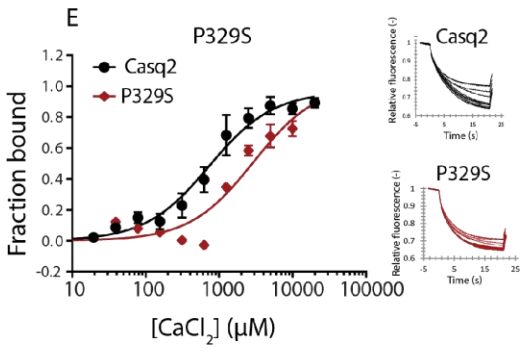

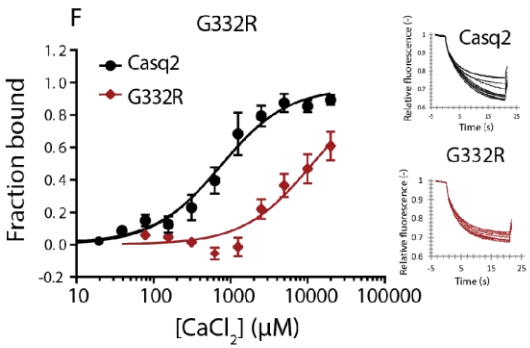

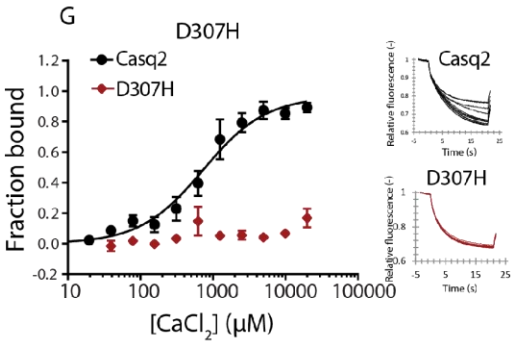

H

	Kd (mM)	P value*
Casq2 wt	0.872 ± 0.283	
R33Q	0.691 ± 0.051	0.546
L167H	0.708 ± 0.036	0.581
K180R	0.683 ± 0.168	0.579
D307H	no fit	N/A
P329S	2.589 ± 0.404	0.023
G332R	13.490 ± 5.568	0.151
D351G	1.052 ± 0.154	0.588

*: two-tailed Student's t-test compare with Casq2 wt
N/A: not applicable

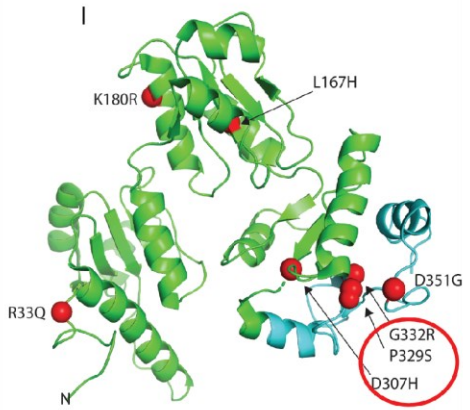

Figure 4-5. Ca^{2+} binding to calsequestrin mutants.

A-G) Microscale thermophoresis analysis of Ca^{2+} binding to mutants Casq2 (red line) and wild-type Casq2 (black line).

H) Calculated Ca^{2+} binding affinities of Casq2 mutants.

I) 3D structure of human Casq2 (adapted from 2VAF) with the location of mutants indicated in the Figure. The red circle depicts the location of mutations that affected Ca^{2} binding to Casq2. All data are representative of more than two biological replicates each with three technical replicates.

4.4.4 Conformational changes and protein folding of Casq2 mutants

Casq2 undergoes conformational change upon Ca^{2+} binding, and this was monitored by circular dichroism (CD) analysis[57]. Upon adding Ca^{2+}, wild-type Casq2 lost 18.3% α-helix and gained 16.79% β-sheet conformation (Figure 4-6)[57]. CD spectra for K180R and D351G mutants overlapped with those of the wild-type Casq2 (Figure 4-6C,D,E,F), indicating no effect of the K180R and D351G mutation on the protein conformation. However, the G332R and P329S mutants, showed altered sensitivity to Ca^{2+}-induced conformational changes (Figure 4-6E,F). This agrees with the reduced Ca^{2+} affinity of these mutants (Figure 4-5). In contrast, the CD spectra of mutants R33Q, L167H, and D307H revealed increased α-helix content that was not sensitive to addition of Ca^{2+} (Figure 4-6A,B,G; Table 4-2).

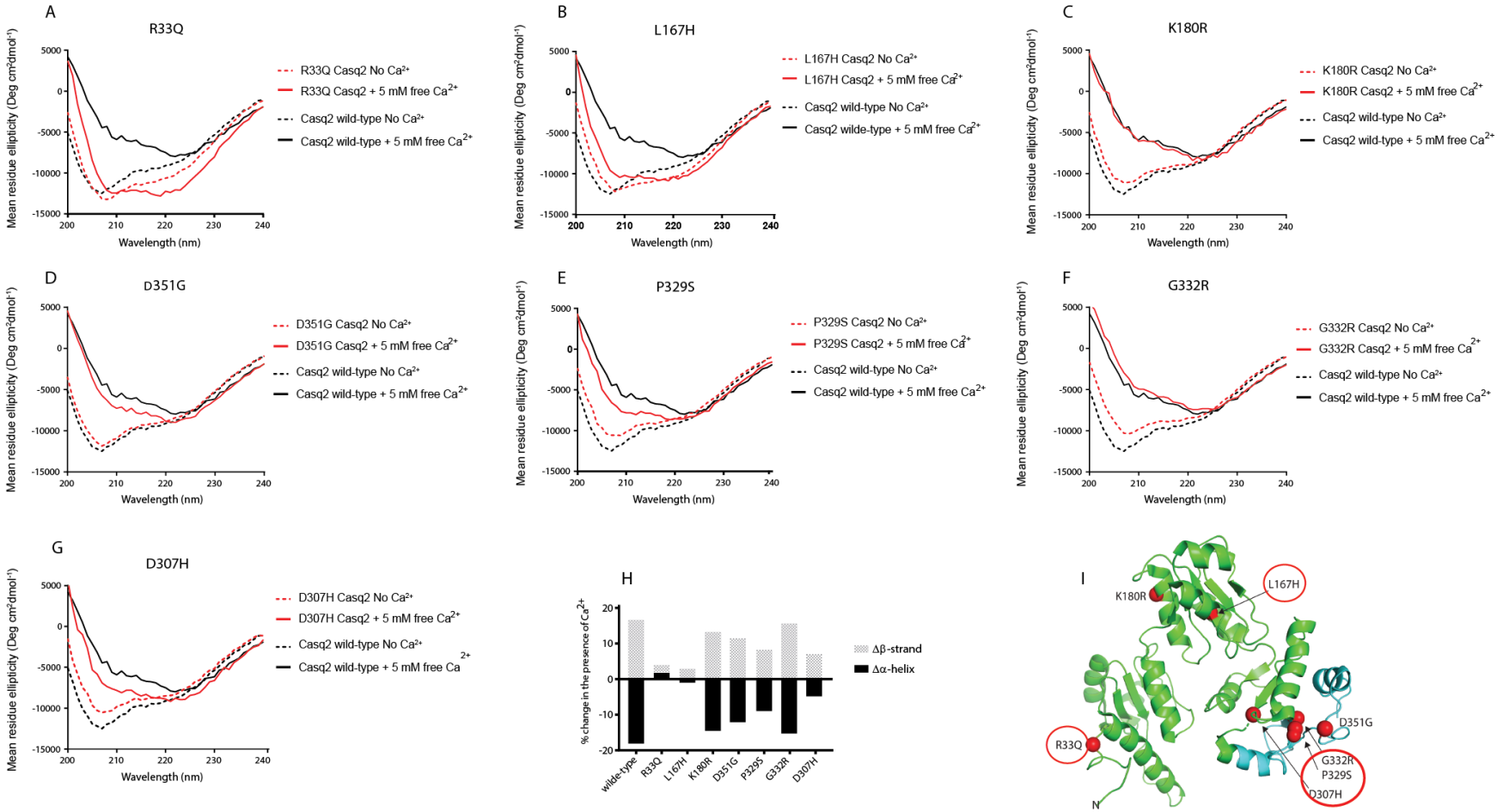
A
R33Q
Mean residue ellipticity (Deg cm²dmol⁻¹)
Wavelength (nm)
R33Q Casq2 No Ca2+
R33Q Casq2 + 5 mM free Ca2+
Casq2 wild-type No Ca2+
Casq2 wild-type + 5 mM free Ca2+
B
L167H
L167H Casq2 No Ca2+
L167H Casq2 + 5 mM free Ca2+
Casq2 wild-type No Ca2+
Casq2 wilde-type + 5 mM free Ca2+
C
K180R
K180R Casq2 No Ca2+
K180R Casq2 + 5 mM free Ca2+
Casq2 wild-type No Ca2+
Casq2 wild-type + 5 mM free Ca2+
D
D351G
D351G Casq2 No Ca2+
D351G Casq2 + 5 mM free Ca2+
Casq2 wild-type No Ca2+
Casq2 wild-type + 5 mM free Ca2+
E
P329S
P329S Casq2 No Ca2+
P329S Casq2 + 5 mM free Ca2+
Casq2 wild-type No Ca2+
Casq2 wild-type + 5 mM free Ca2+
F
G332R
G332R Casq2 No Ca2+
G332R Casq2 + 5 mM free Ca2+
Casq2 wild-type No Ca2+
Casq2 wild-type + 5 mM free Ca2+
G
D307H
D307H Casq2 No Ca2+
D307H Casq2 + 5 mM free Ca2+
Casq2 wild-type No Ca2+
Casq2 wild-type + 5 mM free Ca2+
H
% change in the presence of Ca2+
Δβ-strand
Δα-helix
wilde-type
R33Q
L167H
K180R
D351G
P329S
G332R
D307H
I
K180R
L167H
R33Q
D351G
G332R
P329S
D307H
N

Figure 4-6. CD analysis of Casq2 mutants.

A-G) CD analysis of Casq2 mutants (red solid line) and wild-type Casq2 (black solid line). CD analysis in the presence of 5 mM Ca^{2+} is indicted by black dotted lines for wild-type Casq2 and by red dotted lines for Casq2 mutants.

H) Change in % of α-helix and β-strand content with the absence or presence of Ca^{2+} for wild-type Casq2 and each Casq2 mutant. Negative and positive values indicate a loss or gain of secondary structure content, respectively.

I) Three-dimensional structure of human Casq2 (2VAF). Red circles depict the location of mutations with altered CD spectrum. All data are representative of more than two biological replicates each with three technical replicates.

Table 4-2. CD analysis of calsequestrin mutants

Casq2		WT	R33Q	L167H	K180R	D307H	P329S	G332R	D351G
No Ca^{2+}	% α-helix	26.18	28.83	26.71	23.7	24.06	21.36	20.37	24.31
	% β-sheet	19.65	17.93	19.5	21.78	20.98	22.66	23.41	21.01
5 mM Ca^{2+}	% α-helix	7.88	30.78	25.48	8.95	19.49	12.17	4.86	11.88
	% β-sheet	36.44	20.05	22.56	35.17	26.96	31.05	39.13	32.51
Δ α-helix		-18.3	1.95	-1.23	-14.75	-4.57	-9.19	-15.51	-12.43
Δ β-sheet		16.79	2.12	3.06	13.39	5.98	8.39	15.72	11.5

WT, wild-type

Next, we tested susceptibility of the Casq2 and Casq2 mutants to trypsin digestion to further analyze the impact of Casq2 mutations on protein folding. K180R and D351G mutants showed trypsin digestion patterns similar to wild-type protein indicating no major folding differences between these proteins (Figure 4-7). In support of the CD analysis, R33Q, L167H, and D307H mutants showed limited trypsin susceptibility compared to wild-type protein both in the absence and presence of Ca^{2+} (Figure 4-7). R33Q, L167H, and D307H mutants showed more α-helix (Figure 4-6) and an increased sensitivity to trypsin digestion in the absent of Ca^{2+} (Figure 4-7), indicative of altered protein folding. In agreement with Ca^{2+} binding (Figure 4-5E,F) and CD analysis (Figure 4-6E,F) trypsin digestion of P329S and G332R mutants also showed increased kinetics of digestion in the presence of Ca^{2+} (Figure 4-7C,D), indicative of Ca^{2+}-induced conformational changes of these mutants.

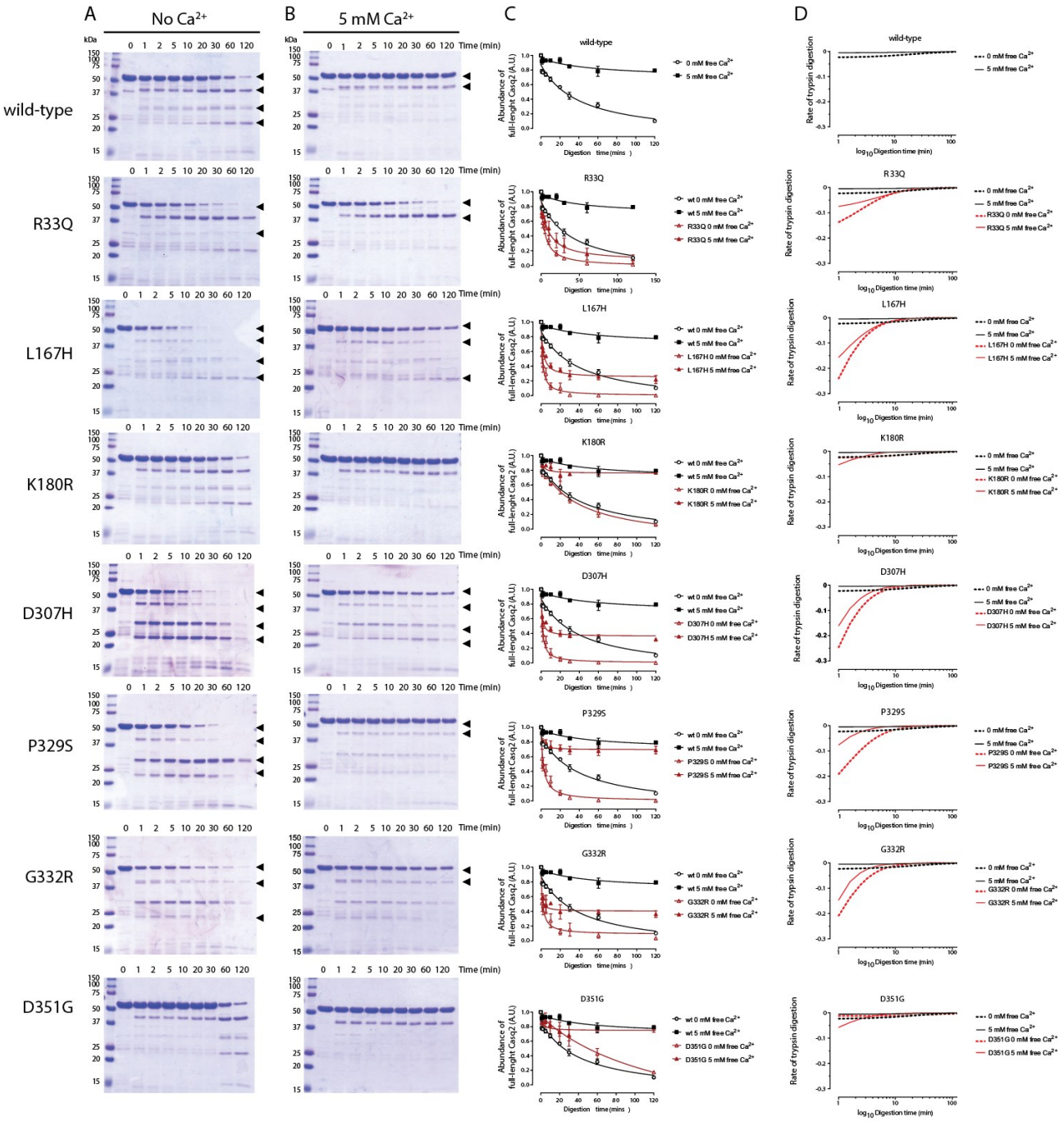

Figure 4-7. Limited trypsin digestion of Casq2 mutants.

A, B) Wild-type Casq2 and Casq2 mutants were subjected to trypsin proteolysis in the absence (A) and presence (B) of 5 mM Ca^{2+} followed by SDS-PAGE. The tryptic fragments, which differed from that of wild-type Casq2 are indicated by the arrowheads.

C) The rate of proteolysis of wild-type and mutant Casq2 as a function of time of trypsin digestion.

D) The rate of proteolysis plotted as the first derivative of the fitted curve from (C). All data are representative of three technical replicates from two independent protein purifications.

Next, we used the Tycho NT.6 system to carry out thermal denaturation analysis of wild-type Casq2 and Casq2 mutants in a label-free environment as another indicator of protein folding. The analysis is based on measurement of the protein's intrinsic tryptophan fluorescence and records a protein's unfolding profile in real-time. Casq2 has 5 tryptophan residues all located in the third thioredoxin-like domain[16, 17] and fully buried in the hydrophobic core. K180R and D351G mutants showed an unfolding profile (Figure 4-8A) and inflection temperature (Ti, proportionally to protein melting temperature) values (Figure 4-8F,G; Table **4-3**) similar to wild-type Casq2. Ti values for R33Q (52.55°C) and G332R (47.23°C) mutants, although close to the wild-type Casq2 (49.89°C), were statistically different (Figure 4-8C,E). P329S, G332R and D307H mutants showed minimal (for P329S and G332R mutants) to no detectable (for D307H mutant) unfolding transition (Figure 4-8; Table **4-3**). These mutants also showed a significantly higher initial ratio (350 nm/330 nm at 35°C), indicating that tryptophan residues in P329S, G332R and D307H mutants were exposed to solvent, and the polarity of the local tryptophan environment was unchanged upon denaturing at higher temperature. The L167H mutant had an intermediate unfolding profile and significantly increased Ti value (Figure 4-8; Table 4-3), indicating partially exposed tryptophan. The L167H mutation resulted in a partial disruption of the third thioredoxin-like domain, whereas, D307H, P329S, and G332R exhibited a large disruption in the third thioredoxin-like domain (Figure 4-8; Table 4-3).

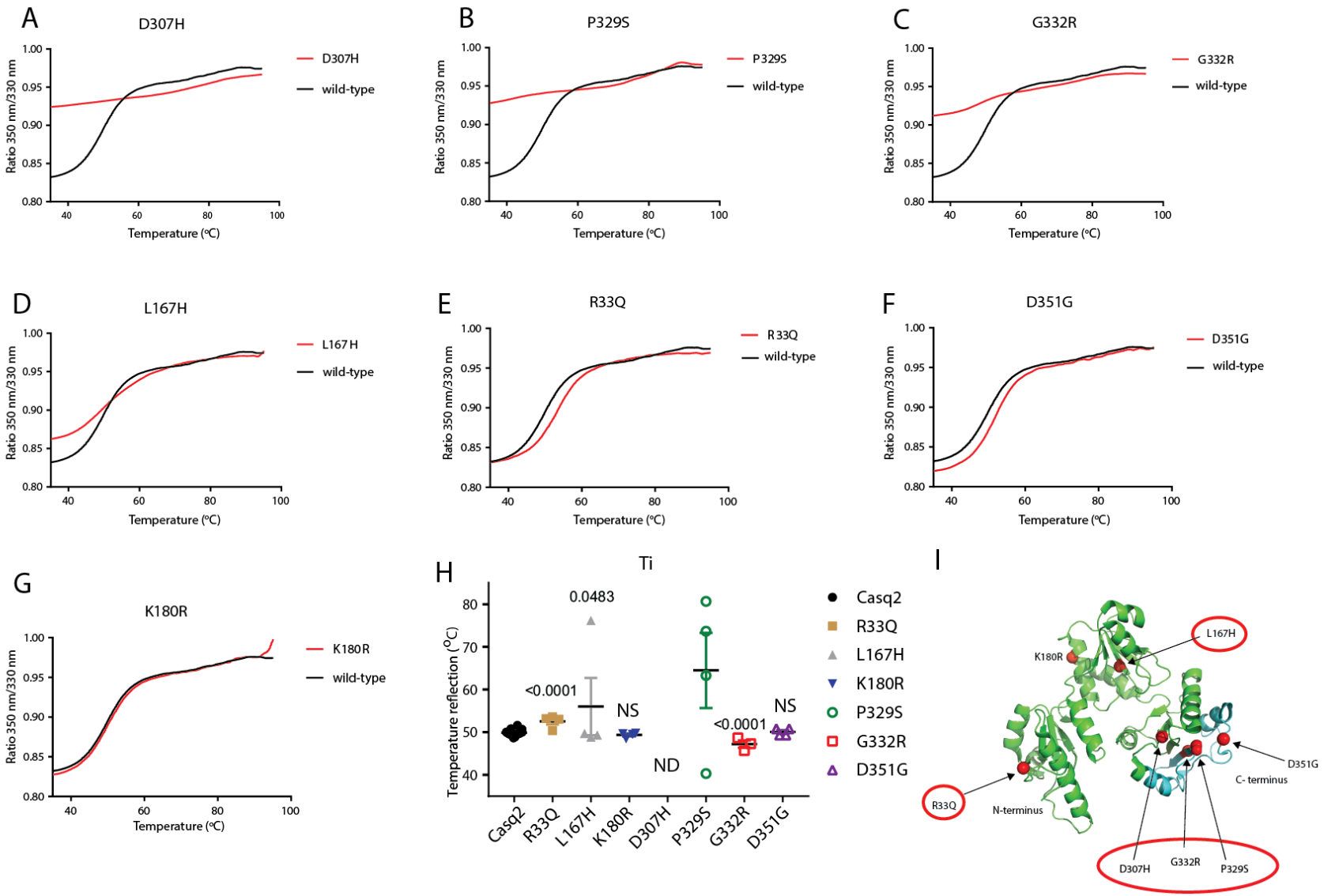
A
D307H
D307H
wild-type
B
P329S
P329S
wild-type
C
G332R
G332R
wild-type
D
L167H
L167H
wild-type
E
R33Q
R33Q
wild-type
F
D351G
D351G
wild-type
G
K180R
K180R
wild-type
Ratio 350 nm/330 nm
Temperature (°C)
H
Ti
Temperature reflection (°C)
0.0483
<0.0001
NS
ND
<0.0001
NS
Casq2
R33Q
L167H
K180R
D307H
P329S
G332R
D351G
I
L167H
K180R
D351G
C- terminus
R33Q
N-terminus
D307H
G332R
P329S

Figure 4-8. Thermal denaturation analysis of Casq2 and Casq2 mutants.

A-G) Thermal denaturation analysis of wild-type Casq2 (black lines) or Casq2 mutants (red lines) was monitored by intrinsic tryptophan fluorescence of proteins in response to increased temperature from 35ºC to 95ºC. Graphs represent 3 independent measurements.

H) Inflection temperature for Casq2 and Casq2 mutants representing the temperature at which the transition from folded protein to unfolded state occurs.

I) Human Casq2 crystal structure (2VAF). Mutants with significant difference in their protein folding are indicated by red circles. The location of tryptophan residues is depicted as yellow sticks. All data are representative of three technical replicates from two independent protein purifications. Error bars represent mean ± standard error. p values calculated from unpaired student t-test.

Table 4-3. Inflection temperature for Casq2 and Casq2 mutants

Calsequestrin (Casq2)	Ti value (°C) mean ± standard error
Wild-type	49.9±0.16 (n=18)
R33Q	52.5±0.73 (n=4)
L167H	56.0±6.73 (n=4)
K180R	49.4±0.29 (n=4)
D351G	50.0±0.43 (n=4)
P329S	64.5±8.82 (n=4)
G332R	47.2±0.87 (n=3)
D307H	Not detectable

Ti: inflection temperature, proportional to protein melting temperature

4.4.5 Ca^{2+} dependent polymerization of Casq2 mutants

Casq2 undergoes monomer to oligomer transition and oligomerization[58]. Upon binding to Ca^{2+}, Casq2 undergoes reversible polymerization, and this affects Casq2 assembly to the junctional SR, which could have direct impact on SR Ca^{2+} supply and RyR2 regulation[58]. We tested for a Ca^{2+}-dependent oligomerization of Casq2 mutants using disuccinimidyl suberate (DSS) cross-linker (Figure 4-9) and native gel electrophoresis techniques (Figure 4-10). Addition of Ca^{2+} to wild-type Casq2 increased oligomerization of the protein (Figure 4-9). A similar pattern of Ca^{2+}-dependent oligomerization was seen for K180R, D351G and D307H mutants (Figure 4-9). Surprisingly, the D307H mutant that did not bind Ca^{2+} (Figure 4-5) and showed Ca^{2+}-dependent oligomerization indistinguishable from the wild-type Casq2 (Figure 4-9) suggesting a role of Ca^{2+} in function of this mutant. R33Q, L167H, P329S and G332R mutants had increased Ca^{2+}-dependent oligomerization whereas R33Q mutant showed no dependence on Ca^{2+} for oligomerization (Figure 4-9). Under conditions of native electrophoresis, wild-type Casq2 and Casq2 mutants exhibited spontaneous oligomerization (Figure 4-10) with R33Q, L167H and G332R mutants having a greater proportion in oligomeric form as compared to wild-type protein (Figure 4-10). This was particularly evident for the R33Q and L167H mutants which existed predominantly (>80% and >60%, respectively) in an oligomeric form (Figure 4-10).

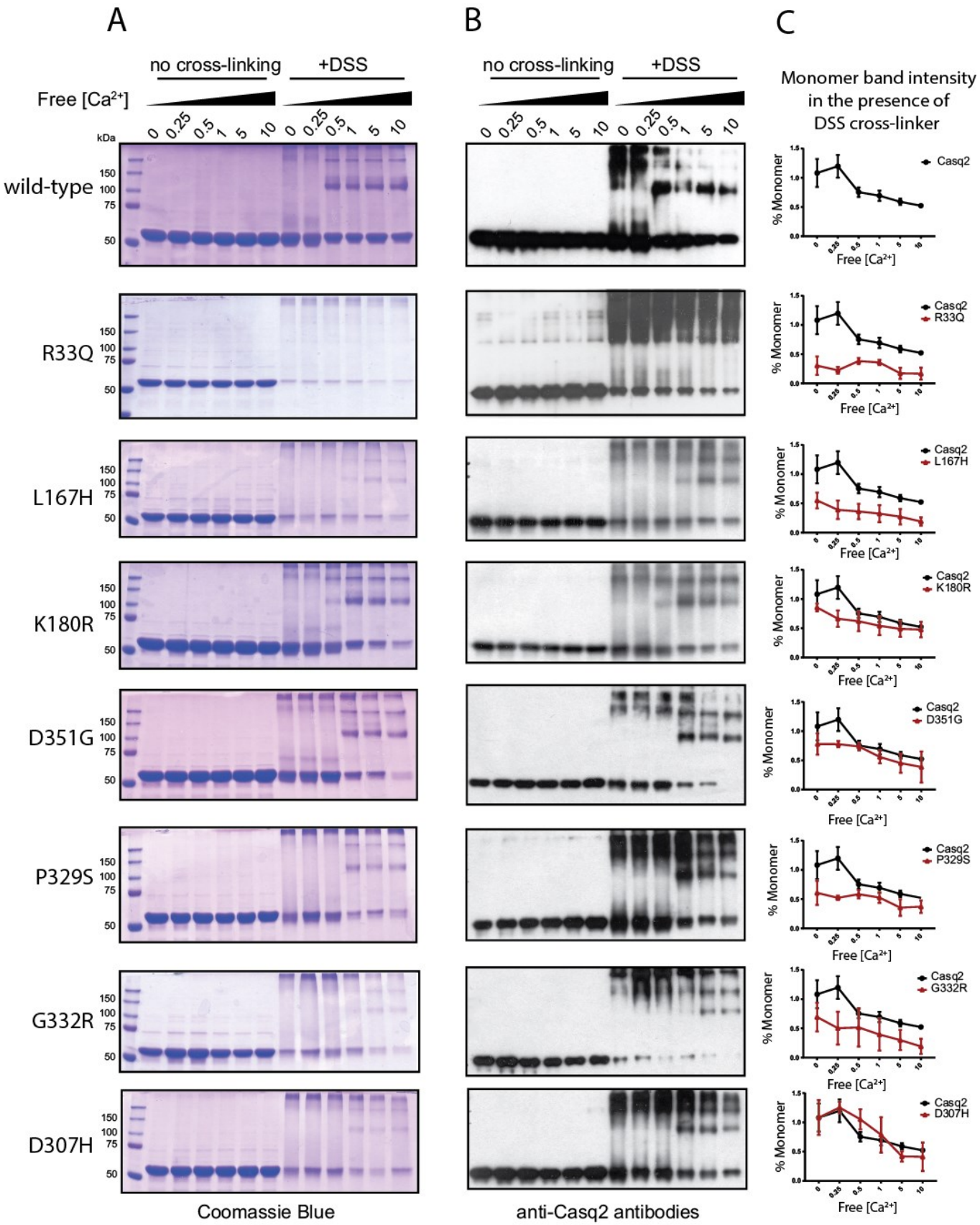
A
B
C
no cross-linking
+DSS
Free [Ca2+]
0 0.25 0.5 1 5 10 0 0.25 0.5 1 5 10
kDa
150
100
75
50
wild-type
R33Q
L167H
K180R
D351G
P329S
G332R
D307H
Coomassie Blue
anti-Casq2 antibodies
Monomer band intensity in the presence of DSS cross-linker
% Monomer
Free [Ca2+]
Casq2
Casq2 R33Q
Casq2 L167H
Casq2 K180R
Casq2 D351G
Casq2 P329S
Casq2 G332R
Casq2 D307H

Figure 4-9. Ca^{2+}-dependent polymerization of Casq2 and Casq2 mutants.

A) Coomassie blue stained SDS-PAGE of Casq2 and Casq2 mutant incubated with or without cross-linker at increasing free Ca^{2+} concentration.

B) Immunoblots were probed with anti-Casq2 antibodies.

C) Quantitative analysis of Casq2 monomer (~50 kDa protein band) of wild-type or mutant proteins in the presence of cross-linker (from A) as a function of increased free Ca^{2} concentration. All data are representative of three technical replicates from two independent protein purifications. Error bars represent mean ± standard error.

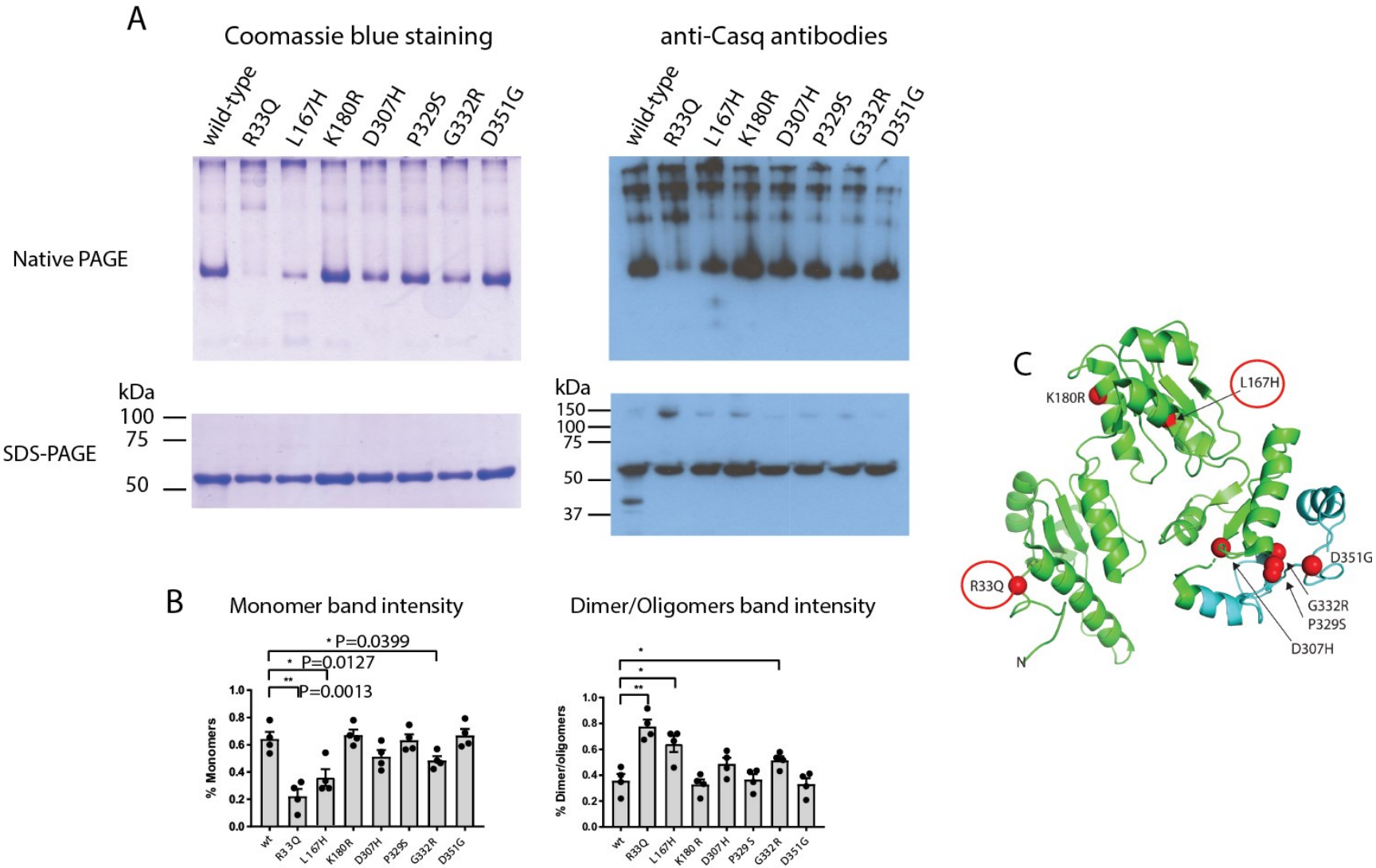
A
Coomassie blue staining
anti-Casq antibodies
wild-type
R33Q
L167H
K180R
D307H
P329S
G332R
D351G
Native PAGE
SDS-PAGE
kDa
100
75
50
150
37
B
Monomer band intensity
Dimer/Oligomers band intensity
* P=0.0399
* P=0.0127
** P=0.0013
% Monomers
% Dimer/oligomers
wt
R33Q
L167H
K180R
D307H
P329S
G332R
D351G
C
K180R
L167H
R33Q
D351G
G332R
P329S
D307H
N

Figure 4-10. Polymerization of Casq2 mutants.

A) Polymerization of Casq2 or Casq2 mutants was carried out at 167 μM free Ca^{2+} followed by SDS-PAGE or native gel electrophoresis. Immunoblots were probed with anit-Casq2 antibodies. A representative of four independent experiments is shown.

B) Quantitative analysis of monomeric and oligomeric forms of Casq2 mutants.

C) Human Casq2 crystal structure (2VAF). Red circles depict the location of Casq2 mutations with highly increased oligomerization. All data are representative of more than three technical replicates from two independent protein purifications. Error bars represent mean ± standard error. P values calculated from unpaired student t-test

4.4.6 Casq2 binding to IRE1α, an ER/SR stress sensor

Casq2 binds to IRE1α, an ER/SR stress sensor and squelches IRE1α activity[47]. We used MST thermophoresis to test whether Casq2 mutations affected Casq2 interaction with the luminal domain of IRE1α. R33Q, L167H, D307H, P329S, G332R and D351G bound to the luminal domain of IRE1α with similar kinetics and affinities as seen for wild-type protein (Figure 4-11). However, the K180R mutant showed increased binding affinity (Figure 4-11) indicating a stronger interaction between the K180R Casq2 mutant and the IRE1α luminal domain. We concluded that all other Casq2 mutants tested bound normally to the IRE1α stress sensor.

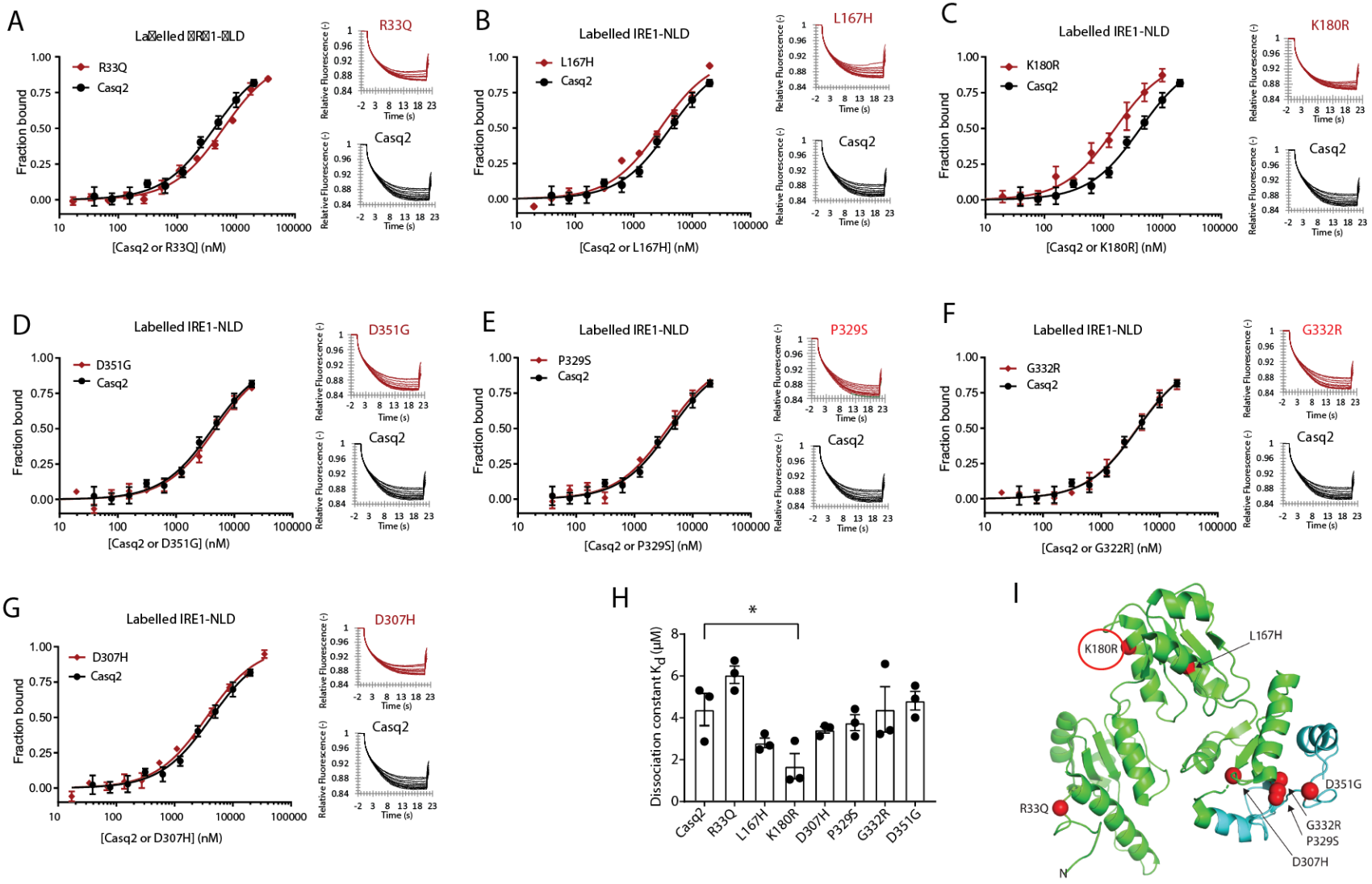
A
Labelled IRE1-NLD
R33Q
Casq2
Fraction bound
[Casq2 or R33Q] (nM)
Relative Fluorescence (-)
Time (s)
B
Labelled IRE1-NLD
L167H
Casq2
[Casq2 or L167H] (nM)
C
Labelled IRE1-NLD
K180R
Casq2
[Casq2 or K180R] (nM)
D
Labelled IRE1-NLD
D351G
Casq2
[Casq2 or D351G] (nM)
E
Labelled IRE1-NLD
P329S
Casq2
[Casq2 or P329S] (nM)
F
Labelled IRE1-NLD
G332R
Casq2
[Casq2 or G322R] (nM)
G
Labelled IRE1-NLD
D307H
Casq2
[Casq2 or D307H] (nM)
H
Dissociation constant K_d (μM)
*
Casq2
R33Q
L167H
K180R
D307H
P329S
G332R
D351G
I
K180R
L167H
D351G
R33Q
G332R
P329S
D307H
N

Figure 4-11. Casq2 mutants binding to the ER luminal domain of IRE1α.

A-G) Recombinant N-terminus luminal domain of IRE1α (IRE1-NLD) protein was covalently labeled with a red fluorescent tag and incubated with increasing amounts of Casq2 or Casq2 mutant as indicated in the Figure. Normalized MST time traces are shown to the right of the graph. Each data point is the average of three independent microscale thermophoresis measurements.

H) Bar graph depicts dissociation constants for different Casq2 mutants. *, $p = 0.05$.

I) Human Casq2 crystal structure (2VAF). The red circle on the Casq2 3D structure depicts the location of mutation with altered IRE1-NLD binding. All data are representative of three technical replicates from two independent protein purifications. Error bars represent mean ± standard error. P values calculated from unpaired student t-test

4.5 Discussion

Our phylogenetic analysis of the calsequestrin genes (*Casq2*, *Casq1*, and pre-duplication *Casq*) revealed that calsequestrin is an ancient protein within the metazoan, and duplication of the calsequestrin gene took place after the divergence of the lancelet but before divergence of Chondrichthyes (Figure 4-1). Duplication of the calsequestrin gene allowed for the eventual differentiation of a muscle-specific form of the protein, namely cardiac calsequestrin (*Casq2*) expressed in cardiomyocytes and Casq1 expressed in skeletal muscle. In the mammalian heart Ca^{2+} release from the calsequestrin (Casq2) rich junctional SR is initiated by the Ca^{2+}-induced Ca^{2+} release mechanism. In skeletal muscle, where Casq1 is expressed, Ca^{2+} release from the junctional SR is initiated by the depolarization-induced Ca^{2+} release mechanism. Notably in mammalian species *Casq1* is almost exclusively expressed in skeletal muscle (Figure 4-12). However, *Gallus gallus* appears to have lost the Casq1 gene and *Casq2* highly expressed in both heart and skeletal muscle tissue (Figure 4-12). Other non-mammalian vertebrates also did not show the tissue-specific expression patterns of Casq1 vs 2 observed consistently in mammalian species suggesting that this evolved later in mammalian-specific trait.

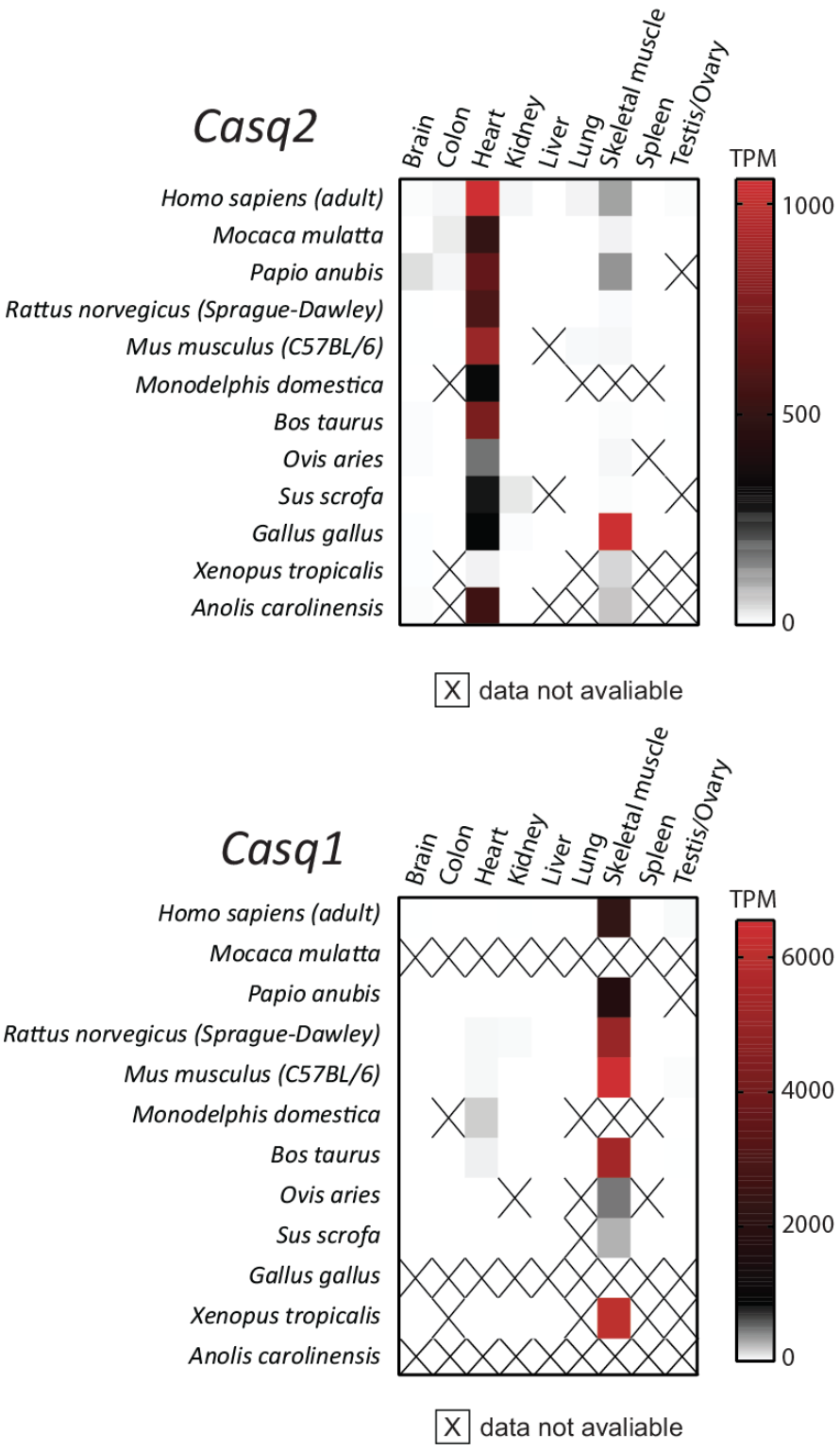

Figure 4-12. Abundance of Casq2 and Casq1 mRNA in selected tissues across species.

Data obtained from Expression Atlas (https://www.ebi.ac.uk/gxa/home). TPM, transcripts per million.

Arthropoda do not have the calsequestrin gene (Figure 4-1), although they have transversely striated muscle similar to the vertebrate skeletal muscle[59] with well-developed T-tubules associated SR cisternae[60, 61]. Considering that Arthropoda move by means of their segmental appendages, they may not require high capacity Ca^{2+} stores. Similar to the loss of the calsequestrin gene in Arthropoda, many genes encoding proteins involved in excitation-contraction coupling have been subject to expansions and losses in different vertebrate classes[61]. For example, amphibian lack the gene encoding RyR2, yet they express both forms of calsequestrin. These results support the notion of the appearance of multiple homologues of junctional SR proteins, including calsequestrin and RyR, which are associated with depolarization-induced Ca^{2+} release (skeletal muscle) or Ca^{2+}-induced Ca^{2+} release (cardiac muscle) mechanisms[61].

Phylogenetic analysis of *casq2* within the metazoan revealed a high level of conservation, especially in the four beta-strands in the hydrophobic core of the third thioredoxin-like fold (Figure 4-4). The C-terminal Asp rich domain of Casq2, responsible for high capacity low affinity Ca^{2+} binding, remained highly conserved throughout many different species. Of note, the pre-duplicated calsequestrin C-terminal domain, however, contains limited numbers of acidic residues, indicating a relatively low Ca^{2+} binding capacity in this basal lineage[62]. There are many highly conserved amino acid residues distributed throughout Casq2 that may be under evolutionary constraints, and mutations in these regions of the protein are expected to impact protein structure and function[63, 64]. Not surprisingly, Casq2 variants associated with CPVT are dispersed throughout different protein regions, but all are highly conserved throughout metazoans some (R33Q, K180R, D307H, P329S and G332R) even including pre-duplication calsequestrin (Figure 4-4). Because of a specific disease phenotype of Casq2 mutants an a priori prediction is that the mutations associated with CPVT would be in sites conserved in Casq2 but divergent in Casq1 and preduplicates. However, this was not what we observed. Instead we found strong conservation at these positions between the paralogues or indeed across all calsequestrin homologues (Figure 4-4). This suggests that the residues at these positions are critical for calsequestrin function. Specificity of cardiac disease seen with Casq2 mutants is likely due to the tissue-specific expression patterns of the paralogues. In humans there is little or no Casq1 paralogue expressed in cardiac tissue to compensate for Casq2 malfunction in CPVT.

For our biochemical studies, we have selected mutants linked to the human CPVT phenotype and located within highly conserved positions, namely, R33Q, L167H, K180R, D307H and three

CASQ2 variants from whole-exome sequencing clinical testing, P329S, G332R, and D351G[24-27, 38, 43, 65, 66]. In agreement with previous reports[25, 31, 33, 46, 67, 68], our studies showed that Casq2^{R33Q}, Casq2^{L167H}, and Casq2^{D307H} differed in their biochemical properties (Figure 4-13): Casq2^{D307H} significantly reduced Ca^{2+} binding affinity and altered protein tertiary structure (Figure 4-5); R33Q and L167H mutants retained Ca^{2+} binding affinity (Figure 4-5), but had increased sensitivity to tryptic cleavage (Figure 4-7) and lost Ca^{2+}-dependent polymerization (Figure 4-9 Figure 4-10).

The Casq2^{R33Q} and Casq2^{L167H} mutants form large oligomers insensitive to Ca^{2+} (Figure 4-9 Figure 4-10), indicating that they lost Ca^{2+} depend polymerization, and are not able to depolymerize in response to Ca^{2+} depletion, a critical function that affects the RyR2 channel gating response to depletion of Ca^{2+} during muscle contraction[58]. Amazingly, Casq2^{D307H} substitution from aspartic acid to histidine, in the highly conserved hydrophobic core of third thioredoxin-like domain of Casq2, results in the loss of low affinity Ca^{2+} binding to Casq2 (Figure 4-5). This is likely due to disruption of the third thioredoxin-like domain, a highly conserved region in Casq2. Surprisingly, Casq2^{D307H} polymerized in a Ca^{2+}-dependent manner (Figure 4-9 Figure 4-10), and, just like the wild-type Casq2, it exhibited Ca^{2+}-dependent confirmation changes[28, 45](Figure 4-6). Nevertheless, the loss of low affinity and high capacity Ca^{2+} binding sites, due to severe Casq2^{D307H} misfolding, results in reduced Ca^{2+} storage at the junctional SR, and impaired Casq2/Ca^{2+}-dependent regulation of RyR2 activity[55, 69].

K180R, P329S, G332R, and D351G mutants have not been previously studied with respect to their biochemical properties. K180R is a newly identified Casq2 mutant, and the first autosomal dominant mutant found of Casq2[27]. Knollman's group recently reported a CPVT-like phenotype in a K180R heterozygous knock-in mouse model[43]. Here we discovered that the Casq2^{K180R} protein has indistinguishable biochemical properties from the wild-type Casq2, including Ca^{2+} binding affinity (Figure 4-5), secondary structure and conformation change in response to increased Ca^{2+} concentration (Figure 4-6), protein flexibility and conformation stability upon trypsin proteolysis (Figure 4-7), protein folding (Figure 4-8), and Ca^{2+} dependent polymerization (Figure 4-9 Figure 4-10). Recently, crystal structure studies of the Casq2^{K180R} maps the mutation to the filament-forming interface[70], and it was proposed that disrupted Casq2 polymer formation may be responsible for Casq2 mutant-associated CPVT. Casq2 binds directly to the luminal domain of ER stress sensor IRE1α at the junctional SR to prevent the activation of IRE1α[47]. Interestingly, of all

mutants tested in this study, only Casq2^{K180R} showed altered binding to the luminal domain of IRE1α (Figure 4-11). Whether this is associated with CPVT remains to be established.

Casq2^{D351G} [38, 39], Casq2^{P329S} [38] and Casq2^{G332R} [38] are three novel Casq2 variants[38, 39] located in a highly conserved third thioredoxin-like domain (Figure 4-4Figure 4-13). Casq2^{P329S} and Casq2^{G332R} have been identified as heterozygous carrier[38]. They are localized in the hydrophobic core of the highly conserved beta-sheet of the third thioredoxin-like domain and are highly conserved throughout the metazoan including Casq1 and pre-duplicate Casq. To our knowledge, there have been no reports on the biochemical and biophysical analysis of these mutants. Casq2^{D351G} showed protein folding and function similar to wild-type protein, whereas Casq2^{P329S} and Casq2^{G332R} showed similar properties to Casq2^{D307H}, including severe disruption in protein folding and impaired Ca^{2+} binding (Figure 4-5), indicative of an important structural and functional role for the highly conserved beta-strands in the third thioredoxin-like domain of Casq2.

Overall, the three CPVT disease causing Casq2 mutants (R33Q, L167H, D307H) and two heterozygous variants (P329S and G332R) may lead to CPVT via different mechanisms (Figure 4-13). The third thioredoxin-like fold domain contains four highly conserved beta-strands, which are essential for correct folding and Ca^{2+} binding, mutations in this region including D307H, P329S, and G332R, and all result in severely misfolded protein with reduced or lost Ca^{2+} binding. R33Q, L167H and K180R are located at the Casq2 front-to-front and back-to-back polymerization interface, causing dysfunction in the protein's Ca^{2+} depend polymerization/depolymerization that would affect filament formation, as proposed by Titus *et al* [70]. This may be the unifying feature of Casq2 mutants association with CPVT [70].

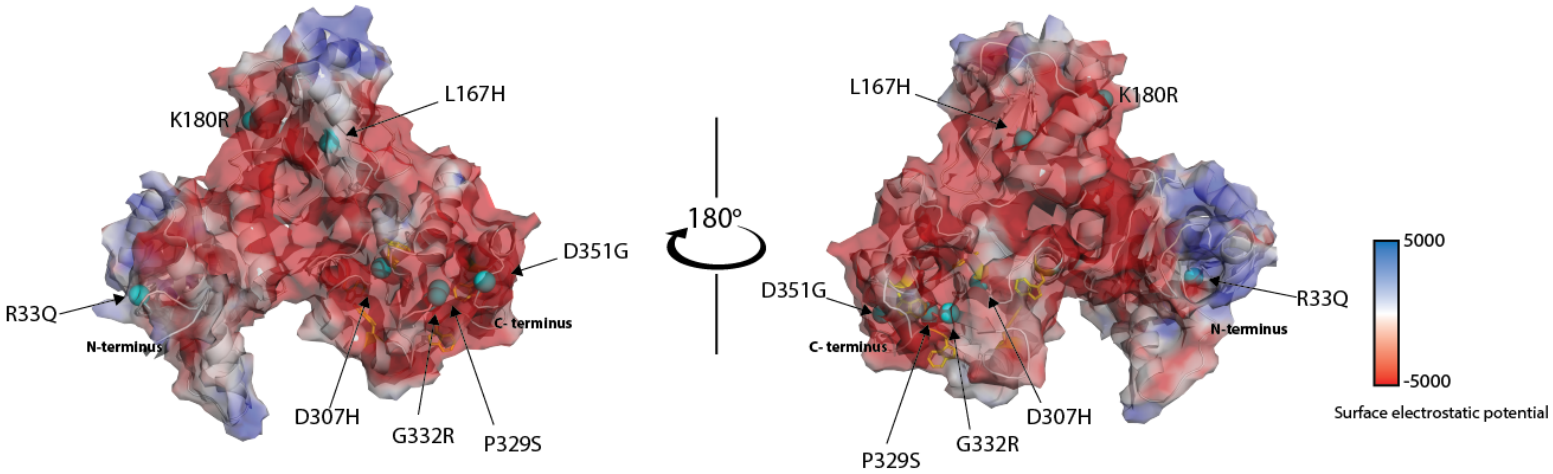

Casq2 mutants	Ca2+ binding Kd (mM)	IRE1NLD binding Kd (μ M)	Polymerization	Protein folding			
				Conformational change in response to increasing [Ca^{2+}] (0 to 5 mM) with CD	Limited proteolysis with trypsin at different [Ca^{2+}]		Domain III folding (at 250 μ [Ca^{2+}])
					absent	5 mM	
wt	0.87 ± 0.28	4.40 ± 0.77	Predominantly monomer at low [Ca2+], increasing [Ca2+] induce polymerization	major conformational change, ↑β sheets by 17% and ↓α-helix by 18%	-	more resistant	Buried typ in the hydrophobic core
R33Q	0.69 ± 0.05	6.06 ± 0.59	Forms high MW aggregates at low [Ca2+]	Minimum to none, ↑β sheets by and ↓α-helix content compares to wt	More susceptible	no observable change	Increased melting temperature
L167H	0.71 ± 0.04	2.81 ± 0.32	Forms high MW aggregates at low [Ca2+]	Not observable, ↑β sheets by and ↓α-helix content compares to wt	Very susceptible	more resistant	Partially misfolded
K180R	0.68 ± 0.17	1.69 ± 0.86	Same as wt	Same as wt	Same as wt	Same as wt	Same as wt
D307H	no detectable binding	3.43 ± 0.31	Slightly more polymerized at low [Ca2+] than wt	Minor change, ↑β sheets by 6% and ↓α-helix by 4.6%	Very susceptible	more resistant	Misfolded, completely exposed typs
P329S	13.49 ± 5.57	4.41 ± 1.09	Same as wt	Smaller change than wt, ↑β sheets by 8% and ↓α-helix by 9%	More susceptible	Same as wt	Misfolded, completely exposed typs
G332R	1.05 ± 0.15	4.82 ± 0.44	More aggregated at low [Ca2+]	Same as wt	Very susceptible	more resistant	Misfolded, completely exposed typs
D351G	2.59 ± 0.40	3.77 ± 0.38	Same as wt	Same as wt	Same as wt	Same as wt	Same as wt

Figure 4-13.Summary of protein characteristics from disease related Casq2 mutants.

Structure of human cardiac calsequestrin (2VAF) shown with surface electrostatic potential. Site of specific mutations is shown as cyan dots. In the Table, mutants with the highest, moderate, or small changes in each parameter measured compare with wild-type (wild-type Casq2) are marked with dark, medium, and light blue, respectively.

4.6 References

1. Rossi AE, Dirksen RT. Sarcoplasmic reticulum: the dynamic calcium governor of muscle. *Muscle & Nerve*. 2006;33:715-731
2. Eisner DA, Caldwell JL, Kistamas K, Trafford AW. Calcium and Excitation-Contraction Coupling in the Heart. *Circulation Research*. 2017;121:181-195
3. Reddish FN, Miller CL, Gorkhali R, Yang JJ. Calcium Dynamics Mediated by the Endoplasmic/Sarcoplasmic Reticulum and Related Diseases. *International Journal of Molecular Sciences*. 2017;18
4. Michalak M, Opas M. Endoplasmic and sarcoplasmic reticulum in the heart. *Trends in Cell Biology*. 2009;19:253-259
5. Wray S, Burdyga T. Sarcoplasmic reticulum function in smooth muscle. *Physiological Reviews*. 2010;90:113-178
6. Bers DM. Cardiac sarcoplasmic reticulum calcium leak: basis and roles in cardiac dysfunction. *Annual Review of Physiology*. 2014;76:107-127
7. Michalak M, Agellon LB. Stress coping strategies in the heart: An integrated view. *Frontiers in Cardiovascular Medicine*. 2018;5:168
8. Barone V, Randazzo D, Del Re V, Sorrentino V, Rossi D. Organization of junctional sarcoplasmic reticulum proteins in skeletal muscle fibers. *Journal of Muscle Research and Cell Motility*. 2015;36:501-515
9. Chopra N, Knollmann BC. Triadin regulates cardiac muscle couplon structure and microdomain Ca^{2+} signalling: a path towards ventricular arrhythmias. *Cardiovascular Research*. 2013;98:187-191
10. Costello B, Chadwick C, Saito A, Chu A, Maurer A, Fleischer S. Characterization of the junctional face membrane from terminal cisternae of sarcoplasmic reticulum. *Journal of Cell Biology*. 1986;103:741-753
11. Lee JM, Rho SH, Shin DW, Cho C, Park WJ, Eom SH, Ma J, Kim DH. Negatively charged amino acids within the intraluminal loop of ryanodine receptor are involved in the interaction with triadin. *Journal of Biological Chemistry*. 2004;279:6994-7000
12. Kobayashi YM, Alseikhan BA, Jones LR. Localization and characterization of the calsequestrin-binding domain of triadin 1. Evidence for a charged beta-strand in mediating the protein-protein interaction. *Journal of Biological Chemistry*. 2000;275:17639-17646
13. Gyorke I, Hester N, Jones LR, Gyorke S. The role of calsequestrin, triadin, and junctin in conferring cardiac ryanodine receptor responsiveness to luminal calcium. *Biophysical Journal*. 2004;86:2121-2128
14. Knollmann BC. New roles of calsequestrin and triadin in cardiac muscle. *The Journal of Physiology*. 2009;587:3081-3087
15. Gyorke S, Stevens SC, Terentyev D. Cardiac calsequestrin: quest inside the SR. *The Journal of Physiology*. 2009;587:3091-3094

16. Wang S, Trumble WR, Liao H, Wesson CR, Dunker AK, Kang CH. Crystal structure of calsequestrin from rabbit skeletal muscle sarcoplasmic reticulum. *Nature Structural Biology*. 1998;5:476-483

17. Kim E, Youn B, Kemper L, Campbell C, Milting H, Varsanyi M, Kang C. Characterization of human cardiac calsequestrin and its deleterious mutants. *Journal of Molecular Biology*. 2007;373:1047-1057

18. Baltogiannis GG, Lysitsas DN, di Giovanni G, Ciconte G, Sieira J, Conte G, Kolettis TM, Chierchia GB, de Asmundis C, Brugada P. CPVT: arrhythmogenesis, therapeutic management, and future perspectives. A brief review of the literature. *Frontiers in Cardiovascular Medicine*. 2019;6:92

19. Mohamed U, Napolitano C, Priori SG. Molecular and electrophysiological bases of catecholaminergic polymorphic ventricular tachycardia. *Journal of Cardiovascular Electrophysiology*. 2007;18:791-797

20. Priori SG, Napolitano C, Memmi M, Colombi B, Drago F, Gasparini M, DeSimone L, Coltorti F, Bloise R, Keegan R, Cruz Filho FE, Vignati G, Benatar A, DeLogu A. Clinical and molecular characterization of patients with catecholaminergic polymorphic ventricular tachycardia. *Circulation*. 2002;106:69-74

21. Postma AV, Denjoy I, Hoorntje TM, Lupoglazoff JM, Da Costa A, Sebillon P, Mannens MM, Wilde AA, Guicheney P. Absence of calsequestrin 2 causes severe forms of catecholaminergic polymorphic ventricular tachycardia. *Circulation Research*. 2002;91:e21-26

22. Nyegaard M, Overgaard MT, Søndergaard MT, Vranas M, Behr ER, Hildebrandt LL, Lund J, Hedley PL, Camm AJ, Wettrell G, Fosdal I, Christiansen M, Børglum AD. Mutations in calmodulin cause ventricular tachycardia and sudden cardiac death. *American Journal of Human Genetics*. 2012;91:703-712

23. Roux-Buisson N, Cacheux M, Fourest-Lieuvin A, Fauconnier J, Brocard J, Denjoy I, Durand P, Guicheney P, Kyndt F, Leenhardt A, Le Marec H, Lucet V, Mabo P, Probst V, Monnier N, Ray PF, Santoni E, Trémeaux P, Lacampagne A, Fauré J, Lunardi J, Marty I. Absence of triadin, a protein of the calcium release complex, is responsible for cardiac arrhythmia with sudden death in human. *Human Molecular Genetics*. 2012;21:2759-2767

24. Faggioni M, Kryshtal DO, Knollmann BC. Calsequestrin mutations and catecholaminergic polymorphic ventricular tachycardia. *Pediatric Cardiology*. 2012;33:959-967

25. Terentyev D, Nori A, Santoro M, Viatchenko-Karpinski S, Kubalova Z, Gyorke I, Terentyeva R, Vedamoorthyrao S, Blom NA, Valle G, Napolitano C, Williams SC, Volpe P, Priori SG, Gyorke S. Abnormal interactions of calsequestrin with the ryanodine receptor calcium release channel complex linked to exercise-induced sudden cardiac death. *Circulation Research*. 2006;98:1151-1158

26. Terentyev D, Kubalova Z, Valle G, Nori A, Vedamoorthyrao S, Terentyeva R, Viatchenko-Karpinski S, Bers DM, Williams SC, Volpe P, Gyorke S. Modulation of SR Ca release by luminal Ca and calsequestrin in cardiac myocytes: effects of CASQ2 mutations linked to sudden cardiac death. *Biophysical Journal*. 2008;95:2037-2048

27. Gray B, Bagnall RD, Lam L, Ingles J, Turner C, Haan E, Davis A, Yang PC, Clancy CE, Sy RW, Semsarian C. A novel heterozygous mutation in cardiac calsequestrin causes autosomal dominant catecholaminergic polymorphic ventricular tachycardia. *Heart Rhythm*. 2016;13:1652-1660

28. Song L, Alcalai R, Arad M, Wolf CM, Toka O, Conner DA, Berul CI, Eldar M, Seidman CE, Seidman JG. Calsequestrin 2 (CASQ2) mutations increase expression of calreticulin and ryanodine receptors, causing catecholaminergic polymorphic ventricular tachycardia. *Journal of Clinical Investigation*. 2007;117:1814-1823

29. Novak A, Barad L, Zeevi-Levin N, Shick R, Shtrichman R, Lorber A, Itskovitz-Eldor J, Binah O. Cardiomyocytes generated from CPVTD307H patients are arrhythmogenic in response to β-adrenergic stimulation. *Journal of Cellular and Molecular Medicine*. 2012;16:468-482

30. Dirksen WP, Lacombe VA, Chi M, Kalyanasundaram A, Viatchenko-Karpinski S, Terentyev D, Zhou Z, Vedamoorthyrao S, Li N, Chiamvimonvat N, Carnes CA, Franzini-Armstrong C, Gyorke S, Periasamy M. A mutation in calsequestrin, CASQ2D307H, impairs sarcoplasmic reticulum Ca^{2+} handling and causes complex ventricular arrhythmias in mice. *Cardiovascular Research*. 2007;75:69-78

31. di Barletta MR, Viatchenko-Karpinski S, Nori A, Memmi M, Terentyev D, Turcato F, Valle G, Rizzi N, Napolitano C, Gyorke S, Volpe P, Priori SG. Clinical phenotype and functional characterization of CASQ2 mutations associated with catecholaminergic polymorphic ventricular tachycardia. *Circulation*. 2006;114:1012-1019

32. Chopra N, Yang T, Asghari P, Moore ED, Huke S, Akin B, Cattolica RA, Perez CF, Hlaing T, Knollmann-Ritschel BE, Jones LR, Pessah IN, Allen PD, Franzini-Armstrong C, Knollmann BC. Ablation of triadin causes loss of cardiac Ca^{2+} release units, impaired excitation-contraction coupling, and cardiac arrhythmias. *Proceedings of the National Academy of Sciences of the United States of America*. 2009;106:7636-7641

33. Bal NC, Sharon A, Gupta SC, Jena N, Shaikh S, Gyorke S, Periasamy M. The catecholaminergic polymorphic ventricular tachycardia mutation R33Q disrupts the N-terminal structural motif that regulates reversible calsequestrin polymerization. *Journal of Biological Chemistry*. 2010;285:17188-17196

34. Cacheux M, Fauconnier J, Thireau J, Osseni A, Brocard J, Roux-Buisson N, Brocard J, Fauré J, Lacampagne A, Marty I. Interplay between Triadin and Calsequestrin in the Pathogenesis of CPVT in the Mouse. *Molecular Therapy*. 2020;28:171-179

35. Josephs K, Patel K, Janson CM, Montagna C, McDonald TV. Compound heterozygous CASQ2 mutations and long-term course of catecholaminergic polymorphic ventricular tachycardia. *Molecular Genetics & Genomic Medicine*. 2017;5:788-794

36. Rajagopalan A, Pollanen MS. Sudden death during struggle in the setting of heterozygosity for a mutation in calsequesterin 2. *Forensic Science, Medicine and Pathology*. 2016;12:86-89

37. Liu B, Ho H-T, Brunello L, Unudurthi SD, Lou Q, Belevych AE, Qian L, Kim DH, Cho C, Janssen PML, Hund TJ, Knollmann BC, Kranias EG, Györke S. Ablation of HRC

alleviates cardiac arrhythmia and improves abnormal Ca handling in CASQ2 knockout mice prone to CPVT. *Cardiovascular Research*. 2015;108:299-311

38. Landstrom AP, Dailey-Schwartz AL, Rosenfeld JA, Yang Y, McLean MJ, Miyake CY, Valdes SO, Fan Y, Allen HD, Penny DJ, Kim JJ. Interpreting incidentally identified variants in genes associated with catecholaminergic polymorphic ventricular tachycardia in a large cohort of clinical whole-exome genetic test referrals. *Circulation: Arrhythmia and Electrophysiology*. 2017;10

39. Neubauer J, Lecca MR, Russo G, Bartsch C, Medeiros-Domingo A, Berger W, Haas C. Post-mortem whole-exome analysis in a large sudden infant death syndrome cohort with a focus on cardiovascular and metabolic genetic diseases. *European Journal of Human Genetics*. 2017;25:404-409

40. Wong CH, Koo SH, She GQ, Chui P, Lee EJ. Genetic variability of RyR2 and CASQ2 genes in an Asian population. *Forensic Science International*. 2009;192:53-55

41. Liu QQ, Oberti C, Zhang XQ, Ke T, Zhang T, Scheinman M, Hu DY, Wang QK. [A Novel mutation of F189L in CASQ2 in families with catecholaminergic polymorphic ventricular tachycardia]. *Zhonghua Yi Xue Yi Chuan Xue Za Zhi*. 2008;25:334-337

42. Laitinen PJ, Swan H, Kontula K. Molecular genetics of exercise-induced polymorphic ventricular tachycardia: identification of three novel cardiac ryanodine receptor mutations and two common calsequestrin 2 amino-acid polymorphisms. *European Journal of Human Genetics*. 2003;11:888-891

43. Wleklinski M, Parikh S, Knollmann BC. An Autosomal Dominant Mutation in Calsequestrin 2 Causes CPVT Without Changing Protein Levels. *Biophysical Journal*. 2019;116:95a-96a

44. Lahat H, Pras E, Olender T, Avidan N, Ben-Asher E, Man O, Levy-Nissenbaum E, Khoury A, Lorber A, Goldman B, Lancet D, Eldar M. A missense mutation in a highly conserved region of CASQ2 is associated with autosomal recessive catecholamine-induced polymorphic ventricular tachycardia in Bedouin families from Israel. *American Journal of Human Genetics*. 2001;69:1378-1384

45. Kalyanasundaram A, Bal NC, Franzini-Armstrong C, Knollmann BC, Periasamy M. The calsequestrin mutation CASQ2D307H does not affect protein stability and targeting to the junctional sarcoplasmic reticulum but compromises its dynamic regulation of calcium buffering. *Journal of Biological Chemistry*. 2010;285:3076-3083

46. Rizzi N, Liu N, Napolitano C, Nori A, Turcato F, Colombi B, Bicciato S, Arcelli D, Spedito A, Scelsi M, Villani L, Esposito G, Boncompagni S, Protasi F, Volpe P, Priori SG. Unexpected structural and functional consequences of the R33Q homozygous mutation in cardiac calsequestrin: a complex arrhythmogenic cascade in a knock in mouse model. *Circulation Research*. 2008;103:298-306

47. Wang Q, Groenendyk J, Paskevicius T, Qin W, Kor KC, Liu Y, Hiess F, Knollmann BC, Chen SRW, Tang J, Chen XZ, Agellon LB, Michalak M. Two pools of IRE1α in cardiac and skeletal muscle cells. *FEBS Journal*. 2019;33:8892-8904

48. Louis-Jeune C, Andrade-Navarro MA, Perez-Iratxeta C. Prediction of protein secondary structure from circular dichroism using theoretically derived spectra. *Proteins*. 2012;80:374-381

49. Schoenmakers TJ, Visser GJ, Flik G, Theuvenet AP. CHELATOR: an improved method for computing metal ion concentrations in physiological solutions. *Biotechniques*. 1992;12:870-874, 876-879

50. Campbell KP, MacLennan DH, Jorgensen AO. Staining of the Ca^{2+}-binding proteins, calsequestrin, calmodulin, troponin C, and S-100, with the cationic carbocyanine dye "Stains-all". *Journal of Biological Chemistry*. 1983;258:11267-11273

51. Damiani E, Volpe P, Margreth A. Coexpression of two isoforms of calsequestrin in rabbit slow-twitch muscle. *Journal of Muscle Research and Cell Motility*. 1990;11:522-530

52. Fliegel L, Leberer E, Green NM, MacLennan DH. The fast-twitch muscle calsequestrin isoform predominates in rabbit slow-twitch soleus muscle. *FEBS Letters*. 1989;242:297-300

53. Biral D, Volpe P, Damiani E, Margreth A. Coexistence of two calsequestrin isoforms in rabbit slow-twitch skeletal muscle fibers. *FEBS Letters*. 1992;299:175-178

54. Eldar M, Pras E, Lahat H. A missense mutation in the CASQ2 gene is associated with autosomal-recessive catecholamine-induced polymorphic ventricular tachycardia. *Trends in Cardiovascular Medicine*. 2003;13:148-151

55. Viatchenko-Karpinski S, Terentyev D, Gyorke I, Terentyeva R, Volpe P, Priori SG, Napolitano C, Nori A, Williams SC, Gyorke S. Abnormal calcium signaling and sudden cardiac death associated with mutation of calsequestrin. *Circulation Research*. 2004;94:471-477

56. Ashkenazy H, Abadi S, Martz E, Chay O, Mayrose I, Pupko T, Ben-Tal N. ConSurf 2016: an improved methodology to estimate and visualize evolutionary conservation in macromolecules. *Nucleic Acids Research*. 2016;44:W344-W350

57. Slupsky JR, Ohnishi M, Carpenter MR, Reithmeier RA. Characterization of cardiac calsequestrin. *Biochemistry*. 1987;26:6539-6544

58. Manno C, Figueroa LC, Gillespie D, Fitts R, Kang C, Franzini-Armstrong C, Rios E. Calsequestrin depolymerizes when calcium is depleted in the sarcoplasmic reticulum of working muscle. *Proceedings of the National Academy of Sciences of the United States of America*. 2017;114:E638-E647

59. Paniagua R, Royuela M, García-Anchuelo RM, Fraile B. Ultrastructure of invertebrate muscle cell types. *Histology & Histopathology*. 1996;11:181-201

60. Smith DS, Gupta BL, Smith UNA. The organization and myofilament array of insect visceral muscles. *Journal of Cell Science*. 1966;1:49

61. Mackrill JJ, Shiels HA. Evolution of excitation-contraction coupling. In: Islam MS, ed. *Calcium Signaling*. Cham: Springer International Publishing; 2020:281-320.

62. Bal NC, Jena N, Chakravarty H, Kumar A, Chi M, Balaraju T, Rawale SV, Rawale JS, Sharon A, Periasamy M. The C-terminal calcium-sensitive disordered motifs regulate

isoform-specific polymerization characteristics of calsequestrin. *Biopolymers*. 2015;103:15-22

63. Miller MP, Kumar S. Understanding human disease mutations through the use of interspecific genetic variation. *Human Molecular Genetics*. 2001;10:2319-2328

64. Guo HH, Choe J, Loeb LA. Protein tolerance to random amino acid change. *Proceedings of the National Academy of Sciences of the United States of America*. 2004;101:9205-9210

65. Kumar S, Patel R. Neutral Theory, Disease Mutations, and Personal Exomes. *Molecular Biology and Evolution*. 2018;35:1297-1303

66. Vitkup D, Sander C, Church GM. The amino-acid mutational spectrum of human genetic disease. *Genome Biology*. 2003;4:R72

67. Valle G, Galla D, Nori A, Priori SG, Gyorke S, de Filippis V, Volpe P. Catecholaminergic polymorphic ventricular tachycardia-related mutations R33Q and L167H alter calcium sensitivity of human cardiac calsequestrin. *Biochemical Journal*. 2008;413:291-303

68. Qin J, Valle G, Nani A, Nori A, Rizzi N, Priori SG, Volpe P, Fill M. Luminal Ca^{2+} regulation of single cardiac ryanodine receptors: insights provided by calsequestrin and its mutants. *The Journal of General Physiology*. 2008;131:325-334

69. Houle TD, Ram ML, Cala SE. Calsequestrin mutant D307H exhibits depressed binding to its protein targets and a depressed response to calcium. *Cardiovascular Research*. 2004;64:227-233

70. Titus EW, Deiter FH, Shi C, Wojciak J, Scheinman M, Jura N, Deo RC. The structure of a calsequestrin filament reveals mechanisms of familial arrhythmia. *bioRxiv*. 2019:672303

Chapter 5: General conclusions

The ER stress is integral part of heart physiology and pathology. In skeletal and cardiac muscle, SR is a specialized ER that is responsible for E-C coupling to support muscle contraction, whereas ER is responsible for vital housekeeping functions. In this work, we identified two distinct pools of IRE1α in skeletal muscle fibers and cardiomyocytes. One localized at the perinuclear ER and other at the junctional SR localized with membrane channel RyR and SR Ca^{2+} binding protein calsequestrin (Figure 5-1). We discovered that, at the junctional SR, calsequestrin interacts directly with the ER luminal domain of IRE1α and inhibiting its dimerization – initiation step of IRE1α mediated UPR activation. However, the localization and regulation of other branch of UPR including PERK and ATF6 in skeletal and cardiac muscle remains to be established (Figure 5-1).

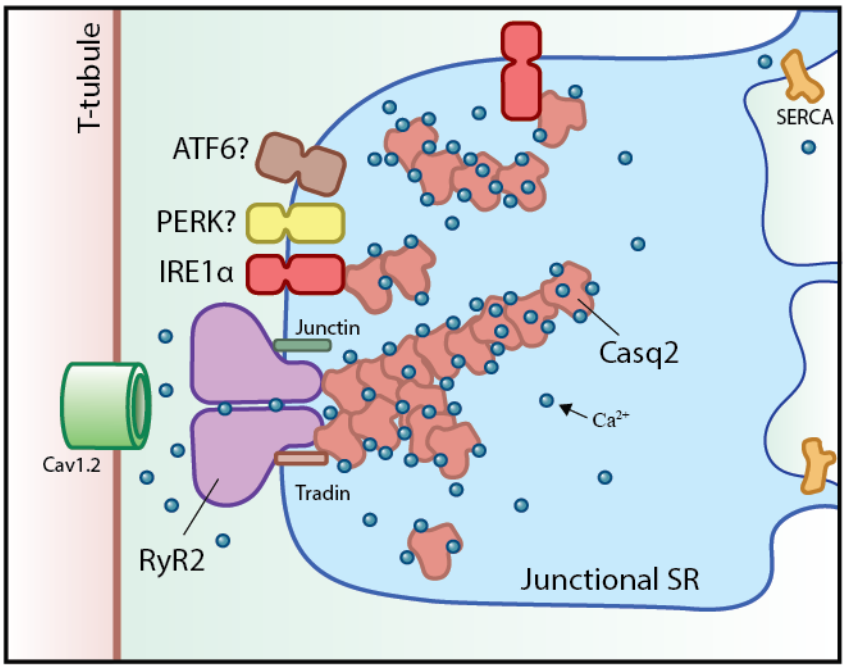

Figure 5-1. Schematic representation of UPR component at the junctional SR.

Ca^{2+} storage/buffering protein calsequestrin is shown to directly interact with IRE1α preventing IRE1α dimerization.

Cav1.2: voltage-gated L-type Ca^{2+} channel

Inhibiting IRE1α have previously been shown to protect heart against cardiac fibrosis[1] and atherosclerosis[2]. To investigate a role of IRE1α and its contribution to cardiac physiology and pathogenesis, we generated a mouse model with cardiomyocyte specific, inducible silencing of the IRE1α gene. Unexpectedly, we discovered that silencing the IRE1α gene in adult heart results in dilated cardiomyopathy with severely impaired cardiac function. This does not, however, cause activation of other branches of UPR including ATF6 nor PERK in cardiomyocytes under non stressed condition. Moreover, IRE1α-deficient cardiomyocytes show impaired Ca^{2+} transient, suggesting IRE1α deficiency in the heart leads to dysfunction in Ca^{2+} handling of the cardiomyocytes. However, the underlying mechanism requires further investigation.

Calsequestrin is the major Ca^{2+} binding protein in the SR, functions as Ca^{2+} storage and buffering, and plays an important role in muscle excitation-contraction E-C coupling. Mutations in the gene encoding for cardiac calsequestrin, CASQ2, cause a stress-induced arrhythmia, CPVT. We investigated the functional impact of six CPVT related Casq2 mutations, including CPVT causing mutations R33Q, L167H, D307H[22, 24-37], newly discovery recessive dominant CPVT associated mutant K180R, and heterozygous variants recently discovered from whole exome sequencing (D351G, G332R, P329S)[3, 4]. We investigated if the stress response role of calsequestrin and its novel interaction with ER stress sensor IRE1α could contribute to CPVT. We found Casq2 mutants do not alter its binding kinetics with IRE1α. However, these mutants exhibit severe impact on Casq2 structure and function, might provide new insights on underlying molecular mechanism of Casq2 related CPVT suggesting that complex formation between calsequestrin and IRE1α may not directly contribute to CPVT pathogenesis.

From phylogenetic analysis, we discovered that calsequestrin is an ancient protein in the metazoans, and these mutations are highly conserved throughout metazoans. Moreover, these six mutations are distributed in diverse locations of the calsequestrin protein and impart structure and functional diversity such as misfolding, aggregation, and severe impaired or reduced Ca^{2+} binding ability from biochemical and biophysical characterization (Figure 5-2). However, remarkably these mutations manifest in a similar phenotype in humans. Ca^{2+}-dependent polymerization is important for regulating RyR2 channel activity, misfolding and aggregation can cause loss of RyR2 regulation and leads to RyR2 dependent arrhythmia. Mutations cause loss of Ca^{2+} binding ability can lead to reduced Ca^{2+} storage and buffering function of calsequestrin, which is important in maintaining free Ca^{2+} pool to sustain muscle contraction under stressed conditions. These

potential mechanisms that can leads to CPVT due to Casq2 mutations can be future research directions.

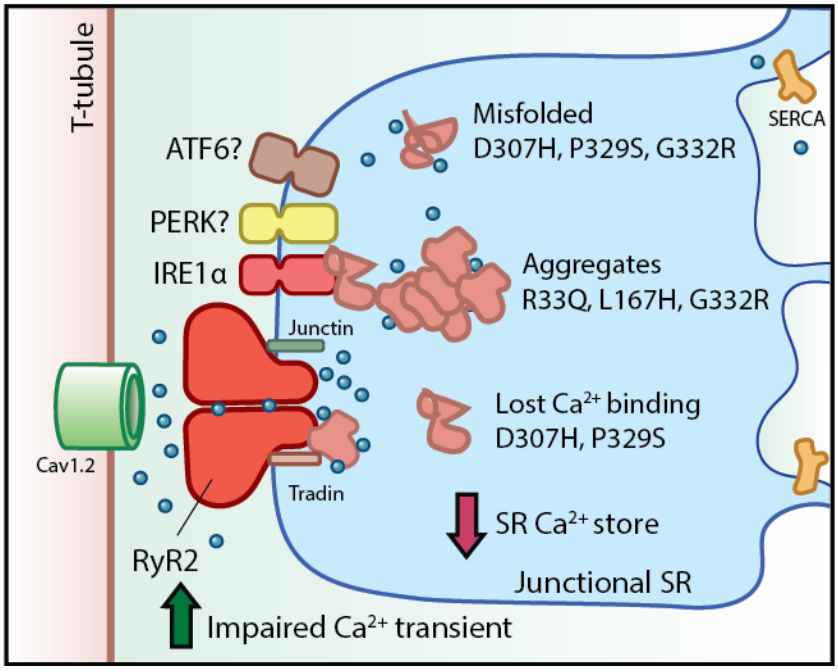

Figure 5-2. Structure and functional impact of CPVT related cardiac calsequestrin mutations

5.1 Reference

1. Groenendyk J, Lee D, Jung J, Dyck JR, Lopaschuk GD, Agellon LB, Michalak M. Inhibition of the Unfolded Protein Response Mechanism Prevents Cardiac Fibrosis. *PLOS One*. 2016;11:e0159682
2. Tufanli O, Telkoparan Akillilar P, Acosta-Alvear D, Kocaturk B, Onat UI, Hamid SM, Cimen I, Walter P, Weber C, Erbay E. Targeting IRE1 with small molecules counteracts progression of atherosclerosis. *Proceedings of the National Academy of Sciences of the United States of America*. 2017;114:E1395-E1404
3. Landstrom AP, Dailey-Schwartz AL, Rosenfeld JA, Yang Y, McLean MJ, Miyake CY, Valdes SO, Fan Y, Allen HD, Penny DJ, Kim JJ. Interpreting incidentally identified variants in genes associated with catecholaminergic polymorphic ventricular tachycardia in a large cohort of clinical whole-exome genetic test referrals. *Circulation: Arrhythmia and Electrophysiology*. 2017;10
4. Neubauer J, Lecca MR, Russo G, Bartsch C, Medeiros-Domingo A, Berger W, Haas C. Post-mortem whole-exome analysis in a large sudden infant death syndrome cohort with a focus on cardiovascular and metabolic genetic diseases. *European Journal of Human Genetics*. 2017;25:404-409

Bibliography

Chapter 1

1. Wang M, Kaufman RJ. Protein misfolding in the endoplasmic reticulum as a conduit to human disease. *Nature*. 2016;529:326-335
2. Schwarz DS, Blower MD. The endoplasmic reticulum: structure, function and response to cellular signaling. *Cellular and Molecular Life Sciences*. 2016;73:79-94
3. Schröder M. Endoplasmic reticulum stress responses. *Cellular and Molecular Life Sciences*. 2008;65:862-894
4. Lam AK, Galione A. The endoplasmic reticulum and junctional membrane communication during calcium signaling. *Biochimica et Biophysica Acta (BBA) - Biomembranes*. 2013;1833:2542-2559
5. Schröder M, Kaufman RJ. The mammalian unfolded protein response. *Annual Review of Biochemistry*. 2005;74:739-789
6. Lombardi AA, Elrod JW. Mediating ER-mitochondrial cross-talk. *Science*. 2017;358:591-592
7. Phillips MJ, Voeltz GK. Structure and function of ER membrane contact sites with other organelles. *Nature Reviews Molecular Cell Biology*. 2016;17:69-82
8. Saheki Y, De Camilli P. Endoplasmic reticulum–plasma membrane contact sites. *Annual Review of Biochemistry*. 2017;86:659-684
9. Michalak M, Opas M. Endoplasmic and sarcoplasmic reticulum in the heart. *Trends in Cell Biology*. 2009;19:253-259
10. Sorrentino V. Sarcoplasmic reticulum: structural determinants and protein dynamics. *International Journal of Biochemistry & Cell Biology*. 2011;43:1075-1078
11. Wray S, Burdyga T. Sarcoplasmic reticulum function in smooth muscle. *Physiological Reviews*. 2010;90:113-178
12. Bers DM. Cardiac sarcoplasmic reticulum calcium leak: basis and roles in cardiac dysfunction. *Annual Review of Physiology*. 2014;76:107-127
13. Pinali C, Bennett H, Davenport JB, Trafford Andrew W, Kitmitto A. Three-dimensional reconstruction of cardiac sarcoplasmic reticulum reveals a continuous network linking transverse-tubules. *Circulation Research*. 2013;113:1219-1230
14. Bers DM. Cardiac excitation–contraction coupling. *Nature*. 2002;415:198-205
15. Allen BG, Katz S. Calreticulin and calsequestrin are differentially distributed in canine heart. *Journal of Molecular and Cellular Cardiology*. 2000;32:2379-2384
16. Lee D, Michalak M. Membrane associated Ca^{2+} buffers in the heart. *BMB Reports*. 2010;43:151-157

17. Doroudgar S, Glembotski CC. New concepts of endoplasmic reticulum function in the heart: programmed to conserve. *Journal of Molecular and Cellular Cardiology*. 2013;55:85-91

18. Slade AM, Severs NJ. Rough endoplasmic reticulum in the adult mammalian cardiac muscle cell. *Journal of Submicroscopic Cytology and Pathology*. 1985;17:531-536

19. Koyabu S, Imanaka-Yoshida K, Ioshii SO, Nakano T, Yoshida T. Switching of the dominant calcium sequestering protein during skeletal muscle differentiation. *Cell Motility and the Cytoskeleton*. 1994;29:259-270

20. Kaisto T, Metsikkö K. Distribution of the endoplasmic reticulum and its relationship with the sarcoplasmic reticulum in skeletal myofibers. *Experimental Cell Research*. 2003;289:47-57

21. Kaakinen M, Papponen H, Metsikkö K. Microdomains of endoplasmic reticulum within the sarcoplasmic reticulum of skeletal myofibers. *Experimental Cell Research*. 2008;314:237-245

22. Volpe P, Villa A, Podini P, Martini A, Nori A, Panzeri MC, Meldolesi J. The endoplasmic reticulum-sarcoplasmic reticulum connection: distribution of endoplasmic reticulum markers in the sarcoplasmic reticulum of skeletal muscle fibers. *Proceedings of the National Academy of Sciences of the United States of America*. 1992;89:6142-6146

23. Mesaeli N, Nakamura K, Zvaritch E, Dickie P, Dziak E, Krause KH, Opas M, MacLennan DH, Michalak M. Calreticulin is essential for cardiac development. *Journal of Cell Biology*. 1999;144:857-868

24. Xiong B, Jha V, Min J-K, Cho J. Protein disulfide isomerase in cardiovascular disease. *Experimental & Molecular Medicine*. 2020;52:390-399

25. Wang X, Bi X, Zhang G, Deng Y, Luo X, Xu L, Scherer PE, Ferdous A, Fu G, Gillette TG, Lee AS, Jiang X, Wang ZV. Glucose-regulated protein 78 is essential for cardiac myocyte survival. *Cell Death and Differentiation*. 2018;25:2181-2194

26. Walter P, Ron D. The unfolded protein response: From stress pathway to homeostatic regulation. *Science*. 2011;334:1081-1086

27. Groenendyk J, Sreenivasaiah PK, Kim DH, Agellon LB, Michalak M. Biology of endoplasmic reticulum stress in the heart. *Circulation Research*. 2010;107:1185-1197

28. Groenendyk J, Agellon LB, Michalak M. Coping with endoplasmic reticulum stress in the cardiovascular system. *Annual Review of Physiology*. 2013;75:49-67

29. Liu CY, Schroder M, Kaufman RJ. Ligand-independent dimerization activates the stress response kinases IRE1 and PERK in the lumen of the endoplasmic reticulum. *Journal of Biological Chemistry*. 2000;275:24881-24885

30. Zhou J, Liu CY, Back SH, Clark RL, Peisach D, Xu Z, Kaufman RJ. The crystal structure of human IRE1 luminal domain reveals a conserved dimerization interface required for activation of the unfolded protein response. *Proceedings of the National Academy of Sciences of the United States of America*. 2006;103:14343-14348

31. Calfon M, Zeng H, Urano F, Till JH, Hubbard SR, Harding HP, Clark SG, Ron D. IRE1 couples endoplasmic reticulum load to secretory capacity by processing the XBP-1 mRNA. *Nature*. 2002;415:92-96

32. Yoshida H, Matsui T, Yamamoto A, Okada T, Mori K. XBP1 mRNA is induced by ATF6 and spliced by IRE1 in response to ER stress to produce a highly active transcription factor. *Cell*. 2001;107:881-891

33. Yamamoto K, Yoshida H, Kokame K, Kaufman RJ, Mori K. Differential contributions of ATF6 and XBP1 to the activation of endoplasmic reticulum stress-responsive cis-acting elements ERSE, UPRE and ERSE-II. *Journal of Biochemistry*. 2004;136:343-350

34. Maurel M, Chevet E, Tavernier J, Gerlo S. Getting RIDD of RNA: IRE1 in cell fate regulation. *Trends in Biochemical Sciences*. 2014;39:245-254

35. Lerner AG, Upton J-P, Praveen PVK, Ghosh R, Nakagawa Y, Igbaria A, Shen S, Nguyen V, Backes BJ, Heiman M, Heintz N, Greengard P, Hui S, Tang Q, Trusina A, Oakes SA, Papa FR. IRE1α Induces Thioredoxin-Interacting Protein to Activate the NLRP3 Inflammasome and Promote Programmed Cell Death under Irremediable ER Stress. *Cell Metabolism*. 2012;16:250-264

36. Upton J-P, Wang L, Han D, Wang ES, Huskey NE, Lim L, Truitt M, McManus MT, Ruggero D, Goga A, Papa FR, Oakes SA. IRE1α cleaves select microRNAs during ER stress to derepress translation of proapoptotic Caspase-2. *Science* 2012;338:818-822

37. Sano R, Reed JC. ER stress-induced cell death mechanisms. *Biochimica et Biophysica Acta (BBA) - Molecular Cell Research*. 2013;1833:3460-3470

38. Harding HP, Zhang Y, Ron D. Protein translation and folding are coupled by an endoplasmic-reticulum-resident kinase. *Nature*. 1999;397:271-274

39. Shi Y, Vattem KM, Sood R, An J, Liang J, Stramm L, Wek RC. Identification and characterization of pancreatic eukaryotic initiation factor 2 α-subunit kinase, PEK, involved in translational control. *Molecular and Cellular Biology*. 1998;18:7499-7509

40. Bravo R, Parra V, Gatica D, Rodriguez AE, Torrealba N, Paredes F, Wang ZV, Zorzano A, Hill JA, Jaimovich E, Quest AFG, Lavandero S. Endoplasmic reticulum and the unfolded protein response: dynamics and metabolic integration. *International Review of Cell and Molecular Biology*. 2013;301:215-290

41. Oyadomari S, Mori M. Roles of CHOP/GADD153 in endoplasmic reticulum stress. *Cell Death & Differentiation*. 2004;11:381-389

42. Kokame K, Kato H, Miyata T. Identification of ERSE-II, a new cis-acting element responsible for the ATF6-dependent mammalian unfolded protein response. *Journal of Biological Chemistry*. 2001;276:9199-9205

43. Yoshida H, Haze K, Yanagi H, Yura T, Mori K. Identification of the cis-acting endoplasmic reticulum stress response element responsible for transcriptional induction of mammalian glucose-regulated proteins. Involvement of basic leucine zipper transcription factors. *Journal of Biological Chemistry*. 1998;273:33741-33749

44. Okada K, Minamino T, Tsukamoto Y, Liao Y, Tsukamoto O, Takashima S, Hirata A, Fujita M, Nagamachi Y, Nakatani T, Yutani C, Ozawa K, Ogawa S, Tomoike H, Hori M,

Kitakaze M. Prolonged endoplasmic reticulum stress in hypertrophic and failing heart after aortic constriction: possible contribution of endoplasmic reticulum stress to cardiac myocyte apoptosis. *Circulation*. 2004;110:705-712

45. Gao G, Xie A, Zhang J, Herman AM, Jeong EM, Gu L, Liu M, Yang KC, Kamp TJ, Dudley SC. Unfolded protein response regulates cardiac sodium current in systolic human heart failure. *Circulation: Arrhythmia and Electrophysiology*. 2013;6:1018-1024

46. Szegezdi E, Duffy A, O'Mahoney ME, Logue SE, Mylotte LA, O'Brien T, Samali A. ER stress contributes to ischemia-induced cardiomyocyte apoptosis. *Biochemical and Biophysical Research Communications*. 2006;349:1406-1411

47. Thuerauf Donna J, Marcinko M, Gude N, Rubio M, Sussman Mark A, Glembotski Christopher C. Activation of the unfolded protein response in infarcted mouse heart and hypoxic cultured cardiac myocytes. *Circulation Research*. 2006;99:275-282

48. Sawada T, Minamino T, Fu HY, Asai M, Okuda K, Isomura T, Yamazaki S, Asano Y, Okada K, Tsukamoto O, Sanada S, Asanuma H, Asakura M, Takashima S, Kitakaze M, Komuro I. X-box binding protein 1 regulates brain natriuretic peptide through a novel AP1/CRE-like element in cardiomyocytes. *Journal of Molecular and Cellular Cardiology*. 2010;48:1280-1289

49. Jin J-K, Blackwood EA, Azizi K, Thuerauf DJ, Fahem AG, Hofmann C, Kaufman RJ, Doroudgar S, Glembotski CC. ATF6 decreases myocardial ischemia/reperfusion damage and links er stress and oxidative stress signaling pathways in the heart. *Circulation Research*. 2017;120:862-875

50. Martindale Joshua J, Fernandez R, Thuerauf D, Whittaker R, Gude N, Sussman Mark A, Glembotski Christopher C. Endoplasmic reticulum stress gene induction and protection from ischemia/reperfusion injury in the hearts of transgenic mice with a tamoxifen-regulated form of ATF6. *Circulation Research*. 2006;98:1186-1193

51. Liu X, Kwak D, Lu Z, Xu X, Fassett J, Wang H, Wei Y, Cavener DR, Hu X, Hall J, Bache RJ, Chen Y. Endoplasmic reticulum stress sensor protein kinase R-like endoplasmic reticulum kinase (PERK) protects against pressure overload-induced heart failure and lung remodeling. *Hypertension (Dallas, Tex. : 1979)*. 2014;64:738-744

52. Guan HS, Shangguan HJ, Shang Z, Yang L, Meng XM, Qiao SB. Endoplasmic reticulum stress caused by left ventricular hypertrophy in rats: effects of telmisartan. *American Journal of the Medical Sciences*. 2011;342:318-323

53. Fu HY, Minamino T, Tsukamoto O, Sawada T, Asai M, Kato H, Asano Y, Fujita M, Takashima S, Hori M, Kitakaze M. Overexpression of endoplasmic reticulum-resident chaperone attenuates cardiomyocyte death induced by proteasome inhibition. *Cardiovascular Research*. 2008;79:600-610

54. Steiger D, Yokota T, Li J, Ren S, Minamisawa S, Wang Y. The serine/threonine-protein kinase/endoribonuclease IRE1α protects the heart against pressure overload-induced heart failure. *The Journal of Biological Chemistry*. 2018;293:9652-9661

55. Wang ZV, Deng Y, Gao N, Pedrozo Z, Li DL, Morales CR, Criollo A, Luo X, Tan W, Jiang N, Lehrman MA, Rothermel BA, Lee A-H, Lavandero S, Mammen PPA, Ferdous A,

Gillette TG, Scherer PE, Hill JA. Spliced X-box binding protein 1 couples the unfolded protein response to hexosamine biosynthetic pathway. *Cell*. 2014;156:1179-1192

56. Yamaguchi O, Higuchi Y, Hirotani S, Kashiwase K, Nakayama H, Hikoso S, Takeda T, Watanabe T, Asahi M, Taniike M, Matsumura Y, Tsujimoto I, Hongo K, Kusakari Y, Kurihara S, Nishida K, Ichijo H, Hori M, Otsu K. Targeted deletion of apoptosis signal-regulating kinase 1 attenuates left ventricular remodeling. *Proceedings of the National Academy of Sciences of the United States of America*. 2003;100:15883-15888

57. Hollien J. Evolution of the unfolded protein response. *Biochimica et Biophysica Acta (BBA) - Molecular Cell Research*. 2013;1833:2458-2463

58. Hourihan JM, Moronetti Mazzeo LE, Fernández-Cárdenas LP, Blackwell TK. Cysteine sulfenylation directs IRE-1 to activate the SKN-1/Nrf2 antioxidant response. *Molecular Cell*. 2016;63:553-566

59. Carreras-Sureda A, Jaña F, Urra H, Durand S, Mortenson DE, Sagredo A, Bustos G, Hazari Y, Ramos-Fernández E, Sassano ML, Pihán P, van Vliet AR, González-Quiroz M, Torres AK, Tapia-Rojas C, Kerkhofs M, Vicente R, Kaufman RJ, Inestrosa NC, Gonzalez-Billault C, Wiseman RL, Agostinis P, Bultynck G, Court FA, Kroemer G, Cárdenas JC, Hetz C. Non-canonical function of IRE1α determines mitochondria-associated endoplasmic reticulum composition to control calcium transfer and bioenergetics. *Nature Cell Biology*. 2019;21:755-767

60. Iwawaki T, Akai R, Yamanaka S, Kohno K. Function of IRE1 alpha in the placenta is essential for placental development and embryonic viability. *Proceedings of the National Academy of Sciences*. 2009;106:16657

61. Tirasophon W, Lee K, Callaghan B, Welihinda A, Kaufman RJ. The endoribonuclease activity of mammalian IRE1 autoregulates its mRNA and is required for the unfolded protein response. *Genes & Development*. 2000;14:2725-2736

62. Tsuru A, Fujimoto N, Takahashi S, Saito M, Nakamura D, Iwano M, Iwawaki T, Kadokura H, Ron D, Kohno K. Negative feedback by IRE1β optimizes mucin production in goblet cells. *Proceedings of the National Academy of Sciences of the United States of America*. 2013;110:2864-2869

63. Imagawa Y, Hosoda A, Sasaka S-i, Tsuru A, Kohno K. RNase domains determine the functional difference between IRE1α and IRE1β. *FEBS Letters*. 2008;582:656-660

64. Li H, Korennykh AV, Behrman SL, Walter P. Mammalian endoplasmic reticulum stress sensor IRE1 signals by dynamic clustering. *Proceedings of the National Academy of Sciences of the United States of America*. 2010;107:16113-16118

65. Gardner BM, Walter P. Unfolded proteins are Ire1-activating ligands that directly induce the unfolded protein response. *Science* 2011;333:1891-1894

66. Credle JJ, Finer-Moore JS, Papa FR, Stroud RM, Walter P. On the mechanism of sensing unfolded protein in the endoplasmic reticulum. *Proceedings of the National Academy of Sciences of the United States of America*. 2005;102:18773-18784

67. Bertolotti A, Zhang Y, Hendershot LM, Harding HP, Ron D. Dynamic interaction of BiP and ER stress transducers in the unfolded-protein response. *Nature Cell Biology*. 2000;2:326-332

68. Okamura K, Kimata Y, Higashio H, Tsuru A, Kohno K. Dissociation of Kar2p/BiP from an ER sensory molecule, Ire1p, triggers the unfolded protein response in yeast. *Biochemical and Biophysical Research Communications*. 2000;279:445-450

69. Kimata Y, Oikawa D, Shimizu Y, Ishiwata-Kimata Y, Kohno K. A role for BiP as an adjustor for the endoplasmic reticulum stress-sensing protein Ire1. *Journal of Cell Biology*. 2004;167:445-456

70. Kopp MC, Nowak PR, Larburu N, Adams CJ, Ali MM. In vitro FRET analysis of IRE1 and BiP association and dissociation upon endoplasmic reticulum stress. *eLife*. 2018;7:e30257

71. Adams CJ, Kopp MC, Larburu N, Nowak PR, Ali MMU. Structure and molecular mechanism of ER stress signaling by the unfolded protein response signal activator IRE1. *Frontiers in Molecular Biosciences*. 2019;6

72. Shen J, Chen X, Hendershot L, Prywes R. ER stress regulation of ATF6 localization by dissociation of BiP/GRP78 binding and unmasking of Golgi localization signals. *Developmental Cell*. 2002;3:99-111

73. Ali Khan H, Mutus B. Protein disulfide isomerase a multifunctional protein with multiple physiological roles. *Frontiers in Chemistry*. 2014;2

74. Groenendyk J, Peng Z, Dudek E, Fan X, Mizianty MJ, Dufey E, Urra H, Sepulveda D, Rojas-Rivera D, Lim Y, Kim DH, Baretta K, Srikanth S, Gwack Y, Ahnn J, Kaufman RJ, Lee SK, Hetz C, Kurgan L, Michalak M. Interplay between the oxidoreductase PDIA6 and microRNA-322 controls the response to disrupted endoplasmic reticulum calcium homeostasis. *Science Signaling*. 2014;7:ra54

75. Vekich JA, Belmont PJ, Thuerauf DJ, Glembotski CC. Protein disulfide isomerase-associated 6 is an ATF6-inducible ER stress response protein that protects cardiac myocytes from ischemia/reperfusion-mediated cell death. *Journal of Molecular and Cellular Cardiology*. 2012;53:259-267

76. Nagata K. Hsp47: a collagen-specific molecular chaperone. *Trends in Biochemical Sciences*. 1996;21:22-26

77. Nagata K, Hosokawa N. Regulation and function of collagen-specific molecular chaperone, HSP47. *Cell Structure and Function*. 1996;21:425-430

78. Sepulveda D, Rojas-Rivera D, Rodríguez DA, Groenendyk J, Köhler A, Lebeaupin C, Ito S, Urra H, Carreras-Sureda A, Hazari Y, Vasseur-Cognet M, Ali MMU, Chevet E, Campos G, Godoy P, Vaisar T, Bailly-Maitre B, Nagata K, Michalak M, Sierralta J, Hetz C. Interactome screening identifies the ER luminal chaperone Hsp47 as a regulator of the unfolded protein response transducer IRE1α. *Molecular Cell*. 2018;69:238-252.e237

79. Groenendyk J, Paskevicius T, Urra H, Viricel C, Wang K, Barakat K, Hetz C, Kurgan L, Agellon LB, Michalak M. Cyclosporine A binding to COX-2 reveals a novel signaling

pathway that activates IRE1α unfolded protein response sensor. *Scientific Reports*. 2018;8:16678

80. Wang Q, Groenendyk J, Paskevicius T, Qin W, Kor KC, Liu Y, Hiess F, Knollmann BC, Chen SRW, Tang J, Chen XZ, Agellon LB, Michalak M. Two pools of IRE1α in cardiac and skeletal muscle cells. *FEBS Journal*. 2019;33:8892-8904

81. Chen Y, Brandizzi F. IRE1: ER stress sensor and cell fate executor. *Trends in Cell Biology*. 2013;23:547-555

82. Hetz C, Glimcher LH. Fine-tuning of the unfolded protein response: Assembling the IRE1alpha interactome. *Molecular Cell*. 2009;35:551-561

83. Urano F, Wang X, Bertolotti A, Zhang Y, Chung P, Harding HP, Ron D. Coupling of stress in the ER to activation of JNK protein kinases by transmembrane protein kinase IRE1. *Science*. 2000;287:664-666

84. Nishitoh H, Matsuzawa A, Tobiume K, Saegusa K, Takeda K, Inoue K, Hori S, Kakizuka A, Ichijo H. ASK1 is essential for endoplasmic reticulum stress-induced neuronal cell death triggered by expanded polyglutamine repeats. *Genes & Development*. 2002;16:1345-1355

85. Ikemoto N, Bhatnagar GM, Nagy B, Gergely J. Interaction of divalent cations with the 55,000-dalton protein component of the sarcoplasmic reticulum. Studies of fluorescence and circular dichroism. *Journal of Biological Chemistry*. 1972;247:7835-7837

86. MacLennan DH, Wong PT. Isolation of a calcium-sequestering protein from sarcoplasmic reticulum. *Proceedings of the National Academy of Sciences of the United States of America*. 1971;68:1231-1235

87. Meissner G, Conner GE, Fleischer S. Isolation of sarcoplasmic reticulum by zonal centrifugation and purification of Ca^{2+}-pump and Ca^{2+}-binding proteins. *Biochimica et Biophysica Acta (BBA) - Biomembranes*. 1973;298:246-269

88. Ikemoto N, Nagy B, Bhatnagar GM, Gergely J. Studies on a metal-binding protein of the sarcoplasmic reticulum. *Journal of Biological Chemistry*. 1974;249:2357-2365

89. Franzini-Armstrong C. STUDIES OF THE TRIAD : I. Structure of the junction in frog twitch fibers. *Journal of Cell Biology*. 1970;47:488-499

90. Franzini-Armstrong C, Kenney LJ, Varriano-Marston E. The structure of calsequestrin in triads of vertebrate skeletal muscle: a deep-etch study. *Journal of Cell Biology*. 1987;105:49-56

91. Perni S, Close M, Franzini-Armstrong C. Novel details of calsequestrin gel conformation in situ. *Journal of Biological Chemistry*. 2013;288:31358-31362

92. Park H, Park IY, Kim E, Youn B, Fields K, Dunker AK, Kang C. Comparing skeletal and cardiac calsequestrin structures and their calcium binding: a proposed mechanism for coupled calcium binding and protein polymerization. *Journal of Biological Chemistry*. 2004;279:18026-18033

93. Sanchez EJ, Lewis KM, Danna BR, Kang C. High-capacity Ca^{2+} binding of human skeletal calsequestrin. *Journal of Biological Chemistry*. 2012;287:11592-11601

94. Park H, Wu S, Dunker AK, Kang C. Polymerization of calsequestrin. Implications for Ca^{2+} regulation. *Journal of Biological Chemistry*. 2003;278:16176-16182

95. Wang S, Trumble WR, Liao H, Wesson CR, Dunker AK, Kang C. Crystal structure of calsequestrin from rabbit skeletal muscle sarcoplasmic reticulum. *Nature Structural Biology*. 1998;5:476-483

96. Titus EW, Deiter FH, Shi C, Wojciak J, Scheinman M, Jura N, Deo RC. The structure of a calsequestrin filament reveals mechanisms of familial arrhythmia. *bioRxiv*. 2019:672303

97. Beard NA, Casarotto MG, Wei L, Varsanyi M, Laver DR, Dulhunty AF. Regulation of ryanodine receptors by calsequestrin: effect of high luminal Ca^{2+} and phosphorylation. *Biophysical Journal*. 2005;88:3444-3454

98. Wei L, Varsányi M, Dulhunty AF, Beard NA. The conformation of calsequestrin determines its ability to regulate skeletal ryanodine receptors. *Biophysical Journal*. 2006;91:1288-1301

99. Fliegel L, Newton E, Burns K, Michalak M. Molecular cloning of cDNA encoding a 55-kDa multifunctional thyroid hormone binding protein of skeletal muscle sarcoplasmic reticulum. *Journal of Biological Chemistry*. 1990;265:15496-15502

100. Scott BT, Simmerman HK, Collins JH, Nadal-Ginard B, Jones LR. Complete amino acid sequence of canine cardiac calsequestrin deduced by cDNA cloning. *Journal of Biological Chemistry*. 1988;263:8958-8964

101. Murphy RM, Larkins NT, Mollica JP, Beard NA, Lamb GD. Calsequestrin content and SERCA determine normal and maximal Ca^{2+} storage levels in sarcoplasmic reticulum of fast- and slow-twitch fibres of rat. *The Journal of Physiology*. 2009;587:443-460

102. Sacchetto R, Volpe P, Damiani E, Margreth A. Postnatal development of rabbit fast-twitch skeletal muscle: accumulation, isoform transition and fibre distribution of calsequestrin. *Journal of Muscle Research and Cell Motility*. 1993;14:646-653

103. Biral D, Volpe P, Damiani E, Margreth A. Coexistence of two calsequestrin isoforms in rabbit slow-twitch skeletal muscle fibers. *FEBS Letters*. 1992;299:175-178

104. Damiani E, Volpe P, Margreth A. Coexpression of two isoforms of calsequestrin in rabbit slow-twitch muscle. *Journal of Muscle Research and Cell Motility*. 1990;11:522-530

105. Beard NA, Wei L, Cheung SN, Kimura T, Varsanyi M, Dulhunty AF. Phosphorylation of skeletal muscle calsequestrin enhances its Ca^{2+} binding capacity and promotes its association with junctin. *Cell Calcium*. 2008;44:363-373

106. Beard NA, Dulhunty AF. C-terminal residues of skeletal muscle calsequestrin are essential for calcium binding and for skeletal ryanodine receptor inhibition. *Skelet Muscle*. 2015;5:6

107. Royer L, Ríos E. Deconstructing calsequestrin. Complex buffering in the calcium store of skeletal muscle. *The Journal of Physiology*. 2009;587:3101-3111

108. Cala SE, Jones LR. Phosphorylation of cardiac and skeletal muscle calsequestrin isoforms by casein kinase II. Demonstration of a cluster of unique rapidly phosphorylated sites in cardiac calsequestrin. *Journal of Biological Chemistry*. 1991;266:391-398

109. Kiarash A, Kelly CE, Phinney BS, Valdivia HH, Abrams J, Cala SE. Defective glycosylation of calsequestrin in heart failure. *Cardiovascular Research*. 2004;63:264-272

110. Sanchez EJ, Munske GR, Criswell A, Milting H, Dunker AK, Kang C. Phosphorylation of human calsequestrin: implications for calcium regulation. *Molecular and Cellular Biochemistry*. 2011;353:195

111. Sanchez EJ, Lewis KM, Munske GR, Nissen MS, Kang C. Glycosylation of skeletal calsequestrin: implications for its function. *Journal of Biological Chemistry*. 2012;287:3042-3050

112. Ryder DJ, Judge SM, Beharry AW, Farnsworth CL, Silva JC, Judge AR. Identification of the acetylation and ubiquitin-modified proteome during the progression of skeletal muscle atrophy. *PLOS One*. 2015;10:e0136247

113. Kalyanasundaram A, Bal NC, Franzini-Armstrong C, Knollmann BC, Periasamy M. The calsequestrin mutation CASQ2D307H does not affect protein stability and targeting to the junctional sarcoplasmic reticulum but compromises its dynamic regulation of calcium buffering. *Journal of Biological Chemistry*. 2010;285:3076-3083

114. Kim E, Youn B, Kemper L, Campbell C, Milting H, Varsanyi M, Kang C. Characterization of human cardiac calsequestrin and its deleterious mutants. *Journal of Molecular Biology*. 2007;373:1047-1057

115. Slupsky JR, Ohnishi M, Carpenter MR, Reithmeier RA. Characterization of cardiac calsequestrin. *Biochemistry*. 1987;26:6539-6544

116. Aaron BM, Oikawa K, Reithmeier RA, Sykes BD. Characterization of skeletal muscle calsequestrin by 1H NMR spectroscopy. *Journal of Biological Chemistry*. 1984;259:11876-11881

117. Wang Q, Paskevicius T, Filbert A, Qin W, Chen X, Tang J, Dacks J, Agellon L, Michalak M. Evolutionary conservation and diversity of human calsequestrin function. *Scientific Report*. 2020; Revisions requested

118. di Barletta MR, Viatchenko-Karpinski S, Nori A, Memmi M, Terentyev D, Turcato F, Valle G, Rizzi N, Napolitano C, Gyorke S, Volpe P, Priori SG. Clinical phenotype and functional characterization of CASQ2 mutations associated with catecholaminergic polymorphic ventricular tachycardia. *Circulation*. 2006;114:1012-1019

119. Wei L, Hanna AD, Beard NA, Dulhunty AF. Unique isoform-specific properties of calsequestrin in the heart and skeletal muscle. *Cell Calcium*. 2009;45:474-484

120. Rosenberg P, Katz D, Bryson V. SOCE and STIM1 signaling in the heart: Timing and location matter. *Cell Calcium*. 2019;77:20-28

121. Qin J, Valle G, Nani A, Nori A, Rizzi N, Priori SG, Volpe P, Fill M. Luminal Ca^{2+} regulation of single cardiac ryanodine receptors: insights provided by calsequestrin and its mutants. *The Journal of General Physiology*. 2008;131:325-334

122. Lewis KM, Munske GR, Byrd SS, Kang J, Cho H, Ríos E, Kang C. Characterization of post-translational modifications to calsequestrins of cardiac and skeletal muscle. *International journal of molecular sciences*. 2016;17:1539

123. Jacob S, Sleiman NH, Kern S, Jones LR, Sala-Mercado JA, McFarland TP, Sabbah HH, Cala SE. Altered calsequestrin glycan processing is common to diverse models of canine heart failure. *Molecular and Cellular Biochemistry*. 2013;377:11-21

124. Manno C, Sztretye M, Figueroa L, Allen PD, Rios E. Dynamic measurement of the calcium buffering properties of the sarcoplasmic reticulum in mouse skeletal muscle. *The Journal of Physiology*. 2013;591:423-442

125. Dainese M, Quarta M, Lyfenko AD, Paolini C, Canato M, Reggiani C, Dirksen RT, Protasi F. Anesthetic- and heat-induced sudden death in calsequestrin-1-knockout mice. *The FASEB Journal*. 2009;23:1710-1720

126. Paolini C, Quarta M, Nori A, Boncompagni S, Canato M, Volpe P, Allen PD, Reggiani C, Protasi F. Reorganized stores and impaired calcium handling in skeletal muscle of mice lacking calsequestrin-1. *The Journal of Physiology*. 2007;583:767-784

127. Royer L, Sztretye M, Manno C, Pouvreau S, Zhou J, Knollmann BC, Protasi F, Allen PD, Ríos E. Paradoxical buffering of calcium by calsequestrin demonstrated for the calcium store of skeletal muscle. *The Journal of General Physiology*. 2010;136:325-338

128. Shin DW, Pan Z, Kim EK, Lee JM, Bhat MB, Parness J, Kim DH, Ma J. A retrograde signal from calsequestrin for the regulation of store-operated Ca^{2+} entry in skeletal muscle. *Journal of Biological Chemistry*. 2003;278:3286-3292

129. Knollmann BC, Chopra N, Hlaing T, Akin B, Yang T, Ettensohn K, Knollmann BE, Horton KD, Weissman NJ, Holinstat I, Zhang W, Roden DM, Jones LR, Franzini-Armstrong C, Pfeifer K. Casq2 deletion causes sarcoplasmic reticulum volume increase, premature Ca^{2+} release, and catecholaminergic polymorphic ventricular tachycardia. *Journal of Clinical Investigation*. 2006;116:2510-2520

130. Song L, Alcalai R, Arad M, Wolf CM, Toka O, Conner DA, Berul CI, Eldar M, Seidman CE, Seidman JG. Calsequestrin 2 (CASQ2) mutations increase expression of calreticulin and ryanodine receptors, causing catecholaminergic polymorphic ventricular tachycardia. *Journal of Clinical Investigation*. 2007;117:1814-1823

131. Canato M, Scorzeto M, Giacomello M, Protasi F, Reggiani C, Stienen GJM. Massive alterations of sarcoplasmic reticulum free calcium in skeletal muscle fibers lacking calsequestrin revealed by a genetically encoded probe. *Proceedings of the National Academy of Sciences of the United States of America*. 2010;107:22326-22331

132. Lai FA, Erickson HP, Rousseau E, Liu QY, Meissner G. Purification and reconstitution of the calcium release channel from skeletal muscle. *Nature*. 1988;331:315-319

133. Wei L, Gallant EM, Dulhunty AF, Beard NA. Junctin and triadin each activate skeletal ryanodine receptors but junctin alone mediates functional interactions with calsequestrin. *International Journal of Biochemistry & Cell Biology*. 2009;41:2214-2224

134. Beard NA, Sakowska MM, Dulhunty AF, Laver DR. Calsequestrin is an inhibitor of skeletal muscle ryanodine receptor calcium release channels. *Biophysical Journal*. 2002;82:310-320

135. Terentyev D, Viatchenko-Karpinski S, Vedamoorthyrao S, Oduru S, Gyorke I, Williams SC, Gyorke S. Protein protein interactions between triadin and calsequestrin are involved

in modulation of sarcoplasmic reticulum calcium release in cardiac myocytes. *The Journal of Physiology*. 2007;583:71-80

136. Zhang L, Kelley J, Schmeisser G, Kobayashi YM, Jones LR. Complex formation between junctin, triadin, calsequestrin, and the ryanodine receptor. Proteins of the cardiac junctional sarcoplasmic reticulum membrane. *Journal of Biological Chemistry*. 1997;272:23389-23397

137. Qin J, Valle G, Nani A, Chen H, Ramos-Franco J, Nori A, Volpe P, Fill M. Ryanodine receptor luminal Ca^{2+} regulation: swapping calsequestrin and channel isoforms. *Biophysical Journal*. 2009;97:1961-1970

138. Gyorke I, Hester N, Jones LR, Gyorke S. The role of calsequestrin, triadin, and junctin in conferring cardiac ryanodine receptor responsiveness to luminal calcium. *Biophysical Journal*. 2004;86:2121-2128

139. Gyorke I, Gyorke S. Regulation of the cardiac ryanodine receptor channel by luminal Ca^{2+} involves luminal Ca^{2+} sensing sites. *Biophysical Journal*. 1998;75:2801-2810

140. Lukyanenko V, Gyorke I, Gyorke S. Regulation of calcium release by calcium inside the sarcoplasmic reticulum in ventricular myocytes. *Pflügers Archiv: European journal of physiology*. 1996;432:1047-1054

141. Prakriya M, Lewis RS. Store-operated calcium channels. *Physiological Reviews*. 2015;95:1383-1436

142. Lewis RS. The molecular choreography of a store-operated calcium channel. *Nature*. 2007;446:284-287

143. Parekh AB, James W. Putney J. Store-operated calcium channels. *Physiological Reviews*. 2005;85:757-810

144. Michelucci A, García-Castañeda M, Boncompagni S, Dirksen RT. Role of STIM1/ORAI1-mediated store-operated Ca^{2+} entry in skeletal muscle physiology and disease. *Cell Calcium*. 2018;76:101-115

145. Boncompagni S, Michelucci A, Pietrangelo L, Dirksen RT, Protasi F. Exercise-dependent formation of new junctions that promote STIM1-Orai1 assembly in skeletal muscle. *Scientific Reports* 2017;7:14286

146. Zhao X, Min CK, Ko J-K, Parness J, Kim DH, Weisleder N, Ma J. Increased store-operated Ca^{2+} entry in skeletal muscle with reduced calsequestrin-1 expression. *Biophysical Journal*. 2010;99:1556-1564

147. Yarotskyy V, Protasi F, Dirksen RT. Accelerated activation of SOCE current in myotubes from two mouse models of anesthetic- and heat-induced sudden death. *PLOS One*. 2013;8:e77633-e77633

148. Faggioni M, Knollmann BC. Calsequestrin 2 and arrhythmias. *American Journal of Physiology: Heart and Circulatory Physiology*. 2012;302:H1250-1260

149. Gyorke S, Stevens SC, Terentyev D. Cardiac calsequestrin: quest inside the SR. *The Journal of Physiology*. 2009;587:3091-3094

150. Faggioni M, Kryshtal DO, Knollmann BC. Calsequestrin mutations and catecholaminergic polymorphic ventricular tachycardia. *Pediatric Cardiology*. 2012;33:959-967

151. Postma AV, Denjoy I, Hoorntje TM, Lupoglazoff JM, Da Costa A, Sebillon P, Mannens MM, Wilde AA, Guicheney P. Absence of calsequestrin 2 causes severe forms of catecholaminergic polymorphic ventricular tachycardia. *Circulation Research*. 2002;91:e21-26

152. Venetucci LA, Eisner DA. Calsequestrin mutations and sudden death: a case of too little sarcoplasmic reticulum calcium buffering? *Circulation Research*. 2008;103:223-225

153. Knollmann BC. New roles of calsequestrin and triadin in cardiac muscle. *The Journal of Physiology*. 2009;587:3081-3087

154. Baltogiannis GG, Lysitsas DN, di Giovanni G, Ciconte G, Sieira J, Conte G, Kolettis TM, Chierchia GB, de Asmundis C, Brugada P. CPVT: arrhythmogenesis, therapeutic management, and future perspectives. A brief review of the literature. *Frontiers in Cardiovascular Medicine*. 2019;6:92

155. Ackerman MJ, Priori SG, Willems S, Berul C, Brugada R, Calkins H, Camm AJ, Ellinor PT, Gollob M, Hamilton R, Hershberger RE, Judge DP, Le Marec H, McKenna WJ, Schulze-Bahr E, Semsarian C, Towbin JA, Watkins H, Wilde A, Wolpert C, Zipes DP. HRS/EHRA expert consensus statement on the state of genetic testing for the channelopathies and cardiomyopathies this document was developed as a partnership between the Heart Rhythm Society (HRS) and the European Heart Rhythm Association (EHRA). *Heart Rhythm*. 2011;8:1308-1339

156. Terentyev D, Kubalova Z, Valle G, Nori A, Vedamoorthyrao S, Terentyeva R, Viatchenko-Karpinski S, Bers DM, Williams SC, Volpe P, Gyorke S. Modulation of SR Ca release by luminal Ca and calsequestrin in cardiac myocytes: effects of CASQ2 mutations linked to sudden cardiac death. *Biophysical Journal*. 2008;95:2037-2048

157. Valle G, Galla D, Nori A, Priori SG, Gyorke S, de Filippis V, Volpe P. Catecholaminergic polymorphic ventricular tachycardia-related mutations R33Q and L167H alter calcium sensitivity of human cardiac calsequestrin. *Biochemical Journal*. 2008;413:291-303

158. Rizzi N, Liu N, Napolitano C, Nori A, Turcato F, Colombi B, Bicciato S, Arcelli D, Spedito A, Scelsi M, Villani L, Esposito G, Boncompagni S, Protasi F, Volpe P, Priori SG. Unexpected structural and functional consequences of the R33Q homozygous mutation in cardiac calsequestrin: a complex arrhythmogenic cascade in a knock in mouse model. *Circulation Research*. 2008;103:298-306

159. Dirksen WP, Lacombe VA, Chi M, Kalyanasundaram A, Viatchenko-Karpinski S, Terentyev D, Zhou Z, Vedamoorthyrao S, Li N, Chiamvimonvat N, Carnes CA, Franzini-Armstrong C, Gyorke S, Periasamy M. A mutation in calsequestrin, CASQ2D307H, impairs sarcoplasmic reticulum Ca^{2+} handling and causes complex ventricular arrhythmias in mice. *Cardiovascular Research*. 2007;75:69-78

160. Lahat H, Pras E, Olender T, Avidan N, Ben-Asher E, Man O, Levy-Nissenbaum E, Khoury A, Lorber A, Goldman B, Lancet D, Eldar M. A missense mutation in a highly conserved region of CASQ2 is associated with autosomal recessive catecholamine-induced

polymorphic ventricular tachycardia in Bedouin families from Israel. *American Journal of Human Genetics*. 2001;69:1378-1384

161. Terentyev D, Nori A, Santoro M, Viatchenko-Karpinski S, Kubalova Z, Gyorke I, Terentyeva R, Vedamoorthyrao S, Blom NA, Valle G, Napolitano C, Williams SC, Volpe P, Priori SG, Gyorke S. Abnormal interactions of calsequestrin with the ryanodine receptor calcium release channel complex linked to exercise-induced sudden cardiac death. *Circulation Research*. 2006;98:1151-1158

162. Gray B, Bagnall RD, Lam L, Ingles J, Turner C, Haan E, Davis A, Yang PC, Clancy CE, Sy RW, Semsarian C. A novel heterozygous mutation in cardiac calsequestrin causes autosomal dominant catecholaminergic polymorphic ventricular tachycardia. *Heart Rhythm*. 2016;13:1652-1660

163. de la Fuente S, Van Langen IM, Postma AV, Bikker H, Meijer A. A case of catecholaminergic polymorphic ventricular tachycardia caused by two calsequestrin 2 mutations. *Pacing and Clinical Electrophysiology*. 2008;31:916-919

164. Liu QQ, Oberti C, Zhang XQ, Ke T, Zhang T, Scheinman M, Hu DY, Wang QK. [A Novel mutation of F189L in CASQ2 in families with catecholaminergic polymorphic ventricular tachycardia]. *Zhonghua Yi Xue Yi Chuan Xue Za Zhi*. 2008;25:334-337

165. Rajagopalan A, Pollanen MS. Sudden death during struggle in the setting of heterozygosity for a mutation in calsequesterin 2. *Forensic Science, Medicine and Pathology*. 2016;12:86-89

166. Landstrom AP, Dailey-Schwartz AL, Rosenfeld JA, Yang Y, McLean MJ, Miyake CY, Valdes SO, Fan Y, Allen HD, Penny DJ, Kim JJ. Interpreting incidentally identified variants in genes associated with catecholaminergic polymorphic ventricular tachycardia in a large cohort of clinical whole-exome genetic test referrals. *Circulation: Arrhythmia and Electrophysiology*. 2017;10

167. Wong CH, Koo SH, She GQ, Chui P, Lee EJ. Genetic variability of RyR2 and CASQ2 genes in an Asian population. *Forensic Science International*. 2009;192:53-55

168. Kirchhefer U, Wehrmeister D, Postma AV, Pohlentz G, Mormann M, Kucerova D, Muller FU, Schmitz W, Schulze-Bahr E, Wilde AA, Neumann J. The human CASQ2 mutation K206N is associated with hyperglycosylation and altered cellular calcium handling. *Journal of Molecular and Cellular Cardiology*. 2010;49:95-105

169. Laitinen PJ, Swan H, Kontula K. Molecular genetics of exercise-induced polymorphic ventricular tachycardia: identification of three novel cardiac ryanodine receptor mutations and two common calsequestrin 2 amino-acid polymorphisms. *European Journal of Human Genetics*. 2003;11:888-891

170. Basaki M, Asasi K, Tabandeh MR, Aminlari M. Polymorphism identification and cardiac gene expression analysis of the calsequestrin 2 gene in broiler chickens with sudden death syndrome. *British Poultry Science*. 2016;57:151-160

171. Neubauer J, Lecca MR, Russo G, Bartsch C, Medeiros-Domingo A, Berger W, Haas C. Post-mortem whole-exome analysis in a large sudden infant death syndrome cohort with a focus on cardiovascular and metabolic genetic diseases. *European Journal of Human Genetics*. 2017;25:404-409

Chapter 2

1. Groenendyk J, Agellon LB, Michalak M. Coping with endoplasmic reticulum stress in the cardiovascular system. *Annual Review of Physiology*. 2013;75:49-67
2. Cao SS, Kaufman RJ. Endoplasmic reticulum stress and oxidative stress in cell fate decision and human disease. *Antioxidants & Redox Signaling*. 2014;21:396-413
3. Dicks N, Gutierrez K, Michalak M, Bordignon V, Agellon LB. Endoplasmic reticulum stress, genome damage, and cancer. *Frontiers in Oncology*. 2015;5:11
4. Wang M, Kaufman RJ. Protein misfolding in the endoplasmic reticulum as a conduit to human disease. *Nature*. 2016;529:326-335
5. Hetz C, Papa FR. The Unfolded Protein Response and Cell Fate Control. *Molecular Cell*. 2018;69:169-181
6. Hollien J. Evolution of the unfolded protein response. *Biochimica et Biophysica Acta (BBA) - Molecular Cell Research*. 2013;1833:2458-2463
7. Acosta-Alvear D, Zhou Y, Blais A, Tsikitis M, Lents NH, Arias C, Lennon CJ, Kluger Y, Dynlacht BD. XBP1 controls diverse cell type- and condition-specific transcriptional regulatory networks. *Molecular Cell*. 2007;27:53-66
8. Schwarz DS, Blower MD. The endoplasmic reticulum: structure, function and response to cellular signaling. *Cellular and Molecular Life Sciences*. 2016;73:79-94
9. Krebs J, Agellon LB, Michalak M. Ca^{2+} homeostasis and endoplasmic reticulum (ER) stress: An integrated view of calcium signaling. *Biochemical and Biophysical Research Communications*. 2015;460:114-121
10. Braakman I, Hebert DN. Protein folding in the endoplasmic reticulum. *Cold Spring Harbor Perspectives in Biology*. 2013;5:a013201
11. Rossi AE, Dirksen RT. Sarcoplasmic reticulum: the dynamic calcium governor of muscle. *Muscle & Nerve*. 2006;33:715-731
12. Reddish FN, Miller CL, Gorkhali R, Yang JJ. Calcium Dynamics Mediated by the Endoplasmic/Sarcoplasmic Reticulum and Related Diseases. *International Journal of Molecular Sciences*. 2017;18
13. Eisner DA, Caldwell JL, Kistamas K, Trafford AW. Calcium and Excitation-Contraction Coupling in the Heart. *Circulation Research*. 2017;121:181-195
14. Barone V, Randazzo D, Del Re V, Sorrentino V, Rossi D. Organization of junctional sarcoplasmic reticulum proteins in skeletal muscle fibers. *Journal of Muscle Research and Cell Motility*. 2015;36:501-515
15. Chopra N, Knollmann BC. Triadin regulates cardiac muscle couplon structure and microdomain Ca^{2+} signalling: a path towards ventricular arrhythmias. *Cardiovascular Research*. 2013;98:187-191
16. Costello B, Chadwick C, Saito A, Chu A, Maurer A, Fleischer S. Characterization of the junctional face membrane from terminal cisternae of sarcoplasmic reticulum. *Journal of Cell Biology*. 1986;103:741-753

17. Gyorke S, Stevens SC, Terentyev D. Cardiac calsequestrin: quest inside the SR. *The Journal of Physiology*. 2009;587:3091-3094

18. Knollmann BC. New roles of calsequestrin and triadin in cardiac muscle. *The Journal of Physiology*. 2009;587:3081-3087

19. Wang S, Trumble WR, Liao H, Wesson CR, Dunker AK, Kang CH. Crystal structure of calsequestrin from rabbit skeletal muscle sarcoplasmic reticulum. *Nature Structural Biology*. 1998;5:476-483

20. Wu J, Ruas JL, Estall JL, Rasbach KA, Choi JH, Ye L, Bostrom P, Tyra HM, Crawford RW, Campbell KP, Rutkowski DT, Kaufman RJ, Spiegelman BM. The unfolded protein response mediates adaptation to exercise in skeletal muscle through a PGC-1alpha/ATF6alpha complex. *Cell Metabolism*. 2011;13:160-169

21. Paul PK, Bhatnagar S, Mishra V, Srivastava S, Darnay BG, Choi Y, Kumar A. The E3 ubiquitin ligase TRAF6 intercedes in starvation-induced skeletal muscle atrophy through multiple mechanisms. *Molecular and Cellular Biology*. 2012;32:1248-1259

22. Pierre N, Deldicque L, Barbe C, Naslain D, Cani PD, Francaux M. Toll-like receptor 4 knockout mice are protected against endoplasmic reticulum stress induced by a high-fat diet. *PLOS One*. 2013;8:e65061

23. Marambio P, Toro B, Sanhueza C, Troncoso R, Parra V, Verdejo H, Garcia L, Quiroga C, Munafo D, Diaz-Elizondo J, Bravo R, Gonzalez MJ, Diaz-Araya G, Pedrozo Z, Chiong M, Colombo MI, Lavandero S. Glucose deprivation causes oxidative stress and stimulates aggresome formation and autophagy in cultured cardiac myocytes. *Biochimica et Biophysica Acta (BBA) - Biomembranes*. 2010;1802:509-518

24. Groenendyk J, Lee D, Jung J, Dyck JR, Lopaschuk GD, Agellon LB, Michalak M. Inhibition of the Unfolded Protein Response Mechanism Prevents Cardiac Fibrosis. *PLOS One*. 2016;11:e0159682

25. Tufanli O, Telkoparan Akillilar P, Acosta-Alvear D, Kocaturk B, Onat UI, Hamid SM, Cimen I, Walter P, Weber C, Erbay E. Targeting IRE1 with small molecules counteracts progression of atherosclerosis. *Proceedings of the National Academy of Sciences of the United States of America*. 2017;114:E1395-E1404

26. Liu CY, Wong HN, Schauerte JA, Kaufman RJ. The protein kinase/endoribonuclease IRE1alpha that signals the unfolded protein response has a luminal N-terminal ligand-independent dimerization domain. *Journal of Biological Chemistry*. 2002;277:18346-18356

27. Groenendyk J, Peng Z, Dudek E, Fan X, Mizianty MJ, Dufey E, Urra H, Sepulveda D, Rojas-Rivera D, Lim Y, Kim DH, Baretta K, Srikanth S, Gwack Y, Ahnn J, Kaufman RJ, Lee SK, Hetz C, Kurgan L, Michalak M. Interplay between the oxidoreductase PDIA6 and microRNA-322 controls the response to disrupted endoplasmic reticulum calcium homeostasis. *Science Signaling*. 2014;7:ra54

28. Gatti G, Trifari S, Mesaeli N, Parker JM, Michalak M, Meldolesi J. Head-to-tail oligomerization of calsequestrin: a novel mechanism for heterogeneous distribution of endoplasmic reticulum luminal proteins. *Journal of Cell Biology*. 2001;154:525-534

29. MacLennan DH, Wong PT. Isolation of a calcium-sequestering protein from sarcoplasmic reticulum. *Proceedings of the National Academy of Sciences of the United States of America*. 1971;68:1231-1235

30. Cala SE, Jones LR. Rapid purification of calsequestrin from cardiac and skeletal muscle sarcoplasmic reticulum vesicles by Ca^{2+}-dependent elution from phenyl-sepharose. *Journal of Biological Chemistry*. 1983;258:11932-11936

31. Milner RE, Baksh S, Shemanko C, Carpenter MR, Smillie L, Vance JE, Opas M, Michalak M. Calreticulin, and not calsequestrin, is the major calcium binding protein of smooth muscle sarcoplasmic reticulum and liver endoplasmic reticulum. *Journal of Biological Chemistry*. 1991;266:7155-7165

32. Schoenmakers TJ, Visser GJ, Flik G, Theuvenet AP. CHELATOR: an improved method for computing metal ion concentrations in physiological solutions. *Biotechniques*. 1992;12:870-874, 876-879

33. McPherson PS, Kim YK, Valdivia H, Knudson CM, Takekura H, Franzini-Armstrong C, Coronado R, Campbell KP. The brain ryanodine receptor: a caffeine-sensitive calcium release channel. *Neuron*. 1991;7:17-25

34. Campbell KP, Knudson CM, Imagawa T, Leung AT, Sutko JL, Kahl SD, Raab CR, Madson L. Identification and characterization of the high affinity [3H]ryanodine receptor of the junctional sarcoplasmic reticulum Ca^{2+} release channel. *Journal of Biological Chemistry*. 1987;262:6460-6463

35. Knudson CM, Chaudhari N, Sharp AH, Powell JA, Beam KG, Campbell KP. Specific absence of the alpha 1 subunit of the dihydropyridine receptor in mice with muscular dysgenesis. *Journal of Biological Chemistry*. 1989;264:1345-1348

36. Hiess F, Vallmitjana A, Wang R, Cheng H, ter Keurs HE, Chen J, Hove-Madsen L, Benitez R, Chen SR. Distribution and Function of Cardiac Ryanodine Receptor Clusters in Live Ventricular Myocytes. *Journal of Biological Chemistry*. 2015;290:20477-20487

37. Hunt DJ, Jones PP, Wang R, Chen W, Bolstad J, Chen K, Shimoni Y, Chen SR. K201 (JTV519) suppresses spontaneous Ca^{2+} release and [3H]ryanodine binding to RyR2 irrespective of FKBP12.6 association. *Biophysical Journal*. 2007;404:431-438

38. Saito A, Seiler S, Chu A, Fleischer S. Preparation and morphology of sarcoplasmic reticulum terminal cisternae from rabbit skeletal muscle. *Journal of Cell Biology*. 1984;99:875-885

39. Lanner JT, Georgiou DK, Joshi AD, Hamilton SL. Ryanodine receptors: structure, expression, molecular details, and function in calcium release. *Cold Spring Harbor Perspectives in Biology*. 2010;2:a003996

40. Young P, Ehler E, Gautel M. Obscurin, a giant sarcomeric Rho guanine nucleotide exchange factor protein involved in sarcomere assembly. *Journal of Cell Biology*. 2001;154:123-136

41. Jorgensen AO, Shen AC, Campbell KP. Ultrastructural localization of calsequestrin in adult rat atrial and ventricular muscle cells. *Journal of Cell Biology*. 1985;101:257

42. Mega T, Oku H, Hase S. Characterization of carbohydrate-binding specificity of concanavalin A by competitive binding of pyridylamino sugar chains. *Journal of Biochemistry*. 1992;111:396-400

43. Eletto D, Eletto D, Dersh D, Gidalevitz T, Argon Y. Protein disulfide isomerase A6 controls the decay of IRE1alpha signaling via disulfide-dependent association. *Molecular Cell*. 2014;53:562-576

44. Kozlov G, Maattanen P, Thomas DY, Gehring K. A structural overview of the PDI family of proteins. *FEBS Journal*. 2010;277:3924-3936

45. Liu CY, Xu Z, Kaufman RJ. Structure and intermolecular interactions of the luminal dimerization domain of human IRE1alpha. *Journal of Biological Chemistry*. 2003;278:17680-17687

46. Park H, Park IY, Kim E, Youn B, Fields K, Dunker AK, Kang C. Comparing skeletal and cardiac calsequestrin structures and their calcium binding: a proposed mechanism for coupled calcium binding and protein polymerization. *Journal of Biological Chemistry*. 2004;279:18026-18033

47. Beard NA, Dulhunty AF. C-terminal residues of skeletal muscle calsequestrin are essential for calcium binding and for skeletal ryanodine receptor inhibition. *Skelet Muscle*. 2015;5:6

48. Zhou J, Liu CY, Back SH, Clark RL, Peisach D, Xu Z, Kaufman RJ. The crystal structure of human IRE1 luminal domain reveals a conserved dimerization interface required for activation of the unfolded protein response. *Proceedings of the National Academy of Sciences of the United States of America*. 2006;103:14343-14348

49. Liu CY, Schroder M, Kaufman RJ. Ligand-independent dimerization activates the stress response kinases IRE1 and PERK in the lumen of the endoplasmic reticulum. *Journal of Biological Chemistry*. 2000;275:24881-24885

50. Li H, Korennykh AV, Behrman SL, Walter P. Mammalian endoplasmic reticulum stress sensor IRE1 signals by dynamic clustering. *Proceedings of the National Academy of Sciences of the United States of America*. 2010;107:16113-16118

51. Baumann O, Walz B. Endoplasmic reticulum of animal cells and its organization into structural and functional domains. *International Review of Cytology*. 2001;205:149-214

52. Michalak M, Opas M. Endoplasmic and sarcoplasmic reticulum in the heart. *Trends in Cell Biology*. 2009;19:253-259

53. Wray S, Burdyga T. Sarcoplasmic reticulum function in smooth muscle. *Physiological Reviews*. 2010;90:113-178

54. Bers DM. Cardiac sarcoplasmic reticulum calcium leak: basis and roles in cardiac dysfunction. *Annual Review of Physiology*. 2014;76:107-127

55. Beard NA, Wei L, Dulhunty AF. Ca^{2+} signaling in striated muscle: the elusive roles of triadin, junctin, and calsequestrin. *European Biophysics Journal*. 2009;39:27-36

56. Lee JM, Rho SH, Shin DW, Cho C, Park WJ, Eom SH, Ma J, Kim DH. Negatively charged amino acids within the intraluminal loop of ryanodine receptor are involved in the interaction with triadin. *Journal of Biological Chemistry*. 2004;279:6994-7000

57. Kobayashi YM, Alseikhan BA, Jones LR. Localization and characterization of the calsequestrin-binding domain of triadin 1. Evidence for a charged beta-strand in mediating the protein-protein interaction. *Journal of Biological Chemistry*. 2000;275:17639-17646

58. Gyorke I, Hester N, Jones LR, Gyorke S. The role of calsequestrin, triadin, and junctin in conferring cardiac ryanodine receptor responsiveness to luminal calcium. *Biophysical Journal*. 2004;86:2121-2128

59. Zhang L, Kelley J, Schmeisser G, Kobayashi YM, Jones LR. Complex formation between junctin, triadin, calsequestrin, and the ryanodine receptor. Proteins of the cardiac junctional sarcoplasmic reticulum membrane. *Journal of Biological Chemistry*. 1997;272:23389-23397

60. Gaburjakova M, Bal NC, Gaburjakova J, Periasamy M. Functional interaction between calsequestrin and ryanodine receptor in the heart. *Cellular and Molecular Life Sciences*. 2013;70:2935-2945

61. Wang L, Zhang L, Li S, Zheng Y, Yan X, Chen M, Wang H, Putney JW, Luo D. Retrograde regulation of STIM1-Orai1 interaction and store-operated Ca^{2+} entry by calsequestrin. *Scientific Reports*. 2015;5:11349-11349

62. Kraskiewicz H, FitzGerald U. InterfERing with endoplasmic reticulum stress. *Trends in Pharmacological Sciences*. 2012;33:53-63

63. Hetz C. The unfolded protein response: controlling cell fate decisions under ER stress and beyond. *Nature Reviews Molecular Cell Biology*. 2012;13:89-102

64. Bertolotti A, Zhang Y, Hendershot LM, Harding HP, Ron D. Dynamic interaction of BiP and ER stress transducers in the unfolded-protein response. *Nature Cell Biology*. 2000;2:326-332

65. Oikawa D, Kimata Y, Kohno K, Iwawaki T. Activation of mammalian IRE1alpha upon ER stress depends on dissociation of BiP rather than on direct interaction with unfolded proteins. *Experimental Cell Research* 2009;315:2496-2504

66. Ma K, Vattem KM, Wek RC. Dimerization and release of molecular chaperone inhibition facilitate activation of eukaryotic initiation factor-2 kinase in response to endoplasmic reticulum stress. *Journal of Biological Chemistry*. 2002;277:18728-18735

67. Oikawa D, Kimata Y, Kohno K. Self-association and BiP dissociation are not sufficient for activation of the ER stress sensor Ire1. *Journal of Cell Science*. 2007;120:1681-1688

68. Kimata Y, Oikawa D, Shimizu Y, Ishiwata-Kimata Y, Kohno K. A role for BiP as an adjustor for the endoplasmic reticulum stress-sensing protein Ire1. *Journal of Cell Biology*. 2004;167:445-456

69. Sepulveda D, Rojas-Rivera D, Rodríguez DA, Groenendyk J, Köhler A, Lebeaupin C, Ito S, Urra H, Carreras-Sureda A, Hazari Y, Vasseur-Cognet M, Ali MMU, Chevet E, Campos G, Godoy P, Vaisar T, Bailly-Maitre B, Nagata K, Michalak M, Sierralta J, Hetz C. Interactome screening identifies the ER luminal chaperone Hsp47 as a regulator of the unfolded protein response transducer IRE1α. *Molecular Cell*. 2018;69:238-252.e237

70. Groenendyk J, Paskevicius T, Urra H, Viricel C, Wang K, Barakat K, Hetz C, Kurgan L, Agellon LB, Michalak M. Cyclosporine A binding to COX-2 reveals a novel signaling

pathway that activates IRE1α unfolded protein response sensor. *Scientific Reports*. 2018;8:16678

Chapter 3

1. Westrate LM, Lee JE, Prinz WA, Voeltz GK. Form follows function: the importance of endoplasmic reticulum shape. *Annual Review of Biochemistry*. 2015;84:791-811

2. Groenendyk J, Agellon LB, Michalak M. Coping with endoplasmic reticulum stress in the cardiovascular system. *Annual Review of Physiology*. 2013;75:49-67

3. Groenendyk J, Sreenivasaiah PK, Kim DH, Agellon LB, Michalak M. Biology of endoplasmic reticulum stress in the heart. *Circulation Research*. 2010;107:1185-1197

4. Doroudgar S, Thuerauf DJ, Marcinko MC, Belmont PJ, Glembotski CC. Ischemia activates the ATF6 branch of the endoplasmic reticulum stress response. *Journal of Biological Chemistry*. 2009;284:29735-29745

5. Okada K, Minamino T, Tsukamoto Y, Liao Y, Tsukamoto O, Takashima S, Hirata A, Fujita M, Nagamachi Y, Nakatani T, Yutani C, Ozawa K, Ogawa S, Tomoike H, Hori M, Kitakaze M. Prolonged endoplasmic reticulum stress in hypertrophic and failing heart after aortic constriction: possible contribution of endoplasmic reticulum stress to cardiac myocyte apoptosis. *Circulation*. 2004;110:705-712

6. Li SY, Gilbert SA, Li Q, Ren J. Aldehyde dehydrogenase-2 (ALDH2) ameliorates chronic alcohol ingestion-induced myocardial insulin resistance and endoplasmic reticulum stress. *Journal of Molecular and Cellular Cardiology*. 2009;47:247-255

7. Severino A, Campioni M, Straino S, Salloum FN, Schmidt N, Herbrand U, Frede S, Toietta G, Di Rocco G, Bussani R, Silvestri F, Piro M, Liuzzo G, Biasucci LM, Mellone P, Feroce F, Capogrossi M, Baldi F, Fandrey J, Ehrmann M, Crea F, Abbate A, Baldi A. Identification of Protein Disulfide Isomerase as a Cardiomyocyte Survival Factor in Ischemic Cardiomyopathy. *Journal of the American College of Cardiology*. 2007;50:1029-1037

8. Myoishi M, Hao H, Minamino T, Watanabe K, Nishihira K, Hatakeyama K, Asada Y, Okada K, Ishibashi-Ueda H, Gabbiani G, Bochaton-Piallat ML, Mochizuki N, Kitakaze M. Increased endoplasmic reticulum stress in atherosclerotic plaques associated with acute coronary syndrome. *Circulation*. 2007;116:1226-1233

9. Jia LX, Zhang WM, Zhang HJ, Li TT, Wang YL, Qin YW, Gu H, Du J. Mechanical stretch-induced endoplasmic reticulum stress, apoptosis and inflammation contribute to thoracic aortic aneurysm and dissection. *Journal of Pathology*. 2015;236:373-383

10. Martindale Joshua J, Fernandez R, Thuerauf D, Whittaker R, Gude N, Sussman Mark A, Glembotski Christopher C. Endoplasmic reticulum stress gene induction and protection from ischemia/reperfusion injury in the hearts of transgenic mice with a tamoxifen-regulated form of ATF6. *Circulation Research*. 2006;98:1186-1193

11. Jin J-K, Blackwood EA, Azizi K, Thuerauf DJ, Fahem AG, Hofmann C, Kaufman RJ, Doroudgar S, Glembotski CC. ATF6 decreases myocardial ischemia/reperfusion damage and links er stress and oxidative stress signaling pathways in the heart. *Circulation Research*. 2017;120:862-875

12. Liu X, Kwak D, Lu Z, Xu X, Fassett J, Wang H, Wei Y, Cavener DR, Hu X, Hall J, Bache RJ, Chen Y. Endoplasmic reticulum stress sensor protein kinase R-like endoplasmic reticulum kinase (PERK) protects against pressure overload-induced heart failure and lung remodeling. *Hypertension (Dallas, Tex. : 1979)*. 2014;64:738-744

13. Steiger D, Yokota T, Li J, Ren S, Minamisawa S, Wang Y. The serine/threonine-protein kinase/endoribonuclease IRE1α protects the heart against pressure overload-induced heart failure. *The Journal of Biological Chemistry*. 2018;293:9652-9661

14. Thuerauf Donna J, Marcinko M, Gude N, Rubio M, Sussman Mark A, Glembotski Christopher C. Activation of the unfolded protein response in infarcted mouse heart and hypoxic cultured cardiac myocytes. *Circulation Research*. 2006;99:275-282

15. Wang ZV, Deng Y, Gao N, Pedrozo Z, Li DL, Morales CR, Criollo A, Luo X, Tan W, Jiang N, Lehrman MA, Rothermel BA, Lee A-H, Lavandero S, Mammen PPA, Ferdous A, Gillette TG, Scherer PE, Hill JA. Spliced X-box binding protein 1 couples the unfolded protein response to hexosamine biosynthetic pathway. *Cell*. 2014;156:1179-1192

16. Wang X, Deng Y, Zhang G, Li C, Ding G, May Herman I, Tran Diem H, Luo X, Jiang D-S, Li Dan L, Wei X, Xu L, Ferdous A, Gillette Thomas G, Scherer Philipp E, Jiang X, Wang Zhao V. Spliced x-box binding protein 1 stimulates adaptive growth through activation of mTOR. *Circulation*. 2019;140:566-579

17. Sano R, Reed JC. ER stress-induced cell death mechanisms. *Biochimica et Biophysica Acta (BBA) - Molecular Cell Research*. 2013;1833:3460-3470

18. Wang S, Binder P, Fang Q, Wang Z, Xiao W, Liu W, Wang X. Endoplasmic reticulum stress in the heart: insights into mechanisms and drug targets. *British Journal of Pharmacology*. 2018;175:1293-1304

19. Terai K, Hiramoto Y, Masaki M, Sugiyama S, Kuroda T, Hori M, Kawase I, Hirota H. AMP-activated protein kinase protects cardiomyocytes against hypoxic injury through attenuation of endoplasmic reticulum stress. *Molecular and Cellular Biology*. 2005;25:9554-9575

20. Yamaguchi O, Higuchi Y, Hirotani S, Kashiwase K, Nakayama H, Hikoso S, Takeda T, Watanabe T, Asahi M, Taniike M, Matsumura Y, Tsujimoto I, Hongo K, Kusakari Y, Kurihara S, Nishida K, Ichijo H, Hori M, Otsu K. Targeted deletion of apoptosis signal-regulating kinase 1 attenuates left ventricular remodeling. *Proceedings of the National Academy of Sciences of the United States of America*. 2003;100:15883-15888

21. Fu HY, Minamino T, Tsukamoto O, Sawada T, Asai M, Kato H, Asano Y, Fujita M, Takashima S, Hori M, Kitakaze M. Overexpression of endoplasmic reticulum-resident chaperone attenuates cardiomyocyte death induced by proteasome inhibition. *Cardiovascular Research*. 2008;79:600-610

22. Nishitoh H, Matsuzawa A, Tobiume K, Saegusa K, Takeda K, Inoue K, Hori S, Kakizuka A, Ichijo H. ASK1 is essential for endoplasmic reticulum stress-induced neuronal cell death triggered by expanded polyglutamine repeats. *Genes & Development*. 2002;16:1345-1355

23. Pendse AA, Arbones-Mainar JM, Johnson LA, Altenburg MK, Maeda N. Apolipoprotein E knock-out and knock-in mice: atherosclerosis, metabolic syndrome, and beyond. *Journal of Lipid Research*. 2009;50 Suppl:S178-S182

24. Erbay E, Babaev VR, Mayers JR, Makowski L, Charles KN, Snitow ME, Fazio S, Wiest MM, Watkins SM, Linton MF, Hotamisligil GS. Reducing endoplasmic reticulum stress through a macrophage lipid chaperone alleviates atherosclerosis. *Nature Medicine*. 2009;15:1383-1391

25. Tufanli O, Telkoparan Akillilar P, Acosta-Alvear D, Kocaturk B, Onat UI, Hamid SM, Cimen I, Walter P, Weber C, Erbay E. Targeting IRE1 with small molecules counteracts progression of atherosclerosis. *Proceedings of the National Academy of Sciences of the United States of America*. 2017;114:E1395-E1404

26. Groenendyk J, Lee D, Jung J, Dyck JR, Lopaschuk GD, Agellon LB, Michalak M. Inhibition of the Unfolded Protein Response Mechanism Prevents Cardiac Fibrosis. *PLOS One*. 2016;11:e0159682

27. Guan HS, Shangguan HJ, Shang Z, Yang L, Meng XM, Qiao SB. Endoplasmic reticulum stress caused by left ventricular hypertrophy in rats: effects of telmisartan. *American Journal of the Medical Sciences*. 2011;342:318-323

28. Fu Hai Y, Okada K-i, Liao Y, Tsukamoto O, Isomura T, Asai M, Sawada T, Okuda K, Asano Y, Sanada S, Asanuma H, Asakura M, Takashima S, Komuro I, Kitakaze M, Minamino T. Ablation of C/EBP homologous protein attenuates endoplasmic reticulum–mediated apoptosis and cardiac dysfunction induced by pressure overload. *Circulation*. 2010;122:361-369

29. Wiersma M, Meijering RAM, Qi X-Y, Zhang D, Liu T, Hoogstra-Berends F, Sibon OCM, Henning RH, Nattel S, Brundel BJJM. Endoplasmic reticulum stress is associated with autophagy and cardiomyocyte remodeling in experimental and human atrial fibrillation. *Journal of the American Heart Association*. 2017;6:e006458

30. Ayyappan JP, Lizardo K, Wang S, Yurkow E, Nagajyothi JF. Inhibition of ER stress by 2-aminopurine treatment modulates cardiomyopathy in a murine chronic chagas disease model. *Biomolecules & Therapeutics (Seoul)*. 2019;27:386-394

31. Iwawaki T, Akai R, Yamanaka S, Kohno K. Function of IRE1 alpha in the placenta is essential for placental development and embryonic viability. *Proceedings of the National Academy of Sciences*. 2009;106:16657

32. Lee D, Oka T, Hunter B, Robinson A, Papp S, Nakamura K, Srisakuldee W, Nickel BE, Light PE, Dyck JRB, Lopaschuk GD, Kardami E, Opas M, Michalak M. Calreticulin induces dilated cardiomyopathy. *PloS one*. 2013;8:e56387-e56387

33. Schipke J, Brandenberger C, Rajces A, Manninger M, Alogna A, Post H, Mühlfeld C. Assessment of cardiac fibrosis: a morphometric method comparison for collagen quantification. *Journal of Applied Physiology*. 2017;122:1019-1030

34. Ackers-Johnson M, Li PY, Holmes AP, O'Brien SM, Pavlovic D, Foo RS. A simplified, langendorff-free method for concomitant isolation of viable cardiac myocytes and nonmyocytes from the adult mouse heart. *Circulation Research*. 2016;119:909-920

35. Cojan-Minzat BO, Zlibut A, Agoston-Coldea L. Non-ischemic dilated cardiomyopathy and cardiac fibrosis. *Heart Failure Reviews*. 2020

36. Liu T, Song D, Dong J, Zhu P, Liu J, Liu W, Ma X, Zhao L, Ling S. Current understanding of the pathophysiology of myocardial fibrosis and its quantitative assessment in heart failure. *Frontiers in Physiology*. 2017;8

37. Kaprielian RR, Stevenson S, Rothery SM, Cullen MJ, Severs NJ. Distinct patterns of dystrophin organization in myocyte sarcolemma and transverse tubules of normal and diseased human myocardium. *Circulation*. 2000;101:2586-2594

38. Crossman DJ, Young AA, Ruygrok PN, Nason GP, Baddelely D, Soeller C, Cannell MB. T-tubule disease: Relationship between t-tubule organization and regional contractile performance in human dilated cardiomyopathy. *Journal of Molecular and Cellular Cardiology*. 2015;84:170-178

39. Bhavanandan VP, Katlic AW. The interaction of wheat germ agglutinin with sialoglycoproteins. The role of sialic acid. *Journal of Biological Chemistry*. 1979;254:4000-4008

40. Campbell KP, Kahl SD. Association of dystrophin and an integral membrane glycoprotein. *Nature*. 1989;338:259-262

41. Pandya K, Kim H-S, Smithies O. Fibrosis, not cell size, delineates β-myosin heavy chain reexpression during cardiac hypertrophy and normal aging in vivo. *Proceedings of the National Academy of Sciences of the United States of America*. 2006;103:16864-16869

42. Balijepalli RC, Lokuta AJ, Maertz NA, Buck JM, Haworth RA, Valdivia HH, Kamp TJ. Depletion of T-tubules and specific subcellular changes in sarcolemmal proteins in tachycardia-induced heart failure. *Cardiovascular Research*. 2003;59:67-77

43. Emde B, Heinen A, Gödecke A, Bottermann K. Wheat germ agglutinin staining as a suitable method for detection and quantification of fibrosis in cardiac tissue after myocardial infarction. *European Journal of Histochemistry*. 2014;58:2448-2448

44. Richards MA, Clarke JD, Saravanan P, Voigt N, Dobrev D, Eisner DA, Trafford AW, Dibb KM. Transverse tubules are a common feature in large mammalian atrial myocytes including human. *American Journal of Physiology. Heart and Circulatory Physiology*. 2011;301:H1996-H2005

45. Bensley JG, De Matteo R, Harding R, Black MJ. Three-dimensional direct measurement of cardiomyocyte volume, nuclearity, and ploidy in thick histological sections. *Scientific Reports*. 2016;6:23756

46. Crossman DJ, Shen X, Jüllig M, Munro M, Hou Y, Middleditch M, Shrestha D, Li A, Lal S, dos Remedios CG, Baddeley D, Ruygrok PN, Soeller C. Increased collagen within the transverse tubules in human heart failure. *Cardiovascular Research*. 2017;113:879-891

47. Priori SG, Chen SRW. Inherited dysfunction of sarcoplasmic reticulum Ca^{2+} handling and arrhythmogenesis. *Circulation Research*. 2011;108:871-883

48. Acimovic I, Refaat MM, Moreau A, Salykin A, Reiken S, Sleiman Y, Souidi M, Přibyl J, Kajava AV, Richard S, Lu JT, Chevalier P, Skládal P, Dvořak P, Rotrekl V, Marks AR, Scheinman MM, Lacampagne A, Meli AC. Post-translational modifications and diastolic

calcium leak associated to the novel RYR2-D3638A mutation lead to cpvt in patient-specific hipsc-derived cardiomyocytes. *Journal of Clinical Medicine*. 2018;7:423

49. Knollmann BC, Chopra N, Hlaing T, Akin B, Yang T, Ettensohn K, Knollmann BE, Horton KD, Weissman NJ, Holinstat I, Zhang W, Roden DM, Jones LR, Franzini-Armstrong C, Pfeifer K. Casq2 deletion causes sarcoplasmic reticulum volume increase, premature Ca^{2+} release, and catecholaminergic polymorphic ventricular tachycardia. *Journal of Clinical Investigation*. 2006;116:2510-2520

50. Iyer V, Hajjar Roger J, Armoundas Antonis A. Mechanisms of abnormal calcium homeostasis in mutations responsible for catecholaminergic polymorphic ventricular tachycardia. *Circulation Research*. 2007;100:e22-e31

51. Mishiba K-I, Iwata Y, Mochizuki T, Matsumura A, Nishioka N, Hirata R, Koizumi N. Unfolded protein-independent IRE1 activation contributes to multifaceted developmental processes in Arabidopsis. *Life Science Alliance*. 2019;2:e201900459

52. Chen Y, Brandizzi F. IRE1: ER stress sensor and cell fate executor. *Trends in Cell Biology*. 2013;23:547-555

53. Reimold AM, Etkin A, Clauss I, Perkins A, Friend DS, Zhang J, Horton HF, Scott A, Orkin SH, Byrne MC, Grusby MJ, Glimcher LH. An essential role in liver development for transcription factor XBP-1. *Genes & Development* 2000;14:152-157

54. Duan Q, Ni L, Wang P, Chen C, Yang L, Ma B, Gong W, Cai Z, Zou M-H, Wang DW. Deregulation of XBP1 expression contributes to myocardial vascular endothelial growth factor-A expression and angiogenesis during cardiac hypertrophy in vivo. *Aging cell*. 2016;15:625-633

55. Liu M, Dudley SC, Jr. The role of the unfolded protein response in arrhythmias. *Channels (Austin, Tex.)*. 2018;12:335-345

56. Liu M, Shi G, Zhou A, Rupert CE, Coulombe KLK, Dudley SC, Jr. Activation of the unfolded protein response downregulates cardiac ion channels in human induced pluripotent stem cell-derived cardiomyocytes. *Journal of Molecular and Cellular Cardiology*. 2018;117:62-71

57. Carreras-Sureda A, Jaña F, Urra H, Durand S, Mortenson DE, Sagredo A, Bustos G, Hazari Y, Ramos-Fernández E, Sassano ML, Pihán P, van Vliet AR, González-Quiroz M, Torres AK, Tapia-Rojas C, Kerkhofs M, Vicente R, Kaufman RJ, Inestrosa NC, Gonzalez-Billault C, Wiseman RL, Agostinis P, Bultynck G, Court FA, Kroemer G, Cárdenas JC, Hetz C. Non-canonical function of IRE1α determines mitochondria-associated endoplasmic reticulum composition to control calcium transfer and bioenergetics. *Nature Cell Biology*. 2019;21:755-767

58. Fan G, Baker ML, Wang Z, Baker MR, Sinyagovskiy PA, Chiu W, Ludtke SJ, Serysheva, II. Gating machinery of InsP3R channels revealed by electron cryomicroscopy. *Nature*. 2015;527:336-341

59. Peng W, Shen H, Wu J, Guo W, Pan X, Wang R, Chen SR, Yan N. Structural basis for the gating mechanism of the type 2 ryanodine receptor RyR2. *Science*. 2016;354

60. Seo M-D, Enomoto M, Ishiyama N, Stathopulos PB, Ikura M. Structural insights into endoplasmic reticulum stored calcium regulation by inositol 1,4,5-trisphosphate and ryanodine receptors. *Biochimica et Biophysica Acta (BBA) - Molecular Cell Research*. 2015;1853:1980-1991
61. Mackrill JJ. Ryanodine receptor calcium release channels: an evolutionary perspective. *Advancesin Experimental Medicine and Biology*. 2012;740:159-182

Chapter 4

1. Rossi AE, Dirksen RT. Sarcoplasmic reticulum: the dynamic calcium governor of muscle. *Muscle & Nerve*. 2006;33:715-731
2. Eisner DA, Caldwell JL, Kistamas K, Trafford AW. Calcium and Excitation-Contraction Coupling in the Heart. *Circulation Research*. 2017;121:181-195
3. Reddish FN, Miller CL, Gorkhali R, Yang JJ. Calcium Dynamics Mediated by the Endoplasmic/Sarcoplasmic Reticulum and Related Diseases. *International Journal of Molecular Sciences*. 2017;18
4. Michalak M, Opas M. Endoplasmic and sarcoplasmic reticulum in the heart. *Trends in Cell Biology*. 2009;19:253-259
5. Wray S, Burdyga T. Sarcoplasmic reticulum function in smooth muscle. *Physiological Reviews*. 2010;90:113-178
6. Bers DM. Cardiac sarcoplasmic reticulum calcium leak: basis and roles in cardiac dysfunction. *Annual Review of Physiology*. 2014;76:107-127
7. Michalak M, Agellon LB. Stress coping strategies in the heart: An integrated view. *Frontiers in Cardiovascular Medicine*. 2018;5:168
8. Barone V, Randazzo D, Del Re V, Sorrentino V, Rossi D. Organization of junctional sarcoplasmic reticulum proteins in skeletal muscle fibers. *Journal of Muscle Research and Cell Motility*. 2015;36:501-515
9. Chopra N, Knollmann BC. Triadin regulates cardiac muscle couplon structure and microdomain Ca^{2+} signalling: a path towards ventricular arrhythmias. *Cardiovascular Research*. 2013;98:187-191
10. Costello B, Chadwick C, Saito A, Chu A, Maurer A, Fleischer S. Characterization of the junctional face membrane from terminal cisternae of sarcoplasmic reticulum. *Journal of Cell Biology*. 1986;103:741-753
11. Lee JM, Rho SH, Shin DW, Cho C, Park WJ, Eom SH, Ma J, Kim DH. Negatively charged amino acids within the intraluminal loop of ryanodine receptor are involved in the interaction with triadin. *Journal of Biological Chemistry*. 2004;279:6994-7000
12. Kobayashi YM, Alseikhan BA, Jones LR. Localization and characterization of the calsequestrin-binding domain of triadin 1. Evidence for a charged beta-strand in mediating the protein-protein interaction. *Journal of Biological Chemistry*. 2000;275:17639-17646
13. Gyorke I, Hester N, Jones LR, Gyorke S. The role of calsequestrin, triadin, and junctin in conferring cardiac ryanodine receptor responsiveness to luminal calcium. *Biophysical Journal*. 2004;86:2121-2128

14. Knollmann BC. New roles of calsequestrin and triadin in cardiac muscle. *The Journal of Physiology*. 2009;587:3081-3087

15. Gyorke S, Stevens SC, Terentyev D. Cardiac calsequestrin: quest inside the SR. *The Journal of Physiology*. 2009;587:3091-3094

16. Wang S, Trumble WR, Liao H, Wesson CR, Dunker AK, Kang CH. Crystal structure of calsequestrin from rabbit skeletal muscle sarcoplasmic reticulum. *Nature Structural Biology*. 1998;5:476-483

17. Kim E, Youn B, Kemper L, Campbell C, Milting H, Varsanyi M, Kang C. Characterization of human cardiac calsequestrin and its deleterious mutants. *Journal of Molecular Biology*. 2007;373:1047-1057

18. Baltogiannis GG, Lysitsas DN, di Giovanni G, Ciconte G, Sieira J, Conte G, Kolettis TM, Chierchia GB, de Asmundis C, Brugada P. CPVT: arrhythmogenesis, therapeutic management, and future perspectives. A brief review of the literature. *Frontiers in Cardiovascular Medicine*. 2019;6:92

19. Mohamed U, Napolitano C, Priori SG. Molecular and electrophysiological bases of catecholaminergic polymorphic ventricular tachycardia. *Journal of Cardiovascular Electrophysiology*. 2007;18:791-797

20. Priori SG, Napolitano C, Memmi M, Colombi B, Drago F, Gasparini M, DeSimone L, Coltorti F, Bloise R, Keegan R, Cruz Filho FE, Vignati G, Benatar A, DeLogu A. Clinical and molecular characterization of patients with catecholaminergic polymorphic ventricular tachycardia. *Circulation*. 2002;106:69-74

21. Postma AV, Denjoy I, Hoorntje TM, Lupoglazoff JM, Da Costa A, Sebillon P, Mannens MM, Wilde AA, Guicheney P. Absence of calsequestrin 2 causes severe forms of catecholaminergic polymorphic ventricular tachycardia. *Circulation Research*. 2002;91:e21-26

22. Nyegaard M, Overgaard MT, Søndergaard MT, Vranas M, Behr ER, Hildebrandt LL, Lund J, Hedley PL, Camm AJ, Wettrell G, Fosdal I, Christiansen M, Børglum AD. Mutations in calmodulin cause ventricular tachycardia and sudden cardiac death. *American Journal of Human Genetics*. 2012;91:703-712

23. Roux-Buisson N, Cacheux M, Fourest-Lieuvin A, Fauconnier J, Brocard J, Denjoy I, Durand P, Guicheney P, Kyndt F, Leenhardt A, Le Marec H, Lucet V, Mabo P, Probst V, Monnier N, Ray PF, Santoni E, Trémeaux P, Lacampagne A, Fauré J, Lunardi J, Marty I. Absence of triadin, a protein of the calcium release complex, is responsible for cardiac arrhythmia with sudden death in human. *Human Molecular Genetics*. 2012;21:2759-2767

24. Faggioni M, Kryshtal DO, Knollmann BC. Calsequestrin mutations and catecholaminergic polymorphic ventricular tachycardia. *Pediatric Cardiology*. 2012;33:959-967

25. Terentyev D, Nori A, Santoro M, Viatchenko-Karpinski S, Kubalova Z, Gyorke I, Terentyeva R, Vedamoorthyrao S, Blom NA, Valle G, Napolitano C, Williams SC, Volpe P, Priori SG, Gyorke S. Abnormal interactions of calsequestrin with the ryanodine receptor calcium release channel complex linked to exercise-induced sudden cardiac death. *Circulation Research*. 2006;98:1151-1158

26. Terentyev D, Kubalova Z, Valle G, Nori A, Vedamoorthyrao S, Terentyeva R, Viatchenko-Karpinski S, Bers DM, Williams SC, Volpe P, Gyorke S. Modulation of SR Ca release by luminal Ca and calsequestrin in cardiac myocytes: effects of CASQ2 mutations linked to sudden cardiac death. *Biophysical Journal*. 2008;95:2037-2048

27. Gray B, Bagnall RD, Lam L, Ingles J, Turner C, Haan E, Davis A, Yang PC, Clancy CE, Sy RW, Semsarian C. A novel heterozygous mutation in cardiac calsequestrin causes autosomal dominant catecholaminergic polymorphic ventricular tachycardia. *Heart Rhythm*. 2016;13:1652-1660

28. Song L, Alcalai R, Arad M, Wolf CM, Toka O, Conner DA, Berul CI, Eldar M, Seidman CE, Seidman JG. Calsequestrin 2 (CASQ2) mutations increase expression of calreticulin and ryanodine receptors, causing catecholaminergic polymorphic ventricular tachycardia. *Journal of Clinical Investigation*. 2007;117:1814-1823

29. Novak A, Barad L, Zeevi-Levin N, Shick R, Shtrichman R, Lorber A, Itskovitz-Eldor J, Binah O. Cardiomyocytes generated from CPVTD307H patients are arrhythmogenic in response to β-adrenergic stimulation. *Journal of Cellular and Molecular Medicine*. 2012;16:468-482

30. Dirksen WP, Lacombe VA, Chi M, Kalyanasundaram A, Viatchenko-Karpinski S, Terentyev D, Zhou Z, Vedamoorthyrao S, Li N, Chiamvimonvat N, Carnes CA, Franzini-Armstrong C, Gyorke S, Periasamy M. A mutation in calsequestrin, CASQ2D307H, impairs sarcoplasmic reticulum Ca^{2+} handling and causes complex ventricular arrhythmias in mice. *Cardiovascular Research*. 2007;75:69-78

31. di Barletta MR, Viatchenko-Karpinski S, Nori A, Memmi M, Terentyev D, Turcato F, Valle G, Rizzi N, Napolitano C, Gyorke S, Volpe P, Priori SG. Clinical phenotype and functional characterization of CASQ2 mutations associated with catecholaminergic polymorphic ventricular tachycardia. *Circulation*. 2006;114:1012-1019

32. Chopra N, Yang T, Asghari P, Moore ED, Huke S, Akin B, Cattolica RA, Perez CF, Hlaing T, Knollmann-Ritschel BE, Jones LR, Pessah IN, Allen PD, Franzini-Armstrong C, Knollmann BC. Ablation of triadin causes loss of cardiac Ca^{2+} release units, impaired excitation-contraction coupling, and cardiac arrhythmias. *Proceedings of the National Academy of Sciences of the United States of America*. 2009;106:7636-7641

33. Bal NC, Sharon A, Gupta SC, Jena N, Shaikh S, Gyorke S, Periasamy M. The catecholaminergic polymorphic ventricular tachycardia mutation R33Q disrupts the N-terminal structural motif that regulates reversible calsequestrin polymerization. *Journal of Biological Chemistry*. 2010;285:17188-17196

34. Cacheux M, Fauconnier J, Thireau J, Osseni A, Brocard J, Roux-Buisson N, Brocard J, Fauré J, Lacampagne A, Marty I. Interplay between Triadin and Calsequestrin in the Pathogenesis of CPVT in the Mouse. *Molecular Therapy*. 2020;28:171-179

35. Josephs K, Patel K, Janson CM, Montagna C, McDonald TV. Compound heterozygous CASQ2 mutations and long-term course of catecholaminergic polymorphic ventricular tachycardia. *Molecular Genetics & Genomic Medicine*. 2017;5:788-794

36. Rajagopalan A, Pollanen MS. Sudden death during struggle in the setting of heterozygosity for a mutation in calsequesterin 2. *Forensic Science, Medicine and Pathology*. 2016;12:86-89

37. Liu B, Ho H-T, Brunello L, Unudurthi SD, Lou Q, Belevych AE, Qian L, Kim DH, Cho C, Janssen PML, Hund TJ, Knollmann BC, Kranias EG, Györke S. Ablation of HRC alleviates cardiac arrhythmia and improves abnormal Ca handling in CASQ2 knockout mice prone to CPVT. *Cardiovascular Research*. 2015;108:299-311

38. Landstrom AP, Dailey-Schwartz AL, Rosenfeld JA, Yang Y, McLean MJ, Miyake CY, Valdes SO, Fan Y, Allen HD, Penny DJ, Kim JJ. Interpreting incidentally identified variants in genes associated with catecholaminergic polymorphic ventricular tachycardia in a large cohort of clinical whole-exome genetic test referrals. *Circulation: Arrhythmia and Electrophysiology*. 2017;10

39. Neubauer J, Lecca MR, Russo G, Bartsch C, Medeiros-Domingo A, Berger W, Haas C. Post-mortem whole-exome analysis in a large sudden infant death syndrome cohort with a focus on cardiovascular and metabolic genetic diseases. *European Journal of Human Genetics*. 2017;25:404-409

40. Wong CH, Koo SH, She GQ, Chui P, Lee EJ. Genetic variability of RyR2 and CASQ2 genes in an Asian population. *Forensic Science International*. 2009;192:53-55

41. Liu QQ, Oberti C, Zhang XQ, Ke T, Zhang T, Scheinman M, Hu DY, Wang QK. [A Novel mutation of F189L in CASQ2 in families with catecholaminergic polymorphic ventricular tachycardia]. *Zhonghua Yi Xue Yi Chuan Xue Za Zhi*. 2008;25:334-337

42. Laitinen PJ, Swan H, Kontula K. Molecular genetics of exercise-induced polymorphic ventricular tachycardia: identification of three novel cardiac ryanodine receptor mutations and two common calsequestrin 2 amino-acid polymorphisms. *European Journal of Human Genetics*. 2003;11:888-891

43. Wleklinski M, Parikh S, Knollmann BC. An Autosomal Dominant Mutation in Calsequestrin 2 Causes CPVT Without Changing Protein Levels. *Biophysical Journal*. 2019;116:95a-96a

44. Lahat H, Pras E, Olender T, Avidan N, Ben-Asher E, Man O, Levy-Nissenbaum E, Khoury A, Lorber A, Goldman B, Lancet D, Eldar M. A missense mutation in a highly conserved region of CASQ2 is associated with autosomal recessive catecholamine-induced polymorphic ventricular tachycardia in Bedouin families from Israel. *American Journal of Human Genetics*. 2001;69:1378-1384

45. Kalyanasundaram A, Bal NC, Franzini-Armstrong C, Knollmann BC, Periasamy M. The calsequestrin mutation CASQ2D307H does not affect protein stability and targeting to the junctional sarcoplasmic reticulum but compromises its dynamic regulation of calcium buffering. *Journal of Biological Chemistry*. 2010;285:3076-3083

46. Rizzi N, Liu N, Napolitano C, Nori A, Turcato F, Colombi B, Bicciato S, Arcelli D, Spedito A, Scelsi M, Villani L, Esposito G, Boncompagni S, Protasi F, Volpe P, Priori SG. Unexpected structural and functional consequences of the R33Q homozygous mutation in cardiac calsequestrin: a complex arrhythmogenic cascade in a knock in mouse model. *Circulation Research*. 2008;103:298-306

47. Wang Q, Groenendyk J, Paskevicius T, Qin W, Kor KC, Liu Y, Hiess F, Knollmann BC, Chen SRW, Tang J, Chen XZ, Agellon LB, Michalak M. Two pools of IRE1α in cardiac and skeletal muscle cells. *FEBS Journal*. 2019;33:8892-8904

48. Louis-Jeune C, Andrade-Navarro MA, Perez-Iratxeta C. Prediction of protein secondary structure from circular dichroism using theoretically derived spectra. *Proteins*. 2012;80:374-381

49. Schoenmakers TJ, Visser GJ, Flik G, Theuvenet AP. CHELATOR: an improved method for computing metal ion concentrations in physiological solutions. *Biotechniques*. 1992;12:870-874, 876-879

50. Campbell KP, MacLennan DH, Jorgensen AO. Staining of the Ca^{2+}-binding proteins, calsequestrin, calmodulin, troponin C, and S-100, with the cationic carbocyanine dye "Stains-all". *Journal of Biological Chemistry*. 1983;258:11267-11273

51. Damiani E, Volpe P, Margreth A. Coexpression of two isoforms of calsequestrin in rabbit slow-twitch muscle. *Journal of Muscle Research and Cell Motility*. 1990;11:522-530

52. Fliegel L, Leberer E, Green NM, MacLennan DH. The fast-twitch muscle calsequestrin isoform predominates in rabbit slow-twitch soleus muscle. *FEBS Letters*. 1989;242:297-300

53. Biral D, Volpe P, Damiani E, Margreth A. Coexistence of two calsequestrin isoforms in rabbit slow-twitch skeletal muscle fibers. *FEBS Letters*. 1992;299:175-178

54. Eldar M, Pras E, Lahat H. A missense mutation in the CASQ2 gene is associated with autosomal-recessive catecholamine-induced polymorphic ventricular tachycardia. *Trends in Cardiovascular Medicine*. 2003;13:148-151

55. Viatchenko-Karpinski S, Terentyev D, Gyorke I, Terentyeva R, Volpe P, Priori SG, Napolitano C, Nori A, Williams SC, Gyorke S. Abnormal calcium signaling and sudden cardiac death associated with mutation of calsequestrin. *Circulation Research*. 2004;94:471-477

56. Ashkenazy H, Abadi S, Martz E, Chay O, Mayrose I, Pupko T, Ben-Tal N. ConSurf 2016: an improved methodology to estimate and visualize evolutionary conservation in macromolecules. *Nucleic Acids Research*. 2016;44:W344-W350

57. Slupsky JR, Ohnishi M, Carpenter MR, Reithmeier RA. Characterization of cardiac calsequestrin. *Biochemistry*. 1987;26:6539-6544

58. Manno C, Figueroa LC, Gillespie D, Fitts R, Kang C, Franzini-Armstrong C, Rios E. Calsequestrin depolymerizes when calcium is depleted in the sarcoplasmic reticulum of working muscle. *Proceedings of the National Academy of Sciences of the United States of America*. 2017;114:E638-E647

59. Paniagua R, Royuela M, García-Anchuelo RM, Fraile B. Ultrastructure of invertebrate muscle cell types. *Histology & Histopathology*. 1996;11:181-201

60. Smith DS, Gupta BL, Smith UNA. The organization and myofilament array of insect visceral muscles. *Journal of Cell Science*. 1966;1:49

61. Mackrill JJ, Shiels HA. Evolution of excitation-contraction coupling. In: Islam MS, ed. *Calcium Signaling*. Cham: Springer International Publishing; 2020:281-320.

62. Bal NC, Jena N, Chakravarty H, Kumar A, Chi M, Balaraju T, Rawale SV, Rawale JS, Sharon A, Periasamy M. The C-terminal calcium-sensitive disordered motifs regulate isoform-specific polymerization characteristics of calsequestrin. *Biopolymers*. 2015;103:15-22

63. Miller MP, Kumar S. Understanding human disease mutations through the use of interspecific genetic variation. *Human Molecular Genetics*. 2001;10:2319-2328

64. Guo HH, Choe J, Loeb LA. Protein tolerance to random amino acid change. *Proceedings of the National Academy of Sciences of the United States of America*. 2004;101:9205-9210

65. Kumar S, Patel R. Neutral Theory, Disease Mutations, and Personal Exomes. *Molecular Biology and Evolution*. 2018;35:1297-1303

66. Vitkup D, Sander C, Church GM. The amino-acid mutational spectrum of human genetic disease. *Genome Biology*. 2003;4:R72

67. Valle G, Galla D, Nori A, Priori SG, Gyorke S, de Filippis V, Volpe P. Catecholaminergic polymorphic ventricular tachycardia-related mutations R33Q and L167H alter calcium sensitivity of human cardiac calsequestrin. *Biochemical Journal*. 2008;413:291-303

68. Qin J, Valle G, Nani A, Nori A, Rizzi N, Priori SG, Volpe P, Fill M. Luminal Ca^{2+} regulation of single cardiac ryanodine receptors: insights provided by calsequestrin and its mutants. *The Journal of General Physiology*. 2008;131:325-334

69. Houle TD, Ram ML, Cala SE. Calsequestrin mutant D307H exhibits depressed binding to its protein targets and a depressed response to calcium. *Cardiovascular Research*. 2004;64:227-233

70. Titus EW, Deiter FH, Shi C, Wojciak J, Scheinman M, Jura N, Deo RC. The structure of a calsequestrin filament reveals mechanisms of familial arrhythmia. *bioRxiv*. 2019:672303

Chapter 5

1. Groenendyk J, Lee D, Jung J, Dyck JR, Lopaschuk GD, Agellon LB, Michalak M. Inhibition of the Unfolded Protein Response Mechanism Prevents Cardiac Fibrosis. *PLOS One*. 2016;11:e0159682

2. Tufanli O, Telkoparan Akillilar P, Acosta-Alvear D, Kocaturk B, Onat UI, Hamid SM, Cimen I, Walter P, Weber C, Erbay E. Targeting IRE1 with small molecules counteracts progression of atherosclerosis. *Proceedings of the National Academy of Sciences of the United States of America*. 2017;114:E1395-E1404

3. Landstrom AP, Dailey-Schwartz AL, Rosenfeld JA, Yang Y, McLean MJ, Miyake CY, Valdes SO, Fan Y, Allen HD, Penny DJ, Kim JJ. Interpreting incidentally identified variants in genes associated with catecholaminergic polymorphic ventricular tachycardia in a large cohort of clinical whole-exome genetic test referrals. *Circulation: Arrhythmia and Electrophysiology*. 2017;10

4. Neubauer J, Lecca MR, Russo G, Bartsch C, Medeiros-Domingo A, Berger W, Haas C. Post-mortem whole-exome analysis in a large sudden infant death syndrome cohort with a

focus on cardiovascular and metabolic genetic diseases. *European Journal of Human Genetics*. 2017;25:404-409

Appendix I: IRE1α and Casq2 knockout in mouse embryonic stem cells

To investigate function of IRE1α and stress response role of Casq2 in cardiomyocytes, I generated IRE1α or Casq2 knockout in mouse embryonic stem cells by using CRISPR/Cas9 (clustered regularly interspaced short palindromic repeats) genetic editing tool. Embryonic stem cells able to differentiate to cardiomyocytes provide an important model to investigate mechanism and involvement of IRE1α in the cardiac development[1]. Cardiomyocytes derived from *IRE1α*$^{-/-}$ or *Casq2*$^{-/-}$ embryonic stem cells are useful tools to study functional impact of these two proteins in cardiomyocytes biology and pathology.

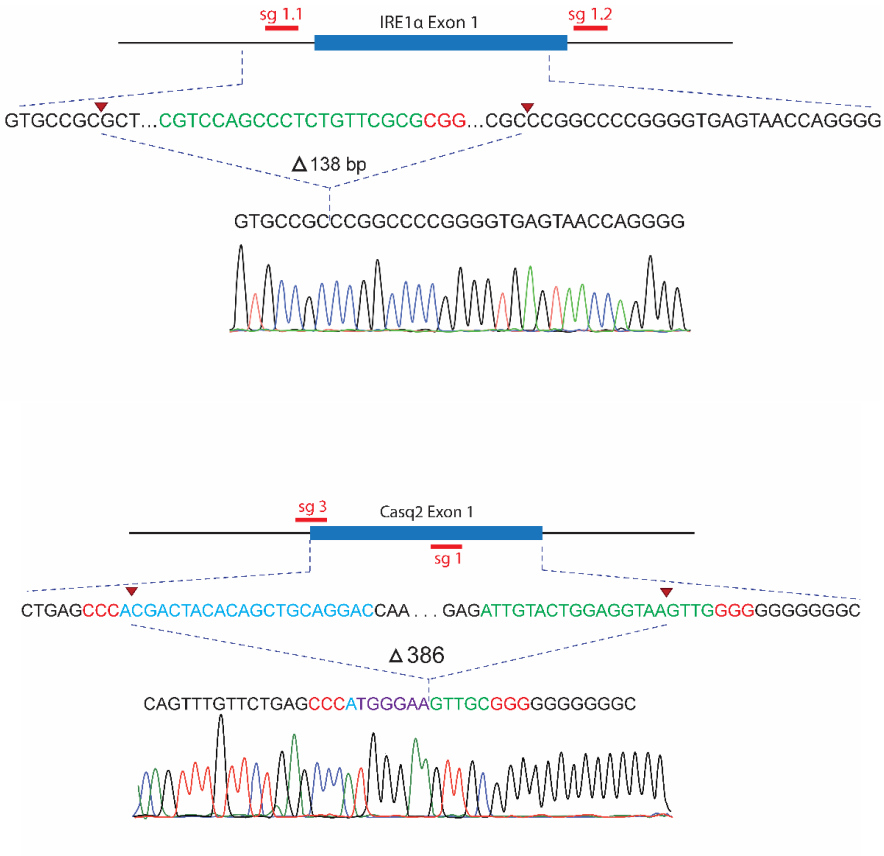

Figure A-1. CRISPR/Cas9 knockout of the IRE1α or Casq2 gene in mouse embryonic stem cells.

Sequencing confirmation of the gene deletions from genomic DNA.

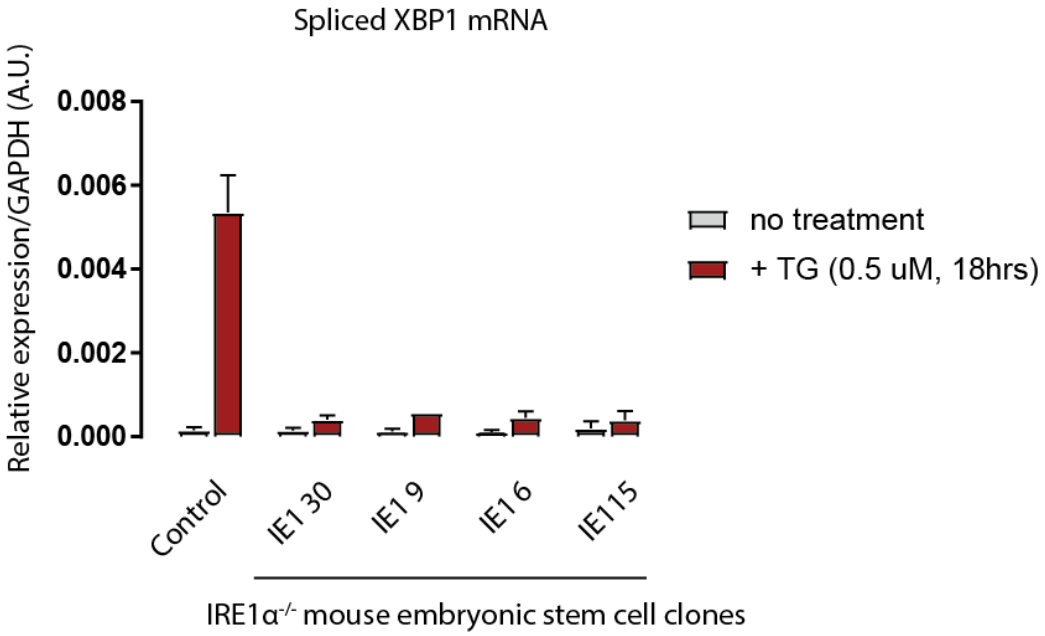

Figure A-2. *IREα*$^{-/-}$ mouse embryonic stem cells lost RNase activity.

Four clones selected after CRISPR/Cas9 gene editing and nucleotide sequence analysis confirming silencing of the IREα gene. Cells treated with thapsigargin, an inhibitor of sarco/endoplasmic reticulum Ca^{2+} ATPase (SERCA) to induce ER stress. n=3, Data presented are mean ± standard error.

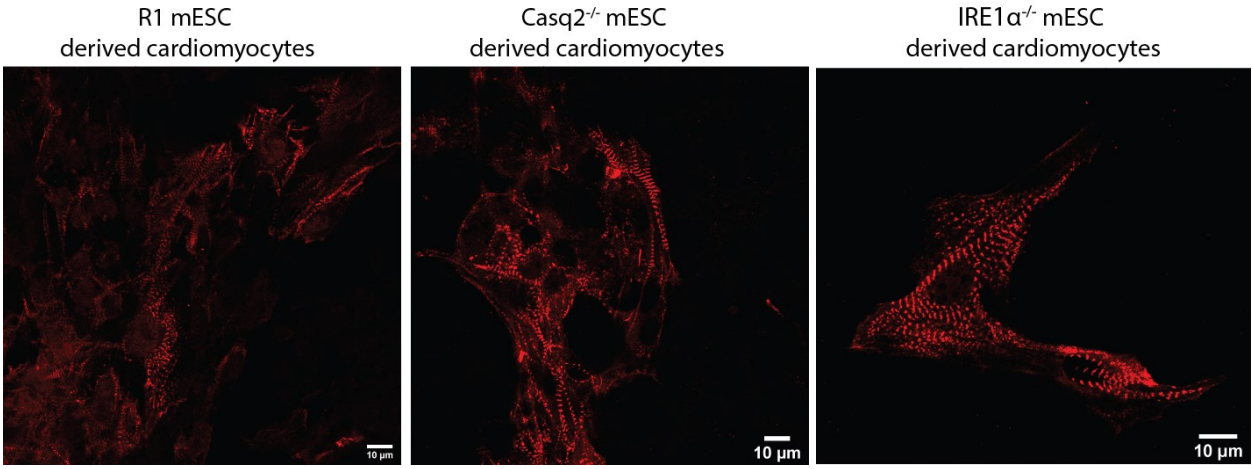

Figure A-3. IRE1α- and Casq2-deficient mouse embryonic stem cells able to differentiated into beating cardiomyocytes.

R1: wild-type mouse embryonic stem cell (mESC).

The embryonic bodies generated from mouse embryonic stem cells were plated onto 24 mm circle coverslip with gelatin coating. Cells were fixed with 3.7% paraformaldehyde (PFA) at day 12 of differentiation (counting start from embryonic body hanging drop). Embryonic bodies were stained with sarcomere protein α-actinin (Alexa 647) and imaged with Leica SP5 confocal (n=2).

Appendix II: The overexpression of Casq2 in non-muscle cells

To investigate functional impact of Casq2 on IRE1α mediated UPR, I overexpressed Casq2 in HEK293 cells and measured IRE1α mediated UPR activity under non-stress and stressed condition.

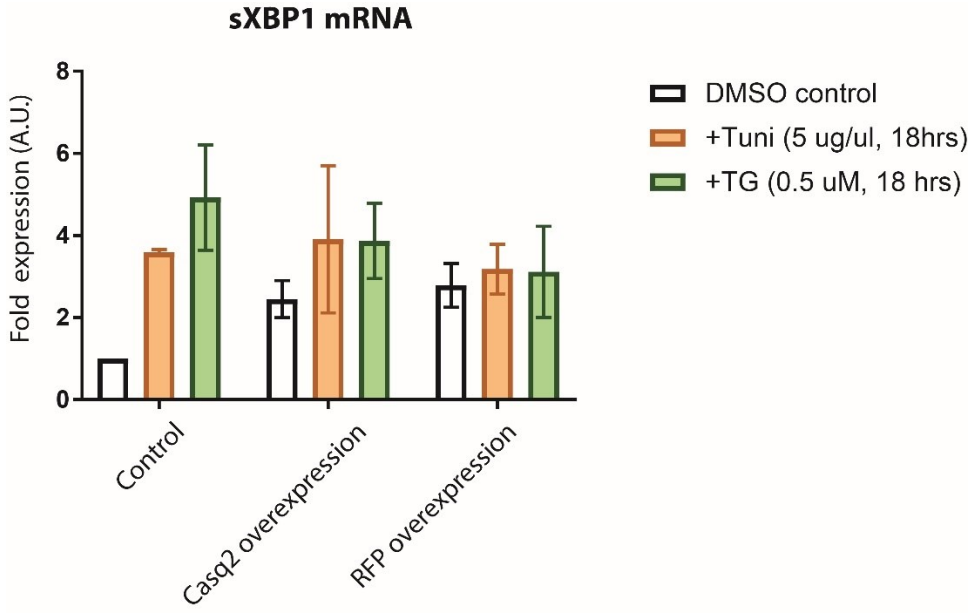

Figure B-1. Overexpression of Casq2 in HEK293 cell induces activation of IRE1α mediated UPR as monitored by XBP1 mRNA splicing.

HEK293 cells were transient transfected with pcDNA3.1 containing cDNA encoding full-length dog Casq2 or red fluorescent protein (RFP). Both Casq2 and RFP able to induce activation of IRE1α measured by increased spliced XBP1 activity in absence of addition stress agents. XBP1 splicing activity of IRE1α can be further induced slightly by treating cells with tunicamycin (induce ER stress by inhibiting protein glycosylation) or thapsigargin (induces ER stress by depleting ER Ca^{2+} store). Since both Casq2 and RFP induced activation of IRE1α by transient transfection, indicating transient transfection can activate UPR may be due to ER protein overload. Data presented are mean ± standard error.

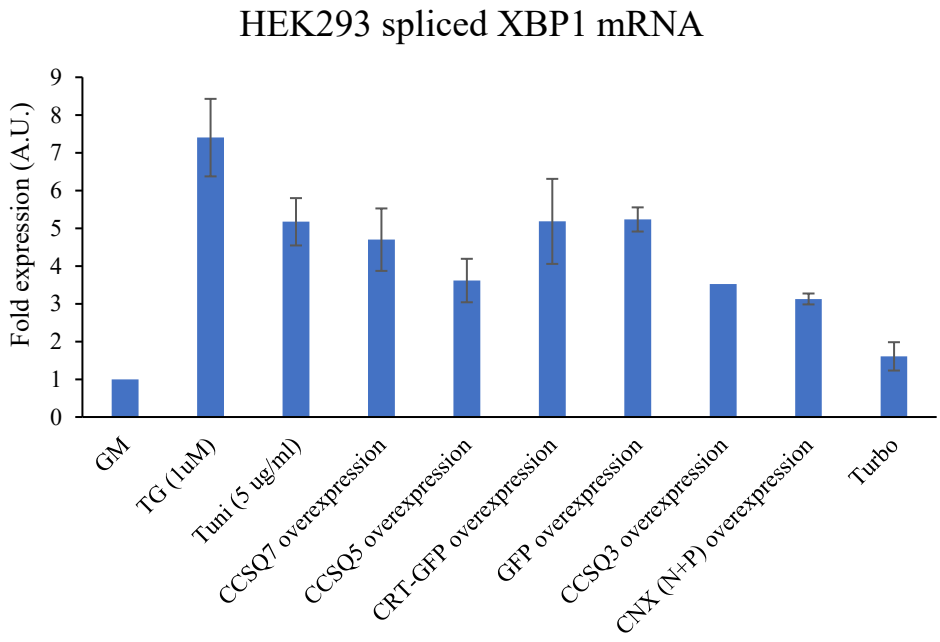

Figure B- 2. Transient transfection to overexpress proteins can induce ER stress in HEK293 cells.

GM: Growth media, non-stress control (n=5)
TG: Thapsigargin treatment for 8 hours, induced ER stress control (n=4)
Tuni: Tunicamycin treatment for 8 hours, induced ER stress control (n=3)
CCSQ7: Full-length Casq2 (n=4)
CCSQ5: Truncated Casq2 with deletion of the third thioredoxin-like fold domain (n=3)
CRT-GFP: Full-length calreticulin fused with green fluorescence protein (GFP) (n=2)
CCSQ3: Truncated Casq2 with deletion of third and second thioredoxin-like fold domain. (n=1)
CNX (N+P): Truncated calnexin containing calnexin globular N-domain and P domain (n=2)
Turbo: TurboFect transfection regents (ThermoFisher, R0533) treatment without any plasmids (n=2)
Data presented are mean ± standard error

To eliminate ER protein overload induced ER stress due to transient transfection, I generated stable HEK293 cell line express full-length dog Casq2. HEK293 cells were transfected with pcDNA3.1 plasmid containing cDNA of full-length dog Casq2 with HA tag at the C-terminus by using TurboFect transfection regents (ThermoFisher, R0533). After 48 hours transfection, cells were selected with 0.4 mg/ml neomycin (G418) for 6 days. Single cells were selected by limited dilution.

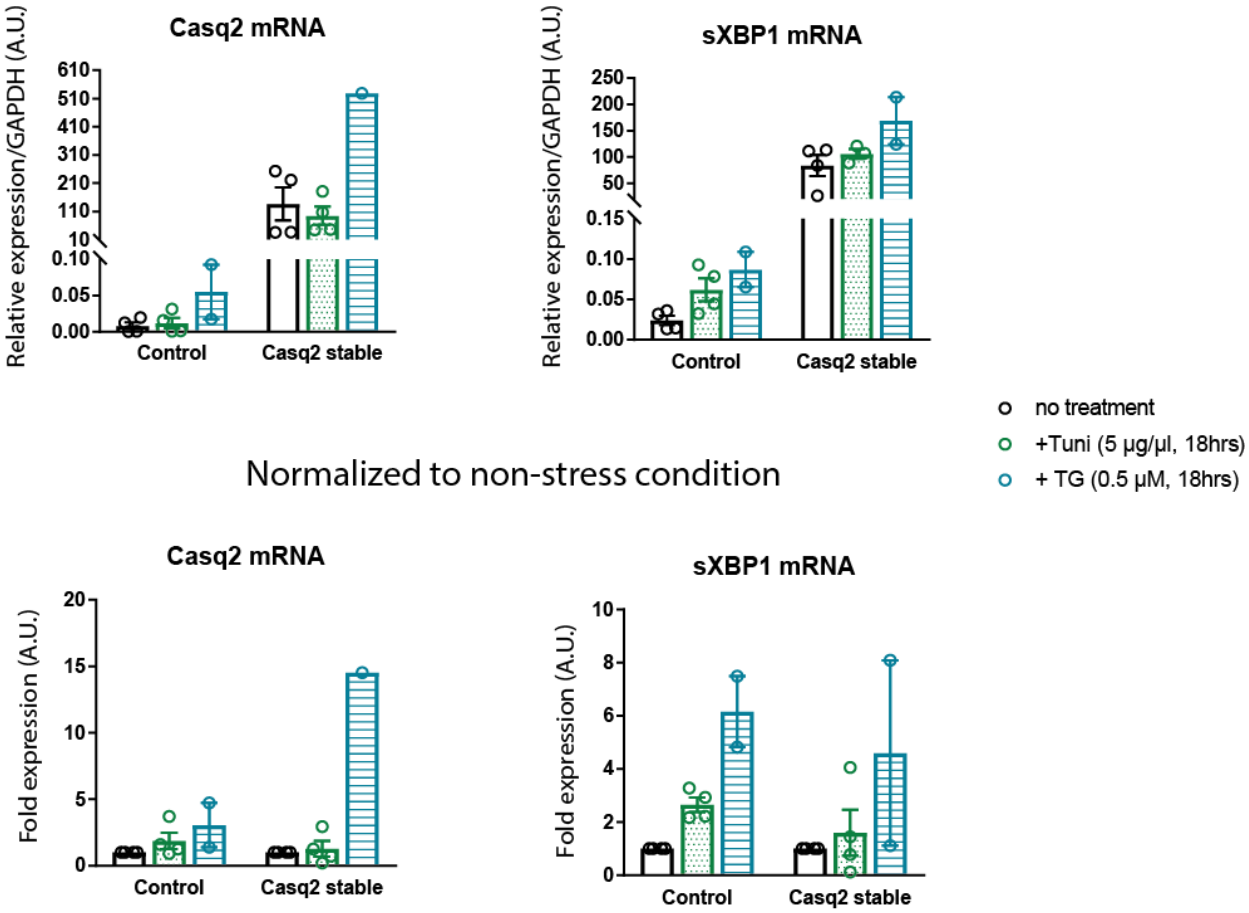

Figure B-3. HEK293 cell line stable expressing Casq2 has elevated IRE1α-mediated UPR activation.

TG: Thapsigargin treatment
Tuni: Tunicamycin treatment
Data presented are mean ± standard error

Appendix III: Unfolded protein response in Casq2 deficient cardiomyocytes

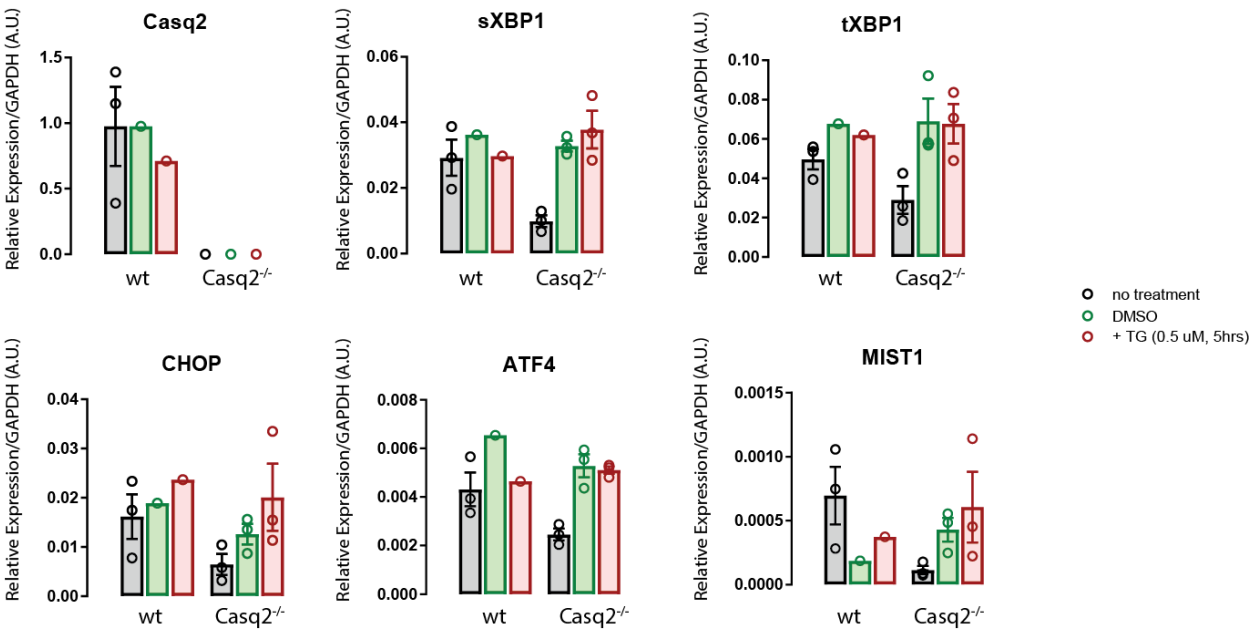

Figure C-1. qPCR of mRNA isolated from wild-type and *Casq2*$^{-/-}$ cardiomyocytes.

wt: Cardiomyocyte isolated from C57BL/6J wild-type hearts

Casq2$^{-/-}$: Cardiomyocytes isolated from mice with the whole body knockout of the Casq2 gene, where *Casq2*$^{-/-}$ allele consist of 1.1 kb deletion that removes entire exon 1 with 561 bp upstream and 107 bp downstream.

DMSO: solvent for thapsigargin

Thapsigargin: ER stress inducer by depleting ER Ca^{2+} store. Treated for 5 hr after cardiomyocyte isolation with 0.5 μM concentration.

Cardiomyocytes were prepared by Kaylen Kor from laboratory of Dr. Bjorn C. Knollmann at Vanderbilt University School of Medicine, Nashville, U.S.A. global knockout of Casq2 mice were generated by Dr. Bjorn C. Knollmann's group[2].

Data presented are mean ± standard error

Appendix IV: IRE1α and Calsequestrin co-localization using super-resolution imaging

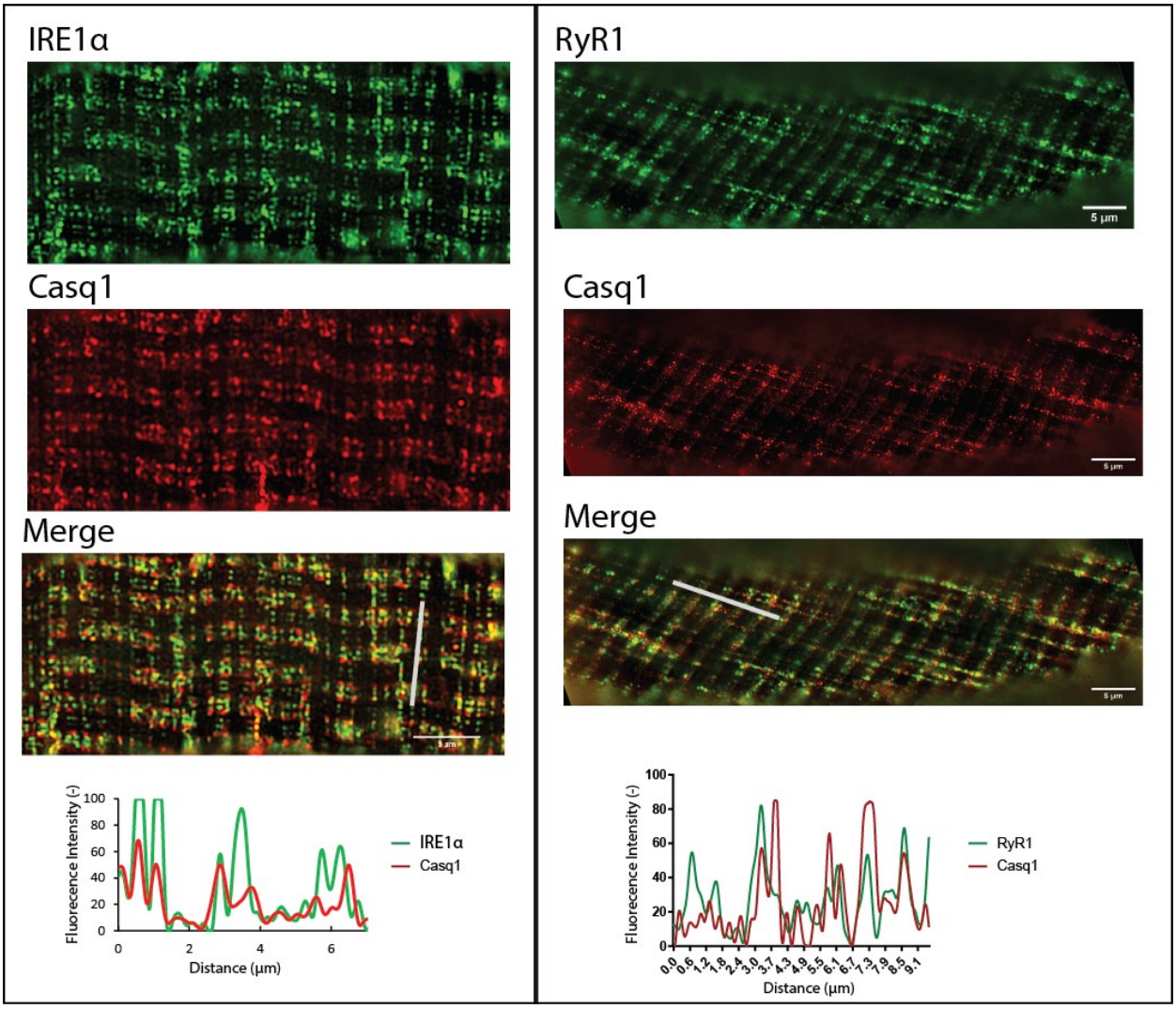

Figure D-1. Skeletal muscle tissue immunostaining imaged with Nikon structured illumination microscopy (SIM, N-SIM S system)

IRE1α (Alexa 488) and Casq1 (Alexa 647) colocalized in skeletal muscle tissue. Fluorescence intensity profile were measured and plotted from indicated line. (n=1)

RyR1 (Alexa 488) and Casq1 (Alexa 647) shown in right. (n=1)

Appendix references

1. Sachinidis A, Fleischmann BK, Kolossov E, Wartenberg M, Sauer H, Hescheler J. Cardiac specific differentiation of mouse embryonic stem cells. *Cardiovascular Research*. 2003;58:278-291

2. Knollmann BC, Chopra N, Hlaing T, Akin B, Yang T, Ettensohn K, Knollmann BE, Horton KD, Weissman NJ, Holinstat I, Zhang W, Roden DM, Jones LR, Franzini-Armstrong C, Pfeifer K. Casq2 deletion causes sarcoplasmic reticulum volume increase, premature Ca^{2+} release, and catecholaminergic polymorphic ventricular tachycardia. *Journal of Clinical Investigation*. 2006;116:2510-2520